Bridging the Gap in Clinical Translation:

Optimising an Ovine Model of Traumatic Brain Injury

A thesis submitted in fulfilment for degree of

DOCTOR OF PHILOSOPHY

In

The Discipline of Anatomy and Pathology

Adelaide Medical School

The University of Adelaide

Jessica Sharkey

June 2021

TABLE OF CONTENTS

THESIS ABSTRACT

Traumatic brain injury (TBI) is a life-threatening injury, affecting approximately 69 million people worldwide annually. TBI is characterised as an acute physical injury to brain tissue, and is typically inflicted by external mechanical force which results in a diminished or altered state of consciousness, often leading to subsequent neurological impairment. Damage to the axonal white matter tracts within the brain is a key cause of neurological impairment and long-term disability following TBI. This diffuse axonal injury (DAI) presents across the spectrum of mild, moderate and severe TBI and increases relative to injury severity. To date, most pre-clinical studies investigating DAI following TBI have been limited to the use of lissencephalic species which respond differently to traumatic shear injury than the gyrencephalic brain of humans due to structural and neuroanatomical differences. The human brain presents a higher ratio of white matter (60%) and more intricate cortical structure compared to the rodent brain (10%), which is of particular relevance given evidence that DAI develops predominantly in the white matter of the brain. Additionally, DAI pathology is largely influenced by the mechanical forces of injury. For these reasons, translation of therapies from rodent to human have been largely unsuccessful. Therefore, an intermediary species which more closely represents the human brain is required to better understand DAI pathology. As such, the aim of this research was to optimise an ovine model of moderate TBI with the absence of skull fracture in order to characterise DAI and associated pathologies following injury. These studies also explored the effects of post-traumatic hypoxia (PTH) on the development of DAI. Additionally, studies within this thesis investigated the relationship between angular and linear head acceleration following impact on the development of DAI. Finally, this thesis determined the centre of mass of the sheep head in order to develop an anatomical coordinate system (ACS) which would allow more representative calculation of head acceleration specific to the anatomy of the sheep.

This will better inform the understanding of DAI pathology and development following impact in the sheep. Despite extensive troubleshooting, these findings presented suggest this model of TBI with the addition of PTH to be insufficient to effectively produce marked DAI in the absence of significant skull fracture and gross pathological lesions within the sheep. Additional modelling is required in order to reduce the incidence of skull fracture and increase the inertial force transmitted to the brain parenchyma which will encourage the production of DAI and additional microscopic TBI pathologies.

DECLARATION

I certify that this work contains no material which has been accepted for the award of any other degree or diploma in my name, in any university or other tertiary institution and, to the best of my knowledge and belief, contains no material previously published or written by another person, except where due reference has been made in the text. In addition, I certify that no part of this work will, in the future, be used in a submission in my name, for any other degree or diploma in any university or other tertiary institution without the prior approval of the University of Adelaide and where applicable, any partner institution responsible for the joint-award of this degree.

I acknowledge that copyright of published works contained within this thesis resides with the copyright holder(s) of those works.

I also give permission for the digital version of my thesis to be made available on the web, via the University's digital research repository, the Library Search and also through web search engines, unless permission has been granted by the University to restrict access for a period of time.

I acknowledge the support I have received for my research through the provision of an Australian Government Research Training Program Scholarship.

Jessica Sharkey

ACKNOWLEDGEMENTS

First and foremost, I would like to thank my primary PhD supervisor A/Prof Renée Turner along with Dr Frances Corrigan and Dr Anna Leonard for being my co-supervisors. Thank you for seeing my potential and giving me a world of opportunity to develop skills I could never have dreamt of having. Somehow, in the midst of you all having babies over these last 4 years you have made inconceivable time to teach me, comfort me and mentor my growth as a researcher at any needed time. You may as well have raised me too! I am forever grateful for having such strong and influential female role models in science which have inspired me to be the best version of myself, despite the odds. I hold each of you as not only mentors, but now as friends.

To my co-supervisor Dr Claire Jones and mentor and friend Dr Ryan Quarrington from the Adelaide Spinal Research Group - thank you for your unwavering patience and support in passing on your knowledge of biomechanical engineering to someone who didn't even complete year 12 maths! Thank you for believing I had the potential to take on a project focussing on something completely brand new.

I would also like to thank Rebecca Dowden, Lola Kaukas and Justin Krieg. Developing large animal experiments is no easy feat, and one I could not have done without any of you. Thank you for scratching my nose whenever I was sterile, making me laugh when I was stressed, and providing invaluable research and data support (that last part is all you Justin!).

I would also like to thank the members past and present of our enormous group in the Translational Neuropathology Lab. But in particular, Annabel Sorby-Adams and Bianca Guglietti. I never imagined coming into this PhD and forming two lifelong friendships. Thank you for experiencing every moment of frustration, sadness, joy and success along-side me not only in work but in our personal lives (even planning B's wedding mid PhD, are we crazy?).

The two of you are more valuable than any doctorate and I couldn't be more grateful for this time bringing us together.

To my best friends Emily and Bonnie – I wish I could put into words how I feel about the love and support each of you have given me, not only over the last 4 years but over the last decade of our friendship. Having one of you going through this with me (Bon) and one of you on the out (Em) has been the perfect balance. I hope one day I can give this back to you both.

To Cam – you gave me hope when I thought it was all lost many times over the last year. Meeting me in the last year of my PhD was a bold move on your behalf, but one you took on whole heartedly. Thank you for believing I could do this.

Finally, to my parents (mum, dad, Lynn), my brother Thomas, and all my family – I have never once doubted your pride and support in my journey over the last 10 years. Thank you for being by my side the whole way and only thinking I'm a little bit crazier than when I started.

I also extend my thanks to the staff at SAHMRI LARIF/PIRL at Gilles Plains for their instrumental research support over the years.

I acknowledge the support of my PhD through an Australian Government Research Training Program Scholarship. I also acknowledge funding from the Neurosurgical Research Foundation and National Health and Medical Research Council for projects conducted as part of my candidature.

This thesis is dedicated to all of my sheepies, each one of you was the most important part

TABLE OF ABBREVIATIONS

Arterial blood gas	ABG	Intraventricular	IV
Arterial blood pressure	ABP	Inspired : expired	I:E
Anatomical coordinate system	ACS	Ionized calcium binding adaptor molecule-1	IBA-1
Activities of daily life	ADL	Large animal research and imaging facility	LARIF
Axonal injury	AI	Magnetic resonance imaging	MRI
Alpha	α	Mean arterial blood pressure	mABP
Autonomic nervous system	ANS	Messenger ribonucleic acid	mRNA
Amyloid precursor protein	APP	Mild traumatic brain injury	mTBI
Base excess	BE	Myelin basic protein	MBP
Beta	β	Neurofilament	NF
Bicarbonate	HCO_3	Neurofilament compaction	NFC
Blood-brain-barrier	BBB	Neurofilament medium	RMO-14
Blood pressure	BP	Neuron specific enolase	NSE
Brain tissue oxygenation	$PbtO_2$	Nitrogen	N
Calcium	Ca^{2+}	Non-phosphorylated neurofilament-H	SMI-32
Carbon dioxide	CO_2	N-terminal proteolytic fragment of spectrin	SNTF
Central nervous system	CNS	Oxygen	O_2
Centre of mass	CoM	Partial pressure of carbon dixoide	pCO_2
Cerebrospinal fluid	CSF	Partial pressure of oxygen	pO_2
Coordinate system	CS	Peripheral capillary oxygen saturation	SpO_2
Compact DAQ	cDAQ	Positive	+ve
Computed tomography	CT	Post-traumatic hypoxia	PTH
Diffuse axonal injury	DAI	Potassium	K^+
Diffusion tensor imaging	DTI	Polymethyl methacrylate	PMMA
Enzyme-linked immunosorbent assay	ELISA	Region of interest	ROI
End tidal carbon dioxide	$EtCO_2$	Severe traumatic brain injury	sTBI
Endotracheal tube	ET	Sodium	Na^+
Finite element	FE	South Australian health and medical research institute	SAHMRI
Gamma	γ	Sports concussion assessment tool	SCAT
Glasgow coma scale	GCS	Standard deviation	SD
Glial fibrillary acidic protein	GFAP	Standard error of mean	SEM
Haematocrit	Hc	Subarachnoid haemorrhage	SAH
Haematoxylin & eosin	H&E	Subdural haemorrhage	SDH
Haemoglobin	Hb	Three dimensional	3D
Hounsfield units	HU	Toll-like receptor	TLR
Immunohistochemistry	IHC	Total carbon dioxide	$(t)CO_2$
Interleukin	IL	Traumatic brain injury	TBI
Intracranial pressure	ICP	Tumour necrosis factor-alpha	TNF

PUBLICATIONS ARISING FROM OUTSIDE THIS THESIS

Sharkey, JM, McDonald, SJ, Sun, M, Kaukas, LM, Schultz, SR, Turner, RJ, Leonard AV, Brady, RD, Corrigan, F 2020, 'Beyond the brain: Peripheral interactions following traumatic brain injury', *Journal of Neurotrauma*., vol. 37, no. 5.

PDF of manuscript in press can be found in Appendix IV.

CONFERENCE ABSTRACTS ARISING FROM THIS THESIS

Sharkey, JM, Turner, RJ, Leonard, AV, Corrigan, F 2019, 'INVESTIGATING THE PATTERN OF AXONAL INJURY FOLLOWING TRAUMATIC BRAIN INJURY OF VARYING INTENSITY IN A LARGE ANIMAL MODEL', *Journal of Neurotrauma.*, vol. 36, no. 13.

CHAPTER 1

General Introduction

CHAPTER 1: GENERAL INTRODUCTION

1.1 Traumatic Brain Injury (TBI)

Traumatic brain injury (TBI) is a life-threatening injury, with more moderate-severe forms typically resulting in extensive neurological impairment. TBI is the leading cause of death and major disability in people under 45 years of age in Western-industrialised countries, with young adults being especially susceptible (Finnie, & Blumbergs 2002; Maas, Stocchetti & Bullock 2008). Approximately 10 million people worldwide die as a result of TBI annually, with the WHO estimating by 2030, brain injuries due to traffic accidents and falls are expected to rise to the 7th and 17th major cause of death, respectively (Fehily & Fitzgerald 2017; Langlois, Rutland-Brown & Wald 2006; Pozzato et al. 2019; World Health Organization 2014). TBI is evidently a huge public health and socio-economic issue in Australia. The Australian Institute of Health and Welfare (AIHW) has reported TBI incidence rates to be approximately 107 per 100,000 in the Australian population (Jagnoor & Cameron 2014). Additionally, approximately 10,000 people die each year due to TBI in Australia, with trauma alone accounting for 1-20 of all hospital admissions (Health & Welfare 2010). In 2004 to 2005 TBI resulted in over 26,000 episodes of hospitalisation in Australia with an estimated direct cost of hospital care of $184 million (Moorin, Miller & Hendrie 2014). The total estimated cost of TBI on the Australian health care system is estimated to be approximately $8.6 billion, with lifetime cost of $2.5 million per moderate TBI case and $4.8 million per severe TBI (sTBI) case (Access Economics 2009; Moorin, Miller & Hendrie 2014).

Deficits resulting from TBI can manifest as motor, sensory and physical disability, such as dependency for activities of daily life (ADL), voluntary muscle dysfunction (sphincter control) and paralysis (Andelic et al. 2010). Cognitive, emotional and behavioural/psychosocial impairment such as, spatial reasoning and conceptualisation deficits, attention and concentration deficits, information processing and skills in executive functioning and

withdrawal, anxiety, depression, irritability and impulsivity are also common side effects of TBI (Rassovsky et al. 2015). Neuropsychiatric deficits (*i.e.* behavioural and cognitive changes) typically overshadow the neurophysical symptomology (such as incontinence and ataxia) as the major cause of disability (Fleminger & Ponsford 2005). Regardless of patient age, it is these cognitive and behavioural changes that represent the greatest burden to families and support services following TBI (Ponsford et al. 2003). Given the diverse nature of TBI, it is unsurprising that these deficiencies are generally heterogenous to each individual case (Bazarian et al. 2009; Langlois, Rutland-Brown & Wald 2006). There has been an improvement in TBI prevention with public education/safety campaigns, mandating the use of helmets, airbags, and seatbelts, as well as in clinical management of TBI with advanced monitoring and specialised imaging techniques now available. Nevertheless, TBI remains one of the major community health problems worldwide and there is still currently no existing effective treatment (O'Leary & Nichol 2018).

1.2 Classification of TBI

A comprehensive, universal definition of TBI is still yet to be cemented in the literature (Bigler 2001), with the terms head injury and brain injury being used interchangeably in many instances (Povlishock 2013; Pushkarna, Bhatoe & Sudambrekar 2010). Broadly, TBI encompasses the spectrum of concussion, mild TBI (mTBI), and moderate-severe TBI. Specifically, TBI refers to acute physical injury to brain tissue, inflicted by external mechanical force, which results in a diminished or altered state of consciousness, often leading to temporary, or in some cases, permanent neurological impairment (Greve & Zink 2009; Hawryluk & Manley 2015). TBI can be classified as either an open or closed injury to the head. Open injuries are those occuring with penetration of the skull and underlying dura mater, in

most cases resulting from injuries such as gunshot wounds, with the macroscopic brain damage showing a focal point of destruction.

Closed injuries encompass those occurring without penetration of the skull and dura, but rather from blunt force trauma (Pushkarna, Bhatoe & Sudambrekar 2010) and present with a more diffuse pattern of damage in the brain (Castellanos-Pinedo et al. 2012; Maas, Stocchetti & Bullock 2008). Pathologically; however, closed head injuries can also present with focal cerebral damage including lesions, contusions, laceration and haematomas; all of which can occur in the absence of skull penetration (Zhang et al. 2014).

In clinical practice, the most common tool used to diagnose the severity of TBI is the Glasgow Coma Scale (GCS) developed by Teasdale and Jennett in 1974 (*Table 1.1*) (Teasdale & Jennett 1974). TBI can be classified into three main categories based on the immediate effects following injury: mild, moderate, or severe. However, the GCS scoring is symptom-based, assessing motor, verbal, and eye-opening responses, and does not allow targeting of specific pathologies (Hawryluk & Manley 2015).

Table 1.1: GCS score is obtained by adding the value for each category: 3 = deep unconsciousness; 15 = complete consciousness (Teasdale & Jennett 1974).

Score	Eye Opening	Verbal Response	Motor Response
1	None	None	No movements
2	Open to painful stimulation	Incomprehensible sounds	Extended to pain
3	Open to voice	Inappropriate words	Abnormal flexion to pain
4	Open spontaneously	Confused, disoriented	Withdraws to pain
5	-	Oriented converses	Localises to painful stimulus
6	-	-	Obeys commands

1.2.1 Mild TBI

mTBI is the most common form of TBI, accounting for 90% of all cases and is particularly prevalent in teenagers and the elderly (Fehily & Fitzgerald 2017; World Health Organisation 2006). The predominating cause of mTBI is sports-related incidents (McCrory et al. 2013). The subsequent cerebral injury typically results from the application of both linear and rotational acceleration and deceleration to the brain, inducing non-penetrating diffuse rather than focal brain damage (Dashnaw, Petraglia & Bailes 2012; Meaney & Smith 2011). Patients typically experience a period of unconsciousness lasting 30 minutes or less and a GCS of 13-15 with symptoms including photophobia and headache, dizziness/drowsiness, transient amnesia, confusion and nausea and vomiting, which are typically short lived (Fehily & Fitzgerald 2017).

1.2.2 Concussion

An estimated 42 million people worldwide sustain concussive injuries each year (Gardner & Yaffe 2015). The term concussion and mTBI are often used interchangeably, although there is evidence to suggest that concussion is an injury category of its own (Laskowski, Creed & Raghupathi 2015). Concussion is characterised by biomechanical force emitted to the brain resulting in subsequent pathophysiology (Guskiewicz et al. 2000). However, this force which is transmitted to the brain is not always from a direct blow to the head but can also arise from impact to the body causing the head to undergo whiplash acceleration/deceleration (Dowdell et al. 2018; Guskiewicz et al. 2000). Concussion does not always cause loss of consciousness or lead to structural abnormalities on standard imaging, such as magnetic resonance imaging (MRI) or X-Ray (McCrory et al. 2013). Some clinicians and scientists argue that with the high variability and transient nature of symptoms, it is contradictory to use the term concussion as a diagnosis in practice (Sharp & Jenkins 2015). This subset of specialists suggest that the use of vague terminology to describe the post-traumatic sequelae following concussion leads to

misconceptions and biases in the diagnostic process, producing uninterpretable science, poor clinical guidelines and confused policy (Sharp & Jenkins 2015). As a result, describing the severity of TBI in clinical practice results in more accurate diagnoses. The symptoms of concussion are typical of those seen in a mTBI, presenting with many transient neuropsychological symptoms, such as: impaired verbal retrieval, depression and irritability, blurred vision, and emotional distress (Giza & Hovda 2014). Symptoms generally appear immediately following the event and typically subside within 10 days post-injury for most patients. However, in some cases symptoms can persist for days to weeks following the insult, with 10–40% of patients developing the phenomenon post-concussion syndrome, which is associated with long-term cognitive deficits and white matter changes (Binder, Rohling & Larrabee 1997; Kraus et al. 2007; Mittenberg et al. 2001; Rivara & Graham 2014; Willer & Leddy 2006). Post-concussion syndrome is generally transient, where studies have shown neurological impairment to resolve within three-six months (Evans 1992; Hall, Hall & Chapman 2005). Given that a major proportion of concussions are sustained in sporting activities (Daneshvar et al. 2011), a sideline assessment has been developed for immediate diagnosis, this being the Sports Concussion Assessment Tool (SCAT) Test, a questionnaire and evaluation of symptoms ('Sports concussion assessment tool - 5th Edition ' 2017).

1.2.3 Moderate-Severe TBI

Moderate-severe TBI represents approximately 5-10% of all head injury cases but a disproportionate burden of morbidity and mortality (Hillier, Hiller & Metzer 1997). Approximately 5.48 million people worldwide are estimated to sustain moderate-severe TBI each year (73 cases per 100,000 people). The majority of moderate-severe TBIs are caused by falls (54%) and are predominantly seen in the elderly population (>65 years of age) (Iaccarino et al. 2018). Moderate-severe TBI generally results in loss of consciousness for more than 30

minutes, and an accompanying GCS of 9-12 for moderate TBI and <8 for severe, coupled with comatose state, and in most cases, substantial disability (Collins-Praino & Corrigan 2016).

Moderate TBI

Considering the symptomology of moderate TBI, in most cases these vary depending on patient age and location of injury (Myburgh et al. 2008). However, evidence has demonstrated these symptoms to persist for years post-injury (Stocchetti & Zanier 2016). The most commonly associated symptoms of moderate TBI include cognitive impairments such as: memory impairment, depression, anxiety, and attention deficits (Schonberger et al. 2011; van der Naalt et al. 1999). Other reported deficits in moderate TBI include mild/moderate sensory and motor impairments, deficits in executive functioning, decision making, planning, and thinking, as well as difficulty in tracking conversation (Ghawami et al. 2017; Lippert-Gruner et al. 2006). Finally, behavioural changes may also occur as a result of moderate TBI, specifically erratic behaviour, aggressive outbursts, increased impulsivity and emotional insensitivity (Lippert-Gruner et al. 2006).

Severe TBI

One of the key differences between moderate and severe TBI (sTBI) is the survival rates. Although sTBI only represents 5% of overall TBI rates, Australian studies have found a 30-35% mortality rate of all sTBI patients within six months post-injury (Brown et al. 2004; Fearnside et al. 1993). Furthermore, if patients do survive, symptoms are unlikely to resolve fully, leaving many patients with permanent disability or in some cases, in a vegetative state (Wijdicks & Cranford 2005). The number of patients suffering from vegetative state is unclear, and inaccurate diagnoses are often common (O'Donnell et al. 2019). However, it has been

estimated in previous studies that one in five patients did not return to work within a year following injury due to permanent disability resulting from TBI (Selassie et al. 2008). Patients often experience difficulties with language, hearing, vision and memory, along with motor speech, which can remain prominent long term, but also in some cases dissipate over time to become more subtle (Wang, et al. 2004). It is important to note that this constellation of symptoms place a severe burden on the quality of life of patients suffering sTBI. Such a burden can influence social withdrawal and many mood disorders and behavioural changes, which studies have shown to often be overlooked in comparison to the detrimental physical deficits, with patients describing negative emotional state following recovery in a disability (Deb, Lyons & Koutzoukis 1999). There is increasing awareness for neuropsychosocial disorders which can develop long-term following TBI, such as depression, post-traumatic stress disorder, delusional disorders, and potential for substance abuse (Bjork & Grant 2009; Fleminger & Ponsford 2005). In many cases, patients who suffer more severe forms of TBI have also been shown to experience seizures post-injury or develop post-traumatic epilepsy (Semple et al. 2019). More severe forms of TBI will also demonstrate gross pathological lesions within the brain such as contusions, subarachnoid haemorrhage (SAH), subdural haemorrhage (SDH) and skull fractures. Other pathological changes may include, intraparenchymal haemorrhage, increased intracranial pressure (ICP) and decreases in brain tissue oxygenation levels (Van den Heuvel et al. 1999). It is important to note that these are less likely to present in more mild forms of TBI.

1.3 Biomechanics of Brain Injury

The different pathological and clinical presentations that are seen between severities of TBI are largely due to the biomechanics of injury which varies from mild to moderate-severe TBI.

Biomechanics is the study of forces and physical responses in both stationary (static) and moving (dynamic) biological systems (LaPlaca et al. 2007). The basic terms used in biomechanics to describe applied loads on brain tissue are force and stress, whereas deformations and strains are those used to describe the outcome on tissue following loading (LaPlaca et al. 2007). Force is defined as the action of one body on another, which will cause acceleration of the second body. When forces are generated in brain tissue, deformations may result depending on the physical properties and the nature of the force itself (Ommaya & Hirsch 1971). Deformation is defined as the change in shape of the brain tissue subject to force. Stress refers to the distribution of force relative to the area on which it acts. There are two types of stress which are relevant in discussing the biomechanics of brain injury; normal stress which acts perpendicular to the surface, and shear stress which acts within the brain tissue (Holbourn 1943). Each specific tissue tolerance is a point at which a specific load can cause structural and functional failure of the tissue (LaPlaca et al. 2007). Defining the mechanical environment in which brain injuries occur and understanding how mechanical loads are transferred to the brain structures is crucial for the development of preventative measures which could reduce the pathological response to injury (Meaney, Morrison & Bass 2014).

The severity of TBI depends on the nature, direction, duration, and magnitude of the forces applied to the head, as well as on the anatomical site of impact (Margulies, Thibault & Gennarelli 1990). The initiation of primary injury mechanisms of brain trauma is usually resultant from energy transfer to brain tissue by contact or rapid acceleration/deceleration movements (LaPlaca et al. 2007; Margulies, Thibault & Gennarelli 1990). There are two types of forces or loading that are responsible for the mechanical damage to the brain and other peripheral tissue, these being dynamic or static, with dynamic loading being much more common (Johnson et al. 2018; Ommaya, Goldsmith & Thibault 2002). These two types of force application can generate damage to the skull and its contents that produce different injuries.

Static loading, although very rare, is where the load varies with subsequent further compression of the cranium (*i.e.* slow crush injury) (Ommaya, Goldsmith & Thibault 2002). Alternatively, dynamic loading changes rapidly relative to the structure's (*i.e.* brain) resting state and is typically represented by two sub-categories: inertial loading and impact loading, both of which are distinct mechanisms resulting in vastly different consequences (Ommaya, Goldsmith & Thibault 2002). Specifically, inertial/impulse loading consists of movement of elements induced by applied motion at an entirely different position (*i.e.* vehicular occupant whose car has sustained an impact; the load is applied to the seat, and transmitted through the torso and neck to the head) resulting in differential motion of the brain and skull, typically amplified by the movement behaviour of the neck (Ommaya, Goldsmith & Thibault 2002). However, impact loading, on the other hand consists of the rapid contact of two solid objects, such as the skull and a rigid surface (*i.e.* table or floor, both of which are typical in the case of falls) (Ommaya, Goldsmith & Thibault 2002).

The shear stress and strain applied to the brain tissue typically results in either focal, diffuse injuries, or a combination of these injuries. Exactly which type of injury manifests in the brain tissue is dependent upon the type of force the tissue is exposed to. Both focal and diffuse injuries will result in subsequent angular and/or linear acceleration/deceleration. Typically, linear acceleration can be attributed to more focal injuries, where angular acceleration arises more so from diffuse impacts (Kleiven 2013). Further to this, angular acceleration occurs more commonly and results in worse pathological outcome following TBI, specifically DAI (Carroll et al. 2004; Gennarelli, Adams & Graham 1981). Upon impact, these forces cause the brain to rotate and strike the skull, which exposes cerebral tissue to momentary shear strain that deforms the shape of the brain, thereby resulting in the tearing and disconnection of axons (Gultekin & Smith 1994; Ommaya, Goldsmith & Thibault 2002; Povlishock & Katz 2005). Whilst impact forces have been shown to correlate with injury severity, linear accelerations are not the

primary cause of injury. Animal studies have shown that purely linear acceleration produces minimal brain deformation or distortion (Cullen et al. 2016; Hardy et al. 2001; Ommaya & Gennarelli 1974; Ommaya, Grubb & Naumann 1971). Brain tissue strain fields and the resulting TBI are primarily caused by head angular acceleration following impact (*Fig. 1.1*) (Cullen et al. 2016; Kleiven 2013). Strain within the human brain is most sensitive to angular loading and there is a small sensitivity of strain associated with linear kinematics (Kleiven 2013). However, it is important to note that the vast majority of TBIs result from a combination of linear and angular head motion (Cullen et al. 2016).

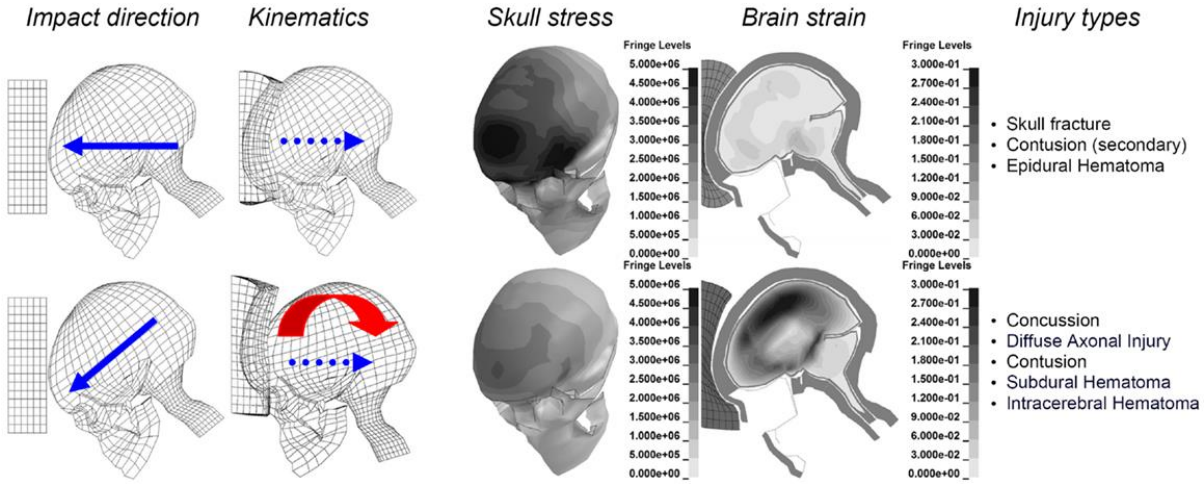

<u>Figure 1.1:</u> Biomechanics of a perpendicular impact (linear accelerations) compared to an oblique impact (angular acceleration) and resulting levels of skull stress and brain strain, when impacted against the same padding using an identical initial velocity of 6.7 m/s. Note: solid blue arrow = direction of impact, dotted blue arrow = direction of rebound motion, red arrow = indicating rotational motion (Kleiven 2013).

Ommaya and colleagues (2002) compared the magnitude of the angular acceleration/deceleration required to produce shear stress sufficient to cause varying degrees

of axonal injury (AI) relative to injury severity (*Fig. 1.2*) (Ommaya, Goldsmith & Thibault 2002). The angular acceleration required to produce concussion or mTBI in the adult brain is approximately 4500 radians/second^2 (rad/sec^2), and in comparison, approximately 18,000 rad/sec^2 to produce severe diffuse axonal injury (DAI) in the adult brain (Ommaya, Goldsmith & Thibault 2002).

In moderate-severe TBI, impact loading commonly exerts focal effects such as overt bleeding and contusions on the surface of the brain (Cullen et al. 2016). However, approximately 90% of TBIs are classified as mild, and these are closed-head injuries not associated with apparent bleeds or contusions (Demetriades et al. 2004; Santiago et al. 2012). In concussion, although impact and inertial loading of the head generally act together, the linear forces associated with head impact most often rapidly accelerate or decelerate the head relative to the position of the body, therefore generating rapid angular acceleration/deceleration of the head (Cullen et al. 2016).

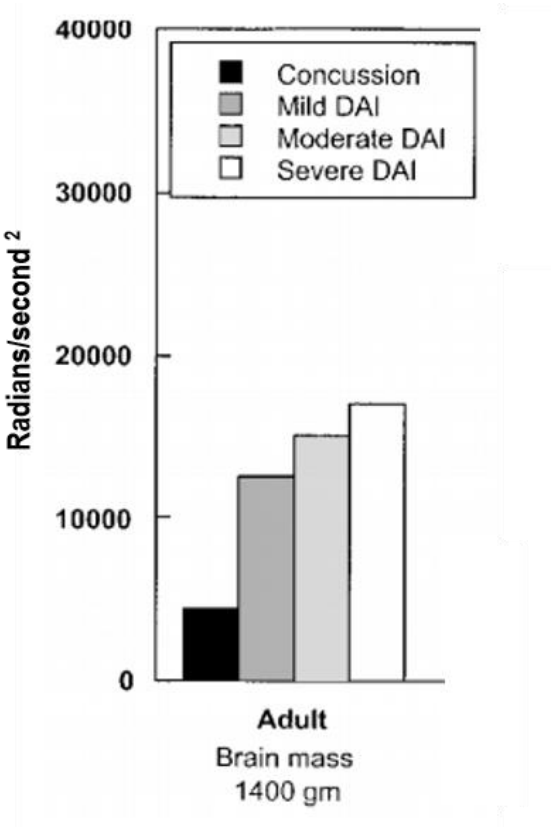

Figure 1.2: Brain injury tolerance scaling in the adult (adapted and used with permission) (Ommaya, Goldsmith & Thibault 2002).

Within the skull, several structures attach the brain to the skull to allow stability in movement of the brain in everyday life, these are the parasinusoidal granulations, parasagittal binding veins, tentorium and cranial nerves. This structural anatomy is intended to anchor the brain in

place within the skull. However, when the brain is subject to forces of injury the brain is subject to free movement within the skull. Specifically, when the brain undergoes forward movement as a result of acceleration following impact, the anterior surface of the frontal and temporal lobes are subject to injury (Ommaya, Goldsmith & Thibault 2002). This distribution and increase in force following severe impacts is why surface contusions are more common in these areas than others in the brain. Additionally, the cortex sits directly beneath specific bony regions of the skull, so when the brain strikes these areas with rapid deceleration forces this can also result in bruising or contusions (Ommaya, Goldsmith & Thibault 2002). Evidently, each individual biomechanical factor has a direct contribution and influence on the pathological response seen following TBI, and the main pathophysiological injury mechanisms are discussed in detail below.

1.4 Pathophysiology of TBI

The extensive neurological damage which arises from TBI occurs via two main injury mechanisms: primary injury and secondary injury.

1.4.1 Primary Injury

Primary injury refers to the initial damage affecting the integrity of cerebral tissue, occurring at the moment of insult, with the mechanical force sustained to the head instigating acceleration/deceleration of the brain causing it to rotate and strike the inside of the skull (Blennow, Hardy & Zetterberg 2012; Povlishock & Katz 2005). The nature, intensity, direction and duration of these forces determines the pattern, presentation and extent of the resultant brain damage (Maas, Stocchetti & Bullock 2008). Damage depicted on the macroscopic level includes shearing and stretching of white matter tracts, focal contusions, haematomas (both

overlying the brain/dura mater and within the brain parenchyma itself), and diffuse cerebral swelling (Maas, Stocchetti & Bullock 2008). Importantly from a TBI management and treatment perspective, primary injury is irreversible and is not amenable to therapeutic intervention. Therefore, primary injury can only be prevented or minimised with the use of safety measures such as seatbelts and helmets.

1.4.2 Secondary Injury

Secondary injury is initiated by the traumatic event (primary injury) and is characterised by a delayed sequence of biochemical and physiological injury cascades that continue to evolve and persist for minutes to weeks, even months following injury. Secondary injury mechanisms such as excitotoxicity, oxidative stress, inflammation, blood-brain-barrier (BBB) disruption and ionic influxes, amongst many others, all contribute to irreversible neuronal death (Blennow, Hardy & Zetterberg 2012; Huang et al. 2013). Secondary injury has been well documented to exacerbate and worsen the amount of brain injury following TBI in both experimental and clinical studies (Collins-Praino et al. 2018; Dixon & MacLeod 2020; Lazaridis, Rusin & Robertson 2019). Indeed, some secondary injury mechanisms have been shown to be exacerbated by post-traumatic hypoxia (PTH) following TBI in the rat, with the reduced tissue oxygenation contributing to a heightened neuroinflammatory response, as well as increased neuronal and axonal damage post-injury (Feng et al. 2012; Hellewell et al. 2010; Thelin et al. 2016). Given that secondary injury, unlike primary injury, develops over time, it provides a potential opportunity for pharmacological intervention to prevent or reduce the level of injury and subsequently improve survival, quality of life and functional outcomes. However, in order to develop such therapies, it is crucial that we initially better understand the factors that

perpetuate these secondary injury mechanisms and at what stage of the injury timeline they occur.

Whilst the neuropathological consequences of TBI are generally heterogeneous, undoubtedly one of the most common features observed across all injury severities, and indeed both primary and secondary injury mechanisms, is DAI (Johnson, Stewart & Smith 2013; Povlishock & Katz 2005).

1.5 Diffuse Axonal Injury

Occurring in 40%-50% of all patients hospitalised as a result of TBI (Meythaler et al. 2001), DAI is a common cause of cognitive dysfunction after TBI (Sugiyama et al. 2007). As the name suggests, DAI generally presents in a diffuse and widespread pattern throughout vulnerable regions of the brain, in comparison to localised regions which are seen with focal injuries (Thomas & Dufour 2009). Given that DAI is one of the most devastating consequences following TBI and a common cause of persistent vegetative state and severe disability, it is essential to better understand its pathophysiology and evolution in order to develop targeted treatments and pharmacotherapies to salvage brain tissue and ultimately function for patients (Smith, Meaney & Shull 2003).

1.5.1 Primary Axonal Injury

DAI can occur as a result of both primary and secondary injury mechanisms (Johnson, Stewart & Smith 2013). Primary AI has been well characterised such that it is accepted that DAI results from the shear and tensile forces transmitted throughout the brain as a result of TBI (Gaetz 2004; Povlishock & Katz 2005). White matter axons appear particularly vulnerable to the rapid

mechanical loading conditions within the brain following TBI, which may be a consequence of their high anisotropic arrangement and/or their inherent structural design (Johnson, Stewart & Smith 2013). Under normal circumstances, axons are pliable under stretch and have the ability to relax back to their original length when stretching forces are removed. However, when exposed to rapid tissue strain axons can behave differently. With the sudden force that is applied to the head during TBI, axons become brittle and subsequently disconnect from the rest of the neuron, a process known as 'primary axotomy' (Smith et al. 1999). Although axonal disconnection and subsequent impairments in axonal transport are rare, the swelling of the axonal membrane, or axolemma, known as 'secondary axotomy' is much more commonly observed. Upon initial exposure, the rapid shearing forces cause the axon to retract and expel a ball of axoplasm, forming a swollen retraction bulb, the pathological feature of traumatically induced axonal damage. (Pettus et al. 1994; Povlishock & Katz 2005). This development of axonal swellings has therefore been shown to lead to progressive changes which result in impaired axonal transport (Christman et al. 1994).

1.5.2 Secondary Axonal Injury

Primary axonal swelling has been shown to impair axonal transport, but this only contributes to a small proportion of axons demonstrating impairment as a result of localised swellings. In contrast, the majority of impaired axonal transport is attributable to axons suffering pathophysiological changes that lead to axonal dysfunction (*Fig. 1.3*) (Johnson, Stewart & Smith 2013). Secondary injury mechanisms which may contribute to axonal dysfunction include altered axolemmal permeability, which is thought to be a major contributor to impaired axonal transport. Such altered axolemmal permeability can result in abnormal influxes of extracellular Ca^{2+} ions, which can in turn activate cysteine proteases, calpains and caspases,

and in turn lead to the disruption of the cytoskeleton and therefore axonal structure and function (Buki & Povlishock 2006; Smith, Meaney & Shull 2003).

Furthermore, alterations to mitochondria, including increased mitochondrial permeability, have also been shown to be particularly detrimental to normal energy metabolism, and therefore negatively impact axonal integrity (Okonkwo & Povlishock 1999). Indeed, intrathecal injection of cyclosporin-A prior to impact acceleration TBI in the rat led to preserved mitochondrial integrity which correlated with a reduction of the number of axons undergoing delayed axotomy (Okonkwo & Povlishock 1999). Additionally, oxidative stress and lipid peroxidation have been linked to the pathophysiology of TBI and associated with mitochondrial dysfunction and break down of the cytoskeleton (Mustafa et al. 2010; Mustafa et al. 2011). Finally, neuroinflammation and subsequent microglial activation in white matter tracts have also been shown to contribute to AI (Loane & Byrnes 2010), and shown to persist for years following injury (Johnson et al. 2013). Given that axons are essential for neuronal structural integrity and are key to neuronal function, such pathological axonal changes following trauma contribute to both the acute and chronic side-effects of TBI, such as an immediate loss of consciousness, long-term cognitive and functional deficits such as coma (Davceva, Sivevski & Basheska 2017). Interestingly, despite the fact that experimental studies examining the long-term axonal pathologies seen following TBI are limited, AI/pathology has been shown to peak at 24 hours post-injury (Gultekin & Smith 1994). Although this may represent the peak of AI, axonal pathologies have been shown to persist for weeks or months post-injury, with some reports of AI pathology presenting up to 12 months post-injury, with particular selectivity for degeneration of white matter tracts such as the corpus callosum, corona radiata and striatum and internal capsule (Pierce et al. 1998). This was identified by immunohistochemical (IHC) analysis for the amyloid precursor protein (APP) which accumulates in damaged axons and is used as a marker of AI (Pierce et al. 1998).

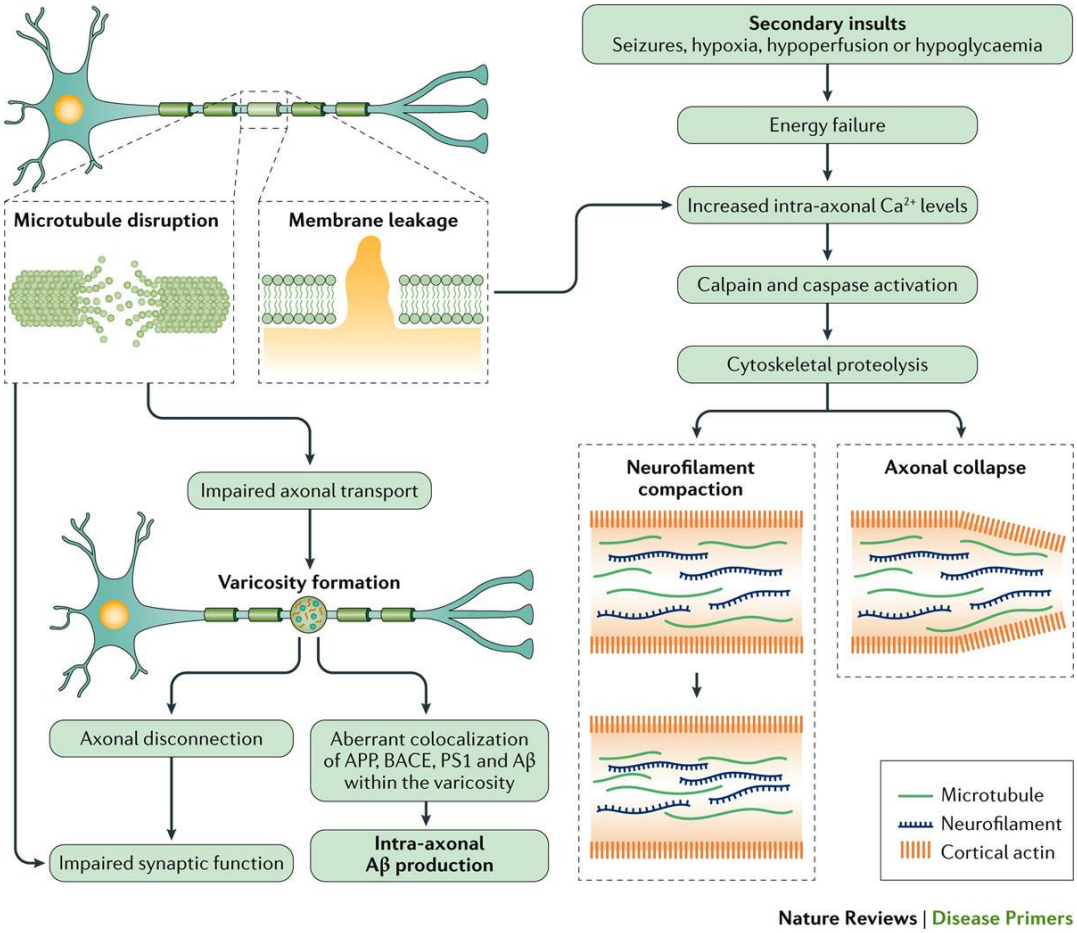

Figure 1.3: Primary and secondary AI pathophysiology following TBI (used with permissions) (Blennow et al. 2016).

1.5.3 Presentation of DAI in TBI Severity

AI is present across spectrum of mild to moderate-severe TBI and increases relative to injury severity (Blumbergs, Jones & North 1989; Davceva, Basheska & Balazic 2015). It is believed that the macroscopic "marker" lesions of DAI are typically in the corpus callosum, however the dorsolateral quadrants of the brain stem are only involved in the brains of those patients with the most severe DAI (Blumbergs, Jones & North 1989). Adams' and colleagues (1989) developed a grading system that highlights the pattern and presentation of DAI in specific brain regions relative to injury severity (*Table. 1.2)* (Adams et al. 1989).

Table 1.2: Classification of DAI, presence of focal lesion and macroscopic injuries individual to TBI severity (Adams et al. 1989).

TBI/DAI Severity	Location of DAI	Presence of Gross Focal Lesions	Macroscopic Injury
Mild	Major white matter tracts (corpus callosum, cerebral cortex, internal capsule)	N/A	N/A
Moderate	Major white matter tracts (corpus callosum, cerebral cortex, internal capsule) & specific grey matter regions (thalamus, hippocampus)	Impact site	Hairline skull fractures Contusions
Severe	Major white matter tracts (corpus callosum, cerebral cortex, internal capsule) & specific grey matter regions (thalamus, hippocampus)	Impact site and brain stem	Severe skull fractures Contusions SDH

A greater understanding of the pathophysiology of AI is required in order to generate new pharmacotherapies and improve patient outcomes. Consequently, the use of clinically relevant and translatable animal models of TBI to provide a means of further understanding the underlying pathologies that result from TBI and therefore trials for potential treatment options is particularly useful and essential.

1.6 Animal Models of TBI

There is a consensus amongst both scientists and clinicians that in order to develop effective treatment options, a greater understanding of the underlying pathophysiology of TBI is crucial. Unfortunately, advances in the field have been slow, due to both patient and injury heterogeneity, which pose major challenges in TBI prevention, diagnosis, and treatment (Vink 2018). Identifying specific mechanisms of injury can be extremely complex in the clinical

setting, largely due to the fact that primary injury in human TBI is executed from multiple different biomechanical influences, such as direct impact to the head, or indirect acceleration/deceleration (Anderson, et al. 2003). Furthermore, the primary mechanical injury initiates secondary injury cascades that are dependent on the mechanism and severity of the primary insult (Finnie, et al. 2001). As such, previous research using a diverse range animal models have greatly enhanced our understanding of the complex primary and secondary pathophysiological cascades seen following TBI. However, interspecies differences in cerebral anatomy, brain size and complexity, are important considerations that may influence experimental outcome and potential translational potential of the findings (Sorby-Adams, Vink & Turner 2018) (*Fig. 1.4*). Rodent TBI models dominate the pre-clinical literature; rodents have small lissencephalic brains, unlike the larger gyrencephalic structure of the human brain (Sorby-Adams, Vink & Turner 2018; Vink 2018).

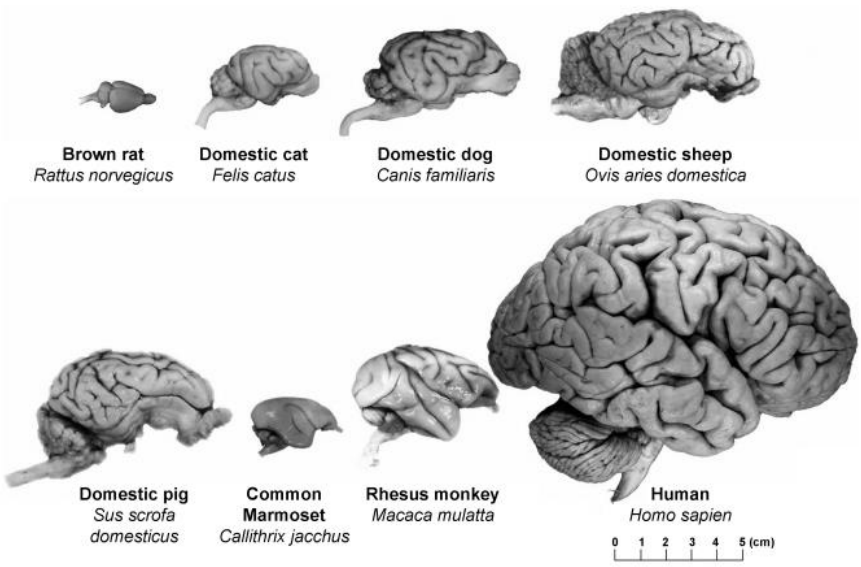

<u>Figure 1.4:</u> Gross comparative neuroanatomy of various large animal species used to model central nervous system (CNS) injury. Note the lissencephalic structure of the brown rat and common marmoset compared with the larger gyrencephalic structure of the dog, pig, sheep and rhesus monkey (used with permissions) (Sorby-Adams, Vink & Turner 2018).

When considering the pathological response to TBI, there are significant differences between lissencephalic and gyrencephalic brains. In particular, the smooth appearance of the lissencephalic brain, due to a lack of gyri and sulci, results in far less tissue deformation upon impact compared to the gyrencephalic brain, given that the gyri influence the movement of the brain within the skull (Finnie, 2001). Humans and non-human primates alike have relatively thick cortices when compared with rodents, containing numerous high velocity neurons which results in the differences seen in enhanced processing capacity (Roth & Dicke 2012). Gyrification and increased surface area also correlate with an increased number of neurons, which has implications for cortical functional organization and development (Cloots et al. 2008). The presence of sulci focuses mechanical stress away from the cortex to the base of the sulci, whereas rodent brains would experience this mechanical stress uniformly across the more superficial layers of the cortex due to the absence of sulci (Cloots et al. 2008; Ho & Kleiven 2009) (*Fig. 1.5*).

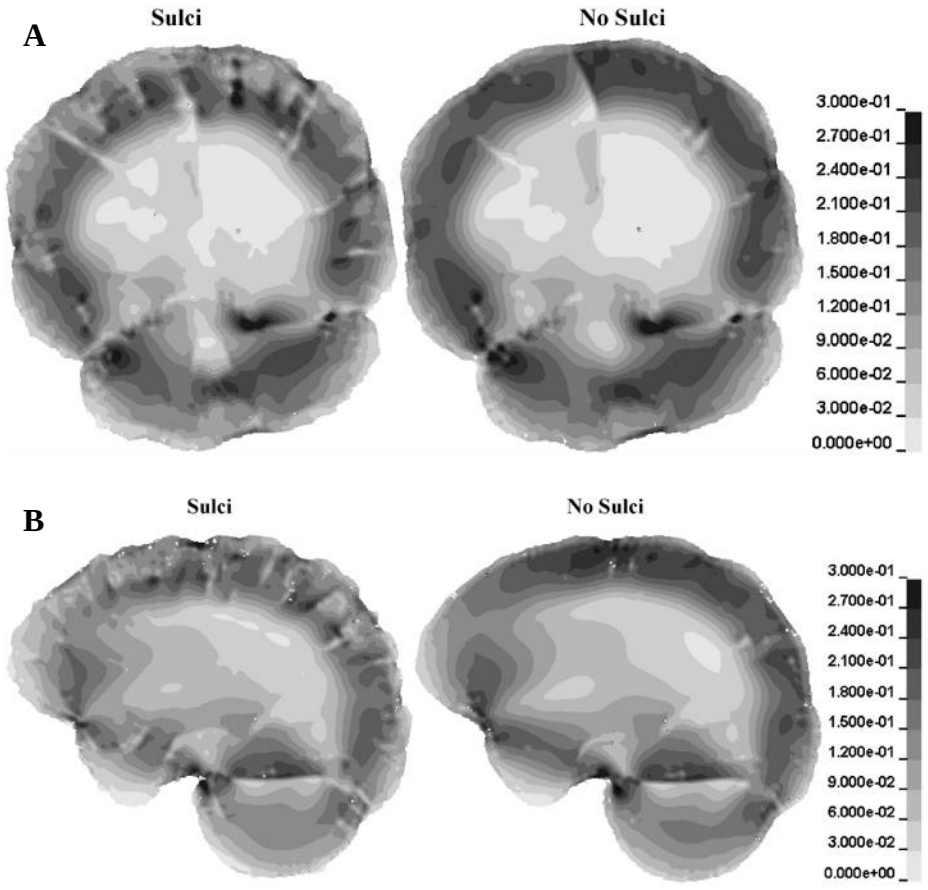

*Figure 1.5: Finite element (FE) model simulation of angular acceleration in the coronal plane (**A**) and the sagittal plane (**B**). Coronal cross-section demonstrating strain distribution in the brain with sulci (left) and without sulci (right). Para-sagittal cross-section demonstrating strain distribution in the brain with sulci (left) and without sulci (right). Strains equal or above 0.3 are indicated as black (Ho & Kleiven 2009).*

As such, the pathological response to rapid acceleration/deceleration in TBI is thought to markedly differ in the lissencephalic brain compared to that seen in the gyrencephalic human brain following TBI. In particular, the distribution of traumatic shear injury and overall pattern of AI seen in the lissencephalic brains following TBI is vastly different to that seen in gyrencephalic brains following TBI, which is the major cause of severe impairment following injury (Su & Bell 2016). As such, choosing an appropriate species to model TBI based on

overall brain size and structure is absolutely vital due to mass regional effects following injury. Additionally, gyrencephalic brains have a higher proportion of sub-cortical white matter to grey matter compared to lissencephalic brains, with white matter distribution correlating with absolute brain weight, such that large animal species generally have a greater brain mass and consequently higher white matter to grey matter ratio (Vink 2018).

Given that DAI is the main cause of severe neurological and neuropsychological impairment following TBI (Buki & Povlishock 2006; Johnson, Stewart & Smith 2013; Smith, Hicks & Povlishock 2013; Smith, Meaney & Shull 2003) and the number of TBI patients presenting with white matter involvement is high, it is therefore critical to select an experimental species of which has a high proportion of white matter in order to effectively model this key clinical feature of injury. Interestingly, grey and white matter have different tissue thresholds to injury (Cai & Wang 2016). White matter, which contains the myelinated axons of neurons, is extremely vulnerable to the effects of ischemia, leading to irreversible AI (Buki & Povlishock 2006). Many neuroprotective agents that have been tested in rodent models have proven to reduce grey matter injury, however when assessed in clinical trials these have proven unsuccessful in reducing the effects of injury, which likely reflects their tissue specificity (Dewar, Yam & McCulloch 1999). Large animals such as porcine, canine, feline and ovine species all have relatively large, gyrencephalic brains, with a high proportion of white matter (Sorby-Adams, Vink & Turner 2018), which gives premise for their use as a translational intermediary between rodent models and clinical TBI studies. As such, various models of TBI have been successfully developed using miniature pigs in the United States (Browne et al. 2011; Chen, et al. 1999; Cullen et al. 2016; Lafrenaye et al. 2020; Lafrenaye et al. 2015; Meaney et al. 1995; O'Donnell et al. 2019; Ross et al. 1994; Smith et al. 2000) to capitalise on these advantages; however, given the lack of availability of these species in Australia, sheep

offer a more prominent option. Indeed, ovine TBI models have been developed and used in Australia for some 20 years (Anderson, et al. 2003; Anderson, 2000; Byard et al. 2009; Byard et al. 2012; Finnie, et al. 1999; Finnie, et al. 2000; Finnie, et al. 2002; Finnie, et al. 2001; Lewis, et al. 1996; Van den Heuvel et al. 1999; Van den Heuvel et al. 1998; Vink, Bahtia & Reilly 2008; Vink, Gabrielian & Thornton 2017).

1.6.1 Ovine Models - Advantages and Disadvantages

Ovine models of TBI offer a number of distinct advantages when modelling the clinical condition compared to rodent TBI models. In Australia and New Zealand, the use of sheep in large animal experiments is common due to high availability but also due to the inability to source other large animals such as miniature pigs. However, anatomically, sheep also have better a brain-to-body ratio than pigs and less developed neck musculature, which facilitates head acceleration and whiplash injury, particularly in immature animals (Finnie, et al. 1999). The large proportion of white matter in the sheep brain is key for modelling TBI and this is essential for studying the evolution of AI. Furthermore, the gyrencephalic structure of the sheep brain enables specialised sub-types of clinical imaging to be used and highlights the similarities to the human brain. Diffusion tensor imaging (DTI) MRI specifically highlights white matter disruption and has been used previously in both rodent and sheep studies (Alahmari et al. 2017; Lee et al. 2015; Mohamed, et al. 2020; Pieri et al. 2019). Of course, there are also disadvantages to using sheep as a model of TBI and these are largely centred on the cost of technical support, infrastructure required to perform experiments and appropriately house and care for the animals. Procedures often require the use of specialist clinical-like surgical and imaging facilities, such as large operating theatres, custom housing facilities, and clinical imaging equipment. Specialised surgical instruments, clinical anaesthetic and monitoring equipment are also required, along with extensive surgical skill and technical expertise to carry out surgical,

monitoring and recovery procedures in large animals. Furthermore, given the relatively long lifespan of the ovine species compared to rodents, chronic investigational studies can take a considerably longer period of time due to the extended timeline required to age animals out to the appropriate age for study.

A crucial element for conducting reproducible large animal TBI experiments is the characterisation of biomechanical parameters, which are directly linked pathological outcomes of TBI. FE models have been a useful tool in characterising the injury mechanics specific to TBI, whilst also predicting patterns of DAI (Hajiaghamemar et al. 2020; Ueno & Melvin 1995). However, given the heterogeneity of TBI pathology, animal models allow a more clinically relevant comparison of the pathological response to TBI that FE models cannot provide. Previous research using non-human primates and pigs have characterised the biomechanics associated with TBI and these have also been linked to specific thresholds for certain pathologies which arise from different injury severities (Adams, Graham & Gennarelli 1981; Atlan, Smith & Margulies 2018; Chen, et al. 1999; Cullen et al. 2016; Gennarelli, Adams & Graham 1981; Lafrenaye et al. 2020; Lafrenaye et al. 2015; Ommaya, Grubb & Naumann 1971; Smith et al. 1997). It should be noted that these studies also use non-impact head acceleration models. Unfortunately, these datasets are rarely reported throughout the literature in sheep models of TBI, which therefore requires pilot studies in order to further characterise injury mechanisms. Finally, as sheep have not been widely used an animal model of disease until a significant increase in recent years, specific anti-sheep antibodies for molecular and IHC applications are scarce. This is further compounded by the limited availability of biochemical and molecular data specific to sheep.

1.6.2 Ovine models of TBI

Sheep have been used for impact acceleration studies of sTBI (Anderson, et al. 2003; Lewis, et al. 1996; Van den Heuvel et al. 1999; Van den Heuvel et al. 1998), with single studies also using fluid percussion (Millen, Glauser & Fairman 1985), penetrating injury (Finnie, JW et al. 2002) and controlled cortical impact (CCI) (Dutschke 2016) models. Ovine impact acceleration TBI is induced with the aid of a humane stunner that is directed at the temporal region of the sheep head (Lewis, et al. 1996), causing rapid angular acceleration of the head away from the impactor. The velocity of the impactor and the resultant injury severity can be altered by varying the explosive charge of the device. Free axial and coronal rotation of the head ensues, due to the head being unrestrained at the time of impact, therefore resulting in DAI (Anderson, et al. 2003). Indeed, the extent of AI has been shown to be significantly correlated with peak ICP which developed in the immediate 10 minute period after TBI, with a subsequent decline to baseline levels within 30 minutes post-injury, suggesting that the severity of injury is reflected in the immediate vascular response to impact. (Anderson, et al. 2003). Finally, brain tissue oxygenation levels have been shown to significantly decrease as ICP increases, supporting an inverse correlation between ICP and brain oxygenation (Vink, Bahtia & Reilly 2008). This particular model of sTBI has been used sporadically throughout the last 20 years by the Neurotrauma Research Group at The University of Adelaide, South Australia. Although this model was used to comprehensively analyse the effects of sTBI on AI, brain oxygenation, ICP and various other factors, this was only evaluated up until four hours post-injury (Lewis, et al. 1996). Indeed, this model has also been used for some biomechanical evaluation of injury dynamics (Anderson, et al. 2003; Anderson 2000). Most importantly, this model has not previously been refined to encompass the entire spectrum of mild, moderate, and sTBI. Furthermore, given that this injury model was only characterised to evaluate sTBI, delivery of brain injury was associated with significant skull fracture and gross macroscopic injuries such

as contusions and SDH. Such features of the sTBI model are not permissive to survival studies which are crucial for investigating the chronic pathophysiological and neurocognitive deficits associated following TBI.

1.7 Synopsis

TBI encompasses a spectrum of disease, ranging from mild to moderate-severe injury. As such, in order to ascertain a comprehensive pathological evaluation of each level of severity, it is important to develop clinically translatable models that encompass the entire spectrum of injury and replicate key features of the clinical injury. Damage to the axonal white matter tracts within the brain is a well-established key cause of neurological impairment and long-term disability following TBI, and this AI presents across the entire TBI spectrum from mild right through to moderate-severe TBI, increasing in an injury-dependent manner. Despite this, a greater understanding of the pathophysiology of AI and the contributing secondary injury mechanisms is required in order to generate targeted and effective therapies to improve patient outcomes.

To date, most pre-clinical TBI studies use lissencephalic species, whose brains respond differently to traumatic shear injury than the gyrencephalic human brain. As a result, it is proposed that the use of large animal models, specifically an ovine TBI model, may provide better translation potential to clinical TBI. Indeed, a pre-clinical ovine model of sTBI has been established and used extensively in our research group, however this model is associated with skull fractures and significant gross macroscopic brain injury meaning that survival studies are not ethically possible or suggested. As such, in order to recover animals following TBI and study outcomes beyond the very acute phase (e.g. four hours), modifications to the model are

required in order to titrate down the level of injury severity and reduce the occurrence of skull fracture, whilst still maintaining extensive microscopic injury (e.g. DAI) throughout the brain.

Further, following sTBI, approximately 55% of patients develop a secondary brain injury in the minutes, hours, days or even weeks after the initial injury, and this is typically due to hypoxia, which is the brain tissue being starved of oxygen post-injury (Dixon, Turner & Christou 2019). TBI studies have shown effective modelling of hypoxia following TBI in rodents; (Arulsamy et al. 2018; Hellewell et al. 2010; Plummer, et al. 2018; Yamamoto et al. 1999) however, this is yet to be modelled in sheep. Importantly, rodent TBI models have demonstrated that PTH exacerbates the development of secondary injury mechanisms, such as neuroinflammation and DAI (Hellewell et al. 2010).

In order to establish a reproducible large animal model of TBI, the complex and crucial biomechanical response to injury must also be characterised, alongside the neuropathological investigations. To achieve this, an anatomical coordinate system (ACS) is required to aid in the accurate description of head acceleration during injury. Accelerations are then calculated through (linear acceleration) or about (angular acceleration) the Centre of Mass (CoM) of the head. The intersection of the anatomical axes defined by the ACS is intended to place the origin point (for acceleration calculation) at or near the CoM of the head, or to define some plane perpendicular to gravity (e.g. the Frankfort plane in primates). Previous work using the sTBI model utilised an ACS defined by surgically visible and readily palpable landmarks on the sheep head, these being the zygomatic notches and bregma. However, this ACS was not dictated by accurate proximity to a known CoM of the sheep head. Consequently, in order to accurately characterise and describe the biomechanics of TBI, the location of the CoM of the sheep head must be ascertained which can therefore be used to define a more anatomically

representative ACS. This would allow the origin to lie in closer proximity to the CoM of the head which will therefore facilitate more accurate calculation of head acceleration in future experiments.

Hypothesis:

Coupling modification of the ovine impact acceleration model of sTBI with extensive biomechanical characterisation of injury will result in the development of a survivable model of moderate TBI in the sheep, with the absence of significant skull fracture.

Aims:

1. Evaluate the effects of altering injury severity on the development of DAI, neuroinflammation, and arterial blood pressure (ABP) response.
2. Evaluate the effects of post-injury hypoxia on the development of DAI, neuroinflammation, myelin microstructure and ABP response.
3. Determine the peak angular and linear accelerations following injury.
4. Determine the location of the CoM of the sheep head.
5. Develop an anatomically representative coordinate system (CS) to the head of the sheep which places the origin in close proximity to the CoM of the head.

CHAPTER 2

Materials and Methods

CHAPTER 2: MATERIALS AND METHODS

2.1 Introduction

Extensive troubleshooting of the methods used in this thesis were undertaken to identify specific injury parameters that would result in the optimal level of AI and therefore represent the spectrum of TBI. This information and data are presented in Chapter 3, along with the improvements made to the method during the troubleshooting process. The final methods, as well as those methods not requiring modification for use in this project, are presented below.

2.2 Animal Care

2.2.1 Ethics

All experimental protocols were approved by the Animal Ethics Committees of the South Australian Health and Medical Research Institute (SAHMRI) (SAM325; SAM396.19) according to guidelines established for the use of large animals in experimental research as outlined by the National Health and Medical Research Council (8th edition, 2013).

2.2.2 Animals

55 Merino Wethers (55-65kgs, 18-24 months) were group housed upon arrival in the conventional sheep pens at the Gilles Plains Large Animal Research and Imaging Facility (LARIF). Each animal was fasted overnight with free access to water in individual pens prior to all procedures requiring anaesthesia, including surgery and imaging. All surgical procedures were non-survival, where animals were maintained under general anaesthesia for the entire duration of the experiments and perfusion procedure.

2.2.3 Anaesthesia

Anaesthetic agents

Isoflurane (Henry Shein, Australia), Ketmaine (Ketamil – Ketamine hydrochloride, Troy Laboratories Australia Pty Ltd.) and Diazepam (Pamlin – Ceva Australia) were stored in a drug safe below 25°C and away from direct heat and sunlight.

Induction of Anaesthesia and Intubation

Anaesthesia was induced with a mix of intravenous ketamine (0.05 mg/kg; Troy Laboratories Australia, Pty Ltd.) and diazepam (0.04 mL/kg; Ceva Australia), administered via the jugular vein, followed by endotracheal intubation (size 8) and mechanical ventilation (Ohmeda 7000 ventilator, Ohmeda Madison, WI, USA) delivering 2-3% isoflurane in a normoxic mix of oxygen (O_2) (30%) and nitrogen (N_2) (70%) at a flow rate of 4 L/min. The tidal volume was calculated using the following equation:

$$\text{Tidal volume (mL)} = \text{Animal Mass (kg)} \times 10 \text{ (mL/kg)}$$

The respiratory parameters were monitored and adjusted so that physiological end-tidal carbon dioxide ($EtCO_2$) levels were maintained between 30-48 millimetres of mercury (mmHg). Animals were then maintained under a mix of isoflurane and ketamine (as outlined below) for the duration of the TBI procedure and post-TBI monitoring period.

Maintenance of General Anaesthesia

Following induction and intubation, the animal was transported to the operating theatre and secured on the operating table, and the level of isoflurane was adjusted to 1.5-2% (in O_2 and

N_2 mixture; $3O_2 : 7N_2$; 4 L/min) in order to reduce its hypotensive properties and maintain physiological blood pressure (BP) within normal limits. To maintain surgical levels of anaesthesia, isoflurane was administered in conjunction with intravenous ketamine at a dose of 2 mL/hour and was administered with compound sodium lactate (Baxter Medical, Australia) via intravenous jugular catheter. This combination regime was based on our experience in previous ovine acute CNS injury studies, as outlined in detail by Wells and colleagues (2012); in order to avoid the intrinsic neuroprotective properties of either above certain doses, whilst maintaining optimal twilight general anaesthesia (Wells et al. 2012).

2.2.4 Insertion of Femoral Arterial Catheter

Previous studies have reported an increase in BP in response to TBI, which is typical across the entire spectrum of TBI (Shiozaki 2005; Trivedi & Coles 2009). As such, in order to capture the BP response to TBI all animals underwent either underwent non-invasive or invasive femoral arterial catheter insertion in order to ascertain an accurate, real time ABP response to injury. Previous research has utilised the invasive catheter insertion method highlighted below (Wells 2014; Wells et al. 2012). However, this method cannot be used in survival studies as it involves permanent occlusion of the distal supply of the femoral artery and therefore impacts blood circulation and delivery to the lower hind limb. Therefore, animals allocated to the pilot study conducted in Chapter 4 underwent percutaneous catheter insertion. This sought to employ a method which would optimise survival of the leg, as a further aim was to eventually transition this model of TBI to encompass survival. However, this method proved insufficient, despite modifications and extensive troubleshooting occlusion of the catheter occurred frequently (as described in *chapter 3.2.3*). Consequently, animals allocated to the study in Chapter 5

underwent the conventional invasive femoral artery catheter insertion procedure.

Non-invasive Catheter Insertion

Following induction of anaesthesia, animals were placed into a supine position to expose the ventromedial aspect of the hind limb. The right femoral artery was located midway between the anterior superior iliac spine and the pubic symphysis, below the inguinal ligament (*Fig. 2.1*). An 18 Fr needle (Cook Medical) was inserted percutaneously under ultrasound guidance (SonixTouch, Ultrasonix) and an intra-arterial catheter (6Fr, Fast-Cath, St Jude Medical) was advanced into the femoral artery with guide wire assistance. A Codman pressure transducer was then attached to a three-way tap (BD connector plus) on the end of the catheter, allowing for continuous, invasive BP monitoring throughout all surgical procedures and the monitoring period, in addition to routine arterial blood sampling for arterial blood gas (ABG) analysis. A 1.0 Vicryl reverse cutting suture (Ethicon, USA) was used to execute a continuous braided stitch in the skin until the catheter was covered and secured into the skin. Following catheter insertion, the groin was packed with sterile drapes to prevent any movement of the catheter during rotation of the animal into the prone sphinx position for TBI induction and monitoring.

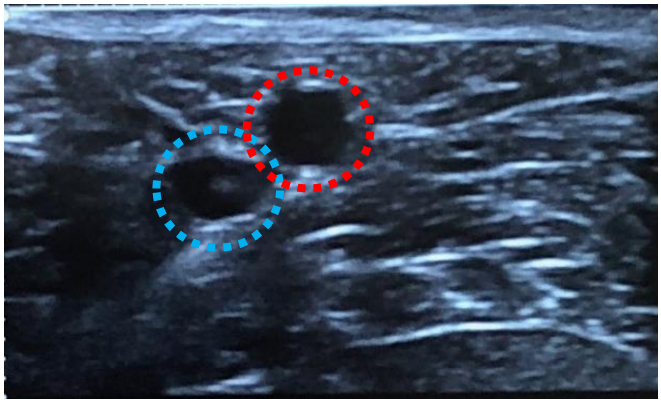

Figure 2.1: Ultrasound image of femoral artery and vein. Image demonstrates the femoral artery (red) and femoral vein (blue).

Invasive Catheter Insertion

Anaesthetised animals were placed in supine position and an incision was made perpendicular to the right femoral triangle. Blunt dissection of the skin and fascia exposed two adjoining muscular layers, which were then carefully retracted using Allis clamps, whilst avoiding two superficial perforating veins (*Fig. 2.2A*). Muscle retraction revealed a cavity of fat and connective tissue concealing the femoral artery, which was superficial and in a clear line of sight. Once the artery was exposed, excess fat and fascia was blunt dissected to clearly expose the artery (*Fig. 2.2B*). In preparation for catheter insertion, any visible arterial branches within the planned insertion site were cauterised, and 3 x 15 cm individual lengths of Dysilk suture (Dynek, Australia) were loosely tied superior, medially, and inferior around the circumference of the artery (*Fig. 2.2C*). A vascular clamp was then placed above the superior suture, whilst the inferior suture was secured and permanently tied off to occlude the passage of blood flow distal to this site. Using surgical scissors, a small incision was made in the femoral artery and the arterial catheter was inserted (12 Fr, Spinal Manometer, Baldwin Medical, Australia). Prior to catheter insertion, the male-taper Luer-slip end was cut off on a bevelled edge and the catheter was primed with sterile saline through a three-way tap attached to the female-taper Luer-Lok. Following insertion, the vascular clamp was then loosened to allow the catheter to be advanced a minimum of 15 cm into the femoral artery; before being re-clamped, the remaining superior and medial sutures were then tied off, followed by an additional three suture lengths around the artery and catheter together to secure the catheter in place within the vessel (*Fig. 2.2D*). The patency of the arterial catheter was immediately checked and then a 1.0 Vicryl reverse cutting suture (Ethicon, USA) was used to execute a continuous braided suture in the skin until the catheter is covered and secured into the skin. The animal was then rotated into the prone sphinx position for induction of TBI and monitoring procedures.

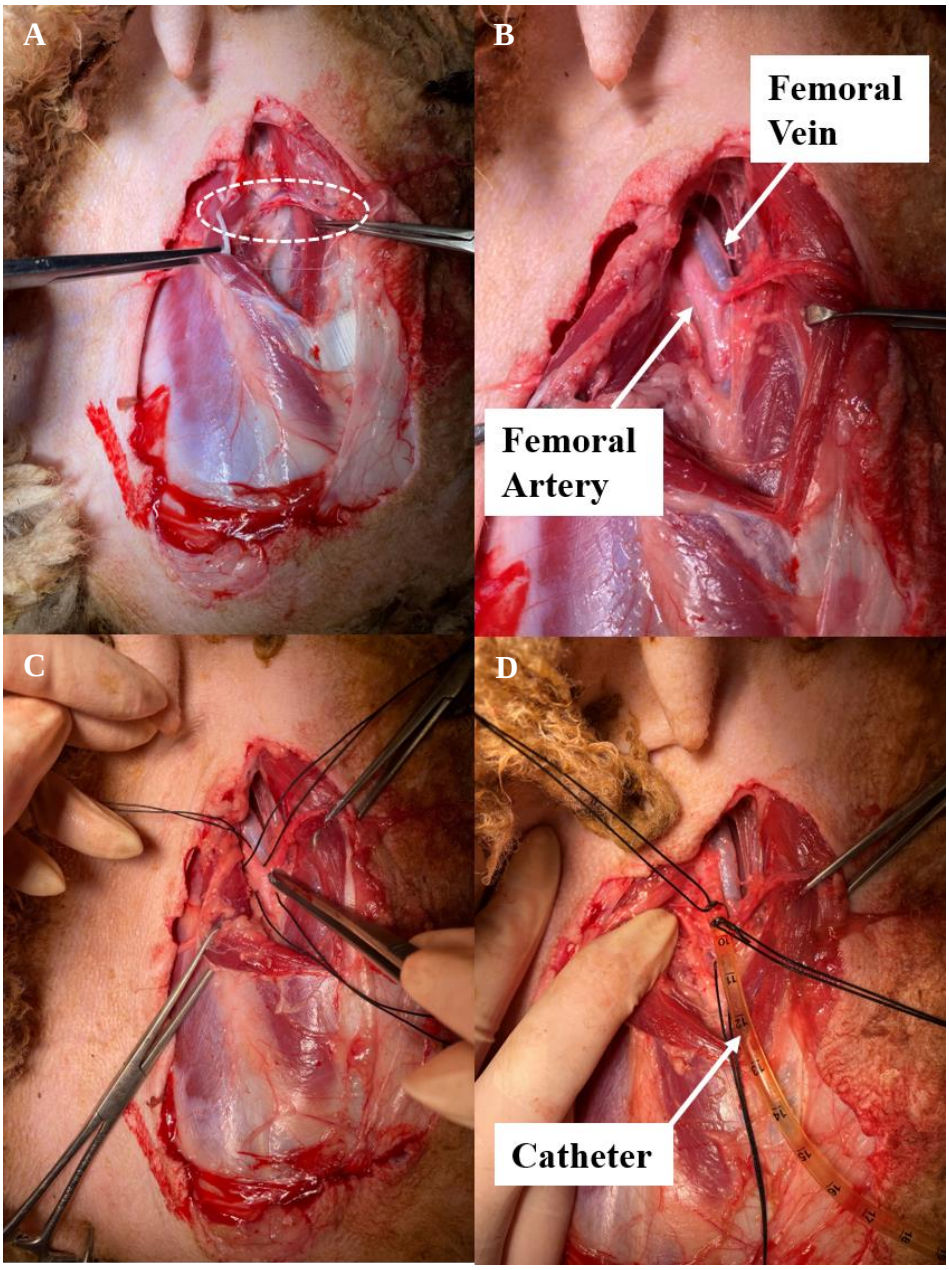

*<u>Figure 2.2:</u> Exposed left femoral triangle, note the perforating veins outlined in white (**A**), exposed femoral artery and vein (**B**), femoral artery and vein isolated with Dysilk (**C**) and invasive catheter inserted into the femoral artery (**D**).*

2.2.5 Cranial surgery and Attachment of Biomechanical Accelerometer Array

With the animals' head supported and held in place by a head frame, a 10 x 10 cm incision was made on the superior surface of the scalp using a monopolar cautery (Covidien/Medtronic, Australia) to expose the skull bone, and clear any adherent muscular and periosteal tissue. A bipolar cautery was used to cauterise large vascular bleeds and the monopolar cautery was run over the bone to ensure all superficial bone bleeding was controlled and minimised. Excess skin flaps were clamped back onto the head with small towel clamps. Acetone was used to clean the bone and dry out the skull surface. 2 x 10 mm burr holes were made 1 cm bilaterally to the midline cranial suture and approximately 25 mm anterior to bregma with an electric bone drill (Medtronic, Australia) and 2 x 14 mm self-taping stainless-steel screws (Bunnings Warehouse, Australia) inserted into the skull with approximately 7 mm prone of the bone surface (*Fig. 2.3A*). Once the screws were inserted into the bone, a 5 cm length of galvanised steel wire was wrapped around the screws in a figure eight pattern (*Fig. 2.3B*). Following this, an 8 cm x 2 cm Polymethyl Methacrylate (PMMA) (Lang Dental, USA: 0834CLR) mantle was moulded over the screws onto the cranial bone in order to create a flattened surface covering the naturally undulating surface of the sheep skull (*Fig. 2.3C*). Initially when mixed, the PMMA was in a putty-like consistency, allowing the mantle to be moulded into shape and anchor to the bone rigidly by forming around screws and wire. The height of the mantle was individual to each animal, depending on the amount of PMMA required to build the mantle into a flat surface on the skull. After the PMMA had cured (~ 20-30 minutes), a stainless-steel adaptor plate was attached to the mantle with 4 x 14 mm cancellous bone screws (CNP4014, Provet, Australia) without the screws penetrating the skull (*Fig 2.3D*). It was important that the screws were inserted prior to complete curation of the PMMA, as once fully cemented, the screws are unable to penetrate the material.

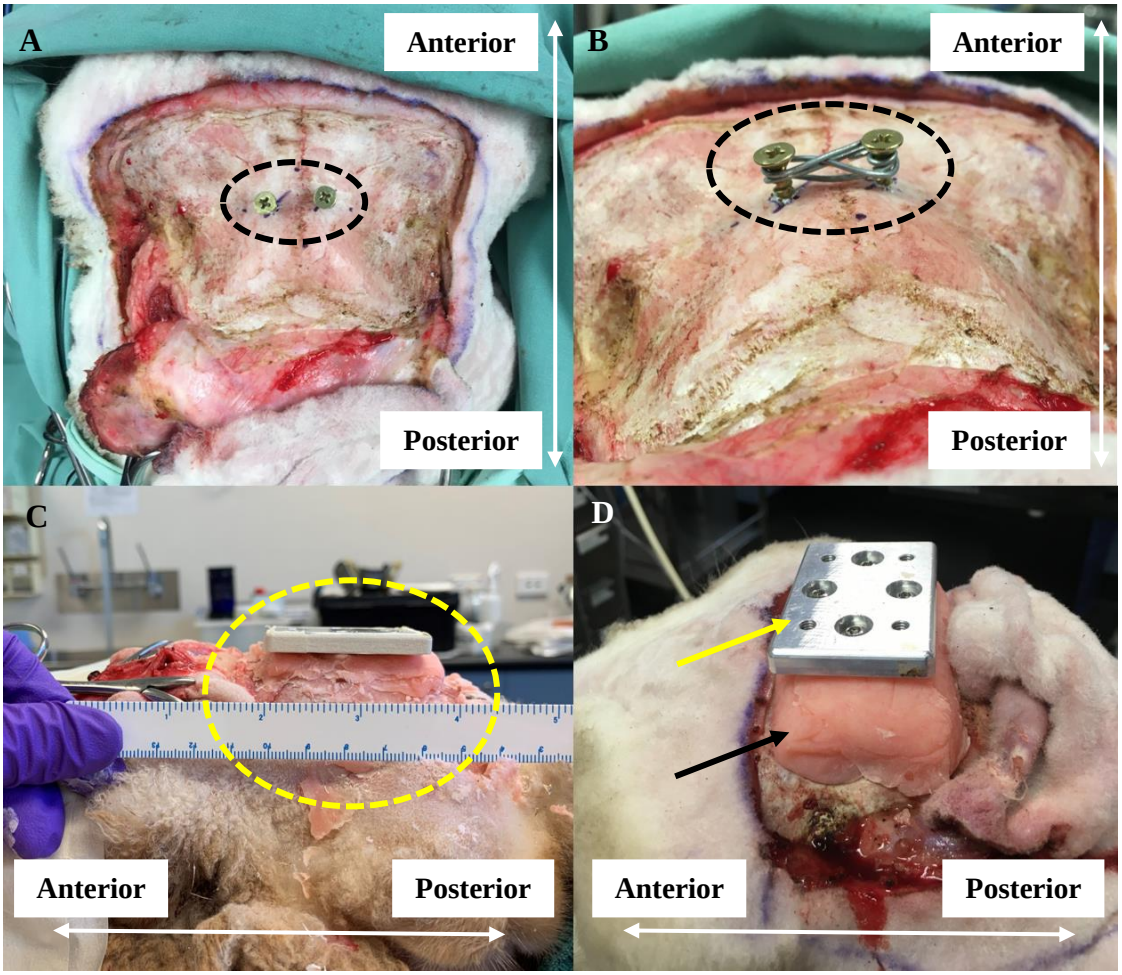

*Figure 2.3: Post-cranial surgery, screws inserted either side of the midline suture - outlined in black (**A**), wire wrapped around the two screws to increase PMMA binding - outlined in black (**B**), PMMA mantle built on the skull - outlined in yellow (**C**) stainless-steel adaptor plate (yellow) screwed into the PMMA mantle (black) (**D**). Bi-directional arrows (white) indicate the location of anterior and posterior surface of the head.*

Accelerometers

A small, lightweight, aluminium fixture incorporating a custom accelerometer array, consisting of four tri-axial accelerometers arranged in a 3-2-2-2 configuration (Endevco Model 35B-2, PCB Piezotronics of North Carolina, Inc.) was attached to the adaptor plate (*Fig. 2.4*). The 3-2-2-2 configuration has been identified as one of the most reliable methods to measure the six-

degree-of-freedom acceleration of a point on a rigid body (Martin et al. 1998). The tri-axial output from each accelerometer was acquired at 50 kHz via custom LabView code using four NI 9232 compact DAQ (cDAQ) modules in a four-slot cDAQ-9174 chassis (National Instruments, Austin, Texas, USA); the outputs from this accelerometer array were used to measure and calculate linear and angular accelerations of the head.

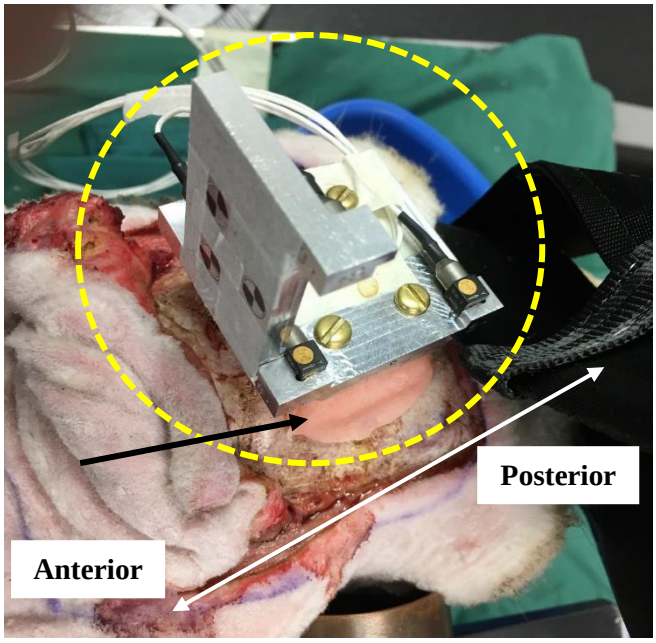

Figure 2.4: Accelerometer array attached to the stainless-steel plate attached to the sheep skull (yellow) via the PMMA mantle (black arrow). Note the location of the bi-directional arrow (white) indicates the location of anterior and posterior surface of the head.

Microscribe and digitisation of anatomical landmarks

To calculate the linear and angular accelerations of the head, the location of the accelerometer array, relative to the animals' head, was determined. Pre-defined location notches on the accelerometer array, and key anatomical landmarks on the head, were digitised using a coordinate measuring device (MicroScribe 3DX, Revware, USA). These anatomical landmarks

were: the left and right notches of the zygomatic processes of the malar bones (*Fig. 2.5A*); and bregma (*Fig. 2.5B*). These landmarks were used to define an ACS of the sheep head, as previously defined by Anderson (Anderson, et al. 2003; Anderson 2000). A transformation matrix was applied to the acceleration data initially captured by the accelerometer array to transform both linear and angular head acceleration data from the array CS to the ACS digitised via the aforementioned anatomical landmarks. The calculation of this transformation matrix is described in detail in the PhD of Dr Robert Anderson (*chapter 3.8.6*) (Anderson, 2000).

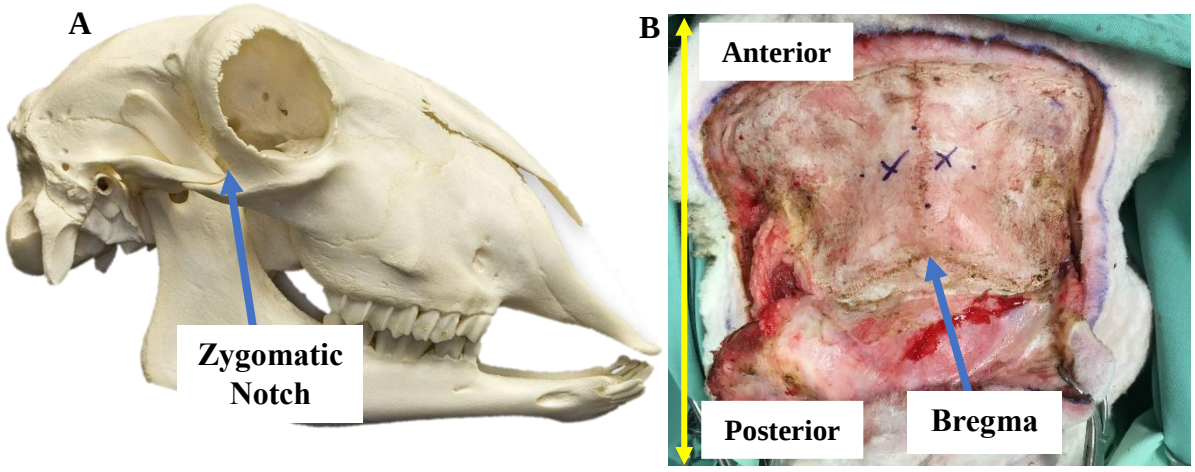

*Figure 2.5: Lateral view of the sheep skull demonstrating the zygomatic notches of the malar bone, note the blue arrow indicating the point of the zygomatic arch (**A**); Superior view of the sheep skull showing the midpoint of bregma (the convergence of sutures joining the left and right parietal bones and frontal bone) indicated by the blue arrow (**B**) Bi-directional arrow (yellow) indicate the location of anterior and posterior surface of the head.*

High-Speed Camera Capture

Stereocalibrated high-speed video footage of the impact event was acquired at 1000 frames per second (1280x512 pixel resolution) using two Olympus i-Speed TR high-speed cameras

(Olympus Corporation, Tokyo, Japan). Images from each camera were distortion-corrected and stereo-calibrated using a checkerboard and a Stereo Camera Calibrator (version, MATLAB, Nattick, MA, USA). The position of three quadrant markers on the accelerometer array, and three quadrant markers on the firing barrel, were tracked with video analysis software (i-SPEED Suite Control Pro v3.1.1.3, iX Cameras, Essex, UK) to determine head kinematics and impact direction, relative to the animals' ACS.

2.2.6 Ovine TBI Model

The ovine impact acceleration head injury device used in this current study was a modified version of the device used initially in the model development by Lewis and colleagues, and has been extensively used in our laboratory (Lewis, et al. 1996; Van den Heuvel, Blumbergs, et al. 2000; Van den Heuvel et al. 1999; Van den Heuvel et al. 1998). However, the device previously used was disposed of and as such, our device required modification in order to more accurately induce the DAI seen in the human condition (as described in *chapters 3.3 & 3.4*).

Following insertion of the femoral artery catheter, cranial surgery and attachment of the accelerometer array, animals were assigned to receive either only sham surgery or undergo induction of TBI using a modified humane captive bolt animal stunner (KL Model, Karl Schermer, Germany) (*Fig. 2.6A*). This device uses a blank gun powder charged cartridge positioned proximally to a captive bolt, that when discharged, propels the bolt in the barrel of the stunning device. The captive bolt weighs 385 g and at its distal end has a flat circular head (4 cm diameter) (*Fig. 2.6B*) which was covered with a custom-made concave silicone tip (*Fig. 2.6C*) (custom printed, RP Prototype Limited, China). To ensure reproducibility, each tip was used for only one injury before being discarded. The barrel velocity depends on the charge rating of the cartridge used. The animals in Chapter 4 that were allocated to receive TBI surgery

were further randomised to receive injury using either an 11, 13 or 15 charge (Karl Schermer, Germany) (n=3/group). The animals assigned to receive TBI in Chapter 5 were injured using a 21-charge. Both sham and TBI animals were further randomised to either undergo a 15 minute period of hypoxia following injury (TBI) or all surgical procedures (sham) or remain on normoxic ventilation (n=3-4/group).

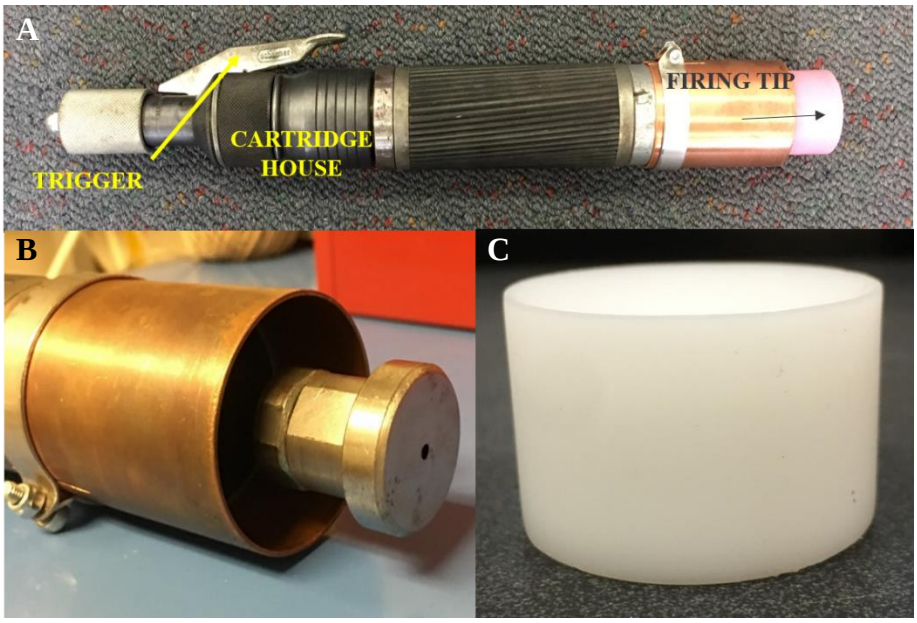

*Figure 2.5: Humane captive bolt animal stun gun (**A**), machined firing pin (**B**) and silicone tip (**C**)*

Surgical Preparation

For the experiments described in Chapter 4, animals were restrained to the table using velcro straps (5 cm width), and the head was supported on sandbags to allow six-degrees-of-freedom of unconstrained motion following impact, leaving the head and neck mobile. The humane animal stunner device was handheld in position at the impact site. In contrast, in Chapter 5 the animal was restrained to the table using velcro straps (5 cm wide), and the head suspended in a cervical sling (Astir, Australia) leaving the head and neck mobile relative to the body. The

humane animal stunner device was secured in a stable tripod that was held down with 80 kg of counterweights.

Induction of TBI

Immediately prior to impact, the animal's endotracheal tube was disconnected from the ventilator, inhalational anaesthesia was discontinued, and intraventricular (IV) fluid lines were disconnected from the jugular catheter. The impactor tip was aligned perpendicular to the skin at the midpoint between the right supraorbital process and the right external auditory meatus (*Fig. 2.6*). Immediately following injury, the ventilator, anaesthesia and IV fluid circuits were reconnected, the animal was stabilised, and any cranial haemorrhage was controlled with sterile gauze packing and pressure, followed by suturing of the wound site using a 1.0 Vicryl reverse cutting suture (Ethicon, USA) if required. Fluids were maintained via continuous infusion with 1000 mL compound sodium lactate via the jugular venous catheter (3 mL/kg/hr – Hartmann's solution, Baxter Health, Australia) to maintain hydration and 1000 mL sodium chloride (30 mL/hr – Baxter Health, Australia) was administered via the arterial catheter to maintain catheter patency. Following induction of TBI or sham surgery, animals were maintained under anaesthesia for four hours before undergoing perfusion.

Figure 2.6: Injury site. Note the outline presented on the skull in black.

2.2.7 Induction of Hypoxia

Immediately following the induction of injury, a sub-set of animals were randomised to undergo a 15 minute period of hypoxia post-TBI. Hypoxia was inducted by adjusting the normoxic gas mixture of 30% O_2 : 70% N_2 down to 10% O_2 : 90% N_2. This produced a drop in peripheral capillary O_2 saturation (SpO_2) levels to between 65% and 70% as monitored via pulse oximetry. O_2 levels were continuously titrated throughout the 15 minute hypoxic period in order to maintain SpO_2 levels within the range. Partial pressure of oxygen (pO_2) levels were confirmed and monitored via ABG samples taken from the femoral artery catheter at 0, 5, 10 and 15 minutes into the hypoxic event. At the end of the 15 minute hypoxic period, the gas mixture was adjusted back to 30% O_2 : 70% N_2 for the remainder of the monitoring period.

2.2.8 Arterial Blood Gas Monitoring

Osmetech OPTI blood gas analyser (CCA, Helena Laboratories, Australia, Pty Ltd) and Osmetech OPTI cassettes were used for routine ABG analysis. Arterial blood samples (0.2 mL) were obtained via the femoral artery catheter using a three-way tap. The key parameters measured were: pO_2, partial pressure of carbon dioxide (pCO_2), pH, base excess (BE), bicarbonate (HCO_3), haemoglobin (Hb), haematocrit (Hct), sodium (Na^+), potassium (K^+) and total (t)CO_2. ABG analyses were conducted at baseline, pre-injury, 30 minutes post-injury, and then hourly until four hours post-injury. Ventilation parameters, including respiratory rate, tidal volume and inspired : expired (I:E) ratio were modified at each blood gas time point, as needed, to maintain pCO_2 within normal limits.

2.2.9 Arterial Blood Pressure Monitoring

Following arterial catheter placement, the animal was placed prone in the sphinx position, a Codman microsensor pressure probe (Codman & Shurtleff Inc., MA) was calibrated and attached to the three-way tap connected to the femoral catheter and further connected to a quad bridge amplifier (Model: FE224, ADInstruments, Australia) and Power Lab system (Model: PL33508, ADInstruments, Australia) for continuous monitoring through LabChart software (v7.2) (Wells 2014). This was used for continual ABP monitoring throughout surgery and the four hour monitoring period following TBI or sham surgery.

2.2.10 Blood and Cerebrospinal Fluid Collection

8 mL peripheral blood samples were collected from the indwelling jugular catheter at the following time points: 0 hour baseline, 30 minutes and four hours post-injury. Blood was collected in a serum separated tube (Product: 367820, BD, Australia), allowed to clot for 30 minutes at room temperature, centrifuged for 15 minutes at 4 °C at 3000 rpm, and the serum harvested and stored in 0.5 mL aliquots at -80 °C until use. Concurrent with blood sample collection (except only 1 x 0 hr baseline sample collected), 2 mL cerebrospinal fluid (CSF) samples were extracted via lumbar puncture using an intrathecal needle at the lumbar region of L3/L4. Samples were immediately centrifuged following collection for 15 minutes at 4 °C at 3000 rpm, supernatant harvested and stored in 0 mL aliquots at -80 °C.

2.2.11 Perfusion and Tissue Collection

At four hours post-injury, animals remained under general anaesthesia and were transported to the post-mortem room and humanely perfused. Specifically, a midline incision was made

overlying the trachea to expose the bilateral common carotid arteries and internal jugular vein. Perfusion was executed by flushing either 10 L of 10% formalin or 5 L of 10% Tris-saline solution under pressure (120-140 mmHg) via catheters inserted and secured bilaterally into the common carotid arteries, with accompanying dissection of the jugular veins to allow outflow of blood. Both carotid arteries were tied off distal to the catheter insertion site to ensure isolated cerebral perfusion. After perfusion was complete, the skull was opened, and the brain was removed. Brains were not weighed in the studies performed in this thesis; however, previous studies using the ovine model of impact acceleration TBI have shown the 2 year old Merino sheep brain to on average weigh approximately 120 g. Following extraction, the brain was segmented into either 1 cm (formalin perfusion) or 0.5 cm thickness sections (Tris-saline perfusion). Collection of both fresh and post-fixed (10% formalin) sections was possible in the Tris-saline perfused animals, with alternating sections being either flash frozen in liquid nitrogen and stored at -80 °C until use, or immersion of samples in 10% formalin solution where they remained for a minimum of two weeks to achieve post-fixation of the tissue.

2.3 Histology and Immunohistochemistry

2.3.1 Tissue Processing

Paraffin embedding and sectioning

All specimens (formalin-fixed or post-fixed) were post-fixed in 10% neutral buffered formalin for a minimum of 14 days before further processing. Processing consisted of 20 minutes in each graded ethanol bath (50%, 70%, 80% and 95% submerged once and 100% submerged twice), followed by two xylene baths for 1.5 hours each and four paraffin baths of increasing time (30, 60, 60 and 90 minutes). Samples were then embedded in paraffin wax. 5 μm thick sections were cut using a microtome (Leica Biosystems, Australia) from 1, 2, 3, 4, 5, 6 and 8

cm anteroposterior segments and subsequently floated onto sodalime coated glass slides (Cat No. XS5176-PLUS - InstrumeC Pty Ltd, Australia). Slides were then dried in a heated oven set at 37 °C for a minimum of 72 hours.

2.3.2 Immunohistochemistry

IHC staining of slides was conducted for distribution and levels of AI, neuroinflammation and myelin integrity (*Table 2.1*). Prepared sections were de-waxed and blocking of endogenous peroxidase activity was conducted with a 30 minute incubation in 0.5% hydrogen peroxide/methanol followed by citrate antigen retrieval. Non-specific binding was then blocked using normal horse serum for one hour prior to overnight incubation with specific primary antibody (*Table 2.1*). Appropriate secondary antibody application (Vector Laboratories 1:250) was applied for 30 minutes followed by streptavidin peroxidase conjugate (Sigma-Aldrich, 1:1000) for one hour. Primary antibody binding was detected via application of 3,3'-Diaminobenzidine (Sigma-Aldrich, D-5637) followed by counterstaining with haematoxylin.

Table 2.1: Panel of IHC markers

Marker	Primary Antibody	Secondary Antibody	Rationale
APP	Mouse-monoclonal, 22C11, 1:150	Horse anti-mouse, Vector Laboratories 1:250	Axonal injury
Ionized calcium binding adaptor molecule 1 (IBA-1)	Rabbit-polyclonal, Wako; 019-19741, 1:1000	Horse anti-rabbit, Vector Laboratories 1:250	Neuroinflammation
Glial fibrillary acidic protein (GFAP)	Rabbit-polyclonal, Dako; Z0334, 1:40,000	Horse anti-rabbit, Vector Laboratories 1:250	Neuroinflammation
Myelin basic protein (MBP)	Mouse-monoclonal, Abcam; ab62631, 1:7,500	Horse anti-mouse, Vector Laboratories 1:250	Microstructure via myelination

2.3.3 Histological Analysis

APP Analysis

Regions of interest (ROI) were determined based on previous literature that highlighted major white matter tracts and specific grey matter regions of the brain where AI is particularly abundant following TBI (Adams et al. 1989; Johnson, Stewart & Smith 2013; McGinn & Povlishock 2015; Su & Bell 2016; Van den Heuvel et al. 1998). Slides were scanned digitally using Nanozoomer technology and viewed using NDP.view2 software (v.U12388-01, Hamamatsu, Japan). Each ROI was outlined, and all clear APP immunoreactive cells were manually counted, and data was presented as total cellular counts per ROI. In Chapter 4, the ROI investigated for APP analysis were: white matter of the pre-frontal cortex, grey matter of

the cerebral cortex, hippocampus, cingulum, internal capsule, reticular thalamic nucleus, medullary lamina, optic tract, corpus callosum, fornix, thalamus, cerebellum, superior colliculus and brainstem (*Fig. 2.7*). The ROIs were refined for analyses in Chapter 5, and the following regions were analysed: grey matter of the cerebral cortex, cingulum, striatum, internal capsule, corpus callosum and thalamus (*Fig. 2.8*).

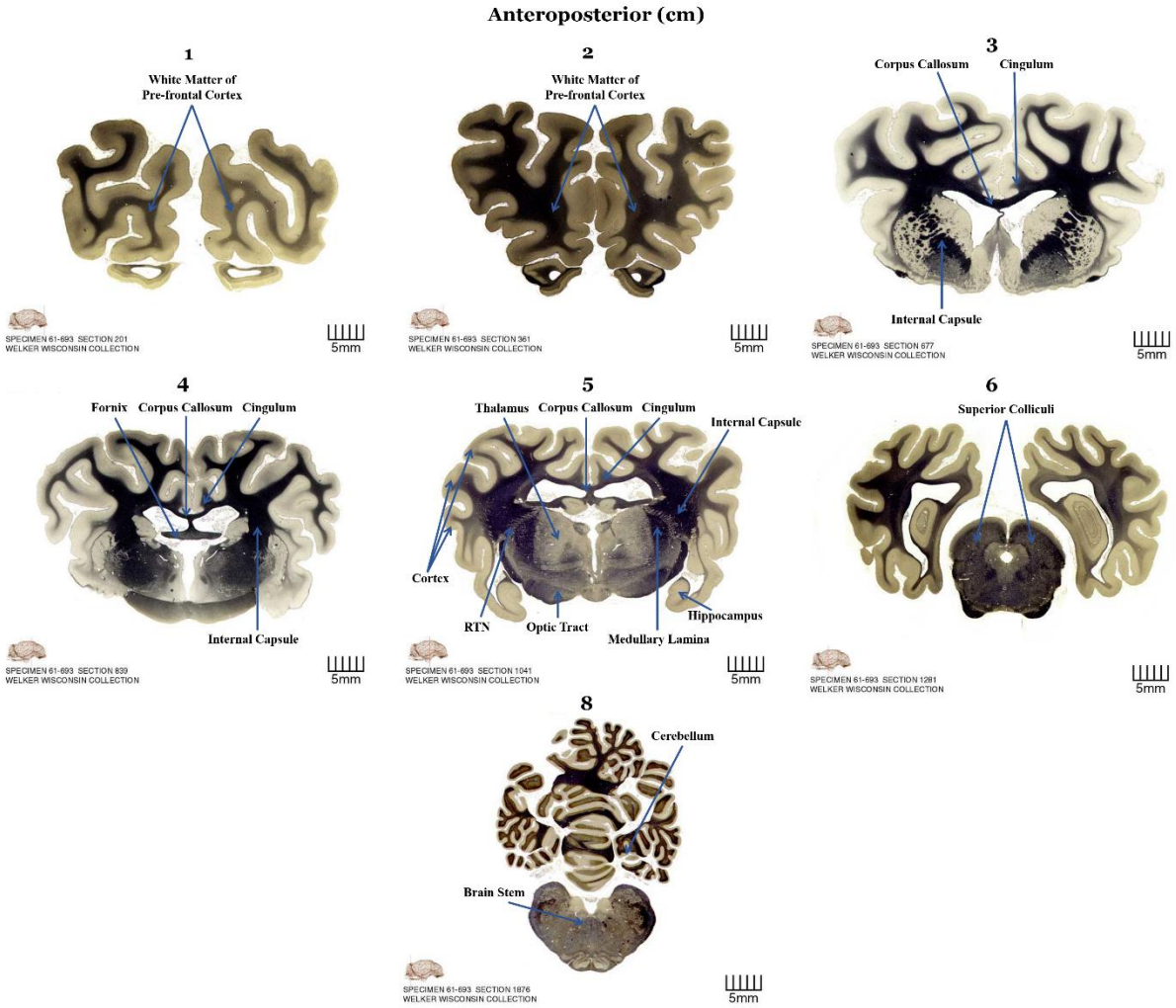

Figure 2.7: 7, 1 cm anteroposterior brain regions outlining ROIs analysed for APP immunoreactivity in each individual level for Chapter 4. Arrows indicate the anatomical location of each ROI. Note the delineation of the grey matter (light stain) and white matter tracts (dark stain).

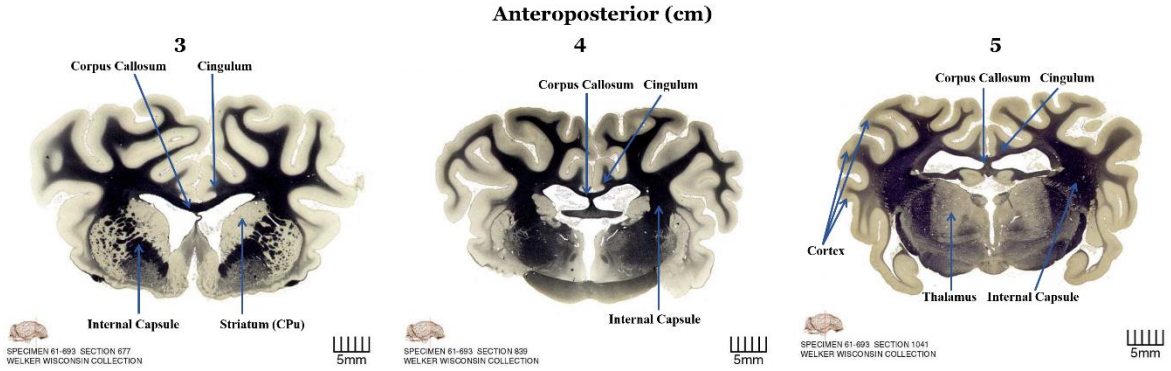

Figure 2.8: 3, 1 cm anteroposterior brain regions outlining ROIs analysed for APP immunoreactivity in each individual level for Chapter 5. Arrows indicate the anatomical location of each ROI. Note the delineation of the grey matter (light stain) and white matter tracts (dark stain).

IBA-1 and GFAP Analysis

Given the paucity of AI throughout the extensive analysis in Chapter 4, a much more targeted ROI analysis was proposed for neuroinflammatory markers. As such, the ROI investigated were as follows:

Chapter 4

Slides were scanned digitally using Zeiss Axio Scanner technology and viewed using Zen Blue software (v2.1 Carl Zeiss, Australia). Various boxes (0.237 mm^2) were randomly placed within the cerebral cortex, hippocampus, cingulum, internal capsule, corpus callosum, fornix and thalamus, within relevant anteroposterior sections and a total of 187 representative images were exported per animal. In ImageJ (v1.5.2), the number of pixels above an automated threshold value was determined and expressed as a percentage of total pixels within the field, with results

expressed as an average value across the sections for each area of interest. Additionally, a manual threshold value was also determined and all immunoreactive cells with clear cell body morphology were automatically counted within that threshold and expressed as cells/mm^2.

Chapter 5

Slides were scanned digitally using Nanozoomer technology and viewed using NDP-view software (v.U12388-01, Hamamatsu, Japan). Various boxes (0.217 mm^2) were randomly placed within the striatum, cerebral cortex, cingulum, internal capsule, corpus callosum and thalamus within relevant anteroposterior sections and a total of 170 representative images were exported per animal. ImageJ (v1.5.2) analysis was performed as per *Chapter 4*.

MBP Analysis

Slides were scanned digitally using Nanozoomer technology and viewed using NDP-view software (v.U12388-01, Hamamatsu, Japan). Various boxes (0.217 mm^2) were randomly placed within the striatum, cerebral cortex, cingulum, internal capsule, corpus callosum and thalamus within relevant anteroposterior sections and a total of 170 representative images were exported per animal. The MBP positive area was determined by setting the manual threshold to include all MBP positive tissue and then measuring the percentage of the field that was positive. Images were analysed via ImageJ software (v1.51w). Coherency of myelinated axons were analysed using the plugin OrientationJ (v2.0.5). Microstructural complexity (fibre length and intersections/kurtosis) was analysed using the plugin DiameterJ (v1.018). Extracted images were initially segmented by removing the background and applying an automated threshold which included all MBP positive staining, prior to measurement with DiameterJ (Mohamed, et al. 2020).

2.4 Enzyme-Linked Immunosorbent Assay (ELISA) Analysis

Biochemical analysis was conducted using the serum of animals subject to TBI (n=3-4/group) and sham (n=3/group). To measure tumour necrosis factor-α (TNF-α) (#MBS778330), interleukin (IL) -1β (#MBS778369) and IL-6 (#MBS778334), samples were loaded onto 96 well plates in duplicate, the assay run accordingly to the manufacturer's instructions and read using a Synergy™ HTX Multi-Mode Microplate Reader. Determination of protein in each sample was run in accordance with the manufacturer's instructions and data was calibrated against standard curves to be expressed as picogram/mL (pg/mL).

2.5 Arterial Blood Pressure Analysis

ABP was analysed using LabChart Reader (v8). Three consecutive pre-injury time points at four second intervals immediately prior to injury were selected to calculate the mean arterial blood pressure (mABP) which was then compared with the mABP post-injury. The maximum change in BP was then calculated from this value. Following injury, once there were five consecutive time points at one minute intervals, this was then used to calculate the time to return to baseline BP. Additionally, a mABP was determined over a 15 minute period following injury, by collecting values from at one minute intervals.

CHAPTER 3

Troubleshooting of Methodology

CHAPTER 3: TROUBLESHOOTING OF METHODOLOGY

3.1 Introduction

In order to optimise the parameters of injury to be as comparable to the human condition as possible, whilst also creating a survivable model of injury which demonstrated the gross pathologies seen in mild-moderate human TBI, various methodologies required extensive troubleshooting and characterisation. It is important to note that smaller cohorts of animals were used throughout these studies. This is due to the significant cost associated with large animal experiments, as well as decisions needing to be made promptly to conduct the desired experiments in Chapters 4 and 5. As such, the purpose of this chapter is to present the methodologies validated within this thesis and explain the rationale for decisions made in the mode development process in order to work towards a more clinically translatable model of TBI.

3.2 Development of a Non-Invasive Approach to Blood Pressure Measurement Using a Percutaneous Arterial Catheter

3.2.1 Rationale

It is abundantly clear that ABP should be monitored as an additional measure of injury severity and further, confirmation of injury in experimental models to validate comparison to the human condition. Transient hypertension followed by sustained hypotension is typical of experimental TBI and has been validated in rodent, porcine and ovine models (Byard et al. 2012; Lewis, et al. 1996; Marmarou et al. 1994; McIntosh et al. 1989; Pfenninger et al. 1989). Indeed, porcine, and ovine models of TBI, report the insertion of an invasive intra-arterial catheter into the femoral artery as described in chapter 2.2.4. However, it is important to note this current method of catheter insertion involves permanent occlusion of the distal branch of the femoral

artery, which does not allow ethical survival of the animal. Therefore, the following aim was addressed:

Develop an alternate method of catheter insertion that was compatible with animal recovery, whilst also allowing for accurate ABP monitoring and ABG sampling during surgical procedures, injury, and monitoring periods.

3.2.2 Methodology

A percutaneous catheter was identified as a more appropriate method to allow patent flow and invasive ABP monitoring within the femoral artery, rather than a direct cut-down approach which results in distal occlusion of the femoral artery.

Initially, percutaneous catheter insertion was trialled on freshly euthanised animals to assess feasibility and plan the more appropriate approach to insertion. Following the initial trials, the percutaneous catheter was then inserted and tested on a series of anaesthetised animals. The percutaneous catheter was inserted non-invasively through the skin and muscle layers of the femoral triangle, into the right femoral artery (*chapter 2.2.4*; *Fig. 3.1A*) under ultrasound guidance. However, following insertion and animal re-positioning prone into the sphinx position for surgery and monitoring, a series of kinks occurred in the catheter within the vessel as a result of the significant pressure within the femoral artery (n=7). Modifications to the internal portion of the catheter were therefore required. In one of these cases the catheter was completely unable to be inserted into the femoral artery due to excessive puncture attempts and resulting haematomas.

As such, a custom-made malleable plastic catheter (Blue Sky Scientific, CA, USA) was designed in order to form to the wall of the artery and prevent kinking. This plastic tubing was designed to fit the percutaneous catheter and form around the head of the catheter once the original internal portion had been removed (*Fig. 3.1B-C*). In order to insert the new tubing

around the head of the catheter, it first required heating to become more pliable to stretch around the opening and then left to cool and set in an air-tight manner.

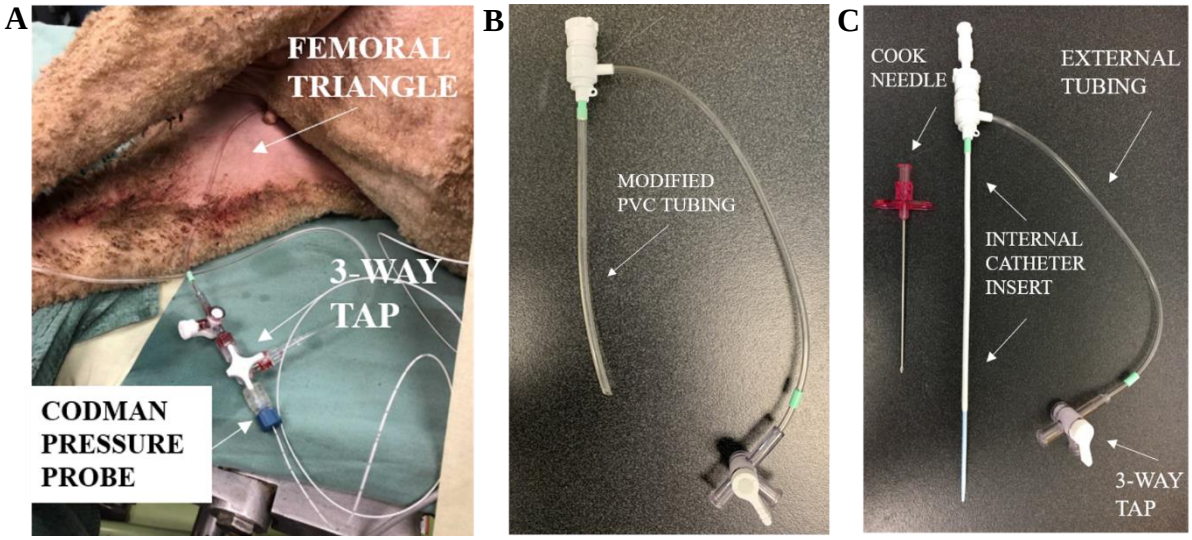

*Figure 3.1: Inserted percutaneous femoral catheter with three-way tap attached (**A**), percutaneous catheter with modified internal PVC tubing (**B**), cook needle and percutaneous catheter with original internal catheter insert (**C**).*

3.2.3 Results and Discussion

This method of catheter insertion was used in 17 animals, including all of those used in experiments described in Chapter 4. Despite insertion of the new catheter being successful, there were various complications which arose. Prior to insertion of the catheter into the vessel, a bevelled edged cook needle was advanced through the skin and muscle into the artery. In order to insert the needle, the femoral artery was visualised under ultrasound guidance, rather than surgically locating the vessel. Insertion of the needle in this manner could lead to multiple unsuccessful attempts to accurately advance the needle into the vessel (n=2) and this did cause major haematomas within the femoral triangle in some animals (n=2).

Following successful vessel puncture and catheter insertion, the catheter was then sutured into the skin to minimise the ability for the internal portion of the catheter to exit the vessel. The standard invasive catheter insertion described in chapter 2.2.4 utilises lengths of Dysilk suture tied around the circumference of the artery to secure the catheter into the vessel and eliminate the risk of the catheter protruding from the vessel (*Fig. 2.2C*). However, this is not possible without dissecting the femoral triangle to locate the artery physically, which would be counterintuitive given the goal of the percutaneous insertion to be as minimally invasive as possible.

As such, given the fluid nature of the modified internal tubing, in some cases this portion of the catheter would coil under the immense pressure within the femoral artery, all whilst remaining sutured into the skin (n=5). In two of these cases the catheter had coiled and protruded from the vessel with only a small portion of the catheter remaining in the vessel (~1-2 cm).

Due to complications arising from percutaneous catheter insertion into the femoral artery, this was deemed inappropriate to proceed with in order to obtain a successful non-invasive ABP trace. Percutaneous insertion of catheters into the auricular artery has been successfully used in both rabbit and pig ears and poses a viable option in place of the femoral artery (Karnabatidis et al. 2006). However, placing a catheter in or around the head of the sheep is not possible given the movement of the head during delivery of TBI and impact would likely cause noise to be present in the ABP trace. As an alternative, a subset of sheep (n=4) were trialled with the insertion of a percutaneous brachial artery catheter in the forelimb, using a 22 G x 25 mm IV cannula (Terumo, Surflo, EU). This brachial artery catheter was inserted in addition to the femoral artery catheter in order to validate comparable tracing values throughout all procedures and monitoring. However, this was only successful in one case, with two animals having the catheter immediately fall out due to the small surface area of the forelimb of the sheep and

large adjoining pressure probe, and in one animal the catheter occluded one hour into the four hour monitoring period.

3.2.4 Conclusions

Despite the percutaneous catheter insertion being uncomplicated in 10/17 animals, it was clear from the results obtained that none of the approaches trialled proved effective in obtaining an acceptable BP trace, compared to our standard cut-down method of invasive catheter insertion. It is important to have reliable tracing of ABP during impact and throughout the entire four hour monitoring period given the injury. As further characterisation in a non-survival model was needed in Chapter 5, the direct and invasive cut-down approach (*chapter 2.2.4*) was used for all experimental animals described in Chapter 5.

3.3 Modification of the Injury Device

3.3.1 Rationale

The previous model of ovine TBI used within our laboratory is classified as sTBI, and the device used to induce impact in this model was a humane animal stunner (MKL model, Karl Schermer, Germany) (*chapter 2.2.6*). This model demonstrated gross macroscopic injuries such as SDH and SAH, contusions, and significant skull fracture in addition to hallmark pathologies such as upregulation of APP and significant increases in ICP (Anderson, et al. 2003; Byard et al. 2009; Byard et al. 2012; Lewis, et al. 1996; Van den Heuvel, Blumbergs, et al. 2000; Van den Heuvel et al. 1999; Van den Heuvel et al. 1998; Vink, Bahtia & Reilly 2008; Vink, Gabrielian & Thornton 2017). It is important to note that in order to allow survival of the animal post-TBI, macroscopic injuries such as skull fracture and significant haemorrhage must be eliminated. Therefore, it was important that specific methodologies were modified in

order to titrate down the severity of injury so we could develop a survivable model of moderate TBI with axonal pathology still present. This was addressed by the following aim:

Evaluate the effects of modifying the original humane animal stunner on the incidence of skull fracture and resulting DAI.

3.3.2 Methodology

The original injury device demonstrates a barrel of 5 cm length and 4.5 cm wide, which allows the captive bolt to extend 5 cm from the barrel normally. It was hypothesised that extending the length of the barrel on the end of the device would increase the length of displacement of the captive bolt from the inner most origin point of the barrel and subsequently decrease the length that the captive bolt would extend from the barrel opening and contact the head. As such, it was further hypothesised that this would reduce the impact velocity of the captive bolt due to friction and air resistance and therefore reduce the kinetic energy of the captive bolt and overall impact force (Campolettano, Gellner & Rowson 2018). Therefore, in order to facilitate this, a brass barrel measuring 7 cm in length and 5 cm wide was affixed to the end of the original barrel of the injury device. By adding this extension, the length of the entire barrel was 8.5 cm and the captive bolt was only able to extend 1.5 cm from the barrel, which theoretically could reduce the acceleration of the head as a result of impact; however, this required biomechanical assessment in order to be confirmed (Campolettano, Gellner & Rowson 2018).

In addition to this, 15 galvanised carbon steel washers [(10: 3 cm wide x 2 mm thick) (5: 3.2 cm wide x 3 mm thick)] were placed around the base of the captive bolt in order to prevent the captive bolt from locking into the base of the barrel. In addition to preventing the lock mechanism of the device, adding these washers only allowed the captive bolt to retract 4 cm into the barrel instead of the standard/original 7.5 cm. It was hypothesised that this could reduce

the acceleration of the captive bolt thereby reducing the impact velocity and force transmitted to the head and consequently the resulting accelerations of the head (Campolettano, Gellner & Rowson 2018).

3.3.3 Results and Discussion

Animals (n=15) were subject to TBI during the optimisation of this device modification, a subset of animals (n=6) received TBI with the device including the extended barrel and the washers around the captive bolt of the device (*modified*), and another subset of animals (n=9) were subject to injury with the barrel extension on the injury device, however without the washers around the captive bolt (*standard*).

Incidence of skull fracture:

Of the nine animals injured with the *standard* device, five of these sustained skull fractures, whilst none of the six animals injured with the *modified* device demonstrated skull fracture (*Table 3.1).* The rationale for skull fracture occurrence in animals injured with the *standard* device is discussed in chapter 3.4.3.

Table 3.1: Incidence of skull fracture when subjected to TBI at with either the standard or modified injury device. Note the incidence of skull fracture in animals injured with the standard device but lack of skull fracture in animals subject to injury with the modified device.

Device	Incidence of Skull Fracture (%)
Standard	5/9 (55.5%)
Modified	0/6 (0%)

DAI

AI was analysed as described in chapter 2.3.3, at the anteroposterior level of injury within the brain (5 cm). AI was quantified within the cerebral cortex, cingulum, internal capsule, reticular thalamic nucleus, medullary lamina, optic tract, corpus callosum, and thalamus (*Table 3.2*). Regional analyses found significantly higher levels of AI within the right reticular thalamic nucleus compared to the left in both injury groups ($p=0.02$). However, further analyses found no significant differences between either injury group.

3.3.4 Conclusions

The resulting AI of animals injured with the *modified* device including the washers around the captive bolt was not significantly different from animals injured with the *standard* device (without the washers around the captive bolt), therefore these 6 animals were not included in results presented in Chapter 4. Indeed, there was a lack of skull fracture in those animals injured with the *modified* device, however given the lack of significant difference in APP it is clear that neither of these were able to produce a significant enough pathological injury. It is hypothesised that the lack of skull fracture occurring in animals injured with the *modified* device is due to a lack of impact force compared to those injured with the use of the *standard* device. However, in order to confirm this, it is critical to biomechanically evaluate the difference in impact force. The use of washers was then excluded from future experiments described in Chapter 5.

*Table 3.2: Total counts for APP+ve cells within specific brain regions. All animals were sustained impact to the right hemisphere. Data are presented as Mean ± standard deviation (SD). Note the significant difference between the left and right hemispheres in both injury groups, within the reticular thalamic nucleus (L&R hemisphere *p=0.02). * = significance.*

Region	Modified Device (n=6)		Standard Device (n=9)	
	L hem	*R hem*	*L hem*	*R hem*
Cerebral Cortex *Injury: p=0.69* *Hemisphere: p=0.70*	1.6 ± 1.8	1.8 ± 1.3	3.1 ± 6.9	1.6 ± 2.3
Corpus Callosum *Injury: p=0.90*	8.8 ± 8.6		8.2 ± 9.9	
Cingulum *Injury: p=0.19* *Hemisphere: p=0.45*	1.2 ± 2.0	5 ± 4.9	6.2 ± 5.1	5.5 ± 7.0
Internal Capsule *Injury: p=0.82* *Hemisphere: p=0.47*	48.2 ± 35.9	68 ± 43.1	41.5 ± 48.9	73.5 ± 87.1
Hippocampus *Injury: p=0.18*	15.5 ± 10.7		26.5 ± 22.7	
Reticular Thalamic Nucleus *Injury: p=0.17* *Hemisphere: ***p=0.02***	313.7 ± 75.7	423.3 ± 92.3	352.2 ± 205.2	580 ± 231.7
Medullary Laminae *Injury: p=0.06* *Hemisphere: p=0.35*	26.5 ± 22.7	48 ± 20.3	59.7 ± 43.6	71.8 ± 15.0
Optic Tract *Injury: p=0.09* *Hemisphere: p=0.95*	3 ± 5.1	1.4 ± 3.1	22.5 ± 43.1	25.7 ± 34.6
Thalamus *Injury: p=0.76* *Hemisphere: p=0.46*	378 ± 228.8	392 ± 215.8	503.8 ± 263.2	331.8 ± 193.9

3.4 Development of the Captive Bolt and Silicone Tip

3.4.1 Rationale

Further to chapter 3.3, the injury device used in previous ovine models of TBI demonstrates a heavy, non-penetrating mushroom-shaped bolt head attached to the end of the captive bolt (*Fig.*

3.2). Upon the induction of injury, this particular captive bolt produces significant macroscopic injury, soft tissue trauma and skull fracture, which as aforementioned is an undesirable outcome when developing a survivable model of TBI.

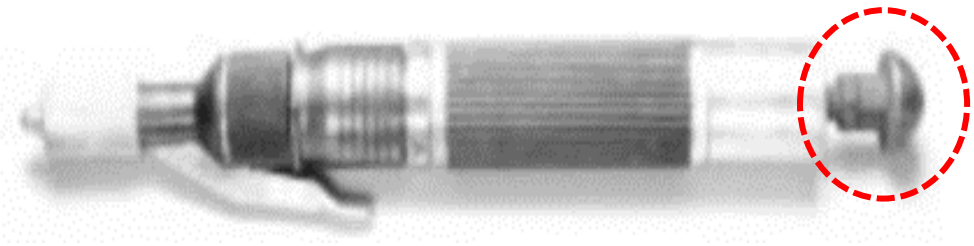

Figure 3.2: Standard Karl Schermer MKL captive bolt humane stunner. Note the mushroom shaped tip (red) on the end of the captive bolt. (Finnie, et al. 2000).

Although the methods described above are effective in avoiding skull fracture whilst still producing significant DAI, it is important to note that the ovine model of impact acceleration TBI is induced temporally rather than superiorly as in the rodent DAI model. Therefore, modifications to the captive bolt were required in order to distribute the impact force more effectively across the skull in order to reduce the risk of external collateral trauma. Additionally, in previous work the injury device had also been angled superiorly at the site of injury in order to promote rotation of the head and increased angular acceleration upon injury, which is the most prominent biomechanical cause of DAI (Cullen et al. 2016; Kleiven 2013; Ommaya, Goldsmith & Thibault 2002; Van den Heuvel et al. 1999).

This was therefore addressed with the following aims:

1: *Evaluate the effects of a convex or concave protective silicone cover over the captive bolt on reducing skull fracture.*

2: *Evaluate the effects of angling the injury device at the impact site.*

3.4.2 Methodology

In addition to the 15 animals discussed in chapter 3.3, an extra five animals were included for the troubleshooting of methods as outlined below. As a result, a total of 21 animals were subject to injury with the various modifications as outlined in chapters 3.3 and 3.4 (*Table 3.3*). Further modifications to the current injury device included modifying the face of the captive bolt tip to be flat (*Fig. 3.3A*) rather than domed or mushroom shaped, in order to implement the use of two silicone covers for the captive bolt tip: concave (*Fig. 3.3B*) and convex (*Fig. 3.3C*). These silicone tips were designed based on the work of Anderson (2000), where a polyurethane tip was developed and used to cover the captive bolt (Anderson, 2000). However, the use of this polyurethane tip caused severe fractures due to the sharp edges of the tip circumference, therefore silicone was chosen the material to cast the tips used in this thesis (Anderson, 2000). The silicone tip was intended to reduce the rate of onset of the force and absorb some of the impact force, whilst avoiding the collateral tissue injury seen with the polyurethane tip. Additionally, a subset of animals were exposed to injury with the device in various angled positions at the site of injury to assess which was most appropriate to proceed with for the larger study.

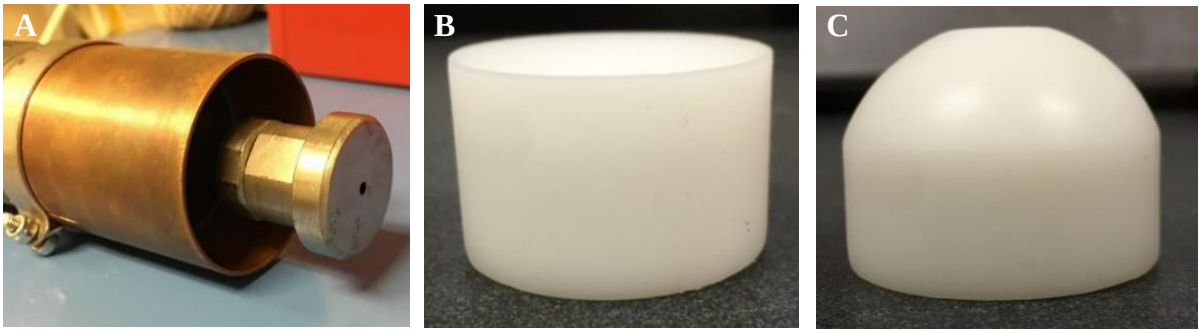

*Figure 3.3: Machined captive bolt tip (**A**), concave silicone cover (**B**) and convex silicone cover (**C**).*

*Table 3.3: Animals subject to TBI with either the concave or convex silicone tip and resulting complications. Direction of injury: P= perpendicular, **p**= posterior angle, **s**= superior angle. +/ - = presence or absence of tip complications, and macroscopic injuries. += zygomatic OR coronoid fracture, ++= zygomatic AND coronoid fracture, +++= zygomatic, coronoid, and orbital rim fracture. Complications are described in more detail in chapter 3.4.3 below.*

Animal	Modified (+) or Standard (-) Device and Charge	Direction of Injury	Tip Complications (+/-)	Skull Fracture (+/-)	Macroscopic Injury (+/-)
Concave Silicone Tip (n=15)					
CONC002	13+	P	-	-	-
CONC003	13+	P	-	-	-
CONC004	13+	P	-	-	-
mTBI001	15+	P	-	-	-
mTBI002	15+	P	-	-	-
mTBI003	15+	P	-	-	-
CONC005	11-	**s**	+	++	-
CONC007	11-	**s**	+	+	-
CONC008	11-	P	+	-	-
mTBI004	13-	**p**	-	-	-
mTBI005	13-	P	-	-	-
mTBI006	13-	P	+	-	-
mTBI007	15-	P	+	+	-
mTBI008	15-	P	+	+	-
mTBI009	15-	P	+	+	-
%			**n= 7/15 (47%)**	**n= 5/15 (33%)**	**n= 0/15 (0%)**
Concave Silicone Tip (n=6)					
mTBI010	15-	P	+	+++	+
mTBI011	11-	**s**	-	-	-
mTBI012	11-	P	+	-	-
mTBI013	11-	P	-	-	+
mTBI014	11-	P	-	-	-
mTBI015	13-	P	-	+	-
%			**n= 2/6 (33%)**	**n= 2/6 (33%)**	**n= 2/6 (33%)**

3.4.3 Results and Discussion

Although the silicone cover was intended to reduce the incidence of skull fracture, many issues with this tip material were encountered throughout the troubleshooting period. Additionally, angling of the injury device with either of the silicone covers also saw many complications.

Concave Silicone Tip

Tip Complications

The trial of the concave silicone cover was implemented in the injury of 15/21 animals in total, encompassing experiments described in Chapter 4. Complications were observed in 7/15 cases of using the concave silicone tip, and all of these were seen in animals injured with the *standard* device (*Table 3.3)*. The centre of the concave silicone cover was split upon impact in a total of 3/15 cases (*Table 3.3; Fig. 3.4*). This is thought to have occurred as the centre of the silicone cover is where the tip is at its thinnest point and therefore would have less strength to absorb the impact force. In 1/15 cases the silicone cover was caught in the barrel upon firing and was unable to make effective contact with the head and 1/15 in another case completely separated from the captive bolt upon impact (*Table 3.3)*.

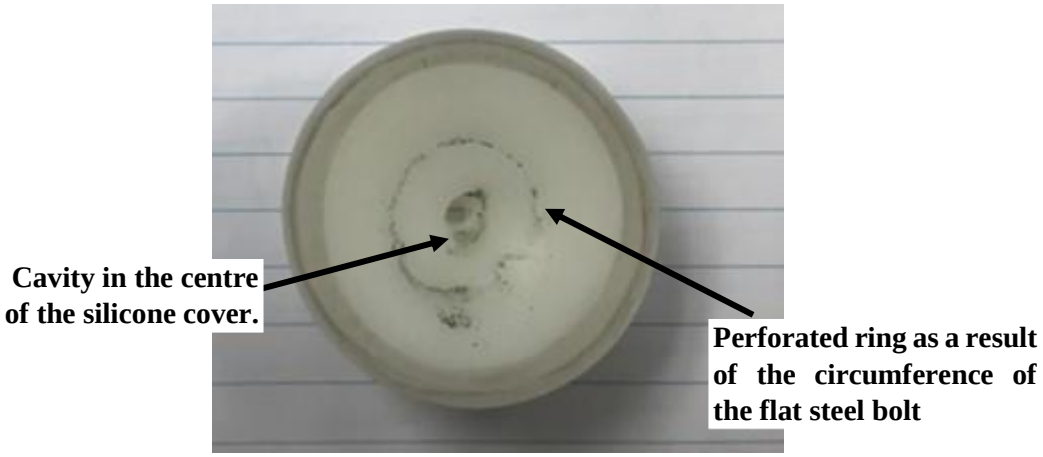

<u>Figure 3.4:</u> Broken concave silicone tip cover. Note the black arrows indicating the cavity in the centre of the tip and the perforated ring surrounding the cavity.

Angling of Impact Direction

3/15 animals (all included in Chapter 4) were subject to angling the injury device against the impact site. In two cases where animals were injured with the 11-charge, the device was angled superiorly, and this resulted in significant soft tissue damage and skull fracture (*Table 3.3 & Fig. 3.5A-B*). One animal subject to injury with a higher charge (13) with the device angled posteriorly at the impact site, resulted in no head movement, nor skull fracture or macroscopic injury following firing of the injury device (*Table 3.3)*. The remaining 12 animals were all subject to injury perpendicular to the impact site. Of these animals, 3/15 sustained skull fracture, however no macroscopic injury was seen (*Table 3.3)*. It is hypothesised that skull fracture in these animals was resultant from injury with the 15-charge, and therefore an increase in impact force compared to other injured animals. However, this would need biomechanical clarification in order to be confirmed.

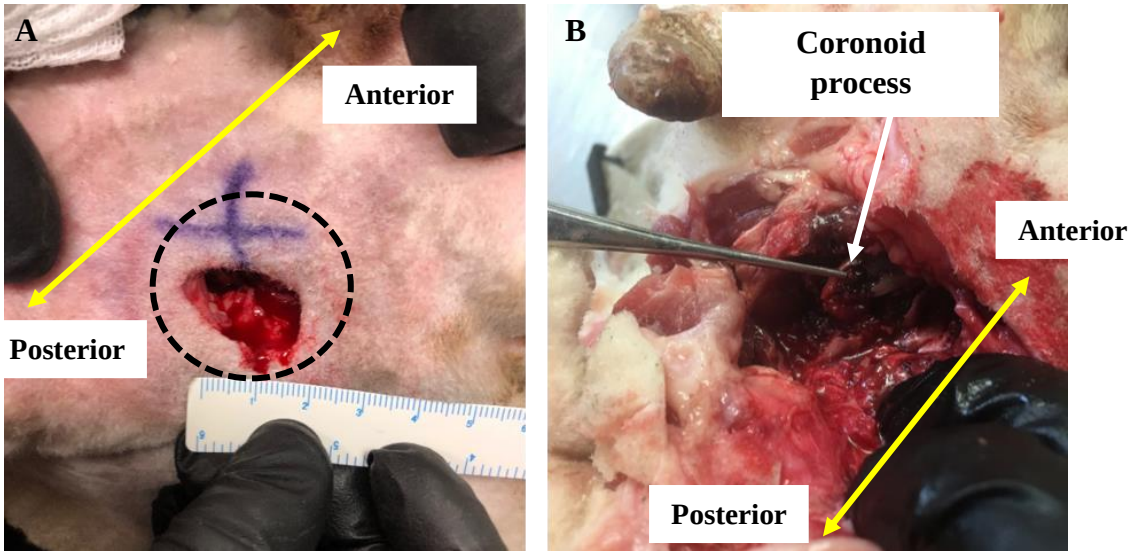

*Figure 3.5: Soft tissue cavity in animal injured with the device angled superiorly (**A**), note the 2cm diameter of the cavity (outlined in black). Skull fracture: note the separation of the top of the coronoid process from the surface of the skull (**B**). Bi-directional arrow (yellow) indicate the location of anterior and posterior surface of the head.*

Convex Silicone Tip

Tip Complications

6/21 animals (not presented in this thesis) were injured with the use of the convex silicone cover on the end of the captive bolt. Whilst complications were only present in 1/6 animals, use of the convex silicone tip resulted in significant skull fracture and macroscopic injuries across these animals.

Angling of Impact Direction

1/6 animals were subject to angling of the impact device superiorly with use of the 11-charge. This angling of the injury device resulted in no movement of the head and no macroscopic injuries so as a result, angling of the device was not pursued further in the remaining 5/6 animals. Soft tissue damage, skull fracture, and contusions were present across within two animals injured perpendicular to the impact site. One animal was injured with the 15-charge with the device perpendicular to the temporal fossa which resulted in significant haemorrhage, soft tissue injury and fracture at the coronoid process and zygomatic arch (*Fig. 3.6A-B*). This injury also resulted in bleeding at the brain stem upon post-mortem examination (*Fig. 3.6C*).

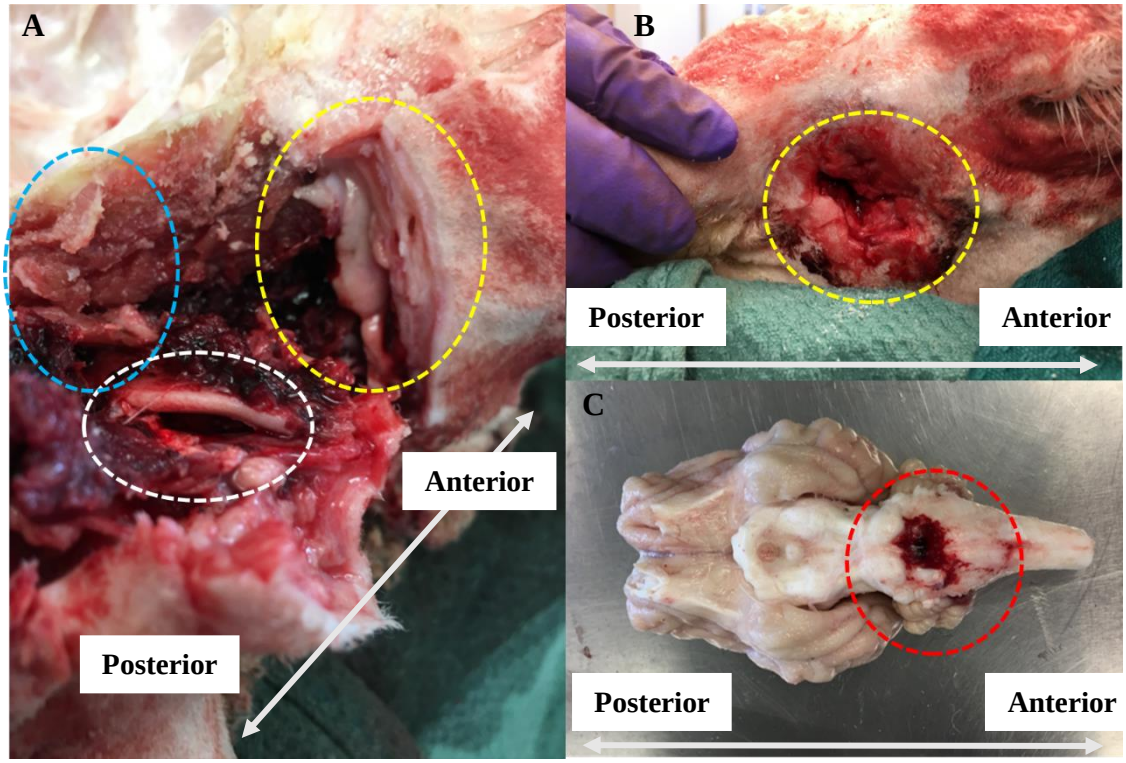

*<u>Figure 3.6:</u> Birds eye (superior) view of right sided zygomatic fracture and separation of the coronoid process (blue), note the separation of the zygomatic arch (white) from the top of the coronoid attached at the skull (yellow) (**B**) soft tissue damage at the impact site, note the cavity outline (yellow) (**B**); and bleed at the base of the brain stem (ventral view) (red) (**C**) seen at post-mortem. Bi-directional arrow (grey) indicate the location of anterior and posterior surface of the head.*

One animal was injured with the 13-charge with the device perpendicular to the impact site. Post-mortem examination revealed a zygomatic arch fracture, however as a result of unsuccessful perfusion the brain examination of macroscopic injuries was difficult. The remaining animals (n=3) were subject to injury with the 11-charge. Of these remaining three animals, in one case the tip came off upon impact (*Fig. 3.7A*), one animal suffered mild subarachnoid bleeding (*Fig. 3.7B*) and bleeding at the brain stem (*Fig. 3.7C*) and one animal sustained no skull fracture or macroscopic injuries.

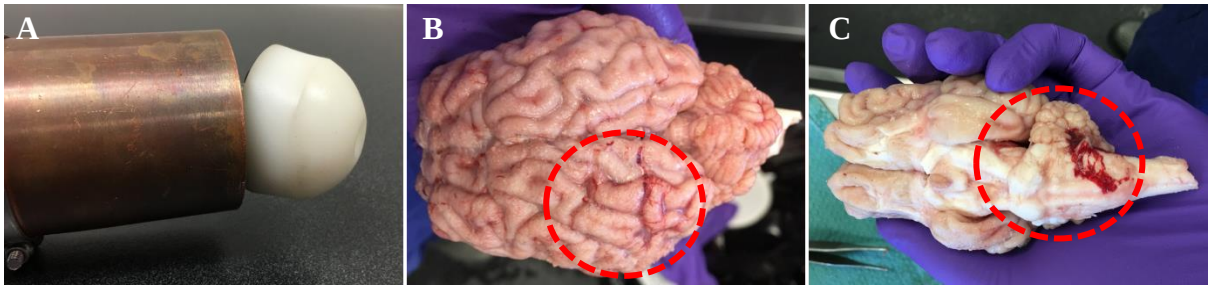

*Figure 3.7: Convex silicone tip peeling off the captive bolt following firing of the injury device (**A**), mild subarachnoid bleeding (red) seen at post-mortem (**B**), bleeding over the brainstem and cerebellum (red) seen at post-mortem (**C**).*

3.4.4 Conclusions

Angling of the injury device in conjunction with the concave silicone cover resulted in skull fracture, whereas angling of the device using the convex silicone cover did not produce movement of the head following firing of the injury device. Additionally, angling of the device did not appear to change the appearance of head motion in animals injured with the concave silicone tip, however biomechanical analyses are required in order to confirm this. As such, angling of the device was not performed in any of the experiments described in Chapter 5, with injury induced with the device perpendicular to the impact site. Furthermore, considering the significant skull fracture and macroscopic injuries demonstrated in animals injured with the convex silicone cover, this tip cover type was not used in any further experiments.

3.5 Development of PMMA Mount

3.5.1 Rationale

Much of the pathology that develops and the severity of neurological outcomes following TBI are dependent on the biomechanics of the brain injury (Ommaya, Goldsmith & Thibault 2002). Biomechanical analyses in the sheep TBI model are presented in Chapter 5, and this was executed with the use of an accelerometer array attached to the skull of the animal (*chapter 2.2.5*). However, in order to accurately measure the accelerations of injury, this accelerometer plate required orientation in a flat plane perpendicular to gravity, which is not achievable via direct attachment to the undulating surface of the sheep skull (Anderson, et al. 2003; Anderson, 2000). Therefore, a buffer between the skull of the sheep and the accelerometer array was required in order to rigidly attach the array to the skull of the animal and ensure uniform motion of the head and the accelerometers. This was addressed via the following aim:

Develop an intermediary flat plane mantle on the skull of the sheep in order to allow effect attachment of an accelerometer array

3.5.2 Methodology

Previous experimental models have implemented the use of dental acrylic (PMMA) to securely attach devices to the head of animals in TBI models, even in rodents using the Marmarou model, where the protective helmet is adhered to the skull with dental acrylic (Marmarou et al. 1994). PMMA forms into a hard bone-like consistency, often used for bone grafting, and has been safely used in previous studies in our laboratory on the skulls of sheep following neurological injury (Wells et al. 2012). Therefore, a PMMA mantle was moulded to the skull of the sheep as outlined in chapter 2.2.5, however various troubleshooting and method refinement was required. It was important to consider that the open wound on the head of the

sheep would remain exposed throughout the course of surgery, injury, and monitoring procedures, which can range anywhere from six - eight hours. Therefore, PMMA that provided antibiotic properties to minimise risk of infection was desirable. As such, PMMA enriched with gentamycin (*chapter 2.2.5*), was used in all troubleshooting experiments and in all experiments presented in Chapter 5.

3.5.3 Results and Discussion

The PMMA mantle was trialled on a subset of deceased, decapitated scavenged sheep heads, in order to ascertain a flat surface of the mantle in the appropriate anatomical location. The exposure of bregma was necessary in order to acquire the appropriate biomechanical digitisation of the ACS required for calculation of impact accelerations. Therefore, an 8 cm^2 PMMA mantle was built proximal to bregma and adhered to the surface of the skull (*Fig. 3.8A*). The size of the mantle was dependant on the initial vertical orientation of the adaptor plate for the attachment of the accelerometer array (*Fig. 3.8B*). However, this was later reoriented to be horizontal, as the PMMA mantle became too large and invasive on the skull of the animal. Therefore, an 8 x 2 cm mantle was built on the skull proximal to bregma (*Fig. 2.3D; chapter 2.2.5*).

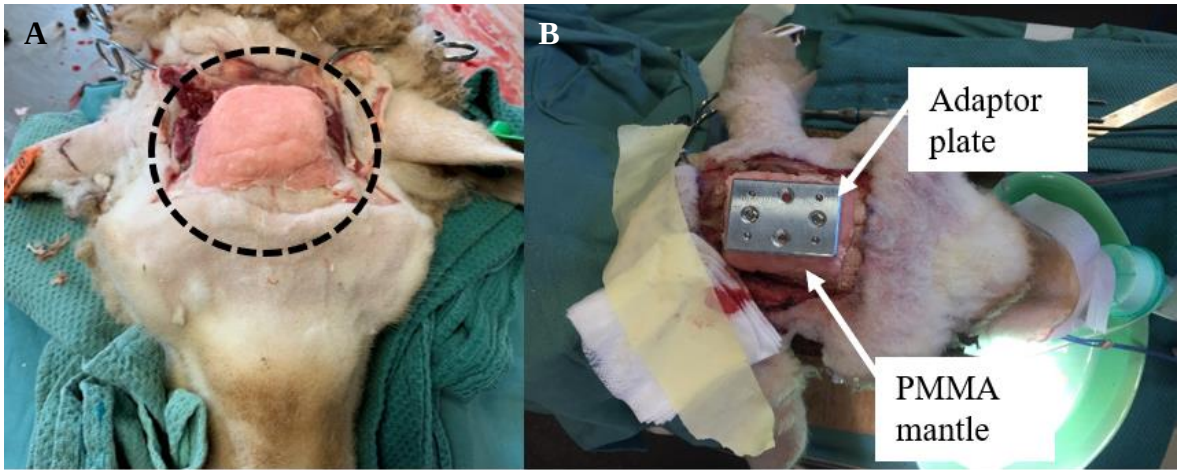

*Figure 3.8: PMMA mantle attached to the skull of the sheep (outlined in black) (**A**), adaptor plate attached to the PMMA mantle on the skull (**B**).*

The PMMA mantle was then trialled on a live animal, however the differences in live compared to deceased tissue proposed further difficulties. The surface of the skull was significantly moist, as a result of increased production of blood and serous fluid, therefore it was necessary to ensure that all exposed blood vessels were cauterised and the surface of the skull was treated with acetone in order to completely dry out the bone prior to mounting of the PMMA mantle to the skull. Once the mantle was built, the PMMA then underwent an exothermic reaction and hardened to the consistency of bone. When this reaction occurred, this caused the mantle to shrink in size and was no longer formed to the shape bone, causing it to detach from the skull. In order to combat this issue two, 14 mm titanium bone screws (Provet, Australia) were inserted into the skull of the animal, and steel wire was wrapped around the screws in order to allow the mantle to form to these and anchor to the skull more rigidly (*chapter 2.2.5*). However, it is important to note that this method meant the mantle was only able be detached from the skull post-mortem, which has implications for survival studies, but was not of concern for the studies presented in this thesis.

3.5.4 Conclusions

Overall, the development of the PMMA mantle allowed successful attachment of the accelerometer array in a flat plane and was adhered to the skull of the animal rigidly. This methodology was therefore implemented in the experiments outlined in Chapter 5.

3.6 Optimisation of Biomechanical Parameters of Injury

3.6.1 Rationale

Previous work using the ovine impact acceleration model of TBI has suspended the head of the sheep on a bed of sandbags prior to and during impact (Lewis, et al. 1996; Van den Heuvel et al. 1999). However, the firm nature of these sandbags restricted the six-degrees of freedom, range of motion of the head to favour more linear motion rather than angular, and as previously mentioned angular acceleration is a more predominating cause of DAI in TBI. In order to confirm the type and amount of acceleration during injury it was essential to conduct biomechanical evaluation. Additionally, studies using this model have induced injury with the device being handheld at the site of injury (Lewis, et al. 1996; Van den Heuvel et al. 1999; Van den Heuvel et al. 1998; Vink, Bahtia & Reilly 2008; Vink, Gabrielian & Thornton 2017). It is important to note that despite these models producing significant DAI, the delivery of force via injury was not controlled as a result of the device being prone to recoil. However, biomechanical analyses of the force were not conducted in these studies to evaluate if the impact produced consistent, reproducible force. Further work by Anderson *et.al.* highlighted that any recoil velocity introduces an error into the velocity of the captive bolt relative to the head and therefore the impact force (Anderson, et al. 2003; Anderson 2000).

Therefore, these were addressed by the following aims:

1. To optimise head suspension in order to incorporate more free angular motion of the head following impact.

2. Evaluate the reproducibility of injury via the use of a stable tripod frame to secure the injury device and minimise recoil.

3.6.2 Methodology

Two methods were incorporated with reference to optimising the free range of motion of the head. Animals injured in the experiments presented in Chapter 4 (n=9) were subject to impact with their heads suspended on sandbags and towels (*Fig. 3.9A*), and an additional subset of 6 animals (not presented in this thesis) were subject to impact with heads suspended on a pillowcase tightly packed with shredded foam (Clark Rubber, Australia) (*Fig. 3.9B*). Furthermore, animals injured in experiments outlined in Chapter 5 (n=8) were impacted with their heads secured in a cervical sling (Model SUSP297, Astir Australia) which was freely hanging suspended via a machine lift (*Fig. 3.9 C&D*).

Figure 3.9: *Head of sheep suspended on sandbags (**A**), head of sheep suspended on shredded foam pillow (**B**), head of sheep suspended in sling (**C**), head of sheep suspended in sling, closer resolution (**D**).*

Animals injured in experiments described in Chapter 4 were impacted with the device handheld against the impact site, however as previously mentioned this does not allow the consistent reproducibility of injury. Therefore, animals injured in experiments described in Chapter 5 were impacted with the injury device secured in a stable tripod (University of Adelaide, Department of Mechanical Engineering), built in the same design as that of Anderson's (2000)

experiments (*Fig. 3.10*) (Anderson, 2000). Attaching the gun to a rigid and secure frame reduces this error and increases the velocity of the captive bolt. A ballast was placed at the front support in order to counter any recoil produced during firing, minimising motion of the frame upon firing.

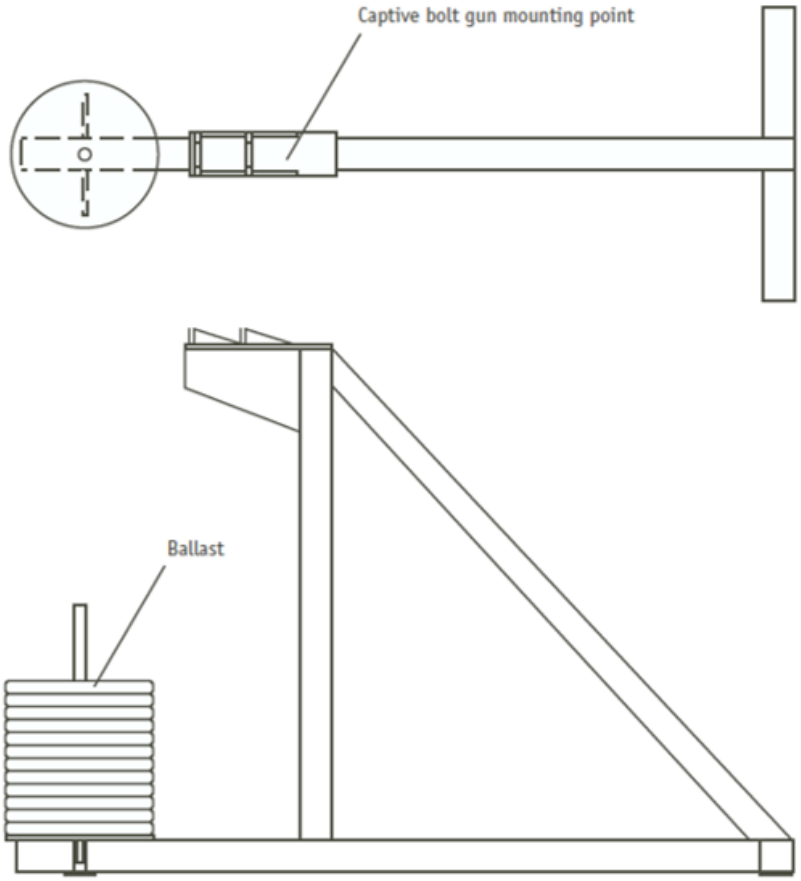

Figure 3.10: Rigid frame for mounting the captive bolt gun (Anderson, 2000).

3.6.3 Results and Discussion

The design of the foam pillow was implemented to more closely represent the foam bed used in Marmarou's impact acceleration model of TBI, and allow the head to accelerate/decelerate in a downward motion (Marmarou et al. 1994). In the absence of biomechanical confirmation,

it appeared that there was no apparent difference seen between this method of head suspension and the use of the sandbags.

3.6.4 Conclusions

Use of the tripod frame was implemented in experiments presented in Chapter 5 due to the tripod allowing the ability for more reproducible impact force. Additionally, given the desire to maximise angular acceleration of the head upon impact, the head of the animals impacted in Chapter 5 were freely suspended in the cervical sling in order to allow a less restricted plane of motion following impact. This was biomechanically evaluated for consistency of both rotational and linear accelerations, as well as head motion in experiments outlined in Chapter 5.

CHAPTER 4

Optimisation of a Closed Head Injury Model of TBI in the Sheep With the Absence of Skull Fracture.

CHAPTER 4: OPTIMISATION OF A CLOSED HEAD INJURY MODEL OF TBI IN THE SHEEP WITH THE ABSENCE OF SKULL FRACTURE

4.1 Introduction

Following TBI, extensive neurological damage occurs throughout the brain. This damage occurs via the initiation of multiple injury events immediately following injury (primary injury) and can persist from hours to days to months following the initial injury (secondary injury) (Plummer, SL et al. 2018). This secondary injury phase involves a destructive cascade of cellular and biochemical events which can exacerbate the existing injury and worsen outcomes (McKee et al. 2015). Common secondary injury mechanisms include excitotoxicity, oxidative stress, reversible cell injury which may progress to cell death, inflammation and BBB disruption (Blennow, Hardy & Zetterberg 2012; Gaetz 2004; Huang et al. 2013).

Whilst TBI produces numerous neuropathological changes, DAI is the most predominant and is the major contributor to morbidity following all severities of TBI (Povlishock & Katz 2005). Interestingly, DAI has been observed across the entire spectrum of mild, moderate and sTBI, with the amount of DAI increasing relative to injury severity (Johnson, Stewart & Smith 2013; Povlishock & Katz 2005). Research suggests that DAI arises from mechanical acceleration/deceleration of the head and brain; however, various secondary mechanisms may also propagate the development and spread of DAI (McGinn & Povlishock 2015). Specifically, pre-clinical studies in animal models have shown that DAI results from changes within the axon cylinder (Buki & Povlishock 2006; Povlishock & Katz 2005), particularly dysregulation of voltage-gated calcium channels which can cause intra-axonal $Ca2^{+}$ influx (Smith, Hicks & Povlishock 2013; Wolf, et al. 2001). Furthermore, shearing forces cause focal impairment of axonal transport at single or multiple loci along an individual axon (McGinn & Povlishock 2015). Following focal impairment, lobulation and local swelling within the axolemma ensues

causing segmentation of the axon cylinder over the course of several hours (Smith, Hicks & Povlishock 2013).

Despite this, a greater understanding of the pathophysiology of DAI is required in order to generate targeted pharmacotherapies to improve patient outcomes. Most pre-clinical studies of TBI have been limited to the use of lissencephalic species, which have proven to be highly valuable for the investigation and understanding of molecular injury mechanisms (Vink 2018). However, there has been a significant lack of successful translation of novel therapeutic agents from rodent studies to clinical trials. This is thought to result from, at least in part, the structural and neuroanatomical differences between the lissencephalic and gyrencephalic brain. The human brain presents a higher ratio of white and grey matter (60% : 40%), more intricate cortical structure and larger size compared to the rodent brain (10% : 90%) (Sorby-Adams, Vink & Turner 2018; Vink 2018). This particularly relevant given the evidence that DAI develops predominantly in the white matter of the brain and that DAI is not only influenced via gyrification, but also brain size, as the inertial effects following injury are dependent on brain mass.

As such, the field has looked to more clinically relevant models of injury to be developed in order to improve clinical translation in TBI. Indeed, research in the United States has highlighted the benefits of using large animals to provide more clinically relevant translation to human TBI, with porcine models of blast injury and rotational acceleration models of TBI having been developed (Bauman et al. 2009; Browne et al. 2011; Cullen et al. 2016; Goodrich et al. 2016; Williams et al. 2020). Interestingly, these models have focussed specifically on the investigation and characterisation of the pattern of DAI across the entire spectrum of TBI, especially in more mild concussive forms (Atlan, Smith & Margulies 2018; Browne et al. 2011; Johnson et al. 2016; Lafrenaye et al. 2015). The ability to investigate the pathological cascade of injury following more mild forms of TBI is extremely important, given that mTBI is the

most common form of TBI, accounting for 90% of all cases and prevalent in both teenagers and the elderly with over 42 million people worldwide suffering concussion and mTBI annually (Gardner & Yaffe 2015; World Health Organisation 2006).

In Australia and New Zealand, the use of sheep in large animal experiments is common due to high availability and inability to access imported miniature pig species due to quarantine regulations. Anatomically, sheep also provide a better brain-to-body ratio than pigs and less developed neck musculature which facilitates head acceleration (Finnie, et al. 1999). Further to this, an ovine model of moderate-severe TBI has previously been developed in our laboratory, which showed comparable DAI pathology to the human condition (Anderson, et al. 2003; Anderson, et al. 2014; Lewis, et al. 1996; Van den Heuvel, et al. 2000; Van den Heuvel et al. 1999; Van den Heuvel et al. 1998). This model used a humane animal stunner to induce injury, where sTBI was achieved by the use of a charged cartridge (17-charge) filled with a controlled amount of gun powder. However, charges ranging from 11 to 21 are also available to induce different levels of brain injury. Although this model comprehensively analysed the effects of sTBI on DAI, brain oxygenation, ICP and various other factors; significant skull fracture and macroscopic injuries such as contusion and SDH were also present, which are not pathologies associated with more mild to moderate forms of TBI (McCrory et al. 2013). Accordingly, the aim of this study was to investigate whether reducing the charge intensity in the ovine impact acceleration model of TBI would lead to significant amounts of DAI, without overt gross pathological lesions and significant skull fracture as seen in clinical mTBI.

4.2 Materials and Methods

4.2.1 Study Design

12 Merino wethers (55-65kgs, 18-24 months) were used under approval of SAHMRI Animal Ethics Committee (ethics number: SAM325). Sheep were group housed upon arrival in the

conventional sheep pens at Gilles Plains LARIF. Animals were fasted overnight prior to surgery, with free access to water, and then underwent induction anaesthesia (as described in *chapter 2.2.3*).

4.2.2 Surgical Procedures, Induction of TBI and Monitoring

Following induction, animals were maintained under anaesthesia (*chapter 2.2.3*) and underwent non-invasive percutaneous intra-arterial catheter insertion (*chapter 2.2.4*). Animals were randomly allocated to receive either sham surgery, TBI: 11-charge, TBI: 13-charge or TBI: 15-charge (*chapter 2.2.6*), and then underwent four hours of physiological monitoring, with blood serum and CSF sample collection during this period (as described in *chapters 2.2.8, 2.2.9, 2.2.10* respectively). Both blood and CSF were stored following collection; however, due to optimisation issues resulting from a lack of sheep-specific antibodies, only blood samples were used for biochemical analyses. At four hours post-injury, anaesthetised animals underwent 10% formalin perfusion and brain removal (*chapter 2.2.11*). Prior to brain removal, the heads of all animals were dissected and inspected for evidence of skull fracture.

4.2.3 Histological Analysis

Following tissue processing (*chapter 2.3.1*), 5 μm thick sections were cut using a microtome (Leica Biosystems, Australia) from 1, 2, 3, 4, 5, 6 and 8 cm anteroposterior brain regions embedded in paraffin blocks. IHC staining of slides was conducted for distribution and levels of AI (APP) and microglial (IBA-1) and astrocytic (GFAP) activation as markers of neuroinflammation (*chapter 2.3.2*). A comprehensive analysis was performed to examine AI with APP, encompassing the following ROIs: cerebral cortex, hippocampus, cingulum, internal

capsule, reticular thalamic nucleus, medullary lamina, optic tract, corpus callosum, fornix, thalamus, cerebellum, superior colliculus and brainstem. However, a more targeted analysis was performed to examine neuroinflammation with IBA-1 and GFAP, with the following ROIs: cerebral cortex, hippocampus, cingulum, internal capsule, corpus callosum, fornix and thalamus. Slides were scanned digitally using Zeiss Axio Scanner and viewed using Zen Blue software (Carl Zeiss, Australia) and then analysed (*chapter 2.3.3*).

4.2.4 ELISA Analysis

Biochemical analysis of pro-inflammatory cytokines IL-6, IL-1β and TNF-α was conducted using the blood serum samples of animals subject to TBI (n=3/group) and sham (n=3) as per manufacturer's instructions (MyBioSource; *chapter 2.4*).

4.2.5 Arterial Blood Pressure Analysis

ABP data was analysed as described in chapter 2.5.

4.2.6 Statistics

All data was analysed using GraphPad Prism® statistical software. A two-way ANOVA followed by a Tukey's post hoc test, was used to analyse basic physiological parameters and the acute histological analysis for APP, IBA-1 and GFAP within the pre-frontal cortex, cerebral cortex, cingulum, internal capsule, thalamus, reticular thalamic nucleus, medullary lamina, and optic tract. All molecular data obtained via ELISA also underwent a two-way ANOVA. A one-way ANOVA followed by Tukey's post-hoc test was used to analyse the ABP data, as well as

acute histological analysis for APP, IBA-1 and GFAP within the corpus callosum, hippocampus, fornix, cerebellum, superior colliculus, and brainstem. Significance was determined as $p<0.05$. Acute histological data are displayed as mean ± SD, whilst all remaining results are expressed as mean ± standard error of mean (SEM).

4.3 Results

4.3.1 Basic Physiological Parameters

All experimental procedures were carried out without complication and there was no premature mortality or unexpected events in any of the groups, with the exception of one animal. All animals were included in the following analysis except for one sham animal. This animal was the first to undergo the non-invasive catheter insertion in this pilot study and catheter insertion was unsuccessful, therefore ABG samples were unable to be obtained from this animal. Physiological parameters were assessed prior to injury (baseline) and then hourly post-injury. No main effect of time was noted; however, a significant main overall effect of injury was seen to increase pH ($p=0.02$) and pCO_2 ($p=0.05$) levels and decrease pO_2 ($p=0.01$) levels (*Table 4.1*). Tukey's post hoc analysis revealed the 11-charge group to have significantly higher pH levels compared to the 15-charge ($p=0.009$) (*Table 4.1*) and the 13-charge group to have significantly higher pCO_2 as compared to sham ($p=0.03$) (*Table 4.1*). Finally, the 15-charge group demonstrated significantly lower pO_2 levels as compared to all other groups (sham: $p=0.03$, 11 $p=0.002$, 13: $p<0.0001$) (*Table 4.1*).

*Table 4.1: Physiological variables measured throughout the course of the four hour monitoring period. Note the significant effect of injury resulting in an increase pH (*p<0.05) and pCO_2 (*p<0.05) levels and decrease pO_2 (****p<0.01). A significant main effect of injury resulted in pH increase with the 11-charge as compared to the 15-charge (**p=0.009). There is also a significant main effect of injury increasing pCO_2 with the 13-charge compared to sham (*p=0.03). Finally, the 15-charge produced significantly lower pO_2 as compared to all other injury groups (sham: *p=0.03, 11 **p=0.002, 13: ****p=<0.0001). All data are expressed mean ± SEM; n = 2-3 per group. * = significance.*

Time point	Sham	11-charge	13-charge	15-charge
pO_2 ***Injury: ****p0.01,*** *Time: p=0.64*				
Baseline	167.5 ± 22.8	154.3 ± 16.8	135 ± 13.6	101.3 ± 5.56
1hr post-injury	134.5 ± 3.8	157.3 ± 23.7	108.3 ± 10.4	104.3 ± 20.4
2hr post-injury	130.5 ± 2.6	152.6 ± 14.2	119 ± 1.5	120 ± 2.45
3hr post-injury	122.5 ± 1.4	154.7 ± 12.2	124 ± 2	108.3 ± 9.7
4hr post-injury	123.5 ± 0.9	154 ± 12.4	126.3 ± 2.9	107.5 ± 4.5
pCO_2 ***Injury: *p0.05,*** *Time: p=0.30*				
Baseline	38.5 ± 2.0	45.7 ± 1.3	44.7 ± 2.0	42.3 ± 1.8
1hr post-injury	35 ± 2.9	38 ± 4.7	44.3 ± 0.9	38.7 ± 3.7
2hr post-injury	35.5 ± 2.0	40.3 ± 4.2	44 ± 1.2	38 ± 0
3hr post-injury	38.5 ± 0.9	39.6 ± 2.6	41 ± 1.7	40 ± 2.5
4hr post-injury	38.5 ± 0.9	39 ± 3.2	39.3 ± 1.7	40 ± 1
pH ***Injury: *p=0.02,*** *Time: p=0.40*				
Baseline	7.45 ± 0.02	7.4 ± 0.03	7.43 ± 0.01	7.44 ± 0.01
1hr post-injury	7.48 ± 0.02	7.47 ± 0.02	7.45 ± 0.01	7.43 ± 0.02
2hr post-injury	7.47 ± 0.01	7.58 ± 0.10	7.45 ± 0.01	7.43 ± 0.01
3hr post-injury	7.45 ± 0	7.58 ± 0.10	7.47 ± 0.01	7.4 ± 0.02
4hr post-injury	7.43 ± 0.01	7.52 ± 0.02	7.49 ± 0.02	7.43 0.01

4.3.2 Acute Blood Pressure Response

All animals were included in the following analysis except for one animal each from the 13 and 15-charge groups. This was due to the percutaneous catheter kinking within the femoral artery during the four hour monitoring period, such that the continuous ABP trace was lost and meaningful data was unable to be extracted or analysed in these animals. Injury appeared to lead to an immediate decrease in BP in all mTBI animals (p=0.18), as calculated relative to pre-injury baseline which was comparable across injury groups with no effect of charge level (sham: 0 ± 0mmHg; 11-charge: -21.45 ± 7.183mmHg; 13-charge: -11.32 ± 5.635mmHg; 15-charge: -13.67 ± 1.3446mmHg) (*Fig. 4.1A*). BP returned to sham levels within four minutes post-injury in all groups (*Fig. 4.1B*), with the time taken to return to sham levels not significantly different between groups (p=0.11). Note the ABP response to TBI *(Fig. 4.1C*), compared to no change in the ABP trace in shams (*Fig. 4.1D*).

4.3.3 Incidence of Skull Fracture

Although significant troubleshooting of methodology was undertaken to reduce the incidence of skull fracture (*chapter 3.4.3*, *Fig.3.6*), it is important to note there were some incidences of skull fracture. Specifically, two animals subject to the 11-charge sustained a fracture of the zygomatic arch (*chapter 3.3*), whilst all animals subject to the 15-charge sustained hairline, non-penetrating skull fractures at the site of injury (*Table 4.2*).

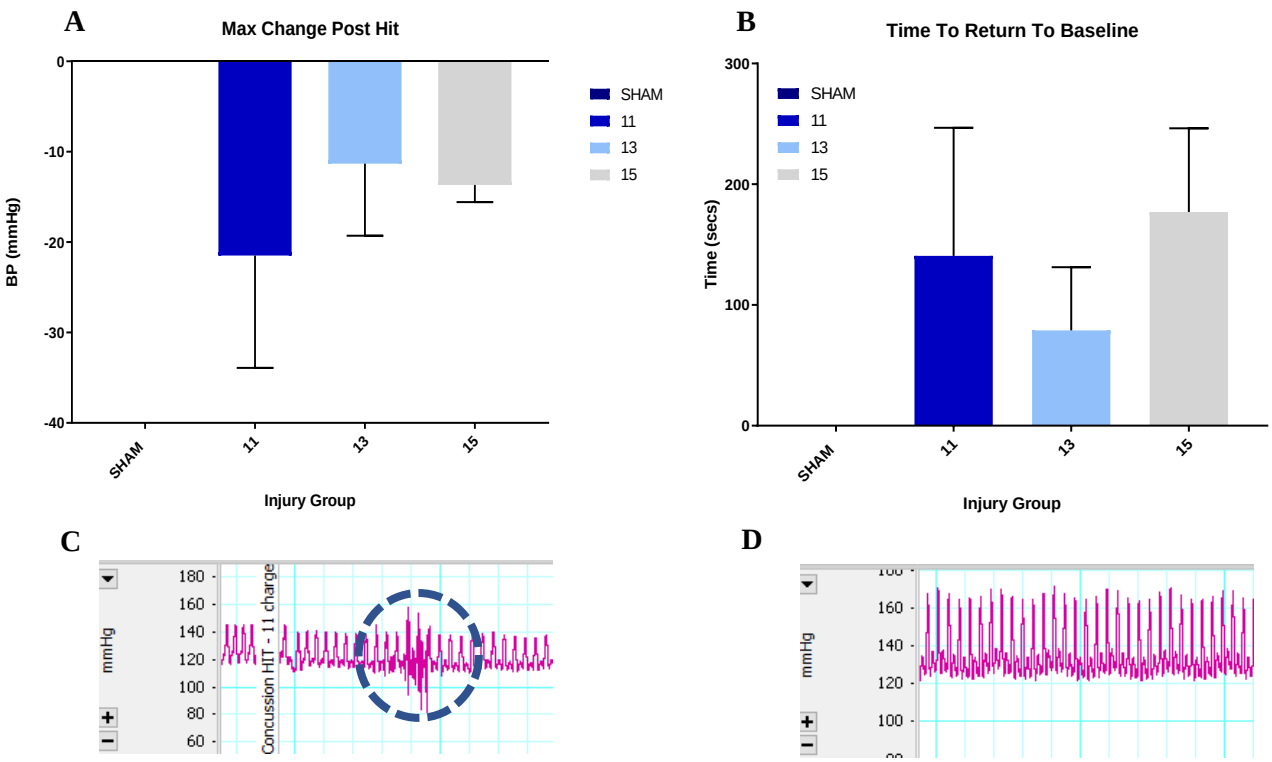

*<u>Figure 4.1:</u> An immediate decrease in BP was seen post-injury in all TBI animals (p=0.18) (**A**), which returned to pre-injury baseline within four minutes post-injury (p=0.11) (**B**). Representative images of amplitude of arterial BP trace, note the drop in BP amplitude following the induction of TBI and return to baseline BP level within seconds post-hit (**C**) compared to absence of change in amplitude in sham trace (**D**). (n=2-3 per group, graphs show mean ± SEM).*

<u>Table 3.2:</u> Incidence of skull fracture when subjected to TBI at each charge intensity. Note the incidence of skull fracture in the 11 and 15-charge but lack of skull fracture in animals subject to injury with the 13-charge.

Charge Level	Incidence of Skull Fracture (%)
11	2/3 (66%)
13	0/3 (0%)
15	3/3 (100%)

4.3.4 Axonal Injury

Distribution and levels of AI were examined, by counting the number of APP positive (+ve) cells within the pre-frontal cortex, cerebral cortex, hippocampus, cingulum, internal capsule, reticular thalamic nucleus, medullary lamina, optic tract, corpus callosum, fornix, thalamus, cerebellum, superior colliculus, and brainstem (*chapter 2.3.3*). Regional AI analysis found minimal significant differences between injury groups and also compared to shams within the thalamus only (injury effect: $p<0.001$; hemisphere effect: $p<0.01$) (*Fig. 4.3; Table 4.3*). Post hoc analysis found the 15-charge to produce a significantly increased number of APP+ve cells as compared to the 13-charge in both the left and right thalamus (L: $p=0.004$, R: $p=0.03$) and to sham in the left thalamus ($p=0.02$) (*Fig. 4.2*). The 13-charge also demonstrated a significantly lower numbers of APP+ve cells in the left thalamus when compared to the 11-charge ($p=0.04$) (*Fig. 4.2*). There was no additional effects of injury or differences between the left and right hemispheres in the remaining brain regions.

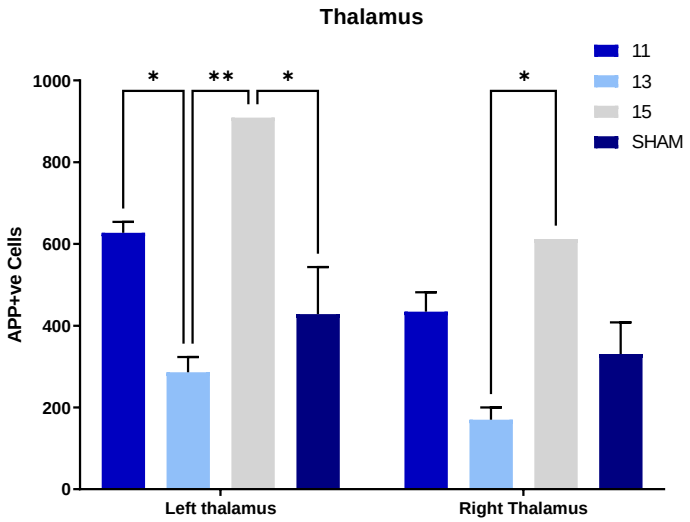

*Figure 4.2: 15-charge resulted in increased APP+ve cells compared to the 13-charge in the left and right thalamus (L: **p<0.005. R: *p<0.05) and to sham in the left hemisphere (*p<0.02). The 11-charge resulted in an increase in APP+ve cells compared to 13-charge in the left hemisphere (*p<0.05). Data expressed mean ± SEM; n = 2-3 per group. * = significance.*

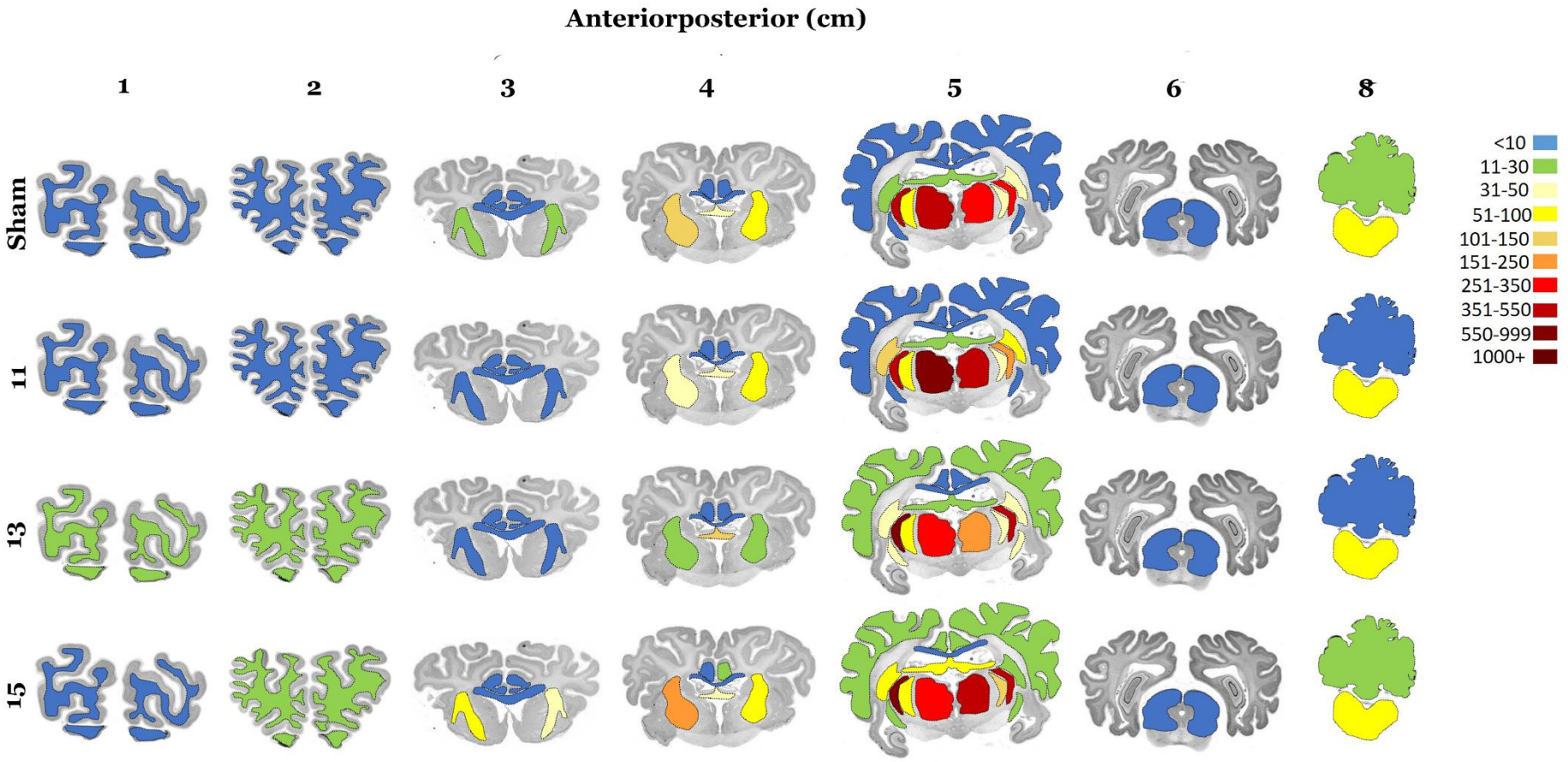

Figure 4.3: Heat map demonstrating the expression and distribution of AI in white matter tracts across seven, 1 cm different anteroposterior brain regions. Scale indicates the number of APP+ve lengths or bulbs within each region. The highest levels of AI were observed within the internal capsule, thalamus, and cingulum, but no significant differences noted between groups.

*Table 4.3: Total counts for APP+ve lengths or bulbs within each brain region analysed. Note the significant effect of injury within the thalamus (injury: ***p=0.0010; L&R hemisphere: *p=0.0155). Note the significant increase with the 15-charge as compared the 13-charge in the left and right thalamus (L: **p<0.005. R: *p<0.05) and to sham in the left hemisphere (*p<0.02). There is also a significant increase in APP+ve lengths/bulbs with the 11-charge compared to 13-charge in the left hemisphere (#p<0.05). All data are expressed mean ± SD; n = 2-3 per group. * and # = significance.*

Region	**Sham**		**11-charge**		**13-charge**		**15-charge**	
	L hem	*R hem*	*L hem*	*R hem*	*L hem*	*R hem*	*L hem*	*R hem*
Pre-frontal Cortex *Injury: p=0.23* *Hemisphere: p=0.59*	1 ± 1	3.3 ± 2.5	0 ± 0	0 ± 0	14.7 ± 25.4	23 ± 39.8	13.5 ± 13.6	18.2 ± 0
Cerebral Cortex *Injury: p=0.22* *Hemisphere: p=0.70*	0 ± 0	1 ± 1	0.5 ± 0.7	0 ± 0	0.7 ± 1.7	1.7 ± 2.9	7.3 ± 11.0	2.7 ± 2.3
Corpus Callosum *Injury: p=0.69*	7.3 ± 6.5		8.33 ± 5.4		13 ± 18.3		17.3 ± 2.5	
Cingulum *Injury: p=0.07* *Hemisphere: p=0.61*	7.3 ± 6.4	13.7± 19.4	12.7 ± 21.1	8.3 ± 12.8	14.7± 7.6	10 ± 8	20 ± 12.5	12 ± 8.7
Internal Capsule *Injury: p=0.12* *Hemisphere: p=0.18*	112.7 ± 100.9	109 ± 102.2	103.3 ± 79.9	123.3 ± 135.4	57.3 ± 61.1	54.7 ± 22.9	104.3 ± 44.4	278.3 ± 87.2
Fornix *Injury: p=0.74*	43 ± 11.3		45 ± 46.7		105 ± 0		47.5 ± 23.3	
Hippocampus *Injury: p=0.051*	21.7 ± 8.1		17.5 ± 7.8		18.3 ± 13.2		69 ± 0	

Region	Sham		11-charge		13-charge		15-charge	
	L hem	*R hem*	*L hem*	*R hem*	*L hem*	*R hem*	*L hem*	*R hem*
Reticular Thalamic Nucleus *Injury: p=0.73* *Hemisphere: p=0.14*	345.7 ± 175.4	461.3 ± 187.9	209.5 ± 173.2	492.5 ± 340.1	404.7 ± 240.1	610 ± 252.5	480 ± 0	665 ± 0
Medullary Laminae *Injury: p=0.15* *Hemisphere: p=0.65*	47 ± 19.08	56.3 ± 35.0	42 ± 15.6	67.5 ± 4.9	48.3± 41.4	66.3 ± 13.1	129 ± 0	97 ± 0
Thalamus *Injury: *****p<0.001*** *Hemisphere: ***p<0.01***	* 331 ± 133.5	428.3 ± 199.4	434.5 ± 67.2	627.5 ± 37.5	** 170 ± 52.2 #	* 286.3 ± 64.5	612 ± 0	909 ± 0
Optic Tract *Injury: p=0.37* *Hemisphere: p=0.94*	3.3 ± 2.1	5.3 ± 5.2	3 ± 1.4	4 ± 5.7	39.3 ± 61.3	42.7 ± 45.3	11 ± 0	18 ± 0
Superior Colliculus *Injury: p=0.12* *Hemisphere: p=0.77*	5 ± 7	9.3 ± 13.7	0.5 ± 0.7	0 ± 0	1 ± 1.7	0.3 ± 0.6	0 ± 0	0 ± 0
Cerebellum *Injury: p=0.057*	27 ± 10.5		9.3 ± 1.5		7.3 ± 1.5		12.7 ± 10.6	
Brain Stem *Injury: p=0.98*	81 ± 37.7		70.7 ± 74.4		73 ± 42.8		67 ± 49.3	

4.3.5 Acute Neuroinflammatory Response

Microglia

Microglial proliferation was assessed with IHC using the classic antibody specific for IBA-1 within the cerebral cortex, hippocampus, cingulum, internal capsule, corpus callosum and thalamus (*chapter 2.3.3*). As such, a more targeted ROI analysis for neuroinflammation was performed, with a focus on only those brain regions which were directly exposed to impact, and only within the higher charge injury groups (13 and 15). Indeed, results were consistent with the AI dataset, with regional analysis revealing minimal differences in the number of IBA-1+ve cells between injury groups. Specifically, a significant effect of injury was only seen in the thalamus ($p=0.02$), where there was a decrease in the number of IBA-1+ve cells in the 13-charge group compared to both the sham and 15-charge groups. Interestingly, there was also a significantly greater ($p=0.03$) number of IBA-1+ve cells observed within the internal capsule of the right hemisphere (*Fig. 4.4; Table 4.4*). Post-hoc analyses did not reveal any further differences, and no additional differences were noted in other brain regions.

Astrocytes

Astrocytic proliferation was assessed with IHC using the classic antibody specific for GFAP within the cerebral cortex, hippocampus, cingulum, internal capsule, corpus callosum and thalamus (*chapter 2.2.3*). Injury did not lead to an increase in GFAP+ve astrocytes in any of the regions examined, with no difference between left and right hemisphere noted (*Fig. 4.5; Table 4.5).*

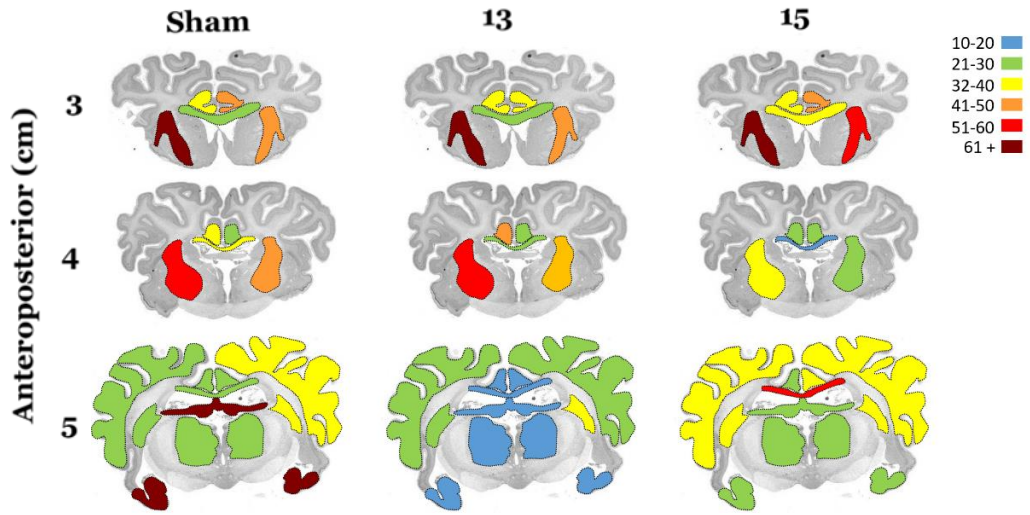

*Figure 4.4: Heat map demonstrating the expression and distribution of microglial proliferation in grey and white matter tracts across three different anteroposterior brain regions. Scale indicates the number of IBA-1+ve cells/mm^2 within the region. Note the significant effect of injury within the thalamus (*p=0.02) and between the left and right hemispheres within internal capsule (*p=0.03). The highest levels of microglial proliferation were noted within the hippocampus with no significant differences noted within groups.*

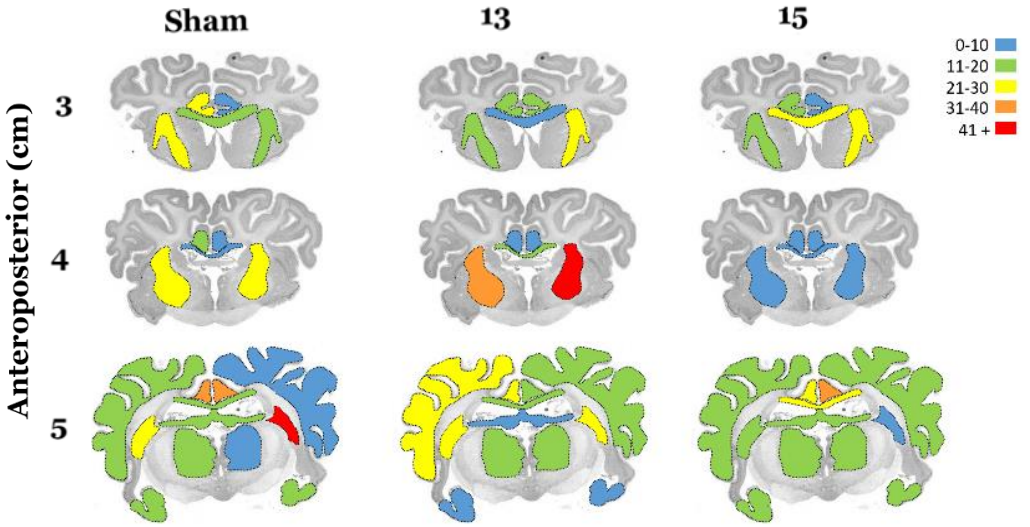

Figure 4.5: Heat map showing the distribution of astrocytic expression. Scale indicates the number of GFAP+ve cells/mm^2 within the region. The highest levels of astrocytic proliferation were noted within the internal capsule and cingulum with no significant differences noted within groups

*Table 4.4: Total counts for IBA-1+ve cells within specific brain regions. Note the significant effect of injury within the thalamus (*p=0.02) and between the left and right hemispheres within internal capsule (*p=0.03). Data are presented as Mean ± SD. * = significance.*

Region	Sham		13-charge		15-charge	
	L hem	***R hem***	***L hem***	***R hem***	***L hem***	***R hem***
Cerebral Cortex *Injury: p=0.22* *Hemisphere: p=0.26*	34.0 ± 13.1	21.1 ± 0	28.7 ± 4.8	30.4 ± 0	39.9 ± 3.4	34.0 ± 1.9
Corpus Callosum *Injury: p=0.62*	78.7 ± 26.3		57.2 ± 23.9		89.9 ± 60.9	
Cingulum *Injury: p=0.60* *Hemisphere: p=0.77*	86.1 ± 32.1	79.0 ± 28.0	66.9 ± 7.9	57.6 ± 28.0	71.4 ± 43.8	73.4 ± 50.0
Internal Capsule *Injury: p=0.58* *Hemisphere: ***p=0.03***	102.9 ± 34.6	155.5 ± 54.4	98.9 ± 17.5	173.3 ± 34.7	94.7 ± 42.4	122.8 ± 74.1
Hippocampus *Injury: p=0.47*	94.5 ± 100.9		19.0 ± 16.7		21.9 ± 4.8	
Thalamus *Injury: ***p=0.02*** *Hemisphere: p=0.34*	29.1 ± 4.8	24.6 ± 10.2	15.4 ± 5.7	13.5 ± 0	28.0 ± 3.8	24.8 ± 6.8

Table 4.5: Total counts for GFAP+ve cells within each brain region examined. Data are presented as Mean ± SD.

Region	Sham		13-charge		15-charge	
	L hem	***R hem***	***L hem***	***R hem***	***L hem***	***R hem***
Cerebral Cortex *Injury: p=0.7693* *Hemisphere: p=0.49*	7.6 ± 5.9	19.1 ± 10.6	13.1 ± 1.8	21.1 ± 0	20.3 ± 13.4	20.8 ± 31.0
Corpus Callosum *Injury: p=0.58*	29.8 ± 8.6		33.9 ± 30.7		45.9 ± 7.7	
Cingulum *Injury: p=0.77* *Hemisphere: p=0.60*	44.3 ± 4.7	62.3 ± 6.3	35.9 ± 26.7	45.9 ± 52.9	50.5 ± 34.9	44.7 ± 20.7
Internal Capsule *Injury: p=0.18* *Hemisphere: p=0.79*	65.2 ± 16.3	84.3 ± 17.5	84.3 ± 43.0	77.7 ± 58.6	44.5 ± 11.0	44.6 ± 33.1
Hippocampus *Injury: p=0.64*	14.8 ± 19.8		0.6 ± 0.3		15.2 ± 20.9	
Thalamus *Injury: p=0.59* *Hemisphere: p=0.74*	5.5 ± 1.3	16.2 ± 11.8	19.0 ± 0.6	12.2 ± 2.4	17.0 ± 18.9	19.3 ± 15.5

4.3.6 Acute Peripheral Inflammatory Response

Peripheral inflammation was assessed in the serum of sham, 13 and 15-charge groups using ELISA for pro-inflammatory cytokines (*chapter 2.4*), which was performed in addition to the histological neuroinflammatory assessment (*chapter 4.3.5*). A significant effect of injury was seen in IL-6 (*Fig. 4.6A*), IL-1β (*Fig. 4.6B*) and TNF-α (*Fig. 4.6C*) expression, with significant increases (IL-6: p=0.009; IL-1β: p=0.04; TNF-α: p=0.02) relative to pre-injury baseline levels. Tukey's post hoc analysis revealed that there was a significant increase in TNF-α levels in the 15-charge group compared to sham at 30 minutes (TNF-α: p=0.01) post-injury. At four hours post-injury there were significantly higher levels of all cytokines detected in the 15-charge group when compared to shams (IL-6: p=0.003; Il-1β: p=0.03; TNF-α: p=0.03). Additionally, at four hours post-injury the 15-charge also produced increased levels of Il-1β compared to 13-charge (p=0.02).

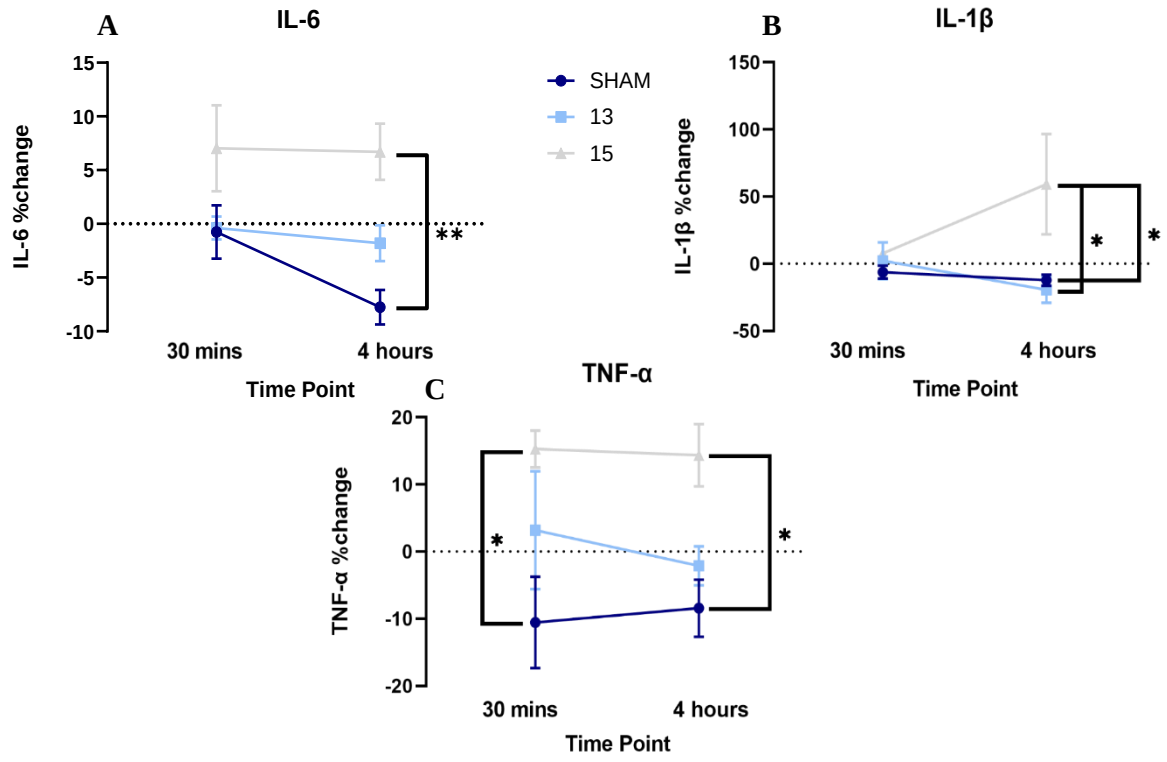

*Figure 4.6: Serum IL-6 (**A**), Il-1β (**B**) and TNF-α (**C**) expression following TBI. An overall significant effect of injury was seen amongst all cytokine expression (IL-6: **p<0.01; Il-1β: *p<0.05; TNF-α:.*p<0.02) Note the significant increase in IL-6 (**A**) at four hours post-injury within the 15-charge group as compared to shams (*p<0.05). At four hours post-injury, Il-1β (**B**) levels were increased with the 15-charge compared to the 13-charge (*p<0.01) and sham (*p<0.01). A significant increase was seen in serum TNF-α (**C**) at 30 minutes and four hours (*p<0.05) post-injury with the 15-charge as compared to shams. (n=2-3 per group, graphs show % change in serum expression compared to pre-injury baseline levels).*

4.4 Discussion

In Australia, no large animal model of moderate TBI has been developed or is currently in use. Given the significant incidence of TBI specifically in Australia and the massive public health burden of injury amongst all age populations, a gyrencephalic model of mild-moderate TBI is urgently required in order to successfully develop and translate new treatments and pharmacotherapies to improved patient outcomes. As such, this study aimed to investigate whether reducing the charge intensity in the established ovine impact acceleration model of sTBI would lead to significant presentation of DAI, without overt gross pathological lesions and significant skull fracture, comparable to that observed clinically in milder forms of TBI.

Whilst no skull fractures were present within the 13-charge group, two animals subjected to the 11-charge, and all animals subject to the 15-charge sustained fractures of the zygomatic arch at the site of injury on the skull. It is proposed that the animals injured with the 11-charge sustained skull fracture as a result of the firing pin of the injury device penetrating through the silicone cover and subsequently making contact with the zygomatic notch which is a protruding palpable landmark on the head of the animal, only covered by a thin soft tissue layer. The higher intensity of the 15-charge is thought to have caused the skull fractures seen in these animals. Additionally, the lack of skull fracture seen in animals injured with the 13-charge could have potentially resulted from issues with the charges themselves not delivering the expected force once ignited upon firing the gun. However, this would need to be probed further. Minimal regional DAI was produced within this model with no overt differences seen between increasing charge levels or compared to shams. Additionally, the regional neuroinflammatory analysis reiterated that there were minimal differences between injury groups compared to shams, as evidenced by the relatively low levels microglial and astrocytic proliferation. However, analysis of pro-inflammatory cytokines within peripheral blood samples revealed

that there was a significant overall effect of injury. At 30 minutes post-injury, increased expression of TNF-α was observed with use of the 15-charge compared to sham. At four hours post-injury, increased expression of IL-6 and TNF-α was observed in animals exposed to the 15-charge compared to sham, and an increased expression of IL-1β cytokines in the 15-charge group compared to both the 13-charge and sham animals.

A significant effect of injury was seen on pO_2, pCO_2 and pH levels. There was a significant increase in pH levels in animals injured with the 11-charge as compared to the 15-charge. There was also a significant increase in pCO_2 in animals injured with the 13-charge compared to sham Finally, the 15-charge produced significantly lower pO_2 as compared to all other injury groups. Whilst there is limited literature describing the acute physiological effects of experimental TBI, it has been reported that breathing problems may arise if there is a reduction in cerebral blood flow (CBF) to the thalamus, and therefore gas exchange between O_2 and carbon dioxide (CO_2) can be disrupted (Siedlecki et al. 2018). Interestingly, CBF has been shown to be compromised following both severe and more mild forms of TBI, with CBF being reduced by up to 50% following concussion, suggesting respiratory issues may arise following even more mild forms of TBI (Bonne et al. 2003; Giza & Hovda 2001; Golding et al. 1999; Len et al. 2013; McQuire, Sutcliffe & Coats 1998). It has been suggested that this alteration in CBF can arise from the neuroautonomic dysregulation of cardiovascular functions (Becelewski & Pierzchała 2003; Jünger et al. 1997; Strebel et al. 1997). Further to this, the autonomic nervous system (ANS) is also responsible for monitoring of subconscious breathing (Mateika & Duffin 1995; Siedlecki et al. 2018). Alterations in CO_2 and O_2 gas exchange has also been demonstrated to effect pH concentration (Patel et al. 2020). However, it should be noted that whilst there was a significant overall effect of injury on these parameters, post hoc analyses revealed individual differences between injury groups, with no effect of change following injury as compared to baseline levels. This likely results as animals were subject to constant mechanical ventilation throughout

surgery and monitoring procedures, and therefore suggests these differences seen between injury groups are likely dependent on changes in the ventilation parameters individual to the animal.

Although this was not significant, ABP analysis revealed the appearance of an immediate decrease in ABP following injury. Cardiovascular abnormalities are commonly reported following TBI (Simard & Bellefleur 1989) (Shiozaki 2005; Trivedi & Coles 2009), with elevations in ABP greater than 160mmHg reported in ~25% of sTBI patients with sTBI, although the average reported ABP is up to 108 ± 11 mmHg. (Clifton et al. 1983; Simard & Bellefleur 1989). However, in this study we observed the opposite response to TBI, with a consistent and immediate decrease in ABP observed in all animals following TBI. In order to understand why we may have seen such a discordant response; it is first necessary to discuss the mechanisms of an increase in ABP following TBI. It has been suggested patients enter a hyperadrenergic state following injury that increases relative to injury severity (Simard & Bellefleur 1989). Indeed, this hyperadrenergic state has been shown to correlate with an increase in circulation, with this surge due to an increase in sympathetic drive. Severe brain parenchymal injury triggers catecholamine release via regional injury to the brain, elevations in ICP, and activation of the brain's lower structures (cerebellum, brain stem and spinal cord), and hypothalamic neuroendocrine pathways (Krishnamoorthy et al. 2017; Krishnamoorthy et al. 2016). This initial brain injury will often increase ICP through local mass effects and diffuse cerebral oedema, and this resulting ICP increase allows a complex interaction with the neuroendocrine response through activation of the ANS, with further release of catecholamines (Kinoshita 2016; Krishnamoorthy et al. 2017; Nguyen & Zaroff 2009). The end result of this systemic catecholamine release is often an increase in ABP. Taken in this context of ABP increases being injury severity-dependent, our results of decrease ABP in response to TBI are

perhaps a little less surprising. Indeed, recent research has begun to expand on the complex relationship between the ANS and CNS following TBI (McDonald et al. 2020). Specifically, studies have suggested possible autonomic dysregulation to follow more mild forms of TBI as indicated by changes in heart rate variability (HRV) (Esterov & Greenwald 2017; Pertab et al. 2018). HRV refers to normal variations in the time between any 2 consecutive heart beats (*i.e.*, R-R interval) and thus the relative contributions of the sympathetic and parasympathetic nervous systems (Baguley et al. 1999; Baguley et al. 2012). However, it is important to note these changes to ANS in the acute phase directly following mTBI have not been extensively studied, and as such, are poorly discussed throughout the literature (McDonald et al. 2020). Whether autonomic dysregulation was a factor in driving a reduction in ABP following TBI in our model requires further investigation with comprehensive cardiovascular monitoring studies.

APP is a membrane spanning glycoprotein, with important roles in neuronal growth and synaptic plasticity (Van den Heuvel, Finnie, et al. 2000). Given that APP has been shown to accumulate in damaged axons following TBI (Van den Heuvel, Finnie, et al. 2000) it has been used as a sensitive marker of neuronal damage in the ovine sTBI model used extensively within our lab previously (Anderson, et al. 2003; Van den Heuvel, Finnie, et al. 2000; Van den Heuvel et al. 1998). APP is transported via fast axonal transmission, with APP messenger ribonucleic acid (mRNA) hybridisation showing that APP is upregulated in axons as early as 30 minutes post-injury, with intense accumulation observed within in axons at two hours and peak accumulation at 24 hours following injury (Gultekin & Smith 1994; Johnson, Stewart & Smith 2013; Van den Heuvel et al. 1999). Specifically, widespread APP immunoreactivity within the cerebral hemispheres and brain stem distant from the impact site consistently in all injured animals at two hours post-injury, with the most prominent AI being within the impacted

hemisphere (Van den Heuvel et al. 1998). APP+ve cells were also noted within regions which were structurally normal when stained with haematoxylin and eosin (H&E) (Van den Heuvel et al. 1998). However, in our study we saw only minimal, non-significant differences in the number of APP+ve cells across all injury groups and no differences compared to shams. At first pass, this suggests that there was a lack of DAI in our study; however, this is based on the assumption that a single marker captures all levels of traumatically injured axons, and does not account for 'sub-lethal' AI. Axons within the white matter tracts of the brain are inherently vulnerable to the stretching and shearing forces sustained in the brain parenchyma as a result of rapid acceleration/deceleration during injury (Browne et al. 2011; Johnson, Stewart & Smith 2013). However, there is a differential sensitivity of different axon subtypes with both *in vivo* and *in vitro* models of TBI indicating that myelinated fibres are more tolerant to mechanical strains of injury compared to unmyelinated fibres. Specifically, unmyelinated fibres more likely to undergo irreversible dysfunction of conduction pathways and secondary degeneration when exposed to stretch injury (Johnson, Stewart & Smith 2013; Reeves et al. 2007; Reeves, Phillips & Povlishock 2005; Staal & Vickers 2011). Furthermore, only subset of axons within any given white matter tract are subject to disrupted axonal transport as a result of traumatic injury and actually go on to develop bulbar swellings which can be detected by accumulation of APP (Johnson et al. 2016). Therefore, this suggests that 'sub-lethal' secondary axonal pathology may be present following mTBI that is not readily detected by routine identification measures. For example, axons that undergo dynamic deformation following stretch, but do not progress with swelling may still suffer subtle pathophysiological changes, including an increase in intra-axonal Ca^{2+} and Na^{+} concentrations, or mitochondrial dysfunction, as suggested by a number of pre-clinical *in vivo* and *in vitro* studies (Iwata et al. 2004; Pettus et al. 1994; Pettus & Povlishock 1996; Smith et al. 1999; Staal et al. 2010; Wolf, et al. 2001; Yuen et al. 2009). All of these factors markedly impede normal axonal, and therefore neuronal,

function. In addition, increased intra-axonal Ca^{2+} concentrations may activate deleterious proteases that initiate or perpetuate damage of the axonal cytoskeleton (Browne et al. 2011). Taken together, this highlights the need for detailed analysis of DAI using more specialised and sensitive histopathological markers that evaluate other axonal pathologies, other than solely APP accumulation within damaged axons, especially when studying the milder forms of TBI.

Previous research has suggested that neuroinflammation, particularly microglial activation, in the white matter may also contribute axonal damage following injury, and may even persist for years following injury (Chen, et al. 2009; Gentleman et al. 2004; Johnson, Stewart & Smith 2013; Loane & Byrnes 2010). The primary DAI sustained at the time of impact signals the recruitment of resident immune cells within the brain (microglia and astrocytes) to potentiate neuronal recovery through the production of both pro- and anti-inflammatory mediators (Begum et al. 2020; Burda, Bernstein & Sofroniew 2016; Lin & Wen 2013). When the neuroinflammatory response was examined in the current study, no differences in microglial or astrocyte number were detected by IBA-1 and GFAP staining respectively. This is not in keeping with previous rodent studies which have identified persistent neuroinflammation following mTBI, evidenced by marked microglial and astrocytic activation, as measured by increases in the IBA-1 and GFAP proteins respectively (Weil, Gaier & Karelina 2014). Activation of such immune/inflammatory cells, allows increased release of pro-inflammatory cytokines such as, IL-1β, IL-6 and TNF-α (Shohami et al. 1994; Weil, Gaier & Karelina 2014; Woodroofe et al. 1991). Microglia also express molecules called toll-like receptors (TLRs) which bind to Damage-Associated Molecular Patterns (DAMPs) such as High-Motility Group Box-1 (HMBG-1), which functions as a potent pro-inflammatory cytokine which is released in the acute phase following mTBI (Singhal et al. 2014). Research using rodent models of TBI

have shown HMGB1-TLR4 binding to increase microglial activation and subsequent pro-inflammatory cytokine release following mTBI (Kim et al. 2008; Teng et al. 2015).

Contrary to the histological assessment which revealed a paucity of neuroinflammation in response to TBI, assessment of the serum pro-inflammatory cytokine response revealed a significant effect of injury, with increased release of IL-6, IL-1β and TNF-α compared to shams. However, it should be noted that microglial activation state was not assessed in this study, rather total microglial population within specific ROI. Assessment of activation state could provide further insight into the release of specific serum cytokine and their resulting levels. The investigation of serum biomarkers following injury is an emerging technology for mTBI diagnosis and early detection of pathology (Agoston, Shutes-David & Peskind 2017). Interestingly, a recent study investigating serum biomarkers and neuropathology at six hours following mTBI in the pig found no correlation between IBA-1 microglial and GFAP astrocytic histological assessment with serum IL-6 levels at any time post-injury (Lafrenaye et al. 2020). Assessment of microglial morphology, indicative of activation state also presented no correlation with cytokine levels (Lafrenaye et al. 2020). Despite both microglia and astrocytes having been shown to release IL-6 (Brett et al. 1995; Kettenmann et al. 2011; Schwaninger et al. 1999; Wolf, Boddeke & Kettenmann 2017), investigation of biomarkers in large animals has been limited to date and certainly warrants further investigation. Although research using rodent models of TBI have demonstrated a correlation between cytokine release within brain tissue and microglial activation (Chio et al. 2013), the relationship between peripheral cytokine expression being indicative of specific CNS pathologies is poorly discussed in the literature and requires further investigation.

4.5 Limitations and Future Directions

Several limitations must be considered when interpreting the findings of this study. Firstly, the absence of biomechanical assessment within this study was a key limitation, as in order to produce the optimal level of DAI seen within mild-moderate TBI, a comprehensive biomechanical assessment is essential in order to accurately measure the accelerations and forces of injury that are being transmitted to the brain. This is addressed in Chapters 5 and 6, where comprehensive biomechanical assessment of injury was performed in order to understand the dynamics of injury and achieve the optimal rotational acceleration/deceleration forces of injury seen in TBI.

Secondly, it may be that the charge level used was insufficient to cause significant brain injury, such that an increase in charge level may be required in order to increase the force of injury, so that the brain tissue is undergoing higher magnitudes of angular/linear acceleration/deceleration. This could potentially increase the expression and pattern of DAI, indeed is explored in Chapter 5. Additionally, implementing a period of PTH may increase injury severity, as it has been well documented that the lack of tissue oxygenation to contributes to a heightened neuroinflammatory response, as well as increased damage to axons post-injury (Hellewell et al. 2010). The impact of the addition of hypoxia in our model will be assessed in Chapter 5. A more detailed histological investigation that includes additional markers of white matter injury, such as MBP, could assist in highlighting the pattern of damage within the subcortical white matter. Implementing more advanced outcome measures such as the use different pathological markers of DAI and specialised MRI may also provide more comprehensive analysis of AI. For example, many recent studies are using DTI/MRI, which has been shown to demonstrate DAI even in mTBI. Finally, we used quite an acute monitoring period in this study of four hours post-TBI. Increasing the monitoring period beyond four hours

post-injury may also allow more time for DAI to develop within the white matter tracts in the brain, allowing for a more chronic evaluation of DAI following mTBI.

4.6 Conclusions

In summary, this pilot study highlights that no significant DAI was produced by any of the 11, 13 or 15-charges compared to sham or within injury groups. These results were in keeping with the neuroinflammatory response, with a paucity of microglial and astrocytic proliferation observed. Taken together, these results suggest that the level of injury achieved in this study was insufficient to produce an appreciable amount of AI within the first four hours post-injury. Therefore, more comprehensive outcome measures including specialised imaging as well as the use of more specialised pathological markers (specifically for DAI) are required in order to highlight the pathological consequences resulting from injury in this model. These measures taken in conjunction with a comprehensive biomechanical assessment should eliminate the risk of skull fracture allow the development of a survivable model of moderate TBI with significant DAI.

CHAPTER 5

Characterising the Effects of Post-Traumatic Hypoxia on the Development of Axonal Injury in an Ovine Model of TBI

CHAPTER 5: CHARACTERISING THE EFFECTS OF POST-TRAUMATIC HYPOXIA ON THE DEVELOPMENT OF AXONAL INJURY IN AN OVINE MODEL OF TBI

5.1 Introduction

The pilot results presented in Chapter 4 described extensive modifications to the ovine model of impact acceleration TBI in order to titrate injury severity to be permissible to survival and prevent the occurrence of skull fracture. However, despite three varying charge levels being tested, skull fracture remained a feature of injury which was present in two animals using the 11-charge, and three animals subject to injury with the 15-charge (*chapter 4.3.3*). Additionally, the IHC results demonstrated a lack of pathological injury response compared to shams, as evidenced by the lack of APP+ve lengths/bulbs or neuroinflammation observed (*chapter 4.3.4 and 4.3.5*). As skull fracture could not be prevented using this model, further modification and model development was required in order to increase the severity of injury and consequently, produce substantial DAI within this model.

TBI typically results from a discrete biomechanical event which induces rapid angular acceleration of the head, and causes dynamic deformation of brain tissue (Cullen et al. 2016) (Frank et al. 2020; Gennarelli, et al. 1982; Ross et al. 1994; Smith et al. 1997). However, replicating the injury biomechanics of human TBI in experimental animal models proposes a substantial challenge, particularly when considering differences in brain size and shape and the way the brain will pathologically respond to injury due to impact force and resulting angular and linear head accelerations (Cullen et al. 2016). Previous studies using both small and large animals have indeed modelled the biomechanical parameters of injury, highlighting the specific injury mechanics and acceleration thresholds for different severities and pathological hallmarks of injury (Cullen et al. 2016; Gennarelli, Adams & Graham 1981; Namjoshi et al. 2014;

Ommaya, Goldsmith & Thibault 2002). It has been widely reported throughout the literature that the presence and severity of DAI correlates with the amplitude of angular head acceleration (Abel, Gennarelli & Segawa 1978; Davidsson & Risling 2011; Gennarelli, et al. 1982; Holbourn 1943; Margulies & Thibault 1992). In contrast, linear kinematics have been demonstrated to be more predictive of skull fracture and contusion rather than resulting diffuse brain injury and axonal pathologies (Kleiven 2013; Ono et al. 1980; Ren et al. 2020). The relationship between (or thresholds of) both angular and linear head accelerations and the presence of DAI in sheep have been assessed previously using the ovine model of sTBI characterised in our laboratory (Anderson, et al. 2003; Anderson 2000). Work by Anderson *et.al.* concluded average resultant angular head accelerations of 81–227 krad/s^2 to be sufficient to produce marked moderate-severe DAI (Anderson, et al. 2003; Anderson 2000).

Following moderate-severe TBI, approximately 55% of patients will go on to develop exacerbated primary injury due to the onset of secondary brain injury in the minutes, hours, days or weeks following the initial insult (Dixon & MacLeod 2020; Dixon, Turner & Christou 2019). Such worsening of injury commonly results from a period of post-injury hypoxia (Dixon & MacLeod 2020). Hypoxia can be initiated by TBI-induced hypoperfusion, post-injury apnoea or hypoventilation, which primarily results from brainstem injury (Adams et al. 1982; Chesnut 1997; Newcombe et al. 2010; Smith et al. 2000; Yan et al. 2011). Intracranial bleeding, increased ICP, hydrocephalus and low ABP have also been found to exacerbate the effects of hypoxia post-injury, in addition to co-existing extracranial injuries such as obstructed airways, lung puncture and excessive blood loss (Maloney-Wilensky et al. 2009; Oddo et al. 2011; Yan et al. 2011). In experimental TBI models, animals are typically subjected to injury under general anaesthesia via intubation, so spontaneous apnoea (and resulting hypoxia) is likely mitigated by the mechanical ventilation of normoxic gases. Therefore, hypoxia must be induced manually following experimental injury models. Mechanical ventilation of animals is

an advantage from this perspective as it enables the gas mix to be manipulated quite easily to achieve a hypoxic episode. Indeed, rodent TBI studies demonstrate that PTH can exacerbate both axonal pathology and cellular inflammation following TBI (Hellewell et al. 2010; Yan et al. 2011). As such, these worsened pathologies are thought to be a driving force for poorer neurological outcomes seen in patients who experience PTH. PTH has been previously modelled in rodent TBI models but not in large animal TBI models (Hellewell et al. 2010; Plummer, et al. 2018; Yan et al. 2011). Hypoxic/ischemic injuries have been modelled independently of TBI in large animal experiments using both sheep and ferrets, but not in conjunction with TBI (Schiffner et al. 2018; Wood et al. 2018).

As such, the aim of this study was to investigate whether the use of a 21-charge, in conjunction with a 15 minute post-injury period of hypoxia, would lead to the production of marked DAI and neuroinflammation. A secondary aim was to evaluate the resultant angular and linear head accelerations produced following the onset of impact and investigate the effects of these accelerations on the amount of DAI produced.

5.2 Materials and Methods

5.2.1 Study Design

14 Merino wethers (55-65 kg, 18-24 months) were used under approval of SAHMRI Animal Ethics Committee (ethics number SAM396.19). Sheep were group housed upon arrival and were fasted overnight prior to surgery and then underwent anaesthesia induction and intubation (*chapter 2.2.3*).

Animals were randomly allocated to receive either sham surgery (n=6/group) or TBI (n=8/group) using a 21-charge (*chapter 2.2.6*), then further randomised to receive either PTH (n=3-4/group) (*chapter 2.2.7*) or normoxia (n=3-4/group), following sham surgery or TBI (*Fig. 5.1*).

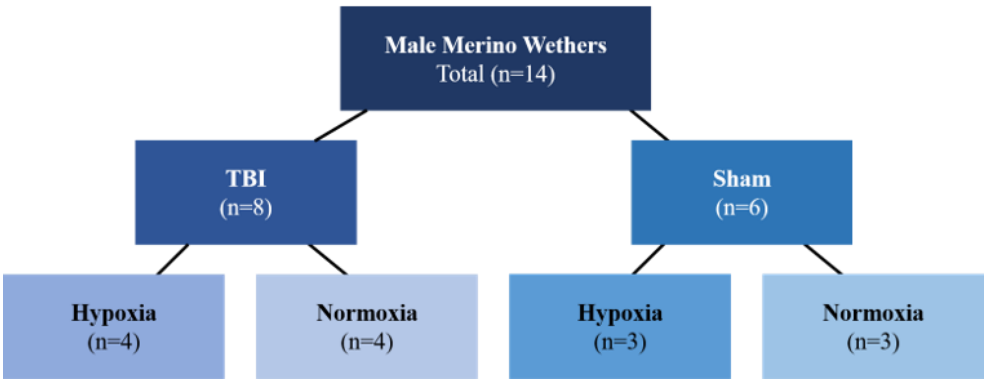

Figure 5.1: Distribution of animals into either TBI or sham injury groups and further randomisation to receive either post-injury hypoxia or normoxia.

5.2.2 Surgical Procedures, Induction of TBI and Monitoring

Following induction, animals were maintained under general anaesthesia (*chapter 2.2.3*) and underwent invasive femoral artery catheter insertion (*chapter 2.2.4*). All animals underwent cranial surgery and attachment of a PMMA mantle to the skull (*chapter 2.2.5*). Following which animals randomised to receive TBI had a biomechanical accelerometer array attached to the PMMA mantle in order to capture impact acceleration data during the delivery of injury (*chapters 2.2.5 and 2.2.6*). High speed camera tracking was implemented to capture translation of the accelerometer array following impact, so to measure head translation (*chapter 2.2.5*). Across the four hour monitoring period, all animals underwent physiological monitoring including measurement of ABG parameters and ABP (*chapters 2.2.8 and 2.2.9*), and collection of serum and CSF samples (*chapter 2.2.10*). As discussed in chapter 4.2.2, CSF samples did not undergo biochemical analyses. Animals were then perfused with 10% Tris-saline (*chapter 2.2.11*). Following perfusion, all animals were decapitated, and heads were dissected, and inspected for skull fracture, and brains were removed for tissue collection and processing (*chapters 2.2.11 and 2.3.1*).

5.2.3 Macroscopic Injury Analysis

Following perfusion, the heads of all animals were examined for presence of soft tissue laceration and oedema at the impact site, as well as skull fracture which was graded from 0-3 (*Table 5.1*). Following removal, each brain was examined for signs of macroscopic injury, such as contusions or haematomas. The skull fracture and macroscopic injury information was used to classify the injury into five main categories of severity (*Table 5.2*).

Table 5.1: Gross pathological features associated with a grading system for macroscopic injury score following TBI.

Grade 0	Brain appears as normal No macroscopic signs of injury or skull fracture
Grade 1	Brain appears as normal Presence of skull fracture
Grade 2	Brain appears as normal Presence of skull fracture Severe soft tissue laceration/cavity – resulting in haemorrhage
Grade 3	Presence of skull fracture Severe soft tissue laceration – resulting in haemorrhage Oedema at impact site Cerebral contusion at impact site
Grade 4	Presence of skull fracture Severe soft tissue laceration/ – resulting in haemorrhage Oedema at impact site SDH on the basal surface of the brain
Grade 5	Presence of skull fracture Severe soft tissue laceration – resulting in haemorrhage Cerebral contusion at impact site SAH surrounding impact contusion SDH on the basal surface of the brain Accessory contusion

Table 5.2: Skull fracture grading system following TBI.

Grade 0	Absence of skull fracture
Grade 1	Hairline skull fracture
Grade 2	Depressed skull fracture resulting in the separation of the coronoid process and fracture of the zygomatic arch
Grade 3	Combination of Grade 1 and 2

5.2.4 Histological Analysis

Following tissue processing (*chapter 2.3.1*), 5 μm thick coronal chapters were cut using a microtome (Leica Biosystems, Australia) from paraffin embedded blocks at 3 cm, 4 cm and 5 cm anteroposterior brain regions. IHC staining was conducted for distribution and levels of AI (APP), myelin microstructure (MBP), and both microglial (IBA-1) and astrocytic (GFAP) activation as markers of neuroinflammation (*chapter 2.3.2*). Slides were scanned digitally using Nanozoomer (Model: 2.0RS) and underwent cellular analyses using NDP.view2 software (v.U12388-01, Hamamatsu, Japan) (*chapter 2.3.3*).

5.2.5 Biochemical Analysis

Biochemical analysis of pro-inflammatory cytokines IL-6, IL-1β and TNF-α was conducted using the serum samples collected at 0 hours, 30 minutes and four hours post-injury, of all animals and then analysed (*chapter 2.4*).

5.2.6 Arterial Blood Pressure Analysis

ABP data was analysed following sham + hypoxia and TBI +/- hypoxia and throughout the four hour monitoring period (*chapter 2.5*).

5.2.7 Head Acceleration and Translation Analysis

Linear and angular impact acceleration and head translation data were provided by our biomechanical engineering collaborators, Dr Claire Jones and Dr Ryan Quarrington of the Adelaide Spinal Research Group at The University of Adelaide. All data were extracted and analysed using custom MATLAB code (v.9.8, R2020a, Mathworks, UK). Peak angular and linear accelerations of the head were described with respect to an ACS of the sheep head (*chapter 2.2.5*). Peak head translations captured by high-speed camera tracking (*chapter 2.2.5*) were additionally calculated with reference to translation of the accelerometer array following impact.

5.2.8 Statistics

All data was analysed using GraphPad Prism® (v.9, GraphPad Software, CA, USA) statistical software. A two and three-way ANOVA followed by a Tukey's post hoc test, was used for ABP analyses as well as basic physiological parameters and histological analysis for APP, MBP, IBA-1 and GFAP within all ROI. ELISA data was analysed using a two-way ANOVA. A paired t-test was used to evaluate the difference between the two peaks in head acceleration for both angular and linear accelerations. Linear regression analysis evaluated the relationship between overall peak angular acceleration and APP+ve number. The relationship between peak head translation and severity of skull fracture was also evaluated via linear regression. Significance level was set at α=0.05, and all data are expressed as mean ± SEM.

5.3 Results

5.3.1 Biomechanical Analyses of Injury – Angular and Linear Head Acceleration

During impact, the head of injured animals underwent both angular and linear head accelerations. Two peaks were observed at the time of impact for both linear and angular acceleration (*for example: see Figs. 1.1A&B – 1.8A&B in Appendix I*) (and this was present in 7/8 cases, with the exception of *JS010*). The initial peak for both angular and linear acceleration occurred on average 5.6 ms following the onset of impact, while the second peak occurred approximately 1.9 ms after the first peak. The resultant angular acceleration was significantly larger in magnitude for the second peak than the first peak in 6/7 cases ($p<0.01$); the resultant linear acceleration was significantly lower for the second peak compared to the first peak in all cases ($p<0.01$) (*Fig. 5.2 A&B*).

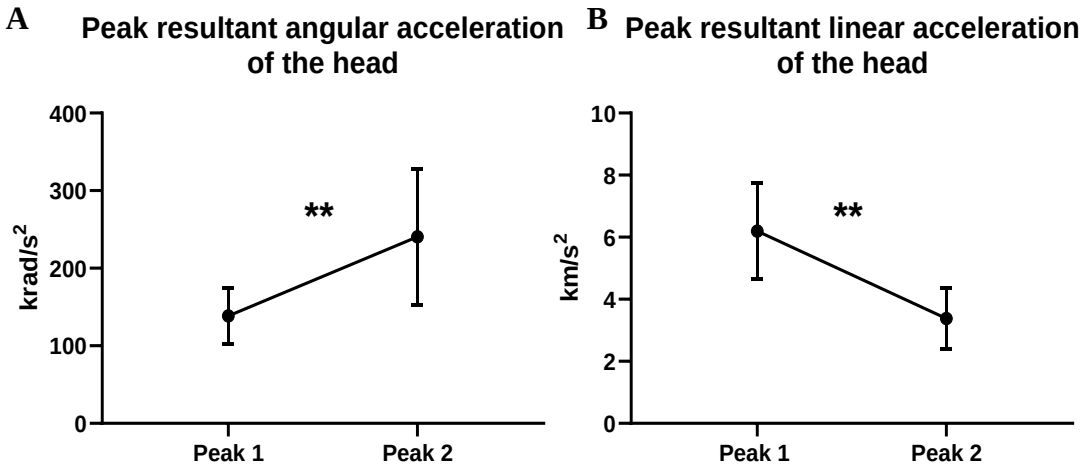

*Figure 5.2: Peak resultant angular accelerations of the head following impact – note the significant increase in angular acceleration from the first to the second acceleration [**p=0.009, (**A**)] and significant decrease in linear acceleration from the first to second peak [**p=0.001, (**B**)].*

The overall peak resultant angular and linear head acceleration was calculated for all injured animals (n=8) and no significant differences were noted between the normoxia and hypoxia groups [n=4/group (angular acceleration: p=0.60, linear acceleration: p>0.99)] (*Fig. 5.3A&B*).

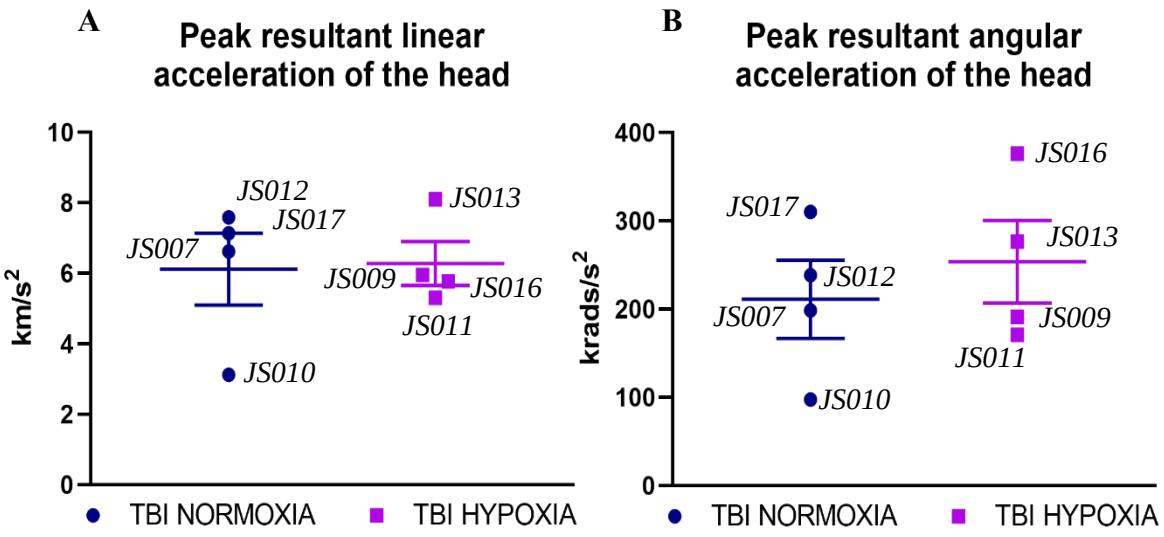

*Figure 5.3: Individual overall peak linear (**A**) and angular (**B**) acceleration values for each injured animal. Note the variability between animals.*

5.3.2 Macroscopic Injury Description

Each of the eight animals subjected to TBI demonstrated vastly different macroscopic injuries (*Table 5.3*). Whilst *JS007, JS010* (TBI + hypoxia) and *JS011* (TBI + normoxia) were categorised into the less severe macroscopic categories of levels 0-2, the remaining five animals all demonstrated more significant macroscopic signs of injury. Specifically, three animals subject to TBI were categorised as level three (TBI + normoxia: *JS009, JS013*; TBI + hypoxia: *JS017*), which included the presence of cerebral contusion on the brain adjacent to the site of impact (*Fig. 5.4A*). Additionally, laceration within the soft tissue resulted in significant haemorrhage, accompanied by severe swelling of the right eye and oedema at the site of impact (*Fig. 5.4B*). *JS012* (TBI + normoxia) was graded at level four, including SDH

over the basal surface of the brain (*Fig. 5.5A&B*). Finally, *JS016* (TBI + hypoxia) was graded at level five, demonstrating significant macroscopic injuries including light SAH overlaying the cerebral contusion as well as accessory contusions on the surface of the cerebellum on the ipsilateral side of the brain (*Fig. 5.5C*).

Table 5.3: Description of macroscopic injury and skull fracture in each animal subject to TBI. These data are presented with reference to the resultant peak angular and linear accelerations of the head in addition to total AI count (discussed in chapter 5.3.5).

Animal	**Skull fracture grading**	**Haemorrhage of soft tissue upon impact**	**Oedema at impact site**	**Impact cortical contusion (*coup*)**	**Focal SAH at impact site**	**Basal sub-dural haematoma (SDH)**	**Accessory contusions**	**Total macroscopic injury grading**	**Total number of APP+ve cells**	**Peak angular acceleration of the head (krad/s^2)**	**Peak linear acceleration of the head (km/s^2)**
JS007	**3**							**1**	602	198.44	6.62
JS009	**2**	●	●	●				**3**	1790	191.21	5.95
JS010	**0**							**0**	1241	97.57	3.12
JS011	**3**	●						**2**	791	170.73	5.30
JS012	**2**	●	●			●		**4**	496	238.58	7.59
JS013	**3**	●	●	●				**3**	1125	276.63	8.10
JS016	**3**	●		●	●	●	●	**5**	1212	376.33	5.77
JS017	**2**	●	●	●				**3**	793	310.17	7.14

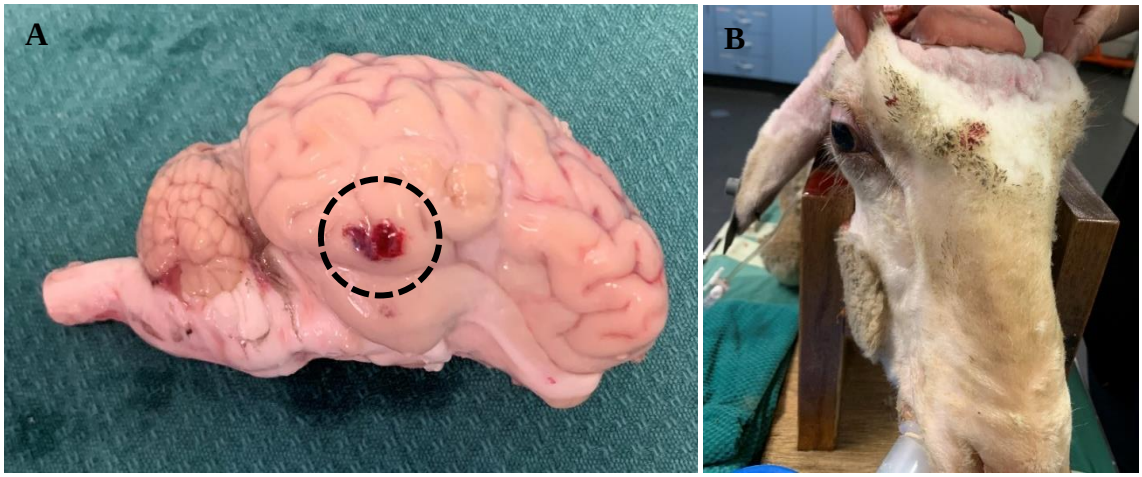

*Figure 5.4: Coup contusion at impact site (**A**), note the outline of the contusion with the black circle. Extensive swelling of the eye on the side of impact post-injury (**B**).*

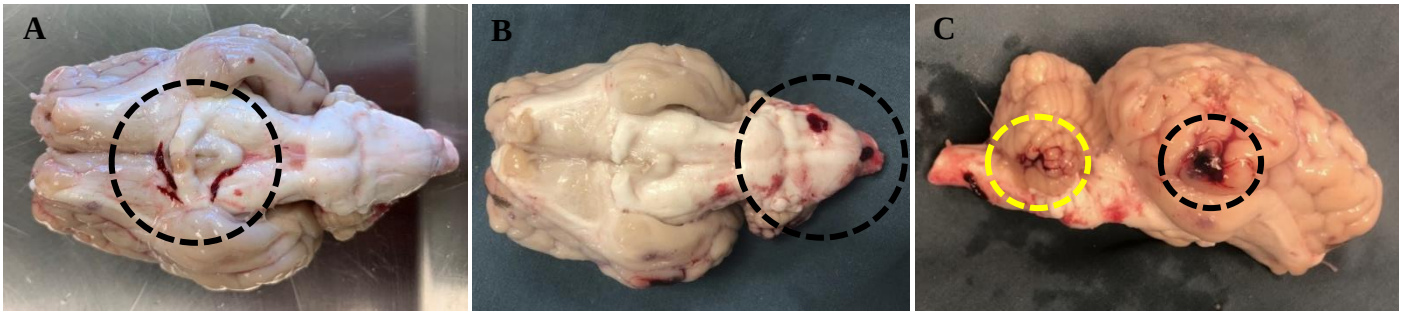

*Figure 5.5: Sub-dural haematoma on the basal surface of the brain following TBI (**A, B**) note the outline in black. Coup cerebellar contusion (note the outline in yellow) and mild SAH overlay surrounding the cerebral contusion (note the outline in black) (**C**). Images demonstrate the ventral surface of the brain (**A**, **B**) and right lateral surface of the brain (**C**).*

5.3.3 Linear Acceleration and Resulting Skull Fracture

The relationship between overall peak resultant linear acceleration values and the severity and presence of skull fracture was evaluated. No relationship was established between linear acceleration and resulting skull fracture severity (*Fig. 5.6*).

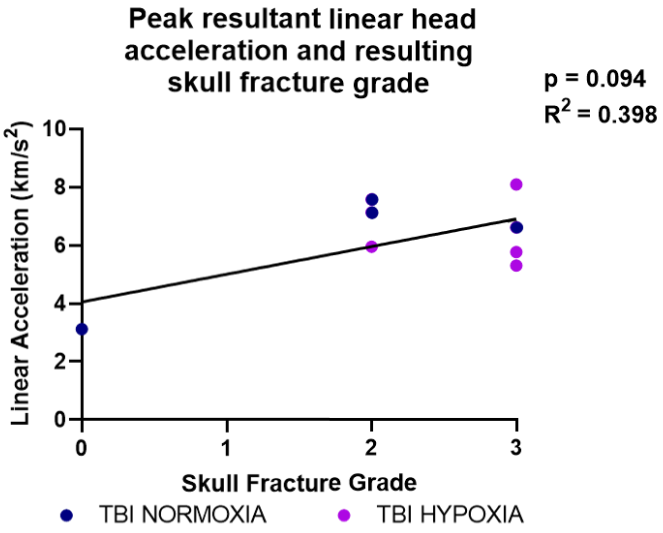

Figure 5.6: Plot of overall peak resultant linear acceleration versus overall skull fracture severity.

5.3.4 Acute Blood Pressure Response

A main effect of both injury ($p<0.001$) and hypoxia ($p<0.001$) led to an immediate significant decrease in BP in the first 13 minutes following injury in all TBI + normoxia, as well as TBI + hypoxia and sham + hypoxia animals compared to sham + normoxia animals, as calculated relative to pre-injury baseline (sham + normoxia: 0±0mmHg, sham + hypoxia: -20.47±3.45 mmHg, TBI + normoxia: -19.98±10.05 mmHg, TBI + hypoxia: -52.49±17.53 mmHg) (*Fig. 5.7*). Post-hoc analysis revealed that animals exposed to TBI + hypoxia demonstrated a significantly lower ABP decrease compared to TBI + normoxia ($p<0.01$) and sham + hypoxia animals ($p<0.01$). ABP returned to baseline levels within 14 minutes post-injury in all injury

groups with the exception of TBI + hypoxia animals which did not recover to baseline levels within the four hour monitoring period. Further to this, the time taken to return to baseline levels was not significantly different between sham + hypoxia and TBI + normoxia groups.

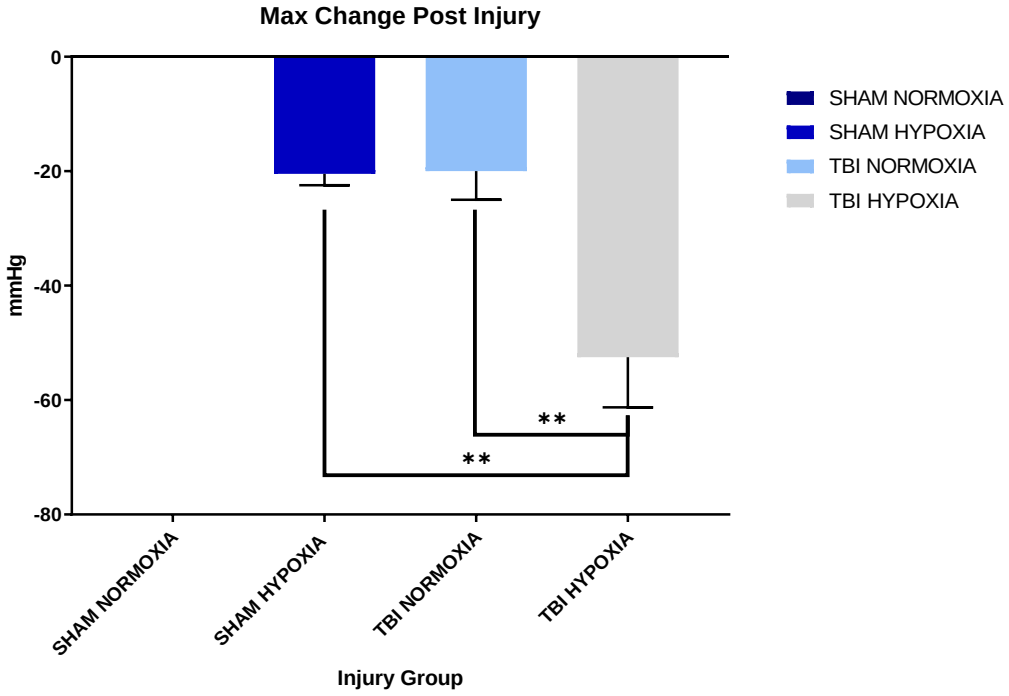

*Figure 5.7: An immediate decrease in BP was seen post-injury. A significant effect of both injury and hypoxia was seen with the TBI + hypoxia group demonstrating a further decrease in ABP post-injury compared to TBI + normoxia (**p=0.005) and sham + hypoxia groups (**p<0.008) (n=3-4 per group, graphs show mean ± SEM).*

5.3.5 Basic Physiological Parameters

Four Hour Monitoring Period

All experimental procedures were carried out without complication and there was no premature mortality or unexpected events in any of the groups. All animals were included in the analysis. Physiological parameters were assessed prior to injury (baseline) and then hourly post-injury. Whilst no significant differences in pO_2 levels were observed, a significant overall effect of

injury was seen to decrease pCO_2 levels ($p<0.05$); however, post-hoc analyses revealed no further differences (*Table 5.4*). Additionally, there was a significant overall effect of hypoxia on pH levels ($p<0.001$) (*Table 5.4*). Post-hoc analyses revealed that sham + hypoxia animals had significantly higher pH levels at two hours post-injury compared to sham + normoxia ($p<0.0001$).

Hypoxic Monitoring Period

Animals exposed to hypoxia underwent physiological monitoring at five minute intervals throughout the 15 minute period of hypoxia, as well as five minutes post-hypoxia. Whilst there was no significance seen within pCO_2 and pH levels, there was a significant effect of time on pO_2 ($p<0.0001$) levels in both sham and injured animals (*Table 5.5*), however these were not significantly different from one another. Both sham and TBI animals had significantly lower levels at 5, 10 and 15 minutes during the hypoxic period as compared to the pre-injury baseline [$p<0.05$ (sham: 5 minutes: -85 mmHg; 10 minutes: -83.7 mmHg; 15 minutes: 65.7 mmHg), (TBI: 5 minutes: 115.7 mmHg; 10 minutes: 119 mmHg; 15 minutes: 123.5 mmHg)], with recovery to baseline by five minutes following the cessation of hypoxia. No main effect of injury was seen in pO_2 levels at any time point post-TBI ($p=0.82$).

*Table 5.4: Data are expressed as pO_2: (mmHg) mean ± SEM, pCO_2: (mmHg) mean ± SEM, pH: (-log[H^+]) mean ± SEM, n = 3-4 per group. Note the significant increase in pH at two hours post-injury in sham + hypoxia animals compared to sham + normoxia animals (****p<0.0001).*

	Sham Normoxia	**Sham Hypoxia**	**TBI Normoxia**	**TBI Hypoxia**
pO_2 *Injury: p=0.057, Hypoxia: p=0.07, Time: p=0.98, Interaction: p=0.99*				
Baseline	179.3 ± 47.2	130.7 ± 8.8	158 ± 14.6	161.5 ± 13.7
1hr post-injury	195 ± 66.1	129 ± 9	141 ± 4.6	147 ± 0.6
2hr post-injury	216 ± 58.8	146 ± 1	124.5 ± 10.5	142.3 ± 0.9
3hr post-injury	180 ± 52.8	142.5 ± 14.5	140.3 ± 4.8	139 ± 3.0
4hr post-injury	204.5 ± 77.2	154 ± 0	127 ± 8	98 ± 0
pCO_2 ***Injury: *p=0.03****, *Hypoxia: p=0.63, Time: p=0.48, Interaction: p=0.49*				
Baseline	43.3 ± 4.8	41.7 ± 2.3	37 ± 1.8	36.3 ± 2.3
1hr post-injury	44.5 ± 0.5	37 ± 1	37.5 ± 1.5	39.3 ± 2.2
2hr post-injury	47.5 ± 2.5	41.5 ± 5.5	39 ± 1.7	38 ± 3.5
3hr post-injury	42.7 ± 0.9	38 ± 4	39.3 ± 1.5	41.8 ± 2.2
4hr post-injury	45 ± 3	42 ± 0	36 ± 2	50 ± 0
pH *Injury: p=0.62,* ***Hypoxia: **p=0.001****, *Time: p=0.11, Interaction: p=0.20*				
Baseline	7.41 ± 0.02	7.45 ± 0.01	7.46 ± 0.01	7.46 ± 0.01
1hr post-injury	7.39 ± 0.04	7.5 ± 0.02	7.49 ± 0.03	7.44 ± 0.01
2hr post-injury	****7.38 ± 0.03	7.72 ± 0.22	7.49 ± 0.02	7.48 ± 0.03
3hr post-injury	7.38 ± 0.04	7.52 ± 0.04	7.47 ± 0.02	7.45 ± 0.01
4hr post-injury	7.36 ± 0.03	7.46 ± 0	7.49 ±0.03	7.43 ± 0

*Table 5.5: Data are expressed as pO_2: (mmHg) mean ± SEM, pCO_2: (mmHg) mean ± SEM, pH: (-log[H^+]) mean ± SEM, n = 3-4 per group. Note the significant main effect of time causing a decrease in pO_2 levels in both sham and TBI animals as compared to pre-injury baseline (**p<0.01, ***p<0.0001, ****p<0.0001) and post-hypoxic levels (, $^{\#}$p<0.05, $^{\#\#}$p<0.001, $^{\#\#\#}$p<0.001, $^{\#\#\#\#}$p<0.0001).*

	Sham Hypoxia	**TBI Hypoxia**
pO_2 *Injury: p=0.82,* ***Time: ****p=<0.0001,** *Interaction: p=0.12*		
Pre-injury Baseline	130.7 ± 8.8	161.5 ± 13.7
Hypoxia - 5 mins	*** 45.7 ± 3.8 ###	**** 45.8 ± 2.7 ####
Hypoxia - 10 mins	*** 47 ± 5.3 ##	**** 42.5 ± 1.3 ####
Hypoxia - 15 minutes	** 65 ± 30.5 #	**** 38 ± 2.4 ####
5 mins post-hypoxia	118.3 ± 8.5	126.5 ± 3.5
pCO_2 *Injury: p=0.09, Time: p=0.86, Interaction: p=0.92*		
Pre-injury Baseline	41.7 ± 2.3	36.25 ± 2.3
Hypoxia – 5 mins	37.7 ± 1.5	35.8 ± 2.9
Hypoxia – 10 mins	38.3 ± 1.9	37 ± 1.9
Hypoxia – 15 minutes	39.3 ± 2.4	35.2 ± 2.2
5 mins post-hypoxia	37 ± 1	37.5 ± 3.2
pH *Injury: p=0.07, Time: p=0.21, Interaction: p=0.59*		
Pre-injury Baseline	7.45 ± 0.01	7.46 ± 0.01
Hypoxia - 5 mins	7.49 ± 0.01	7.46 ± 0.01
Hypoxia - 10 mins	7.5 ± 0.01	7.47 ± 0.01
Hypoxia - 15 minutes	7.49 ± 0.02	7.48 ± 0.01
5 mins post-hypoxia	7.46 ± 0.03	7.45 ± 0.01

5.3.6 Axonal Injury

A heat map representation of ROI analysed with number of APP+ve lengths or bulbs is shown in *Fig. 5.8*. Regional AI analysis showed there were minimal regional differences in the number of APP+ve lengths or bulbs. As there were no differences noted between the left and right hemispheres and as such data is presented with the left and right hemispheres combined (*5.9 A&B*), with no significant effect of injury or hypoxia detected within any of the analysed brain regions [(injury: corpus callosum: p=0.27; cingulum: p=0.20; internal capsule: p=0.42; striatum: p=0.12; thalamus: p=0.97; cerebral cortex: p=0.32) (hypoxia: corpus callosum: p=0.2; cingulum: p=0.74; internal capsule: p=0.58; striatum: p=0.13; thalamus: p=0.25; cerebral cortex: p=0.24)] (*Fig. 5.9*). Representative images of APP staining, with quantification of the number of APP+ve immunoreactive bulbs and lengths can be seen in *Fig. 5.5A* and *B*.

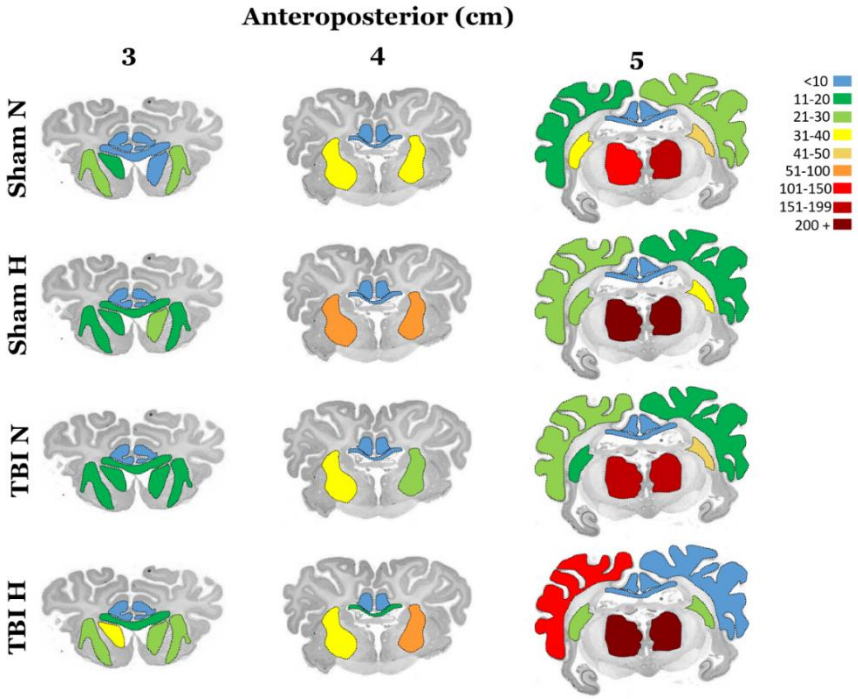

Figure 5.8: Heat map demonstrating the expression and distribution of AI in white matter tracts and grey matter regions across three, 1 cm separated anteroposterior brain regions. Expression of APP+ve cells are shown within both the left and right hemispheres. Scale indicates the number of APP+ve lengths or bulbs within the region. The highest levels of AI were discovered within the internal capsule and thalamus. N = normoxia, H = hypoxia.

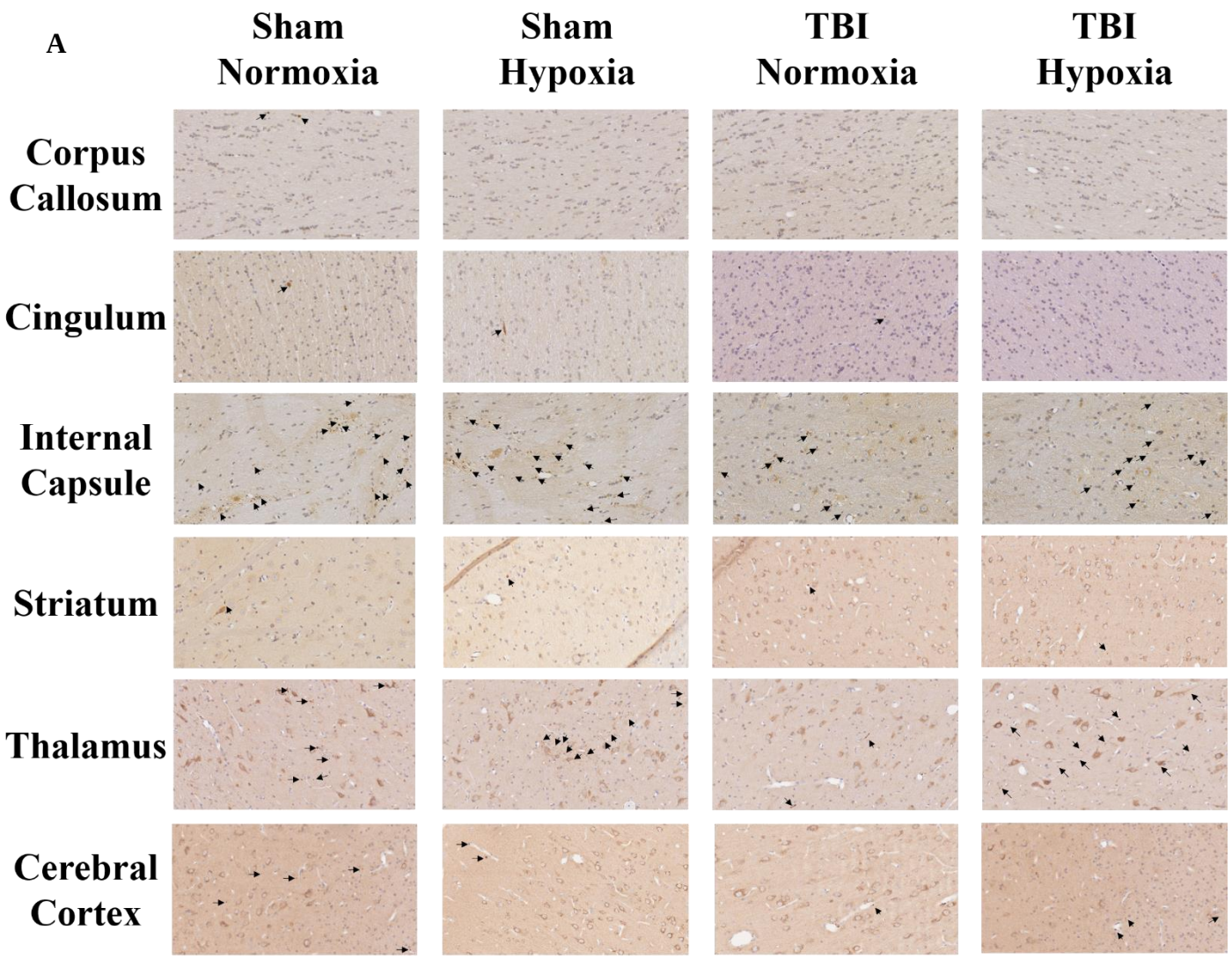

Figure 5.9A: *Representative images of APP IHC from the ROI. Black arrows indicate axonal profiles. Scale = 50 µm.*

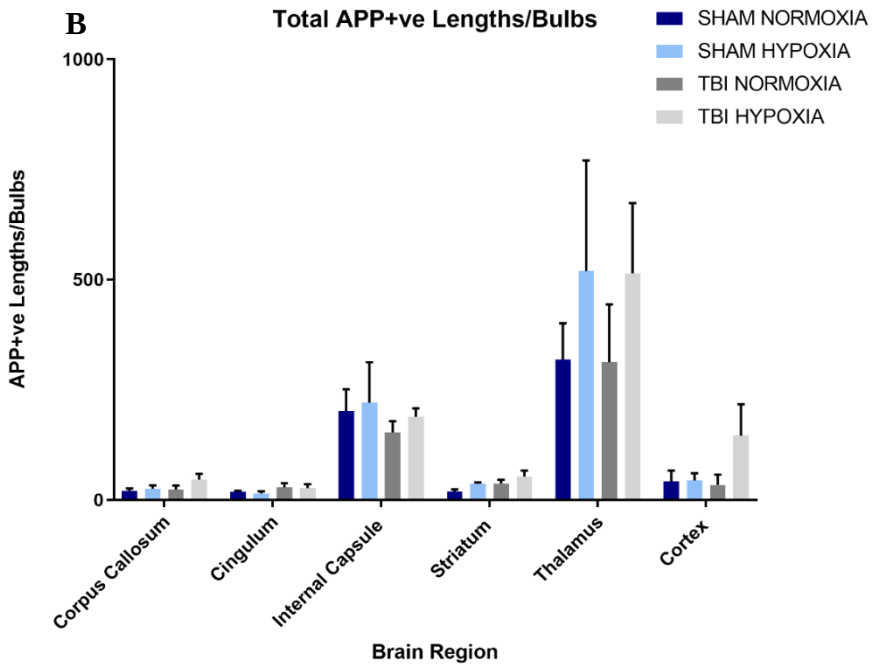

Figure 5.9: Counts of the total number of APP+ve lengths and bulbs.

5.3.7 Microstructural integrity

Myelination and, hence microstructure were assessed via IHC analyses of MBP staining. Representative images of MBP+ve immunoreactivity are presented in *Fig 5.10*, as well as analyses of the total length of MBP+ve fibres (*Fig. 5.11A*), coherence of MBP+ve fibres (*Fig. 5.11B*), the % of MBP+ve area (*Fig. 5.11C*) and kurtosis of MBP+ve fibres (*Fig. 5.11D*).

Analysis of the total length of MBP+ve fibre staining found a significant main effect of hypoxia ($p<0.05$), but not injury ($p=0.08$) within the corpus callosum and cortex. Post-hoc analyses found TBI + hypoxia animals to have increased fibre length as compared to TBI + normoxia animals ($p<0.05$), however no difference was noted between sham + hypoxia and sham + normoxia animals ($p=0.97$) (*Fig. 5.11A*). Finally, a significant interaction was found within the thalamus ($p<0.05$), but no main effect of injury ($p=0.90$) or hypoxia ($p=0.85$). Post-hoc analyses did not reveal any further differences (*Fig. 5.11A*). No main effects of injury or

hypoxia were noted in any of the other regions examined [(injury: cingulum: p=0.08; internal capsule: p=0.07; striatum: p=0.85) (hypoxia: cingulum: p=0.09; internal capsule: p=0.11; striatum: p=0.40)]

Examination of coherence of the MBP+ve fibres found a significant main effect of injury ($p<0.02$), but not hypoxia (p=0.06) causing increased fibre coherency within the cortex. No main effects of injury nor hypoxia were noted in any of the other regions examined [(injury: corpus callosum: p=0.94; cingulum: p=0.69; internal capsule: p=0.68; striatum: p=0.48; thalamus: p=0.66) (hypoxia: corpus callosum: p=0.36; cingulum: p=0.74; internal capsule: p=0.19; striatum: p=0.7; thalamus: p=0.82)] (*Fig. 5.11B*).

Finally, no main effects of hypoxia or injury were noted with analysis of % of MBP+ve area [(injury: corpus callosum: p=0.85; cingulum: p=0.38; internal capsule: p=0.57; striatum: p=0.87; thalamus: p=0.32; cerebral cortex: p=0.98) (hypoxia: corpus callosum: p=0.65; cingulum: p=0.63; internal capsule: p=0.97; striatum: p=0.16; thalamus: p=0.33; cerebral cortex: p=0.13)] (*Fig. 5.11C*), or kurtosis of fibres [(injury: corpus callosum: p=0.96; cingulum: p=0.17; internal capsule: p=0.52; striatum: p=0.49; thalamus: p=0.15; cerebral cortex: p=0.89) (hypoxia: corpus callosum: p=0.58; cingulum: p=0.77; internal capsule: p=0.39; striatum: p=0.44; thalamus: p=0.49; cerebral cortex:0.99)] (*Fig. 5.11D*).

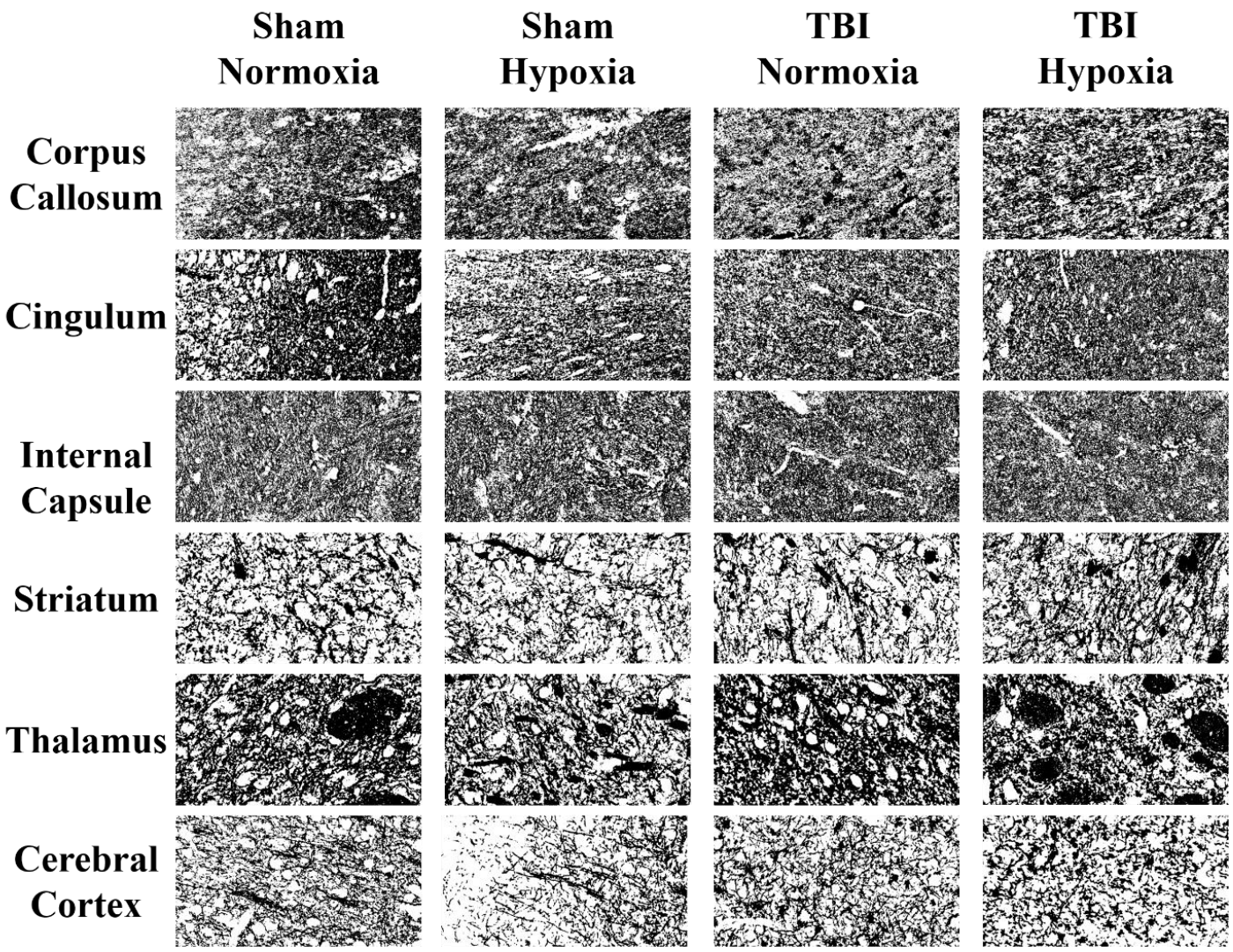

<u>Figure 5.10:</u> Representative images of MBP IHC from the ROI following removal of background, thresholding and creation of a binary image.

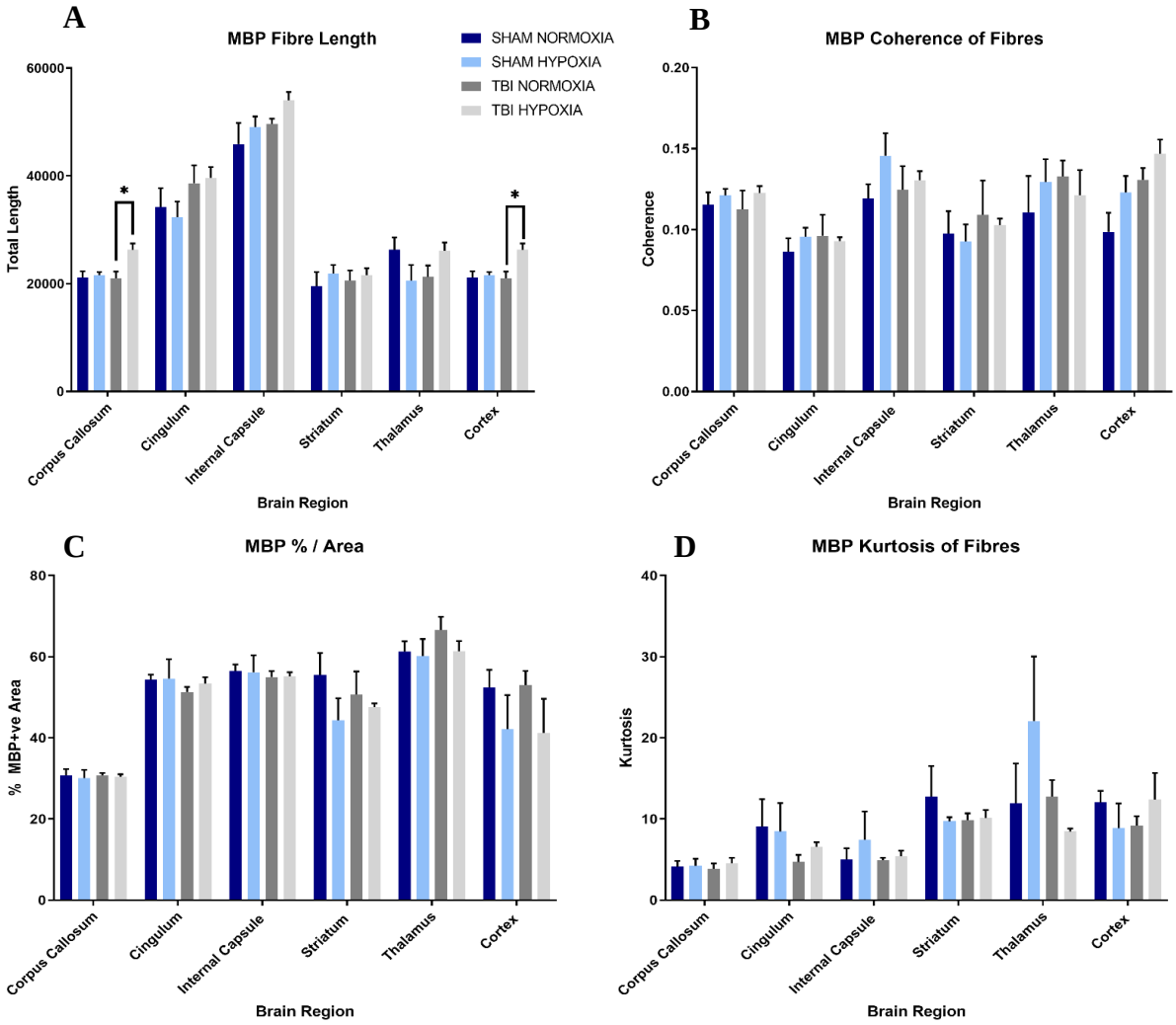

*<u>Figure 5.11:</u> Evaluation of the effects of TBI on expression of MBP as examined via total myelin length (A), coherency (B), % area stained (**C**) and kurtosis of fibres (**D**). Scale bar = 50 µm. Image representative of n = 3-4/group. ***** indicates significantly different compared to TBI + normoxia (* = p<0.05, # = p<0.05). (n=3-4 per group, graphs show mean ± SEM).*

5.3.8 Acute Neuroinflammatory Response

Microglia

A heat map representation of the number of IBA-1+ve microglia per ROI is shown in *Fig. 5.12.* Representative images of IBA-1 immunoreactivity are presented in *Fig. 5.13A*, as well as analyses of the number of IBA-1+ve cells (*Fig. 5.13B*) and % of IBA-1+ve area (*Fig. 5.13C*). Although there were no significant differences noted in expression of APP, regional differences were noted as a result of microglial proliferation. Assessment of microglial number noted a significant interaction ($p<0.05$) and a main effect of injury ($p<0.05$), but not of hypoxia ($p=0.18$) within the thalamus. Post hoc-analysis found a significant decrease in microglial number in TBI + normoxia animals as compared to sham + normoxia animals ($p<0.01$) (*Fig. 5.13B*). A significant main interaction was also noted in the internal capsule ($p<0.05$), but no main effect of injury ($p=0.24$) or hypoxia ($p=0.48$) (*Fig. 5.13B*) Post-hoc analysis did not reveal any further differences. No significant main effects of hypoxia or injury on number of IBA-1+ve cells were seen in any other ROI analysed [(injury: corpus callosum: $p=0.18$; cingulum: $p=0.38$; striatum: $p=0.85$; cerebral cortex: $p=0.36$) (hypoxia: corpus callosum: $p=0.53$; cingulum: $p=0.58$; striatum: $p=0.38$; cerebral cortex: $p=0.06$)].

No significant main effects of hypoxia or injury were detected in the % of IBA-1+ve area in any of the analysed ROI [(injury: corpus callosum: $p=0.94$; cingulum: $p=0.56$; internal capsule: $p=0.54$; striatum: $p=0.37$; thalamus: $p=0.93$; cerebral cortex: $p=0.76$) (hypoxia: corpus callosum: $p=0.65$; cingulum: $p=0.95$; internal capsule: $p=0.23$; striatum: $p=0.70$; thalamus: $p=0.12$; cerebral cortex: $p=0.50$)], (*Fig. 5.13C*).

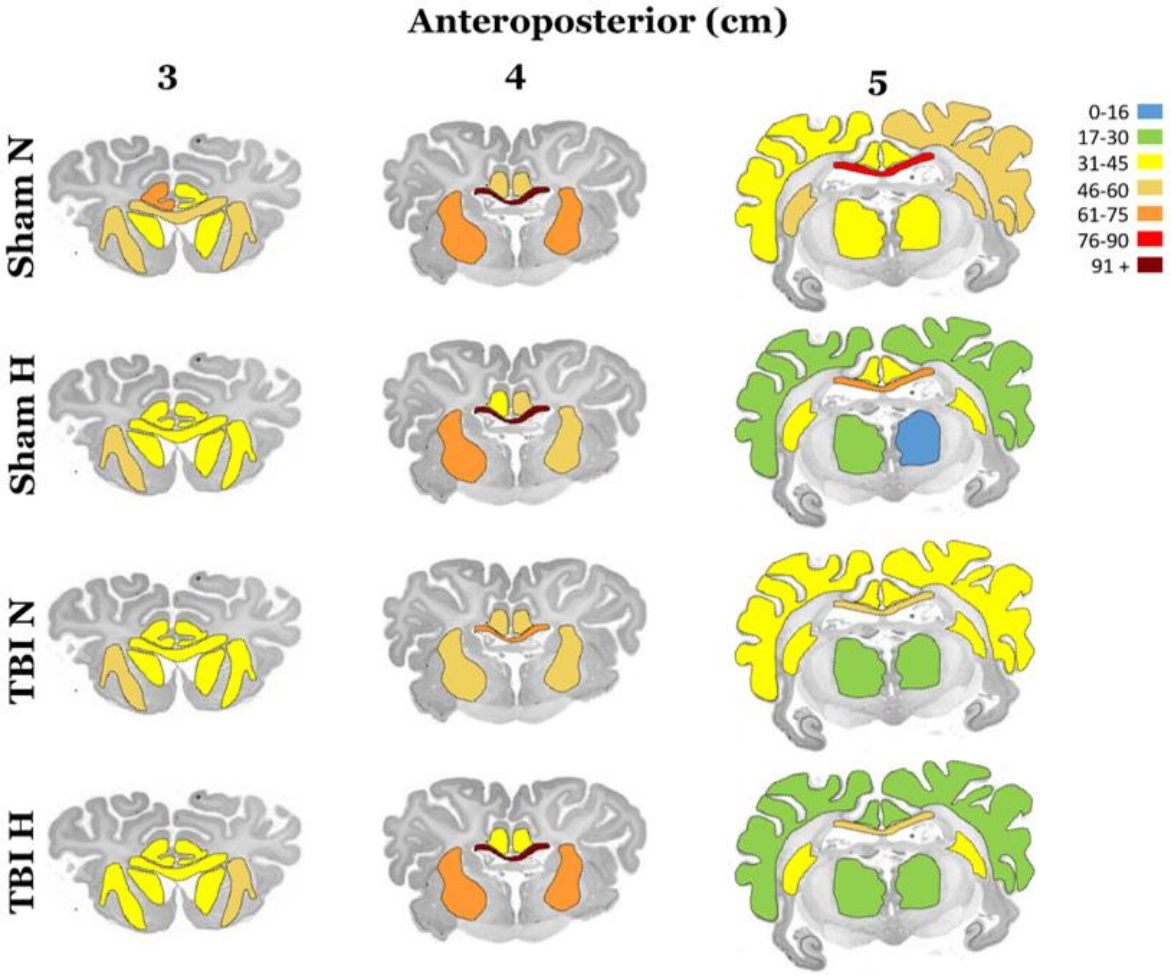

<u>Figure 5.12:</u> Heat map demonstrating the expression and distribution of microglial number in white matter tracts and grey matter regions across three, 1 cm separated anteroposterior brain regions. Scale indicates the number of IBA-1+ve cells within the region. N = normoxia, H = hypoxia. Values calculated as the average of n = 3-4 per group.

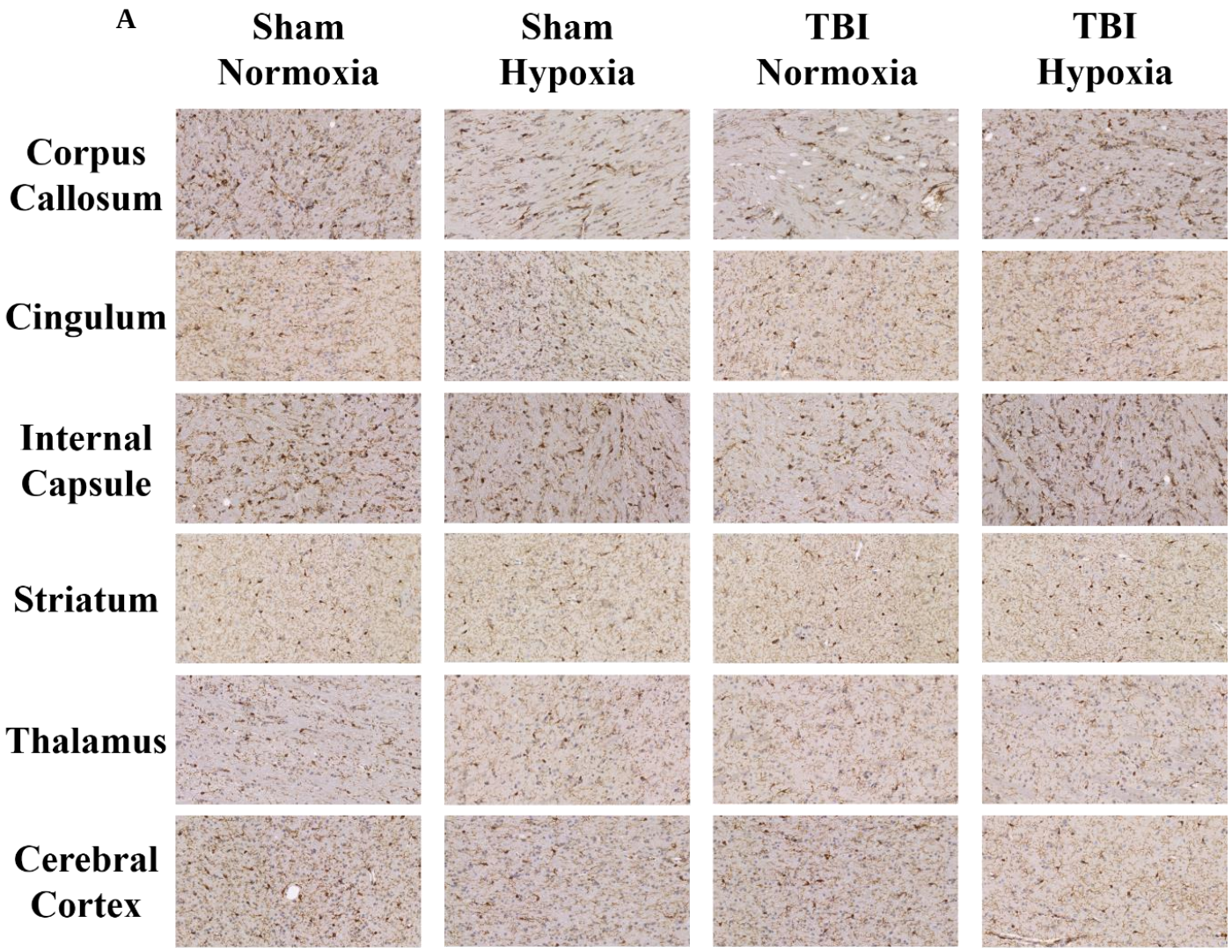

Figure 5.13A: Representative images of IBA-1 IHC from analysed ROI. Scale bar = 50 µm. Image representative of n = 3-4/group.

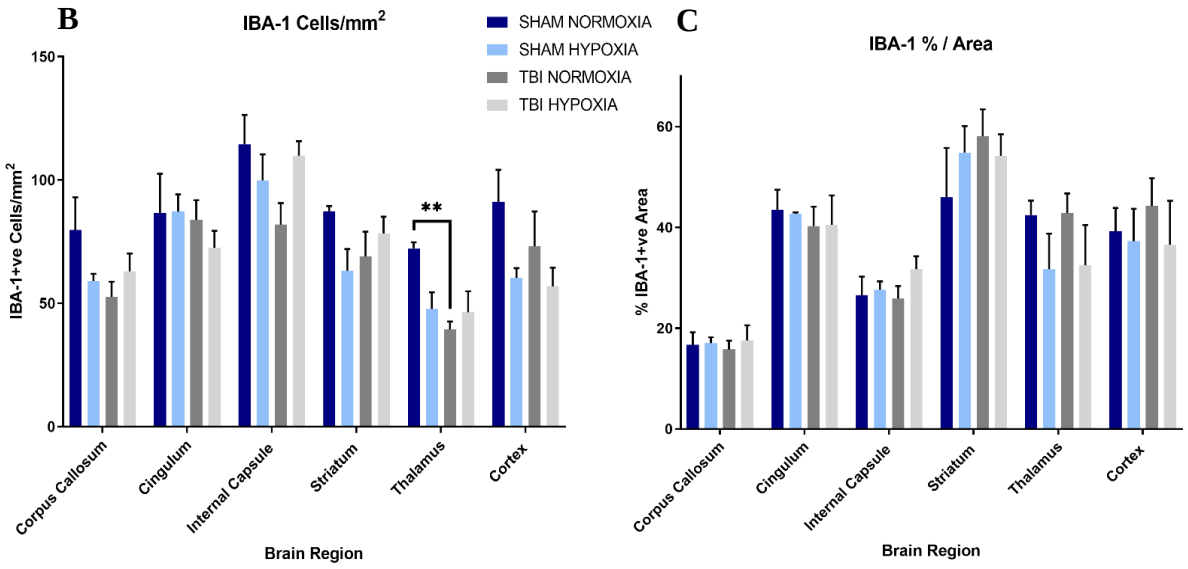

*Figure 5.13: Image representative of n = 3-4/group (**A**), with counts of the number of IBA-1+ve cells/mm2 (**B**) and % of IBA-1+ve area (**C**). * indicates significantly different compared to sham + normoxia (**p<0.01), graphs show mean ± SEM).*

Astrocytes

A heat map representation of the number of GFAP+ve astrocytes per ROI is shown in *Fig. 5.14*. Representative images of GFAP immunoreactivity are presented in *Fig. 5.15A*, as well as analyses of the number of GFAP+ve cells (*Fig. 5.15B*) and % of GFAP+ve area (*Fig. 5.15C*). Indeed, results presented here mimic those seen within microglial proliferation with regional significant differences noted between experimental groups. A significant main effect of hypoxia ($p<0.05$), but not injury ($p=0.11$) was noted within the internal capsule, with post-hoc analyses finding sham + hypoxia animals to have an increase in GFAP+ve cell number as compared to sham + normoxia ($p<0.05$), however no differences were noted between TBI + hypoxia and TBI + normoxia animals ($p=0.97$) (*Fig. 5.15B*). Additionally, a significant main interaction was noted within the striatum ($p<0.05$), with post-hoc analyses finding TBI + hypoxia animals to have an increase in the % of GFAP+ve area as compared to TBI + normoxia

animals ($p<0.05$). However, no main effect of injury ($p=0.82$) or hypoxia ($p=0.18$) was observed (*Fig. 5.15C*). No other main effects of injury nor hypoxia were found in any of the other regions for both GFAP+ve cell number [(injury: corpus callosum: $p=0.83$; cingulum: $p=0.73$; striatum: $p=0.75$; thalamus: $p=0.18$; cerebral cortex: $p=0.89$) (hypoxia: corpus callosum: $p=0.26$; cingulum: $p=0.16$; striatum: $p=0.17$; thalamus: $p=0.35$; cerebral cortex: $p=0.33$)] and GFAP % area [(injury: corpus callosum: $p=0.73$; cingulum: $p=0.99$; internal capsule: $p=0.70$; thalamus: $p=0.79$; cerebral cortex: $p=0.53$) (hypoxia: corpus callosum: $p=0.75$; cingulum: $p=0.50$; internal capsule: $p=0.14$; thalamus: $p=0.60$; cerebral cortex: $p=0.70$)].

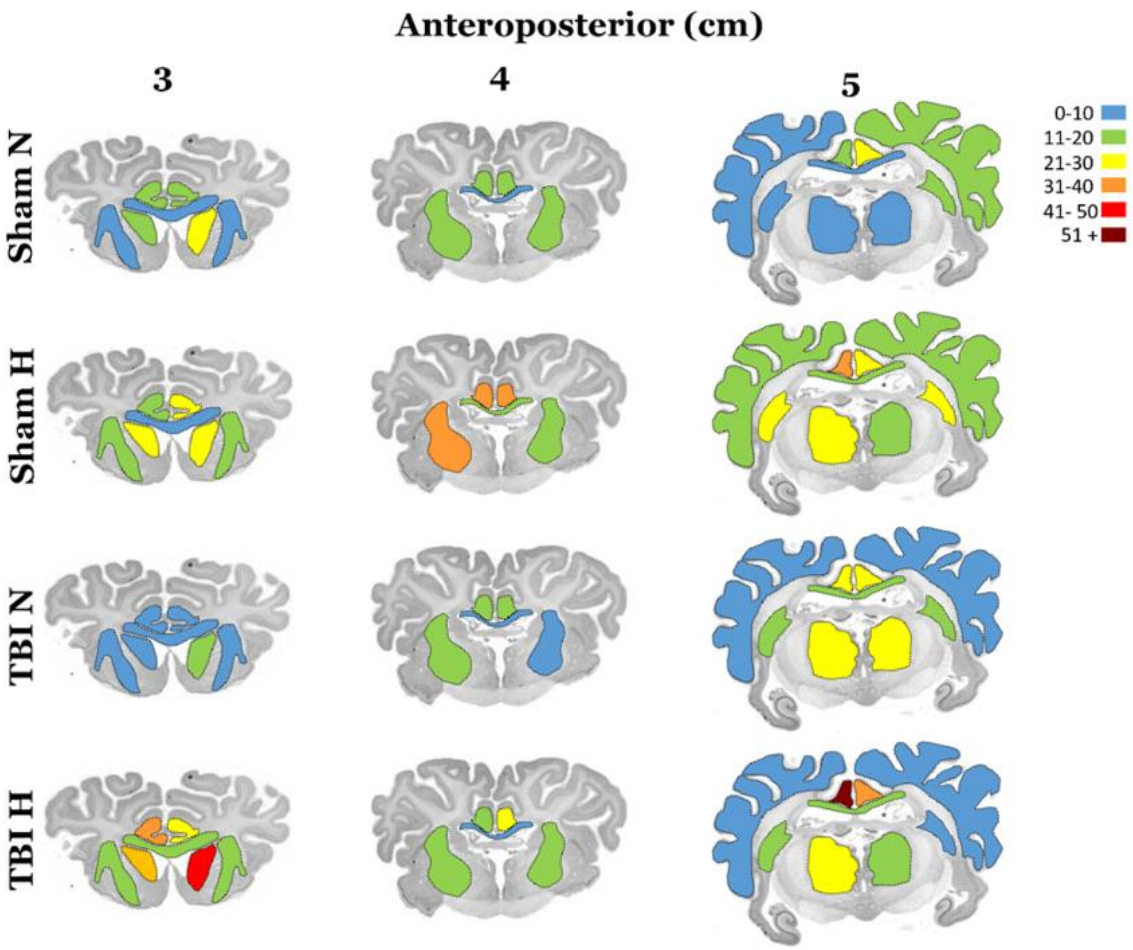

<u>Figure 5.14:</u> Heat map demonstrating the expression and distribution of astrocytes in white matter tracts and grey matter regions across three, 1 cm separated anteroposterior brain regions. Scale indicates the number of GFAP+ve cells within the region. N = normoxia, H = hypoxia.

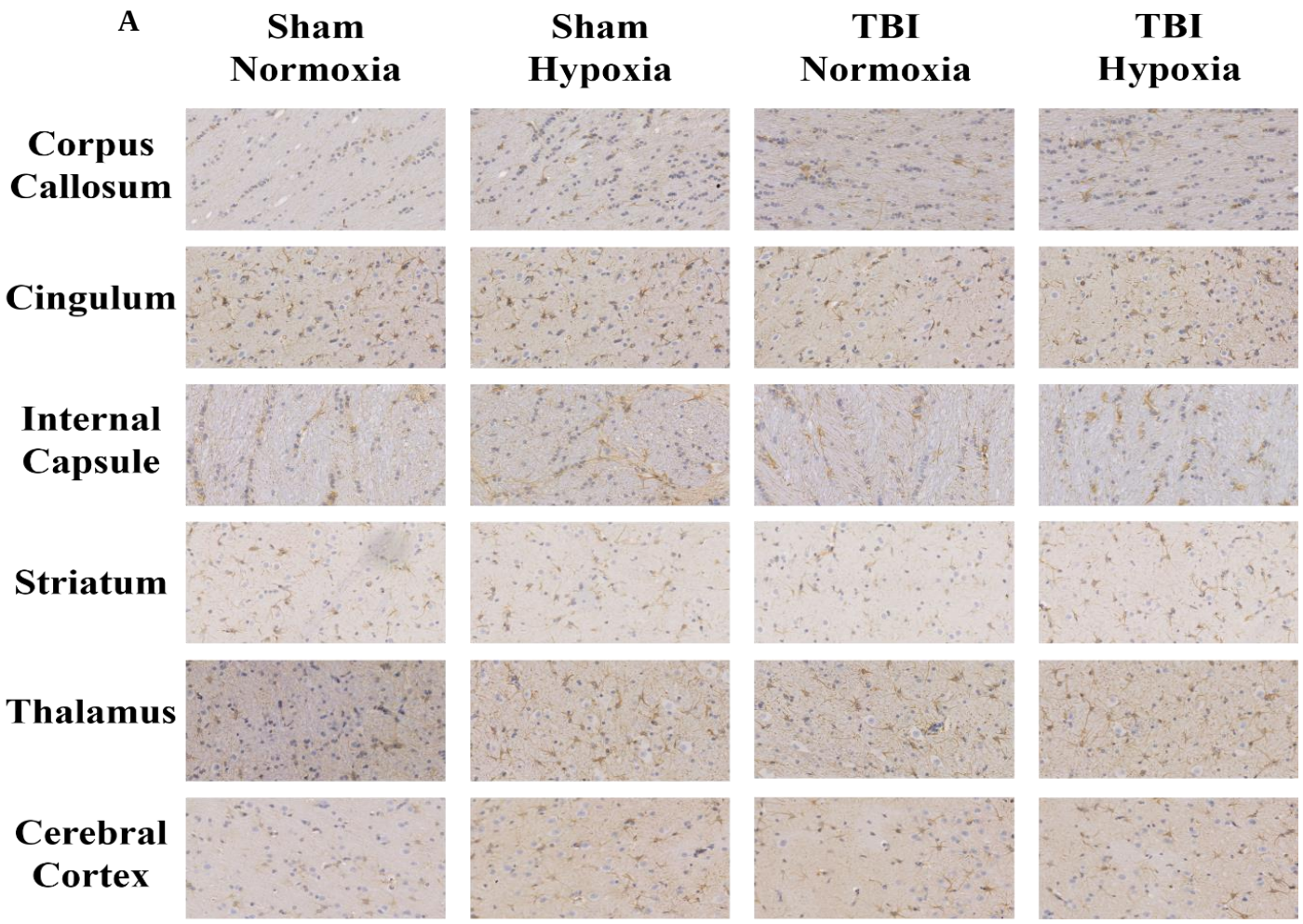

Figure 5.15A: Representative images of GFAP IHC from analysed ROI. Scale bar = 50 µm. Image representative of n = 3-4/group.

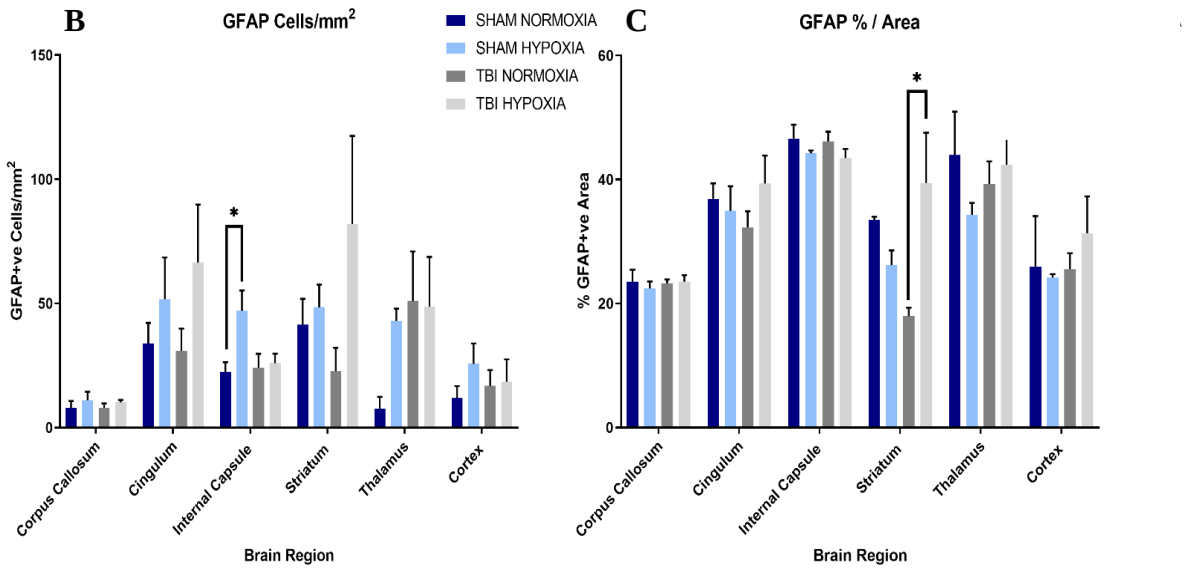

*<u>Figure 5.15:</u> Counts of the number of GFAP+ve cells/mm2 (**B**) and % GFAP+ve area (**C**). * indicates significantly different compared to sham + normoxia (*=p<0.05) (**B**) or TBI + normoxia (*=p<0.05) (**C**), graphs show mean ± SEM.*

5.3.9 Acute Peripheral Inflammatory Response

Peripheral inflammation was assessed within all animals in conjunction with the IHC assessment of neuroinflammation. Serum samples collected before injury and at 30 minutes and four hours post-injury were analysed for the pro-inflammatory cytokines IL-6, IL-1β and TNF-α using ELISA (*chapter 2.4*). Results (*Fig. 5.16 A-C*) are expressed as % change from pre-injury baseline levels. No significant main effect of injury was seen for any of the cytokines investigated, but a significant main effect of hypoxia was noted for both IL-6 ($p<0.05$) and TNF-α ($p<0.01$). No interaction (hypoxia x time; hypoxia x injury; time x hypoxia x injury) was found for either IL-6 or TNF-α (*Fig. 5.16C*).

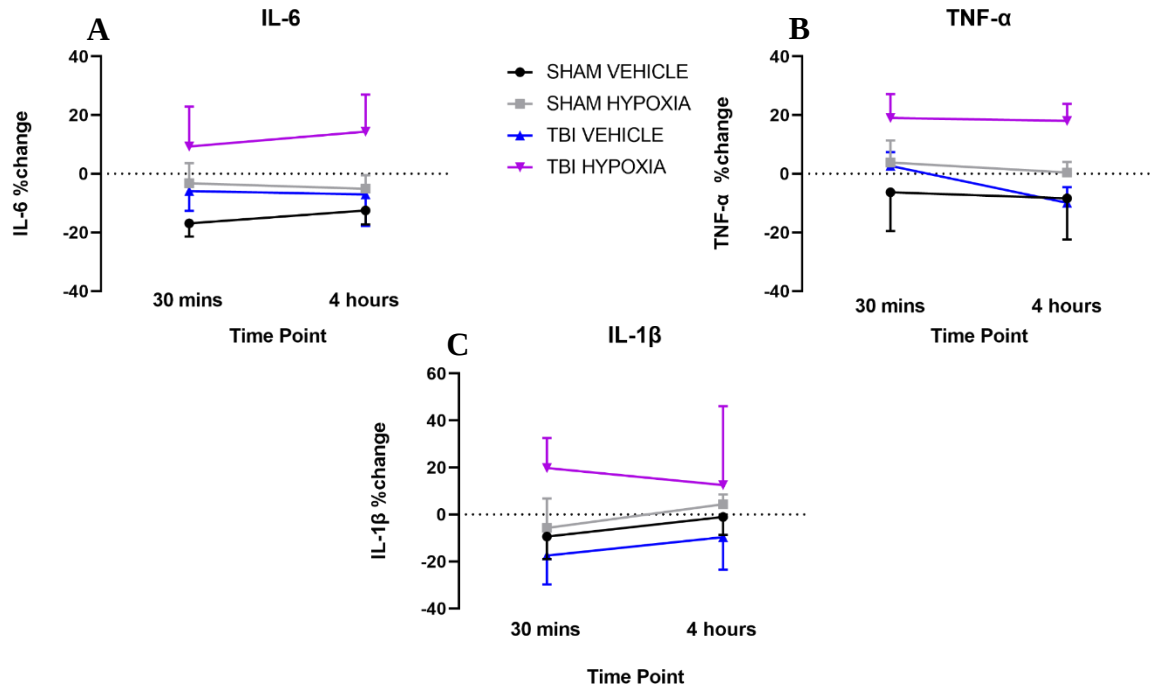

*Figure 5.16: A significant main effect of hypoxia was seen in IL-6 and TNF-α levels: IL-6. [*p=0.04, (**A**)] and TNF-α [**p=0.009, (**B**)], but not injury (IL-6: p=0.09; TNF-α: p=0.09) or time (IL-6: p=0.76; TNF-α: p=0.50). No main effect of injury, time or hypoxia was seen for IL-1β (**C**) (n=3-4 per group, graphs show % change in serum expression compared to pre-injury baseline levels). Data expressed as mean ± SEM.*

5.3.10 Head Acceleration and resulting DAI

The relationship between overall peak resultant angular acceleration values and the total combined number of APP+ve cells within the injured brains was evaluated. No relationship was observed between either angular or linear acceleration and resulting levels of AI (*Fig. 5.17A&B*).

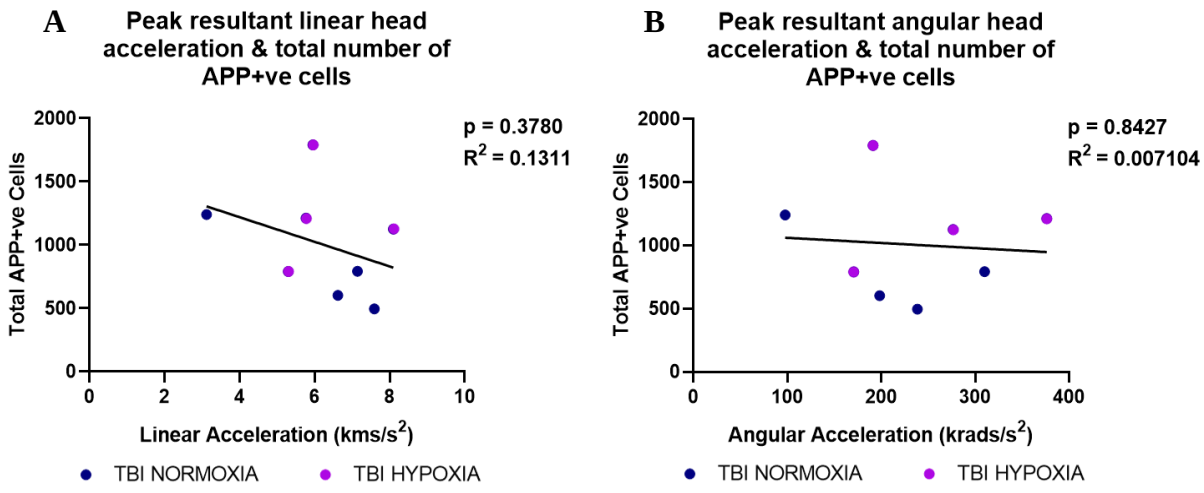

*Figure 5.17: Plot of overall peak resultant angular (**A**) and linear accelerations (**B**), versus total number of APP+ve cells noted in the ROIs evaluated in the injured brain.*

5.4 Discussion

This study aimed to investigate whether the use of a 21-charge, in conjunction with a 15 minute post-injury period of hypoxia, would cause marked DAI production, and whether such DAI would correlate with the peak angular and linear head accelerations generated following the onset of impact.

It was clear from the results of this study that TBI alone or TBI with hypoxia using this injury model was insufficient to produce significant DAI, marked change in myelin microstructure or drive changes in cell number of microglia and astrocytes, nor result in considerable peripheral cytokine expression. However, injury was associated with an acute decrease in ABP, which recovered in TBI + normoxic, but not TBI + hypoxic animals. Despite the paucity of microscopic pathology seen within injured animals compared to shams, substantial macroscopic pathologies were observed in >87% (7/8) animals subject to TBI, including the presence of contusions, SDH and SAH, as well as depressed skull fracture at the site of impact. Whilst no correlation was noted between the amount of DAI and the resultant peak angular

head acceleration, the magnitude of angular acceleration produced in this model was comparable to previous work where marked DAI was produced (Anderson, et al. 2003). No relationship was established between the severity of skull fracture and resultant peak linear acceleration values.

ABP response

Although the literature suggests that an acute hypertensive response is typical following TBI, an immediate significant decrease in ABP was observed in all injury groups following either hypoxia, TBI or TBI with PTH. As discussed in chapter 4.4, the potential mechanisms for an acute immediate decrease in ABP following TBI are poorly addressed in the literature but could be resultant of dysregulation of the ANS (Esterov & Greenwald 2017; McDonald et al. 2020; Pertab et al. 2018). However, this does not address the acute decrease in ABP in animals exposed to hypoxia. Interestingly, a rodent study evaluating the effects of PTH following TBI identified significant decreases in MABP, early after hypoxia induction at 15 minutes, in both hypoxia and TBI rats exposed to PTH compared to either sham animals or their own basal levels prior to hypoxic exposure (Hellewell et al. 2010).

Impact biomechanics

Experimental models have shown that the most typical hallmarks of sTBI, such as SAH, SDH and DAI, are most commonly caused by angular head acceleration (Gennarelli, Thibault & Ommaya 1972; Gennarelli, et al. 1987; Ono et al. 1980). In the human brain, peak resultant magnitudes of angular impact accelerations of approximately 7 krad/s^2 and 18 krad/s^2 are required in order to cause concussive and severe DAI respectively (Ommaya, Goldsmith & Thibault 2002; Ommaya et al. 1967). Production of DAI within the brain is largely dependent on the size and weight of the brain tissue (Cullen et al. 2016). Increased brain mass is associated with smaller thresholds for tissue strain, and therefore higher magnitudes of angular

accelerations are required to produce comparable DAI in smaller brains (Cullen et al. 2016; Ommaya, Goldsmith & Thibault 2002; Ommaya & Hirsch 1971; Ommaya et al. 1967). Large animal models of severe impact acceleration TBI are scarce in the literature; however, non-impact models of head acceleration in both non-human primates and pigs have demonstrated angular acceleration levels of 28–59 krad/s^2 to result in concussive DAI (Cullen et al. 2016; Ommaya et al. 1967). Although average peak angular head accelerations of 232.5 krad/s^2 were produced in this study, there was a lack of DAI as evidenced by APP+ve immunostaining. However, previous work using the ovine impact acceleration model of TBI has reported an average angular acceleration range of 81–227 krad/s^2 whilst also producing marked DAI (Anderson, et al. 2003). As previously mentioned, the presence of two angular acceleration peaks was noted in this study, with the second being greater, and importantly this was not noted in the work of Anderson (Anderson, et al. 2003). It is thought that the skull fracture seen in this study could have potentially dissipated the energy being transmitted to the brain tissue, and that the initial peak in angular acceleration as a result of the onset of impact could be the determinant for the severity of DAI. Although the magnitude of both peaks of angular acceleration generated in this study are comparable to that of Anderson's study, therefore this would require further biomechanical probing to confirm.

In this study, animals were impacted laterally, which produces higher contact forces (due to proximity of the entire surface of the vector contacting the head), and larger linear accelerations of the head, increasing the stresses in the skull bone and therefore the risk of skull fracture (Kleiven 2013). Mean fracture loads of 3.5–3.6 kN have been reported for impact at the temporoparietal area of the human skull (Allsop et al. 1988; Nahum et al. 1968). These can be related to linear acceleration of the head through Newton's second law (Force $_{net}$ = mass x acceleration) (Kleiven 2013). A 5% risk of temporoparietal skull fracture has been estimated to occur with peak linear accelerations of 1.8 km/s^2 and 40% risk for peaks of 2.5 km/s^2 (Mertz,

Prasad & Irwin 1997). Average peak resultant linear accelerations generated within this study were 6.2 km/s^2, therefore being a strong predictor of skull fracture, which occurred in >87% (7/8) cases in this study. As mentioned previously, a smaller second peak in linear acceleration was observed, of approximately 3.2 km/s^2, which still exceeds the threshold for skull fracture suggesting a second skull fracture could have occurred. Peak resultant linear accelerations generated following impact in Anderson's work ranged from 7-18 km/s^2, which far exceed the linear accelerations produced in this study (Anderson, et al. 2003). A crucial difference between Anderson's work and this study was the use of a captive bolt tip that was both different in shape and material. The steel bolt itself in this study was flat in design in comparison to a steel mushroom shaped tip used in all previous ovine impact acceleration work (Anderson, et al. 2003; Byard et al. 2012; Lewis, et al. 1996; Van den Heuvel, Blumbergs, et al. 2000; Van den Heuvel et al. 1999; Van den Heuvel et al. 1998; Vink, Bahtia & Reilly 2008; Vink, Gabrielian & Thornton 2017). The convex silicone cover concealing the captive bolt in this study demonstrated a thick outer wall and a thin pliable centre, whilst no such cover was used in the work of Anderson. The single peak in linear acceleration seen in Anderson's study could be explained by the domed shape of the steel captive bolt tip, contacting the skull upon impact, and causing fracture. In contrast the two peaks in linear acceleration seen in this study could be explained as follows: at the high speed of impact, the *soft* outer rim of the silicone tip cover could be quite *hard*, and the two linear acceleration peaks are caused by initial contact with the rim of the silicone cover and then artefact from the flat face of the steel tip protruding through the thin centre of the convex silicone cover and making secondary contact with the skull, therefore causing further fracture. The silicone cover also could have absorbed partial impact energy, therefore reducing the magnitude of linear acceleration seen in this study compared to the accelerations observed in Anderson's work (Anderson, et al. 2003). Furthermore, partial impact energy could also be being absorbed during the skull fractures themselves, which could

possibly reduce the energy being transmitted to the brain tissue (Ono et al. 1980; Ren et al. 2020). Both clinical and simulation studies have suggested skull fracture may reduce the risk of diffuse brain injury under medium and high velocities, while increasing the risk of contusion under high-impact velocity (Ren et al. 2020; Yavuz et al. 2003), which support the findings in this study. Duration as well as magnitude of acceleration have also been shown to contribute to severity of head injury (*e.g.* the HIC15 head injury criteria) (Mariotti 2019). Indeed, skull fracture was present in animals injured in this study as well as those injured in work by Anderson *et.al.* (2003); however, the lower magnitude of linear acceleration seen in both peaks following impact in this study as compared to Anderson's study could explain lack in APP pathology seen (Anderson, et al. 2003).

As mentioned above, 1/8 animals (*JS010*) subject to injury did not demonstrate signs of macroscopic injury or skull fracture. It is proposed this is as a result of the positioning of the head within the cervical sling being misaligned with the spine, and therefore restraining the range of motion of the head following the onset of impact. This meant that the muzzle/barrel of the impactor wasn't compressed right up against the head, so the head was angled in the direction of impact/vector trajectory. Further to this, it is thought that the gun could have potentially misfired in this experiment, as the explosive volume upon triggering the device was substantially quieter than other experiments. It is postulated that in this case, the kinetic energy of the impactor was reduced and as a result, less contact was made between the captive bolt and the head, therefore reducing the overall impact force delivered. Although impact force would need to be evaluated in order to confirm this, the lack of head motion (*see: Fig. 1.9 in Appendix I*) and significantly lower angular and linear acceleration peaks following impact in this experiment, compared to all other injured animals provides promising justification (*chapter 5.3.1; Fig. 5.3A&B*).

Axonal pathology

The lack of DAI/APP pathology in our model suggests several things, but most notably that APP may not be the most sensitive marker of AI, such that other markers may detect sub-populations of injured axons. APP IHC identifies axons with impaired axonal transport (Otsuka, Tomonaga & Ikeda 1991), as APP is normally transported by fast anterograde axoplasmic transport and therefore rapidly pools at sites of impaired transport in the setting of AI (Smith, Meaney & Shull 2003). However, impaired axonal transport is only one indicator of AI, which suggests the possible presence of DAI that was not fully elucidated in our investigation of AI via APP staining al1 (Mohamed, et al. 2020)). Another key component of AI is neurofilament compaction, where reduction of interfilament spacing occurs as a result of side-arm phosphorylation or proteolysis (Siedler et al. 2014). It has also been suggested that neurofilament compaction may occur in other sub-populations of axons to those that demonstrate impaired axonal transport (DiLeonardi, Huh & Raghupathi 2009; Mohamed, et al. 2020), indicating that a suite of markers may be required in order to capture the full spectrum of AI post-trauma. Furthermore, multiple neurofilament markers exist such as non-phosphorylated neurofilament-H (SMI-32), neurofilament-68 (NF-68) and compacted neurofilament-medium (RMO-14) have been identified to detect populations of damaged axons both in human and animal models of TBI (Browne et al. 2011; Johnson et al. 2016; Wang, et al. 2013). Another major factor of AI is calcium-mediated axonal damage, with an increase in intracellular Ca^{2+} ultimately resulting in the breakdown of the axonal cytoskeleton and disconnection of the axon through activation of calpain and caspases-3 and -9 (Buki & Povlishock 2006). The proteolytic enzyme calpain is responsible for the breakdown of the axolemmal anchoring protein, N-terminal proteolytic fragment of spectrin (SNTF), which has recently been shown to reveal a sub-population of degenerating axons which were not detected by APP, following both mild and severe TBI (Johnson et al. 2016). However, it is important to

note many of these alternate markers are yet to be comprehensively evaluated at more acute time points following TBI.

MBP immunostaining has been used in previous research and demonstrated microstructural damage to axons as acutely as 24 hours post-TBI in a rodent model (Mohamed, et al. 2020). Minimal regional effects of both injury and hypoxia were seen to cause change in MBP+ve fibre length and coherency of MBP+ve fibres; however, our results were not indicative of meaningful change in myelin microstructure. Significant loss of MBP has been shown to be present at 10 days post-injury in a rodent model of TBI (Tu et al. 2016). This suggests that either a time point of four hours post-injury may be too acute to detect widespread demyelination of the white matter tracts or loss of myelinated axons, or that substantial axonal pathology was not achieved in this model. However, given our APP data, the latter is most likely.

Neuroinflammation

As previously mentioned, AI has been shown to both be exacerbated by and drive the neuroinflammatory response following TBI (Chen, et al. 2009; Johnson, Stewart & Smith 2013; Lafrenaye et al. 2015; Wofford, Loane & Cullen 2019). It is well known that microglial proliferation and astrogliosis are increased as a result of TBI (Karve, Taylor & Crack 2016). However, the effects of a single transient hypoxic event on microglial and astrocytic proliferation are poorly addressed in the literature. Although, PTH has been shown to elicit a compounding effect to the already primed inflammatory state of the injured brain following TBI, causing increases in both microglial and astrocyte number (Hellewell et al. 2010; Plummer, et al. 2018). Whilst minimal regional significant increases IBA-1+ve microglia were noted in this study as a result of injury, regional significant increases in astroglial proliferation were seen as a result of hypoxia. Hypoxia resulted in an increase in GFAP+ve astrocyte number

in TBI + hypoxia animals compared to TBI + normoxia animals in the striatum, whilst in the internal capsule, sham + hypoxia animals had an increased % of GFAP+ve staining as compared to sham + normoxia animals. Indeed, whilst minimal neuroinflammation was seen in response to the hypoxic insult in this study, the aforementioned rodent experiments saw widespread significant increases in neuroinflammation following PTH (Hellewell et al. 2010; Plummer, et al. 2018). This could be explained due to the increased severity of hypoxia in these studies, with rodents being exposed to 12% O_2 in Nitrogen resulting in a ~ 50% reduction in arterial blood oxygen saturation for 30 minutes post-injury (Hellewell et al. 2010). Moreover, our results suggest that the 15 minute post-injury hypoxic event was insufficient to increase injury severity in the ovine TBI model. However, as previously mentioned, the translation of neural mechanisms from lissencephalic to gyrencephalic brains is commonly poorly executed, and PTH is yet to be modelled in large animals in conjunction with TBI.

Peripheral inflammatory response

Our results highlighted a hypoxia-dependent increase in peripheral pro-inflammatory cytokines TNF-α and IL-6 regardless of pre-existing injury. This is in keeping with previous studies where hypoxia increased both central and peripheral levels of IL-6 following TBI (Goodman et al. 2011; Yang et al. 2013), and linked to outcome severity in both clinical and experimental TBI (Aly et al. 2006; Hergenroeder et al. 2010). Interestingly, astrocyte-specific overexpression of the pro-inflammatory cytokine IL-6 has been identified following TBI and hypoxia (Penkowa et al. 2003; Quintana et al. 2008), which could be explained by the hypoxia induced increase in GFAP in the brains of both sham + hypoxia and TBI + hypoxia animals. Additionally, both TBI and hypoxia has also been demonstrated to increase peripheral TNF-α levels which were observed in this study (Chio et al. 2013; Lewis & Elks 2019).

5.5 Limitations and Future Directions

There are many limitations to be considered within this study. Firstly, the small sample size must be acknowledged and the impact this potentially had on detecting significant differences between groups. Large animal experiments are extremely costly to conduct, meaning that large group sizes are rarely achievable. Indeed, the inter-group and intra-group variability could be mitigated if sample sizes were increased. Secondly, given the paucity of APP+ve DAI, additional microstructural markers of DAI are required in order to highlight populations of damaged axons that APP may not be able to capture. Such that, IHC for alternate AI markers including SNTF and SMI-32 is suggested for future studies to gain a more complete picture of AI post-trauma in the ovine model. Indeed, SNTF has been observed in peripheral serum samples following human clinical TBI, which could also be investigated in future experiments (Siman et al. 2020). It should also be considered that the 15 minute post-traumatic period of hypoxia may have been too brief with rodent models having previously induced PTH for up to 30 minutes post-injury (Hellewell et al. 2010). As such, future studies in the ovine TBI model should use a PTH period of at least 30 minutes to increase the likelihood of achieving exacerbated pathological injury. Given that regional differences in the acute neuroinflammatory response were observed, the activation state of microglia and astrocytes should be assessed in order to more fully understand if these responses are pro- or anti-inflammatory, and therefore deleterious or protective post-TBI. In addition, molecular analyses of cytokine levels within the brain tissue, in concert with serum and CSF sampling, could also provide more insight into the relationship between peripheral and central cytokine changes post-trauma.

Further biomechanical modelling is required in order to develop optimal impact acceleration that will facilitate the development of appropriate DAI. As mentioned in chapters 2.2.5 and

5.2.7, the ACS used to calculate the resulting head accelerations was based on previous work by Anderson (Anderson, 2000). The intention of an ACS is to describe kinematics and dynamics in anatomically representative directions, and to ensure consistency between animals. Whilst the ACS used by Anderson provides consistent calculations between animals, the location of the anatomical axes defined by this ACS do not allow accurate anatomical description of the direction of injury kinematics and dynamics, particularly non-sagittal motion. Anderson's work was primarily intended for application to a FE model and therefore readily identifiable anatomical landmarks were used rather than landmarks that would allow the development of an ACS with anatomical relevance to the sheep head. Therefore, in order to understand the direction of head acceleration in particular planes/axes following impact more clearly, a more anatomically relevant CS must be developed. This will be addressed further in Chapter 6.

Finally, increasing the monitoring period from four hours post-injury to would allow more time for secondary injury mechanisms to propagate the deleterious pathological cascades seen at more chronic time points following TBI. Other pre-clinical models of large animal TBI have suggested a six hour time point to be sufficient to produce various pathological sequelae, including central and peripheral inflammation (Lafrenaye et al. 2020; Lafrenaye et al. 2015). However, as this study was aiming to transition the previous ovine TBI model from a non-survival to a survivable model of TBI, it was a pre-requisite of the ethics committee that the early four hour time point be used to show the initial ovine TBI model could indeed be replicated whilst incorporating ethical considerations to wake the animal in future experiments.

5.6 Conclusions

This study identified no significant DAI as a result of increased charge level coupled with PTH. This model produced angular acceleration comparable to that of previous work which should have been sufficient to produce substantial amounts of DAI. Significant linear accelerations were also produced and were predictive of skull fracture. Whilst this skull fracture could be responsible for absorbing the impact energy and therefore reducing the DAI produced, this requires further biomechanical probing. Although there were regional significant effects of hypoxia on astroglial proliferation this was not consistent across all ROI analysed. Taken together, these results suggest the model of injury developed within this study was insufficient to produce an appreciable amount of DAI which is seen in moderate or severe clinical TBI. Therefore, further considerations in biomechanical modelling taken together with an increase in the time of PTH and the use of more comprehensive immunopathological markers of injury should increase the viability of this model being able to produce significant DAI.

CHAPTER 6

Determining the CoM of the Sheep Head: Biomechanical Optimisation of the Ovine Model of Impact Acceleration TBI

CHAPTER 6: DETERMINING THE CoM OF THE SHEEP HEAD: BIOMECHANICAL OPTIMISATION OF THE OVINE MODEL OF IMPACT ACCELERATION TBI

6.1 Introduction

Injury biomechanics were assessed in the experiments presented in Chapter 5. The resultant angular and resultant linear head accelerations were described with reference to an ACS of the sheep brain which defined a plane that passed through the brain in previous work using the ovine impact acceleration model of TBI (Anderson, et al. 2003; Anderson 2000). The axes of this ACS were aligned with 3 external landmarks that loosely formed sagittal, coronal and axial planes, and for which the origin point was at the intersection of these axes.

However, CS in other experimental models are designed to place the origin point of the CS in close proximity the CoM of the head, or to define some plane perpendicular to gravity, rather than solely passing through the brain (Anderson, 2000; Cullen et al. 2016). The head CoM in humans and non-human primates is typically defined in a CS based on the Frankfort plane (Hofmann et al. 2016). The anatomical landmarks which identify this plane are the tragion (the most superior central point of the external auditory meatus) and the left and right infraorbital rims (*Fig. 6.1*) (Bussone et al. 2005; Hofmann et al. 2016). These anatomical landmarks define the orthogonal planes and axes of an ACS (x, y and z axes) commonly used in experimental studies investigating the impact mechanics and resulting head kinematics during trauma (Slykhouse et al. 2019; Yoganandan et al. 2009). The Frankfort plane defines a plane which is perpendicular to gravity when the head is in the neutral position (eyes gazing forward). When the head is in this position, the intersection of the left and right tragions (y axis) with the midpoint of the left and right infraorbital rims (x axis) define the origin of the ACS, and further the head CoM (*Fig. 6.2*) (Slykhouse et al. 2019).

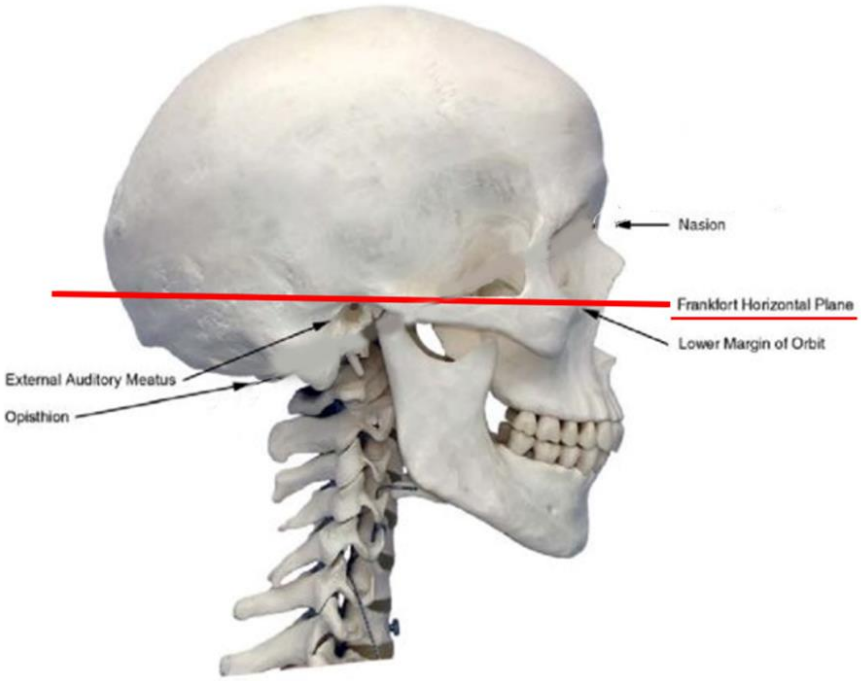

<u>Figure 6.1:</u> Planes of the skull. Note the Frankfort horizontal plane located in anteroposterior direction (red) (Bussone et al. 2005).

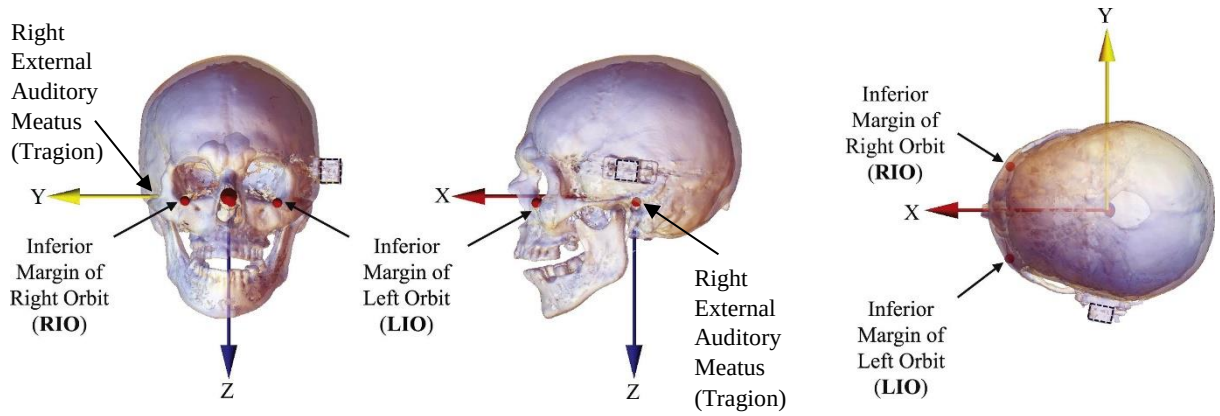

*<u>Figure 6.2:</u> Illustration of a human head local CS as defined by landmarks: Inferior Margin of Right Orbit (**RIO**), Inferior Margin of Left Orbit (**LIO**) and external auditory meatus (tragion). Anterior (left), lateral (center), and superior (right) views shown (Slykhouse et al. 2019).*

The orientation of the anatomical axes and by proxy the location of the origin point, is particularly important when describing the *distribution* of head angular acceleration about each axis following impact. Whilst linear acceleration of the head is described along the anatomical axes, angular head acceleration is described with reference to rotation of the rigid body (the head) about the anatomical axes (*Table 6.1*) (Gennarelli, et al. 1982; Siegler et al. 2015; Slykhouse et al. 2019).

Table 6.1: Anatomical axes and their directional location within the human body. Rotational motion which occurs about each anatomical axis is defined.

Axis	Anatomical Location	Rotation About the Axis
x	Anterior – Posterior	Coronal
y	Lateral – Medial	Sagittal
z	Superior - Inferior	Axial

Early work using non-human primates highlighted that the direction of rotational brain motion is important in predicting the amount of DAI produced by inertial loading. Importantly, non-human primates were chosen due to their similarities to humans both neuroanatomically and in the orientation of the neuroaxis (Gennarelli, Adams & Graham 1981; Gennarelli, et al. 1982; Gennarelli, et al. 1987; Margulies, Thibault & Gennarelli 1990). Acceleration's in these studies were described with reference to an ACS where the origin point was set at an estimated CoM of the brain (pineal gland) (Abel, et al. 1978). Angular accelerations produced by coronal-plane head rotations elicit substantially worse damage to the brain than axial or sagittal-plane rotations, including immediate, prolonged coma (Gennarelli, et al. 1982).

Animals in these studies were subject to pure impulsive non-impact, controlled head rotational acceleration produced by a pneumatic actuator known as the HYGE device. Ethical concerns surrounding the use of non-human primates led to the application of the HYGE model to other species, most notably pigs (Meaney, et al. 1995). However, there are substantial neuroanatomical differences between the non-human primate and the pig. The spinal axis of the pig is parallel to the cerebrum; however, in non-human primates the spinal axis is perpendicular to the cerebrum (Meaney, et al. 1995). It was hypothesised that axial rotation in the pig would produce similar patterns of injury produced by coronal rotations in the non-human primate (Meaney, et al. 1995). The HYGE actuator was customised to produce axial plane rotations which were roughly comparable to coronal plane rotations used in non-human primate experiments (Meaney, et al. 1995). The ACS in both the non-human primate and (more importantly) the pig TBI studies were not developed with reference to a known head CoM.

Defining the repeatability and in a comparable fashion between model species (and humans) is of paramount importance. To our knowledge there is no standardised method for determining an anatomically representative axis of the head using specified anatomical landmarks in quadrupedal large animals; and more specifically, sheep. In order to develop an anatomically relevant CS, the CoM of the sheep head is required, which is currently undefined in the literature. Once the CoM of the sheep head has been determined, anatomical landmarks in close proximity to the head CoM can be located in order to define an anatomically representative CS of the sheep head. This would therefore allow better understanding of the direction of angular head acceleration about the anatomical axes and the pattern of DAI seen as a result of TBI.

As such, the aim of this study was to determine the head CoM of Merino wethers using computed tomography (CT) scans and three dimensional (3D) modelling. The secondary aim of this study was to investigate the effect of the ACS orientation change on the head accelerations presented in Chapter 5, when described in a more anatomically relevant CS.

6.2 Methods

6.2.1 Study Design and CT Procedure

10 male Merino wethers (18-24 months) were used under approval of SAHMRI Animal Ethics Committee (SAM396.19). Nine cadaveric decapitated sheep heads were placed in the prone position and underwent CT imaging (16-slice Philips Brilliance CT scanner). Slice thickness was set at 0.4 mm and the CT image resolution was 0.37 x 0.37 mm / pixel. A single live animal was anaesthetised (*chapter 2.2.3*) and placed in the supine position prior to undergoing CT scan.

6.2.2 Generation of 3D models and Tissue Mass Calculation

MIMICS software (MIS23, Materialise, NV, USA) was used to create a 3D model of the sheep head. CT images were imported and displayed in sagittal, coronal, and axial planes. Segmentation of bone, brain and soft tissue into individual 3D tissue masks was required to account for different tissue densities. Tissue types were separated into independent masks, using specified thresholding bands dictated by Hounsfield units (HU), which describe the radiodensity of the tissue (Dancewicz et al. 2017). Additional manual thresholding was implemented to increase the accuracy of the mask for each of the tissue types.

Soft tissue mask

As a result of decapitation, the pre-set soft tissue mask included a layer of material below the head (blood and serous fluid). This liquid layer, uneven fatty tissue, the neck, and the ears were removed to provide a refined soft tissue mask to increase uniformity of tissue densities across all specimens (*Fig. 6.3A&B*). The ears were not included in the 3D model because they were inconsistently placed in the CT scans, and due to their low mass, symmetry, and that they are

taped back during the impact in injury model, they are unlikely to substantially affect the head CoM.

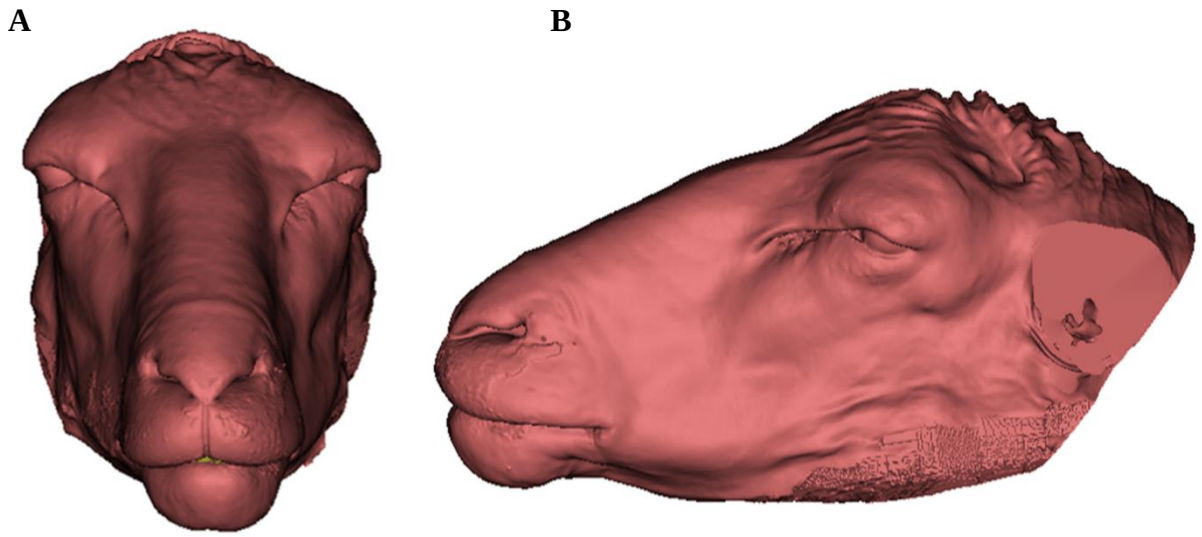

*Figure 6.3: Refined Soft Tissue Mask. Anterior profile (**A**) and lateral profile (**B**).*

Brain

The brain was included in the initial soft tissue mask due to similarities in water content and radiodensity to other soft tissues. In MIMICS, the 'split mask' function was used separate the brain tissue from the refined soft tissue mask (*Fig. 6.3A&B)* into an individual mask (*Fig. 6.4A&B*).

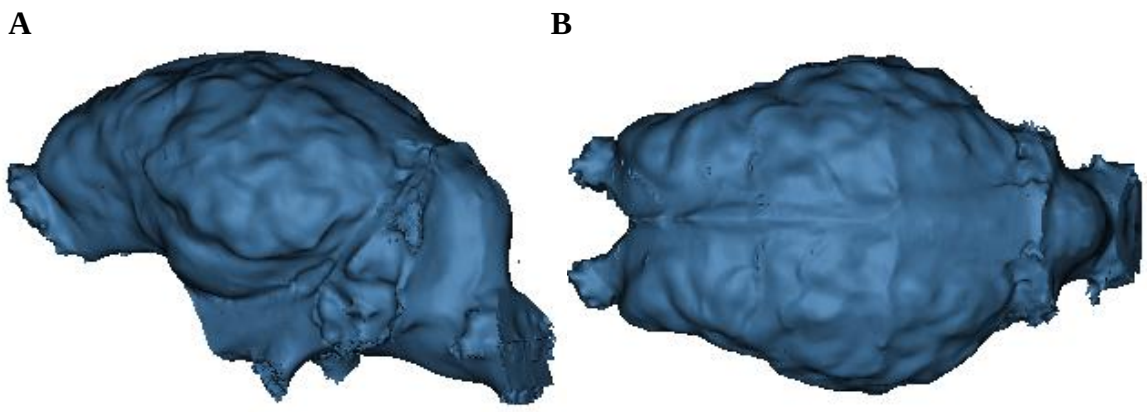

*Figure 6.4: Final brain mask. Lateral profile (**A**) and superior profile (**B**). Note the dura covering the parenchyma and smoothing the gyrencephalic anatomy.*

Bone

Initially, a bone mask was constructed using the pre-set radiodensity threshold limits in MIMICS. The resulting mask included the full bone structure, including animal's teeth (*Fig. 6.5*). Brain and soft tissue have a relatively consistent mass density of 1040 kg/m^3 (Park 1992; Roush 2010); however the mass density of bone and teeth are not consistently the same. Using the pre-set bone mask which encompasses both teeth and bone tissues, would not account for the variation in mass density between bone and teeth and therefore impact the CoM calculation. Therefore, multiple bone/teeth masks were generated with increasing thresholding bands (*chapters 6.2.3 and 6.3.1*; *Fig.6.6*).

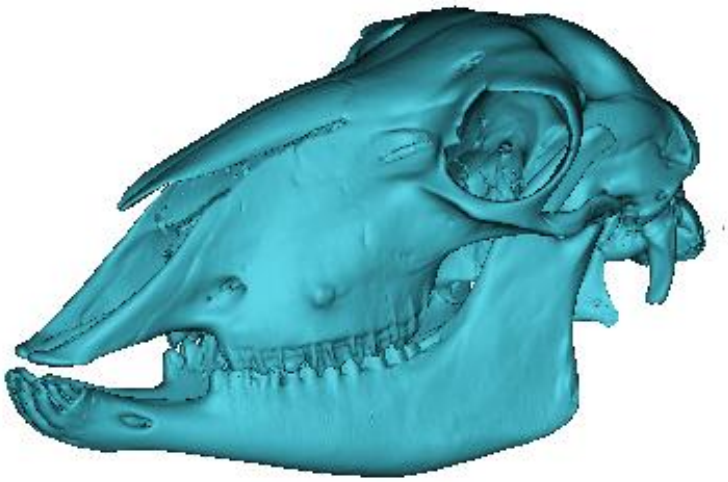

Figure 6.5: Automatically Generated Bone Mask, including teeth.

Tissue Mass Calculation

Tissue volume was automatically calculated by MIMICS, then Equation 1 was used to calculate tissue mass:

$$Mass\ (kg) = \ density\left(\frac{kg}{m^3}\right) \times volume\ (m^3) \tag{1}$$

As previously mentioned, both brain and soft tissue have a known mass density of 1040 kg/m^3; however, the mass density of each individual bone mask was unknown. The mass density (ρ) to apply for each individual bone mask was determined using the following equation, where "H_{mean}" was the average houndsfield unit (HU) of the upper and lower values for each threshold band (Dancewicz et al. 2017) (*chapter 6.3.1; Table 6.3*):

$$\rho\left(\frac{kg}{m^3}\right) = 0.692\ \times\ HU\ + 1000 \tag{2}$$

6.2.3 MIMICS Sensitivity Study

A sensitivity study was performed on the data of one animal to determine comparable differences in head CoM calculation with varying numbers of sub-thresholded bone masks. The sensitivity study consisted of dividing the recommended threshold for bone [226 HU to the maximum detectable HU (~2,800)] into test cases of 1- 9 equally distributed ranges of HU. The resulting tissue volumes were extracted from MIMICS for each mask and used to calculate the CoM. CoM was calculated in MATLAB (*chapter 6.2.4*) (v.9.8, R2020a, Mathworks, UK). Resulting values for the CoM of the head were compared and, the smallest number of sub-thresholds at which the head CoM became most accurate was determined.

6.2.4 CoM Calculation

The brain, soft tissue, and multiple bone/teeth masks were combined to produce the final 3D head model (*Fig. 6.6*).

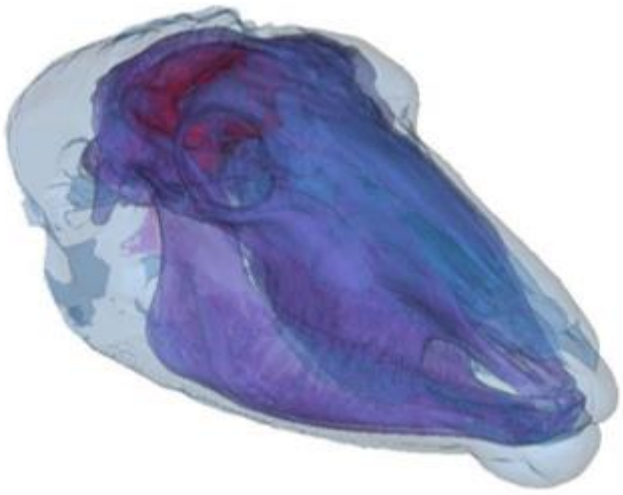

Figure 6.6: All individual masks overlayed to demonstrate completed 3D model of the sheep head.

For each segmented tissue, the x, y, and z coordinates for the CoMs and the volume of each of the tissue types were calculated in MIMICS. The coordinates of the left and right zygomatic processes and bregma, which are used to define orientation of the anatomical axes and location of the origin of Anderson's (2000) ACS, were also exported. Using custom MATLAB code the CoM coordinates ($x_{segment}$, $y_{segment}$, $z_{segment}$) and masses ($m_{segment}$) of the segmented tissues were imported, and Equation 3 was used to calculate the CoM coordinates of the head, x_{head}, y_{head}, and z_{head}:

$$x_{head} = \frac{\sum(x_{segment} \times m_{segment})}{\sum m_{segment}}, y_{head} = \frac{\sum(y_{segment} \times m_{segment})}{\sum m_{segment}}, z_{head} = \frac{\sum(z_{segment} \times m_{segment})}{\sum m_{segment}} \quad (3)$$

6.2.5 Development of An ACS With Reference to Sheep Head Anatomy

A new ACS was developed in order to allow the axes to be more anatomically relevant, whilst simultaneously locating the origin point closer to the CoM of the head. Bony landmarks were identified that would produce a new ACS for which the origin was positioned near the head CoM, and the axes were aligned approximately with the anatomical axes with the head in a forward-gaze posture. These landmarks were visualised and chosen from viewing the 3D model of the sheep skull. The 3D model of the head was oriented to represent the neutral position of the sheep head and a vertical line was plotted from the CoM toward the superior surface of the head and horizontal line was plotted to the lateral surface of the head from the CoM point, on the 3D model of the head. The most identifiable anatomical landmark in close proximity to the point at which the line intercepted bone was then chosen.

6.3 Results

6.3.1 MIMICS Sensitivity Study

Following the analysis of individual bone threshold ranges in MATLAB, it became clear that increasing the number of sub-thresholds increased the accuracy of the CoM calculation. The head CoM converged to an accurate value when four bone/teeth sub-thresholds were used (*Table 6.2*). However, given the inconsistency in CoM calculation prior to the use of four sub-thresholds, the use of five sub-thresholds presented less risk of potential variability when of the protocol was applied to different animals.

Table 6.2: x, y and z coordinates demonstrating the CoM location (in origin ACS) and resulting distance to the anatomical origin point for each threshold range. Note the convergence of solution from the use of 4 thresholding bands onward.

Sub-thresholds	CoM Coordinates in ACS (mm)			CoM Distance to Anatomical Origin (mm)
	x	y	z	
1	-2.1320	-35.0183	-1.3674	35.1098
2	-2.2096	-36.6299	-1.4728	36.7261
3	-2.2730	-39.1769	-1.5640	39.2740
4	**-2.2057**	**-35.8336**	**-1.8376**	**35.9484**
5	-2.2001	-35.7423	-1.9135	35.8611
6	-2.2021	-35.5232	-1.9807	35.6465
7	-2.2078	-35.5555	-1.9530	35.6775
8	-2.2082	-35.2531	-1.9294	35.3748
9	-2.2122	-35.1471	-1.9602	35.2711

Generation of five bone masks was therefore implemented in all future CoM analyses (*chapter 6.2.2; Table 6.3*; *Fig. 6.7*).

Table 6.3: Bone/Teeth mask radio density thresholding and mass density for 5 sub-thresholds. This number of sub-thresholds was applied to all future 3D models.

Mask	Lower Threshold Limit (HU)	Upper Threshold Limit (HU)	Average of Threshold Limits (HU)	Mass Density (kg/m^3)
Bone/Teeth 1	226	745	486	1333
Bone/Teeth 2	745	1264	1005	1693
Bone/Teeth 3	1264	1784	1524	2053
Bone/Teeth 4	1784	2303	2043.5	2413
Bone/Teeth 5	2303	2822	2562.5	2772

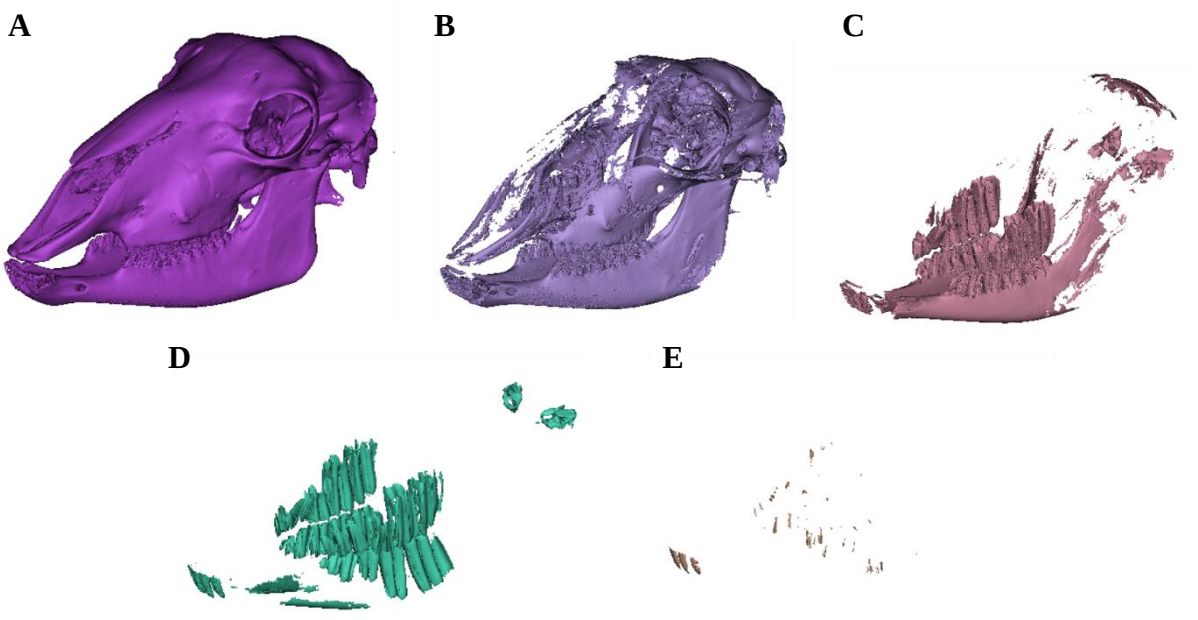

*Figure 6.7: Five independent bone masks created by individual sub-thresholds (Table 6.3) Bone/Teeth 1 (**A**), Bone/Teeth 2 (**B**), Bone/Teeth 3 (**C**), Bone/Teeth 4 (**D**), and Bone/Teeth 5 (**E**). Note the decrease in visible bone as the HU increases in value.*

6.3.2 CoM Calculation

The orientation of Anderson's ACS is as follows: origin = midpoint between the left and right notches of the zygomatic processes, x axis: passes through the left and right zygomatic process, z axis: in the plane perpendicular to the x axis pointing toward bregma, y axis: cross product of the x and z axes (*Fig. 6.8A&B & 6.11D*).

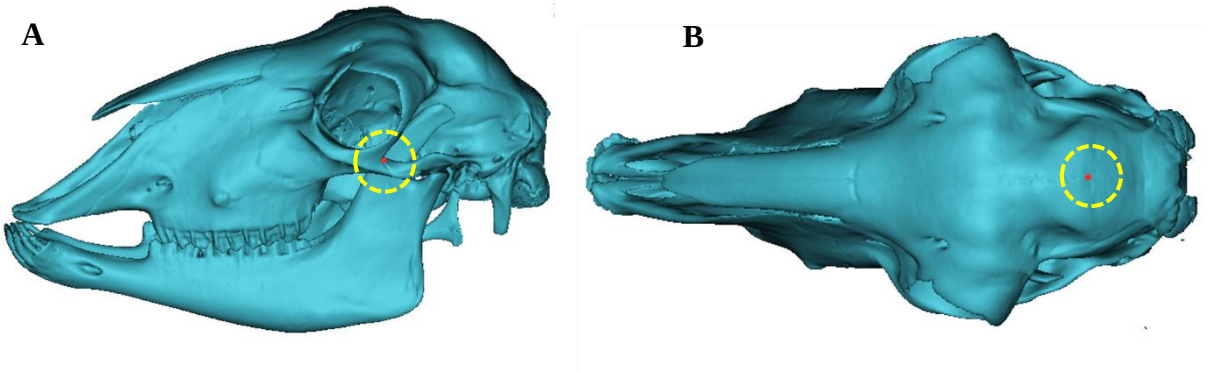

*Figure 6.8: Left zygomatic process (**A**) and bregma (**B**). Note each anatomical landmark is pinpointed in red, with areas highlighted by yellow circles.*

CoM of the head was calculated as described in chapter 6.2.4 and coordinates were reported in each of the the x, y and z axes, with reference to Anderson's ACS. The resulting head CoM was on average was 32.48 ± 2.84 mm from the origin point defined by Anderson's ACS, and typically sat anteroinferior to it. This distance cannot be assumed to have a negligible effect when calculating linear head acceleration and describing the distribution of angular head acceleration about each of the axes in an anatomically representative manner (*Fig. 6.9A&B; Table 6.4).*

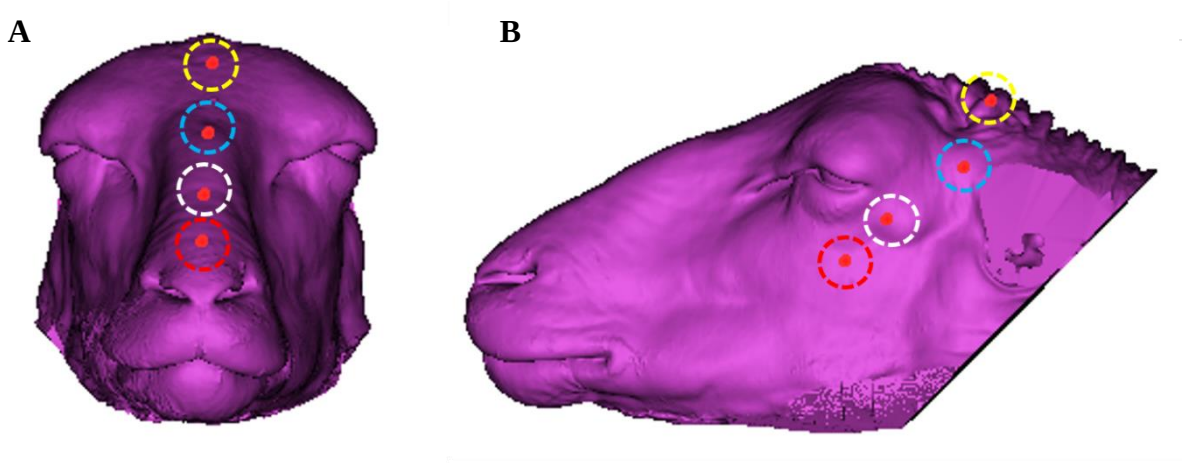

*<u>Figure 6.9:</u> Coronal (**A**) and lateral (**B**) view of 3D model of the sheep head. Highlighted points include bregma (yellow) and the CoM of the brain (blue). Note the distance of the origin (white) to the CoM of the head (red).*

*Table 6.4: Anatomical coordinates of the CoM for each sheep head specimen. Notice the considerable distance of the origin point from the CoM consistently in all animals. ● = live animal. ***** = CoM value furthest from the mean.*

Specimen	CoM Coordinates in Original ACS (mm)			CoM Distance to Anatomical Origin (mm)
	x	y	z	
1	-1.58	-33.21	-4.06	33.49
2	4.66	-31.28	-12.56	34.03
3	-6.25	-28.16	-17.07	33.52
4	-3.98	-26.11	-14.11	29.95
5	2.91	-30.04	-14.44	33.46
6	-4.73	-28.67	-15.14	32.76
7	1.65	-25.41	-11.68	28.01
8	-1.39	-31.28	-16.96	35.61
9	-2.20	-31.91	-16.22	35.86
● 10	-2.89	-27.90	-0.73	● 28.06*
Mean				**32.48 ± 2.84**
Maximum Variation from Mean				**-4.42**

6.3.3 Development of an ACS With Reference to Sheep Head Anatomy and Resulting CoM Calculations

The new anatomical landmarks selected to define the new ACS were the left and right malar maxillary junction to replace the left and right zygomatic notches and the intersection of the supraorbital foramina (*Fig. 6.10A-C*). These landmarks are not palpable and are only visible via CT imaging.

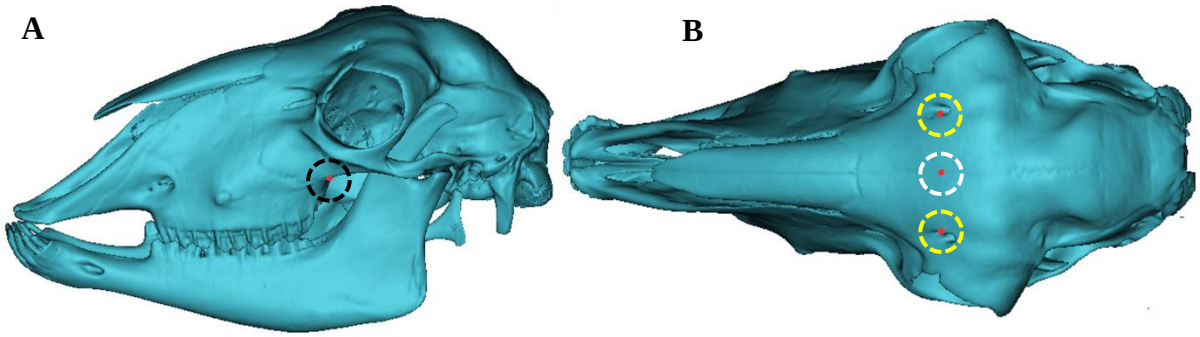

*Figure 6.10: Junction of the right malar and maxillary bones (**A**) highlighted in black. Midpoint of the supraorbital foramina (**B**). Note the midpoint outlined in white and the respective left and right supraorbital foramina outlined in yellow.*

These new anatomical landmarks redefined the axes as follows (*Fig. 6.10D*):

- **Origin:** midpoint of left and right malar/maxillary junctions;
- **x axis:** from origin towards right malar/maxillary junction;
- **z axis:** from origin towards midpoint of the left and right supraorbital foramina;
- **y axis:** orthogonal to x and z-axes.

Although similar to Anderson's CS, the newly defined landmarks result in the placement of the anatomical origin on 8.86 ± 2.39 mm from the head CoM when averaged across the 10 specimens used in this study, in comparison to 32.5 mm using Anderson's ACS (*Fig. 6.11A&B;*

Table 6.5). With the z axis now being more vertically aligned relative to the neutral position of the sheep head (*Fig. 6.11C*), this new ACS better represents the anatomy of the sheep head as compared to Anderson's ACS (*Fig. 6.11D*) and defines a plane of the sheep head perpendicular to gravity, which is currently unreported in literature.

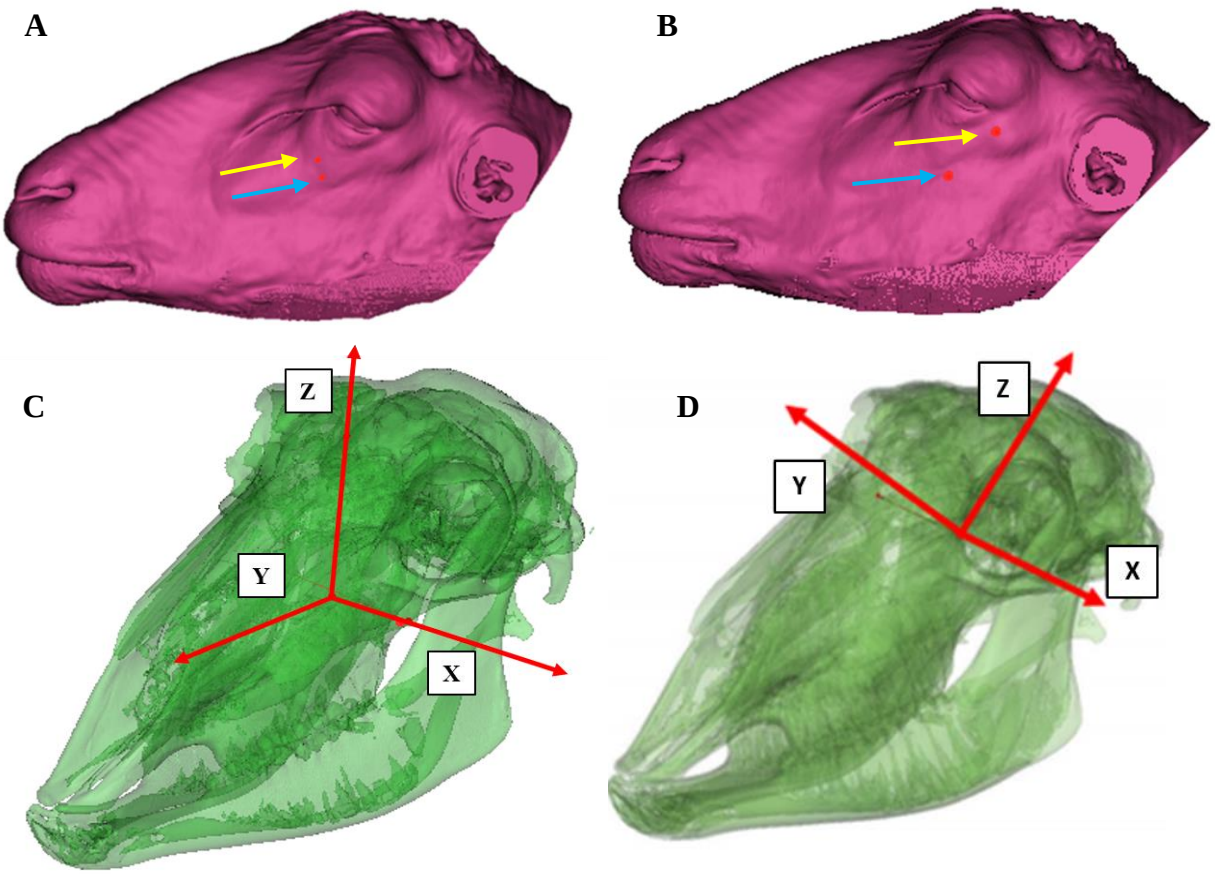

*Figure 6.11: Proximity of the head CoM (blue arrow) to the origin point (yellow arrow) outlined in the new ACS (**A**) and Anderson's ACS (**B**). Note the change in direction of the y and z axes in the new ACS (**C**) compared to Anderson's (**D**).*

Table 6.5: Anatomical coordinates of the sheep head CoM. Notice the proximity the origin point to the CoM consistently in all animals. ● = live animal. ***** *= CoM value furthest from the mean.*

Model	CoM Coordinates in New ACS (mm)			CoM Distance to Anatomical Origin (mm)
	x	y	z	
1	6.80	-7.57	-3.46	10.75
2	-1.67	1.93	-7.75	8.16
3	4.06	-7.43	-6.69	10.79
4	1.50	-2.85	-3.44	4.71*
5	3.21	-4.29	-8.03	9.65
6	1.24	-7.74	-4.91	9.25
7	2.11	-4.59	-2.36	5.57
8	2.53	4.73	-10.61	11.89
9	1.19	-3.87	-9.85	10.65
● 10	3.48	1.86	-6.07	● 7.24
Mean				**8.86 ± 2.39**
Maximum Variation from Mean				**4.15**

6.3.4 Transformation of Head Acceleration Data into The New ACS

Transformation of Coordinates

Given the increased anatomical relevance of the new ACS, acceleration data which was collected in experiments in Chapter 5 be transformed into the new ACS. CT data was not available for these animals, therefore an average of the x, y and z coordinates for each of the

anatomical landmarks and the origin were taken from the 10 animals assessed in this study. Coordinate averages were taken in both Anderson's ACS and the new ACS and average degree of rotation in each of the axes and the origin was then applied to the head acceleration data captured in experiments performed in Chapter 5 in order to estimate the change in accelerations (*Fig. 6.12*).

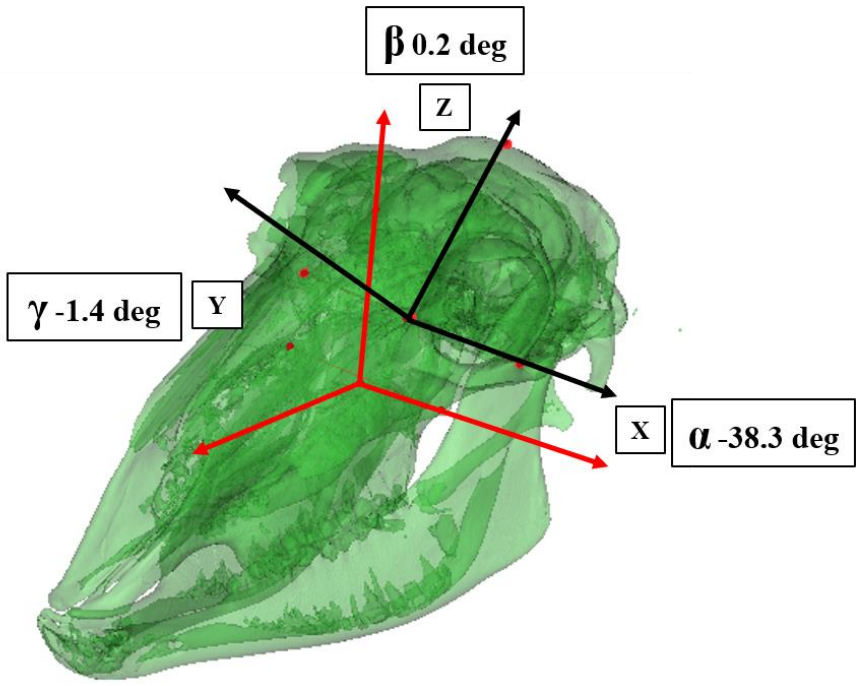

Figure 6.12: Rotation about the anatomical axes from Anderson's ACS (black) to the new ACS (red). Translation of the origin along each axis; x: -0.69 mm, y: 4.75 mm, and z: -28.98 mm.

Resulting Changes in Acceleration

Following the transformation of both linear and angular head acceleration data to the new ACS peak resultant angular and linear accelerations were unchanged in each animal as the resultant acceleration represents a value rather than direction of rotation/motion in each of the axes. The magnitudes of the resultant for each of Anderson's ACS and the new ACS are the same; however, there is a re-distribution of acceleration between the y and z axis in the new ACS, as

these are the two axes that rotated as a result of replacing bregma with the midpoint of the supraorbital foramen. Despite the relocation of the origin point, the orientation of the x axis stayed virtually the same as the plane defined by the zygomatic notches and the malar/maxillary junction is horizontal in both Anderson's and the new ACS, respectively (*For examples see: Figs. 1.1A&B-1.8A-B in appendix II and Figs. 3.1A&B-3.8A-B in appendix IV*).

6.4 Discussion

The primary aim of this study was to determine the CoM of the head of the sheep to develop a more anatomically representative ACS. A novel, standardised method to estimate the CoM of the sheep head was developed using *in vivo* coordinate measurements of external landmarks combined with skull landmarks from CT, as well as determining the actual location of head CoM of the sheep, which is currently unreported in the literature. Being able to locate the CoM allows the calculation of anatomically relevant angular and linear acceleration of the head, which can therefore be comparable to human planes of motion, which is also novel in the sheep. This study was also able to develop a more anatomically representative ACS using anatomical landmarks which are proximal to the CoM of the sheep head, placing the new origin point on average 9 mm from the head CoM, as compared to approximately 32 mm when using the ACS developed by Anderson (Anderson, 2000). As a result of this new ACS, the y and z axes were reoriented to represent the anatomy of the sheep head when in a neutral position more anatomically. Reorienting these axes allows the description of the distribution of head motion and rotation along and about individual axes more anatomically following impact. Results of previous experimental animal studies have shown rotation about specific axes is directly associated with the distribution, presentation, and severity of DAI.

Non-human primate, porcine and ovine TBI studies have all modelled human-like injury mechanics that resulted in the production of marked DAI (Anderson, et al. 2003; Atlan, Smith & Margulies 2018; Browne et al. 2011; Cullen et al. 2016; Gennarelli, Adams & Graham 1981; Gennarelli, et al. 1982; Gennarelli, et al. 1987; Ross et al. 1994). An important difference between the injury models using pigs and monkeys compared to the ovine TBI model is that the device implemented in the former produces pure impulsive non-impact head rotational controlled rotational acceleration levels (Cullen et al. 2016; Gennarelli, Adams & Graham 1981; Gennarelli, T. A. et al. 1982). Because the animal's head is attached to the actuator and undergoes a prescribed head trajectory, the acceleration of the head is the same as the acceleration of the actuator. This means that the manner in which the head is interfaced with the actuator dictates the anatomical plane the acceleration is measured in. However, in the impact-acceleration model of ovine TBI, head acceleration is not dictated by a device. The head is allowed six-degrees-of-freedom unconstrained motion, meaning that its directional response is not dictated or constrained and therefore, head acceleration is measured with the use of an accelerometer array. In order describe the direction of head acceleration captured by the accelerometer array in particular planes or axes accurately, the data must be transformed into an ACS which is anatomically representative of the animal, and the CoM of the head. As previously mentioned, the ACS used in previous work using the ovine model of impact-acceleration TBI was defined without reference to the head CoM of the sheep, as this is unreported in the literature. Therefore, the CoM of the sheep head required definition.

Previous work using decapitated cadaveric human heads has utilised MIMICS software to determine the CoM of the head (Roush 2010). Work by Roush (2010) evaluated the accuracy of CoM calculation with actual weighed tissue mass compared to tissue mass calculated from CT analyses and 3D modelling in MIMICS (Roush 2010). The methodology for Roush's human study compared to the method used in this study was virtually identical, despite creating

a single 3D bone mask, as the teeth were removed from the skull in the human head. The location of CoM for each of the tissue types in both sets of Roush's analyses was comparable and not significantly different. The average coordinates for the CoM calculated with actual tissue weights was: -0.12in (±0.09in) in the x axis, 0.01in (±0.18in) in the y axis, and 0.91in (±0.23in) in the z axis, where the average coordinates for the CoM calculated with 3D modelled tissue weights was -0.15in (±0.09in) in the x axis, 0.03in (±0.12in) in the y axis, and 1.00 (±0.32in) in the z axis (Roush 2010). This suggests 3D modelling to be an accurate means of finding the weight and CoM of the human head. The method in this study implemented additional segmentation of bone and teeth to account for variation is tissue densities, which could have increased the accuracy of CoM calculation even further. However, a direct comparison such as that performed in the aforementioned human study would be required to confirm this.

The method used in this study to determine the head CoM is reliable as supported by other work (Roush 2010). However, when assessing the ten 3D head models, there are considerable anatomical differences between animals, particularly when comparing the length and arc of the snout. Despite this, variation between the location of head CoM between animals was relatively small (~4 mm from mean CoM), and as such, the CoM of heads in future animal testing can be approximated reliably.

Due to locating the CoM of the head, anatomical landmarks which better represent the sheep head were able to be identified to develop a new ACS. With the use of the new ACS, the axes were able to be reoriented on the head of the animal. As aforementioned, this will allow more representative description of head motion in particular planes or rotation about specific axes. Coronal and axial rotation of the head has been shown to produce significantly worse DAI compared to sagittal rotation in experimental models of large animal TBI (Browne et al. 2011; Cullen et al. 2016; Gennarelli, et al. 1982; Ross et al. 1994). When referring to the ovine TBI

model, coronal rotation or lateral bending would occur about the y axis and axial rotation would occur about the z axis (Anderson, et al. 2003; Anderson 2000). The new definition of the ACS resulted in the z axis becoming more vertical, and the y axis being angled more inferiorly (toward the snout of the animal). The distribution of angular acceleration about these two axes can now be described with more anatomical accuracy (Kuo et al. 2018). This is of paramount importance, as understanding the distribution of angular acceleration about the y and z axis will therefore reveal the magnitude of coronal and axial rotation produced respectively as a result of impact, and as such its influence on resulting DAI.

6.5 Limitations and Future Directions

The newly defined ACS was able to relocate the origin point to be in close proximity to the CoM and increase the anatomical relevance to the sheep head anatomy. However, a limitation of this is the method was that the anatomical landmarks were only visible via CT scan. Dissecting the sheep head surgically to expose these landmarks poses extensive risk and is therefore not practical. The supraorbital foramina are located dorsal to the orbital cavity, and house the trochlear nerve and the ophthalmic branch of the trigeminal nerve (Mohamed, Driscoll & Mootoo 2016). Damage to either of these nerves could result in motor and sensory deficits within the forehead and the middle two-thirds of the upper eyelid (Mohamed, Driscoll & Mootoo 2016). The head and face of the sheep is intricately innervated and highly vascularised, and dissection to expose the junction of the malar and maxillary bones would encounter substantial risk of extensive bleeding and damage to the mastication musculature of the face (Allouch, 2017). Therefore, it is suggested the original landmarks defined by Anderson be digitised with use of the microscribe (as this will define a necessary initial spatial relationship between the laboratory and the animal) in future experiments, and all animals

undergo CT scan prior to injury. This would mean an additional, final transformation be applied to the data once the new anatomical landmarks have been identified on the CT in post-processing data analysis.

Another potential concern within this study was that 9/10 CTs were performed on decapitated sheep heads. Upon decapitation of the head, loss of CSF and other circulating fluid such as blood can occur. This could have an effect on the morphology of soft tissues and the brain and subsequently change the tissue mass from that of a live animal, and as such accurate calculation of the CoM. Conversely, a limitation to the use of CT in a live animal is the presence of ET tube and gauze and medical tape to secure the ET tube in the trachea of the animal. This caused significant morphological change in the soft tissue anatomy of this animal which could have also impaired CoM calculation. However, despite this, the variation from the mean CoM, and the morphology of the brain of this animal was comparable to that of the 9 decapitated heads.

6.5 Conclusions

Creating 3D models of sheep heads from CT data allowed specimen-specific differences in tissue mass distribution to be considered. This allowed the CoM of the head to be accurately determined. Using the CoM of the head, an anatomically relevant CS was developed with reference to the anatomy of sheep head in the neutral position. This was applied to acceleration data obtained in Chapter 5, and this demonstrated no effect on the peak resultant angular and linear head accelerations recorded for the current model. However, as expected, this did result in a change in the distribution of acceleration in the y and z axes. The CoM and ACS defined in this study will allow for better clinical translation between linear accelerations and, angular accelerations determined in ovine models of TBI to those seen in human TBI. These findings will contribute to the optimisation of injury mechanics and subsequent patterns and distribution of tissue damage such as DAI, in the ovine impact acceleration model of TBI.

CHAPTER 7

General Discussion

CHAPTER 7: GENERAL DISCUSSION

7.1 Introduction

The over-arching theme of this thesis was to further characterise the ovine model of impact acceleration TBI originally developed in our laboratory at the University of Adelaide in the early 1990's (Lewis, et al. 1996; Van den Heuvel et al. 1999; Van den Heuvel et al. 1998), but with the injury scaled down to produce a mild-moderate TBI. The primary research question in this thesis was to evaluate whether the ovine TBI model could be modified to produce a survivable injury, whilst maintaining a degree of DAI pathology and associated magnitude of angular and linear head acceleration seen in previous work in a non-survival model (Anderson, et al. 2003; Lewis, et al. 1996). As such, the first aim was to eliminate the production of skull fracture and associated soft tissue damage which would prevent ethical recovery of the animal following TBI. However, despite extensive troubleshooting, the modifications implemented to reduce these extraneous injuries associated with impact proved insufficient. Furthermore, extensive DAI was no longer observed post-injury. Therefore, the second aim sought to determine whether we could firstly reproduce the original model of ovine TBI in relation to the biomechanical parameters used to induce injury and the resulting production of DAI and then determine whether PTH could be added to further enhance DAI development. However, despite producing comparable levels of both angular and linear head acceleration, DAI was scantly observed, as assessed via APP+ve immunostaining. Furthermore, the addition of PTH did not influence the development of APP+ve immunostaining.

In order to reconcile this, a more anatomically representative method of describing both the angular and linear head acceleration following TBI in the sheep was developed. As a result of this, the amount of DAI observed in experimental TBI in the sheep can be attributed to the distribution of head acceleration in specific directions and about each of the x, y and z axes,

which has been discussed in previous literature using both pigs and non-human primates (Browne et al. 2011; Cullen et al. 2016; Gennarelli, T. A. et al. 1982; Gennarelli, Thibault & Ommaya 1972). As discussed in chapter 6.4, both coronal (rotation about the y axis) and axial (rotation about the z axis) rotation have been attributed to the development of DAI more so than sagittal rotation (rotation about x the axis), as evidenced by APP+ve immunostaining (Browne et al. 2011; Cullen et al. 2016; Gennarelli, et al. 1982; Gennarelli, Thibault & Ommaya 1972). The acceleration data produced by Anderson *et. al* (2003) using this model showed that during impact, the head executed complex angular motions and that the acceleration could not be described by a single axis of rotation (Anderson, et al. 2003). More specifically, the main axis of angular acceleration passes from the z axis to the y axis; however, the distribution of acceleration within these axes was not described and access to this data is not published in the literature. It could be postulated that, the lack of DAI seen in this model may be attributed to sagittal rotation of the head predominating over axial and coronal rotation. However, this would need further probing in order to fully elucidate. Given the more anatomically relevant ACS which was developed in Chapter 6, this is now possible to discuss and evaluate in future experiments.

7.2 Development of a survival model of impact acceleration in the sheep

Despite extensive troubleshooting (decreasing charge intensity, alterations to the captive bolt, the use of a silicone tip to conceal the steel captive bolt, and the use of a cervical sling) the results of the thesis studies clearly demonstrate that skull fracture was unable to be consistently prevented using this model. Both the pattern of skull fracture and macroscopic injuries seen within the studies in this thesis are consistent with those observed in previous research using this model (Anderson, et al. 2003; Lewis, et al. 1996; Van den Heuvel et al. 1998; Vink, Bahtia

& Reilly 2008). Although the ovine impact acceleration model of TBI has been predominantly utilised in Australia (Anderson, et al. 2003; Bellapart et al. 2016; Bellapart et al. 2018; Byard et al. 2012; Van den Heuvel, Blumbergs, et al. 2000; Van den Heuvel et al. 1999; Van den Heuvel et al. 1998; Vink, Bahtia & Reilly 2008; Vink, Gabrielian & Thornton 2017), a single study outside of Australia, in Germany, has adapted the model to successfully prevent the occurrence skull fracture (Grimmelt et al. 2011). Both 13 and 21-charges were used to induce either mild or sTBI respectively, using a domed rubber bolt to impact the sheep. A transient increase in ICP was observed in mTBI animals as early as one hour post-injury and resolved to sham levels at four hours post-injury, whilst animals exposed to sTBI demonstrated a sustained, prolonged increase in ICP which was higher than both sham and mTBI animals (Grimmelt et al. 2011). However, there were considerable inconsistencies in the pathological response to injury, particularly in sTBI animals, comparable to those observed in Chapter 5 results. Specifically, whilst some sTBI animals demonstrated solitary small intraparenchymal haemorrhages, others of the same group displayed multiple intracranial haemorrhages, including contusions, traumatic SAH and ventricular haemorrhages. (Grimmelt et al. 2011). How this was executed in the absence of skull fracture is poorly discussed; however, it could potentially be attributed to the use of a rubber bolt instead of a steel bolt used in previous work investigating this model (Anderson, et al. 2003; Grimmelt et al. 2011; Lewis, et al. 1996; Van den Heuvel et al. 1999; Van den Heuvel et al. 1998).

In models of impact acceleration TBI using small animals fracture is typically prevented with use of a `helmet'. One of the most popular models of impact acceleration TBI used in pre-clinical research is the Marmarou rodent weight drop model (Marmarou et al. 1994). This model is able to produce graded TBI of varying severity, including mTBI and concussion, by varying both the weight size and drop height used. This model implements the use of a

"helmet", a stainless-steel disc (3mm thick x 10mm diameter), which is cemented to the superior surface of the skull, centred for the direct impact of a brass weight to strike from above (*Fig. 7.1*) (Marmarou et al. 1994). The helmet protects the skull from fracture, whilst still maintaining high kinetic energy levels upon impact via absorbing and distributing the impact force (Marmarou et al. 1994). Given that injury is delivered with the rodent laying prone on a foam bed (*Fig. 7.1*), and that the foam bed has negligible resistance to acceleration, it therefore allows the base of the skull to continue to descend without being compressed significantly, as it would under impact into a resisting hard surface (Marmarou et al. 1994).

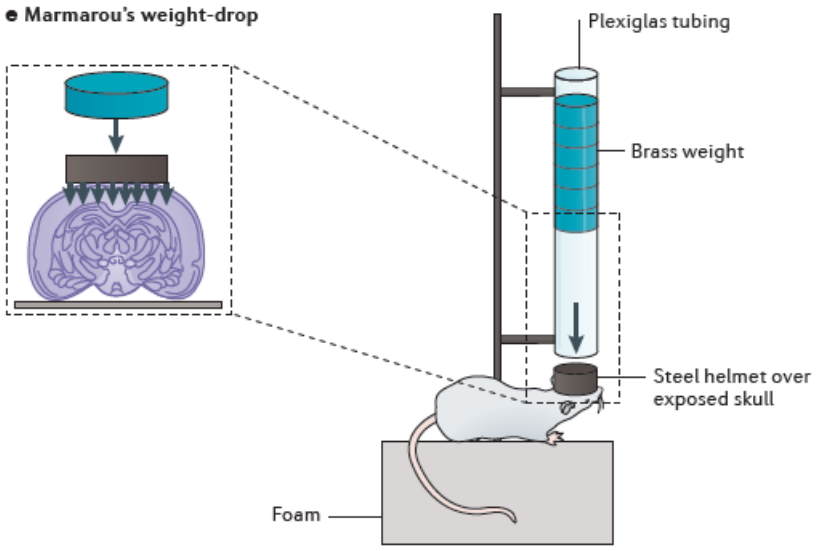

<u>Figure 7.1:</u> Marmarou's impact acceleration model of diffuse AI, as adapted from (Xiong, Mahmood & Chopp 2013)

The earliest work using the ovine model of impact acceleration TBI implemented a similar method to that of the Marmarou model (Lewis, et al. 1996). A vertical incision placed midway between the supraorbital process and the external auditory meatus exposed the parietotemporal suture allowing placement of a contoured steel plate with protruding centrepiece (Lewis, et al. 1996). Most importantly this plate prevented depressed skull fractures; however, superficial

fractures on the outer surface of the skull (coronoid process and zygomatic arch) were still present in 50% of cases. The presence of these superficial skull fractures is likely due to the location of impact. In the ovine model of TBI, animals are impacted laterally at a region of the head particularly vulnerable and prone to fracture when considering the undulating, bony structures protruding from the temporal area of the sheep skull (coronoid process and zygomatic arch). In contrast, the Marmarou model uses an approach where animals are injured on the superior surface of the head, which on the rodent skull is flat (Marmarou et al. 1994). Upon impact, the flat faced weight contacts the flat surface of the 'helmet' and the force of impact is transmitted through to the brain, protecting the skull. Additionally, the rodent skull is much thinner and more pliable compared to the sheep, allowing more flexion of the bone under impact force.

Considering the work in both rodent and ovine impact acceleration models of TBI, studies within this thesis sought to employ various methods which could eliminate skull fracture. Whilst there were benefits in the use of a helmet in the previous ovine model, the domed steel captive bolt still posed considerable risk for skull fracture upon contacting the skull. Therefore, the captive bolt was machined to be flat for use in studies conducted in this thesis (*chapter 3.4*). Additionally, given this model was planned to allow survival of the animal, the surgical procedure which required a steel helmet to be adhered to the skull of the animal with dental cement would have impacted animal survival. In order to attach the helmet, dissection of this region of the head would result in trauma to the masticatory muscles (medial pterygoid, masseter and temporal muscles) which could impact ethical survival (Allouch, 2017). Removal of the helmet could also result in trauma to the temporomandibular region of the head which also could impact ethical waking of the animal. Therefore, the use of a silicone cover on the face of the captive bolt tip was used to emulate a protective intermediary between the impactor and the head of the animal (*chapter 3.4*) However, this proved to be insufficient, still producing

superficial skull fracture in 55.5% (5/9) of animals injured in Chapter 4 and all animals subject to injury in Chapter 5.

7.3 Development of AI in ovine models of TBI

It was postulated in chapter 5.7, that the lacking DAI seen in animals injured in those experiments as opposed to animals injured in Lewis *et.al.* (1996) experiments was due to the skull fracture absorbing the force of impact and subsequently affecting the production of DAI (Lewis, et al. 1996). This could be supported when comparing skull fracture incidence between the two experiments. Granted, this could also be due in part to the use of a 21-charge in Chapter 5 experiments, as compared to a 17-charge used in those conducted by Lewis *et.al* (1996) (Lewis, et al. 1996). Interestingly, experiments conducted by Anderson *et.al.* (2003) did not instrument the temporal bone with a steel protector plate and had increased skull fracture and decreased DAI as compared to Lewis *et.al.* (1996) (Anderson, et al. 2003; Lewis, et al. 1996). Although, as discussed in chapter 5.4, Anderson *et.al.* (2003) did demonstrate substantial peak resultant magnitudes of linear acceleration which likely contributed to the skull fracture further absorbing impact force (Anderson, et al. 2003).

Not only was this study unable to prevent skull fracture, but we were also unable to replicate the widespread DAI that has been observed previously in the ovine TBI model using a 17-charge, as evidenced by upregulation of APP mRNA as acutely as 30 minutes post-injury, in conjunction with diffuse APP immunostaining at two and four hours post-injury (Anderson, et al. 2003; Lewis, et al. 1996; Van den Heuvel, Blumbergs, et al. 2000; Van den Heuvel et al. 1999; Van den Heuvel et al. 1998). Even the survival study conducted by Grimmelt *et al* was able to report DAI in 30% (2/6) of sTBI cases, with no DAI noted in the mildly injured animals (Grimmelt et al. 2011). Although, DAI was assessed histologically with neuron specific enolase (NSE), a glycolytic enzyme which can be used as a marker of neuronal survival, rather than

the gold standard APP immunostaining used in this thesis and previous work using the ovine TBI model to evaluate DAI (Grimmelt et al. 2011; Haque et al. 2018). In contrast, we were unable to observe significant AI in any of our experiments, utilising 11, 13, 15 or a 21-charge, nor with the addition of a PTH period of 15 minutes. DAI was assessed in this thesis via manual counting of total APP+ve axons in the selected ROI. However, it is important to discuss the discrepancies in the analyses of DAI and more specifically, APP, amongst previous studies as compared to the comprehensive quantitative analyses of APP in this thesis. The marked differences in the analysis of DAI make it difficult to directly compare results from this thesis with those reported previously. APP has been used as the hallmark measurement of DAI in previous ovine TBI studies (Anderson, et al. 2003; Lewis, et al. 1996; Van den Heuvel, Blumbergs, et al. 2000; Van den Heuvel et al. 1999; Van den Heuvel et al. 1998). Specifically, the initial studies performed by Lewis *et.al.* allocated a total APP Score (APPS) ranging from 0 to 100, which was derived from segmenting the eight individual, 5 µm coronal brain sections into a total 109 sectors and allocating a positive AI score if AI was present in any given sector. The percentage of sectors demonstrating APP+ve AI was then calculated from the total number of sectors (Lewis, et al. 1996). Whilst this method has many benefits, the analysis itself is quite indiscriminate and does not allow for a quantitative analysis of DAI. Further studies conducted by Van den Heuval *et.al.* (1998) used the same methodology, although specifically assessed the presence of somal APP rather than axonal APP (Van den Heuvel et al. 1998). The presence of somal APP was measured using APP immunocytochemistry and assessing the expression of APP mRNA antigens (Van den Heuvel et al. 1999; Van den Heuvel et al. 1998). The presence of APP in neurons plays an important role in neuronal growth and synaptic plasticity and can be increased following the acute phase following trauma (Van den Heuvel et al. 1999; Van den Heuvel et al. 1998), such that it does not directly assess DAI. The presence of somal APP may be a neuroprotective response to injury whereas the presence of axonal APP suggests there is

disruption to axonal transport as a result of AI (Plummer, et al. 2016). The most recent studies by Anderson *et.al.* (2003) assessed APP+ve axons via immunocytochemistry, using a 4 mm^2 grid that was placed over the three, 5 µm sections selected for analysis, and APP was graded in each sector according to the following system: Level 1: 1-10 axons, Level 2: >10 axons and Level 3: macroscopically visible. This system is quite an arbitrary qualitative method of analysis. Whilst there was a very low-level quantitative threshold set for Level 2, Level 3 was purely qualitative. Indeed, there were sections that demonstrated Level 3 APP staining, although the location of this is never discussed, besides at the location of ICP probe placement which is to be expected following such obvious, direct, physical trauma to the parenchyma. DAI was assessed via a different method in this thesis which employed a purely quantitative method of manually counting the number of APP+ve axons present in clearly delineated brain regions, which included major white matter tracts that would have been most vulnerable to impact and surrounding grey matter regions. This allowed the direct comparison of cellular proliferation among injury groups as compared to sham, which has not been done to date in any large animal model of TBI.

A similar semi-quantitative method for assessment of DAI to that used by Anderson *et.al.* (2003) and Lewis *et.al.* (1996) has been applied in other large animal models of TBI (Browne et al. 2011; Smith et al. 2000). This involves assessment of AI number in much smaller sectors (1.2 mm^2) and is graded to the following system: mild: 1-5 damaged axons, moderate: 6-15 damaged axons and severe: >15 damaged axons (Smith et al. 2000). This same method has been applied to markers of neurofilaments as well as APP+ve axons (Chen, et al. 1999).

Another key difference between the work in this thesis and earlier studies using the ovine model of TBI is the use of male animals, with the earlier studies by Anderson *et al*, Van den Heuvel

et al and Lewis *et al* injuring female sheep (Anderson, et al. 2003; Lewis, et al. 1996; Van den Heuvel et al. 1998). As a result, other factors could have influenced the differences in DAI production. Sex is thought to be a confounding factor which can influence pathological response to injury.

7.3.1 Effect of sexual dimorphism on TBI outcomes

Clinically, females have a decreased incidence of morbidity and mortality after moderate-severe TBI when compared with age-matched males (Berry et al. 2009), with both oestrogen and progesterone thought to be a key contributor to such differences. On the contrary; other work investigating both human and rodent neurons has found female axons to be smaller, with fewer microtubules, and thus are at higher risker of breaking compared to male axons following an equivalent force from simulated TBI (Dollé et al. 2018). Female axons exhibited significantly more axonal swellings and increased loss of calcium signalling function than male axons (Dollé et al. 2018). Therefore, sexual dimorphism of axonal structure in the brain must be considered. This could contribute to worsened axonal pathology in females compared to males exposed to the same mechanical injury (Dollé et al. 2018).

Furthermore, specific to sheep there may be marked differences in the anatomy and thickness of the skull. Rensch's rule describes the pattern of sexual size dimorphism, claiming that in taxa where males are the larger sex, they exhibit higher body size ratios (Parés Casanova 2015; Rensch 1950). Whilst sexual dimorphism has not been directly studied in Australian Merinos, previous research has demonstrated that the Merino breed is sexually dimorphic (Hernández et al. 2017; Parés Casanova 2015). A key anatomical difference between male and female sheep is the growth of horns in males as a protective mechanism for head butting. To our knowledge, the relationship between skull thickness and horn growth in Merino sheep has not been

discussed in the literature. However, a study investigating the morphometric differences between male and female Zell sheep identified that male sheep have a significantly higher overall skull weight compared to females in the absence of horns (Marzban Abbasabadi, Hajian & Rahmati 2020). This suggests a potential link between skull thickness and potential impact force absorption. Although Merino wethers (castrated males) were used in this study in order to control for horn growth, a bony outgrowth of the frontal bone (beginnings of horn core growth) can be seen as early as 118 days gestation in the male Merino sheep (Lyne & Hollis 1973). This suggests that depending on the time of castration, increased circulation of androgens could be contributing to the growth of horns, and by proxy, the skull (Fisher, Bray & Johnstone 2010). Importantly, time of castration was not available for animals used in this thesis, and the size of horn buds varied across the cohort. Energy absorption and local stress distribution of horn bone material during ramming has been simulated via FE modelling of big horn sheep (Drake et al. 2016). Specifically, trabecular bone (which forms the horn core) was shown to absorb impact energy and reduce brain cavity accelerations during high impact ramming of the skull (Drake et al. 2016). However, similar dynamic loading studies should be considered to effectively evaluate the differences between male and female Merino skulls in absorbing force following impact.

Nonetheless, more recent ovine TBI studies have shifted to the use of male sheep (Bellapart et al. 2016; Bellapart et al. 2018; Byard et al. 2012; Vink, Bahtia & Reilly 2008; Vink, Gabrielian & Thornton 2017). Although not the primary outcome measure, two singular studies have investigated DAI following sTBI using the ovine impact model of acceleration TBI (Bellapart et al. 2016; Bellapart et al. 2018). Although the injury model itself was the same with the use of a 17-charge in both studies, the injury in these studies was considered to be either mild (Bellapart et al. 2016) or severe (Bellapart et al. 2018) based on the weight of the injured animals, and not based on the actual pathological outcome. The mild model

injured eight animals weighing 40-45 kg and severe model injured nine animals weighing 65-70 kg. DAI was assessed and graded within the left and right cortices, left thalamus and medulla (*Fig. 7.2A-C*). Each region was qualitatively graded as follows: *Mild*: focal contusion with APP labelling limited to the site of injury or focal APP labelling; *Moderate*: pattern of APP staining greater than one hemisphere, greater than half a hemisphere or less than half a hemisphere; and *Severe*: characterized for the presence of diffuse staining and sub-classified as either diffuse vascular injury, diffuse AI with macroscopic haemorrhage, diffuse AI with microscopic haemorrhage/tissue tears or diffuse AI only (Bellapart et al. 2016; Bellapart et al. 2018). It was clear that in both studies the predominating injury was classified as mild, however toward the thalamus and medulla injury became classified as moderate-severe in some cases (*Fig. 7.2A&B*). It appears as though the weight differential between these studies did not have an effect on the production of DAI. When considering the grading system, the requirement to fit into each category is quite arbitrary. Macroscopic injuries were not discussed in either study and the most severe category of APP grading only requires there to be the presence of DAI of which the definition is not quantified. If animals injured in Chapter 5 of this thesis were categorised based on the grading system used in the studies reported by Bellapart *et.al.* 5/8 animals would be classified as *severe* based on macroscopic injury alone and 8/8 animals had what could be considered DAI in the thalamus (Bellapart et al. 2016; Bellapart et al. 2018). In summary, a grading system which is purely qualitative does not always reflect the true pathological response to injury with reference to DAI.

A

TABLE 1 | Tissue sampling labeling.

Anatomical regions	Anatomical location
AL	Core of contusion, left side
BL	Ischemic penumbra, left side
AR	Mirror region to core of contusion, on the right
BR	Mirror region to ischemic penumbra, on the right
C	Thalamus ipsilateral to injury
D	Medulla

B

TABLE 7 | Amyloid precursor protein (APP) staining qualitative scores by tissue region in a "severe head injury" model showing its distribution among six of the eight subjects for the severe head injury study.

Anatomical regions	Amount of subjects categorized on each qualitative APP score		
	Mild	Moderate	Severe
AL	5	0	1
AR	5	1	0
BL	4	1	1
BR	5	0	1
C	4	1	1
D	5	1	0

APP staining is predominantly of "mild" category at all regions, but an expression of "moderate" and "severe" is also present among all regions.

C

TABLE 8 | Amyloid precursor protein (APP) staining qualitative scores by tissue region in a "mild head injury" model showing its distribution among nine subjects for the mild head injury study.

Anatomical regions	Amount of subjects categorized on each qualitative APP score		
	Mild	Moderate	Severe
AL	9	0	0
AR	9	0	0
BL	9	0	0
BR	9	0	0
C	2	2	5
D	5	2	2

APP staining is predominantly "mild" in category at all regions; categories of "moderate" and "severe" are only present at axial anatomical regions where the highest acceleration–deceleration force mainly concentrates.

*Figure 7.2: Tissue sampling labels from studies conducted by Bellapart et.al. (**A**), APP qualitative scores by tissue region in a 'severe' model of TBI (**B**) APP qualitative scores by tissue region in a 'mild' model of TBI (**C**) (Bellapart et al. 2016; Bellapart et al. 2018).*

Other studies using male sheep have not directly assessed DAI, instead focussing on ICP changes post-injury. Immediate increases in ICP to values as high as 8 times baseline following TBI were observed, before returning to baseline levels within 30 minutes, consistent with a cerebrovascular, event as evidenced by increased ABP response to injury (Byard et al. 2012). Following this, a gradual increase in ICP and subsequent decrease in brain tissue oxygenation ($PbtO_2$) was observed over time post-injury (Byard et al. 2012; Vink, Bahtia & Reilly 2008). Interestingly, the relationship between increased ICP and DAI has been discussed in the

literature, with one clinical study demonstrating approximately 1/3 of patients who have severe DAI as a result of sTBI to have develop increased ICP (Abu Hamdeh, et al. 2018). Whilst changes in ICP and $PbtO_2$ were monitored following trauma in these studies conducted by Byard *et.al.* (2012) and Vink *et.al.* (2008), these were not outcome measures in this thesis.. Additionally, it should be considered that the insertion of probes to measure these parameters can induce AI, which is a possibility for the production of DAI seen in the Bellapart *et.al.* studies also (Bellapart et al. 2016; Bellapart et al. 2018). Thus, it is unclear whether the use of male sheep in this study may have influenced the ability to produce DAI. There are important differences in how injury was generated, such as the use of a different injury device and mushroom shaped captive bolt, which could in part describe some of the pathological differences between the two models. However, the biomechanics of injury must also be considered and the differences in how this was investigated in work by Anderson *et.al.* as compared to the results presented within this thesis (Anderson, et al. 2003).

7.4 Biomechanical influences on the development of DAI

7.4.1 Effect of angular acceleration on the production of DAI

As discussed in chapter 5.4, the resultant magnitude of angular acceleration produced in this model was comparable to that of previous work which should have been sufficient to produce substantial amounts of DAI (Anderson, et al. 2003). However, due to the lack of DAI seen in results in this thesis, this raised the question of how these models may have differed biomechanically in order to affect the amount of DAI produced. Previous work using pigs has highlighted that the magnitude of angular acceleration may not directly influence the number of injured axons produced following impact (Browne et al. 2011). In particular following a mild impact, direction of rotation seems to influence the production of DAI (Browne et al.

2011). Animals were subject to either coronal or axial rotation at a controlled velocity between 95 and 120 rad/sec. DAI was produced in both planes of rotational acceleration; however, a higher number of moderate axonal profiles were observed in the brains of animals injured in the axial plane (Browne et al. 2011). Interestingly, the peak angular acceleration values for axial rotation were considerably lower than that of coronal rotation (axial: 15-26 krad/sec^2, coronal: 30-59 krad/sec^2) (Browne et al. 2011). As previously discussed, the key difference between the pig model when compared to the sheep model, is the induction of injury via controlled angular acceleration in a single plane (Cullen et al. 2016). Injury is induced by impact in the sheep model, which means that the angular acceleration in particular planes cannot be predicted consistently and, must be evaluated via analysis of biomechanical data captured following the onset of impact. This therefore means that the pattern of DAI produced by angular acceleration in specific planes cannot be consistently predicted either. In experiments conducted in Chapter 4, and the previous model of sheep TBI, the head of the animal was suspended on sandbags in order to optimise unrestrained coronal and axial rotation of the head (Anderson, et al. 2003). As described in chapter 3.6, animals injured in experiments conducted in Chapter 5 had their head suspended in a cervical sling, in order to increase the surface area / six-degrees-of-freedom for rotational acceleration. Indeed, the resultant peak magnitudes of angular acceleration were comparable between the model used in this thesis when compared to previous data (Anderson, et al. 2003). However, given that there were differences in the way the head was suspended between the current and previous model of ovine TBI, it could be possible that the magnitude of angular acceleration was distributed within different planes, therefore affecting the amount of DAI produced. However, as previously mentioned, biomechanical analysis of angular acceleration conducted by Anderson *et.al.* revealed that acceleration could not be described by a single axis of rotation but was attributed mainly to the x and y axes (Anderson, et al. 2003). Although, it should be considered

that these axes were not defined with anatomical reference to the sheep head anatomy and therefore the distribution of acceleration within these axes may not be completely representative of the pathological outcomes. The importance of defining an anatomically relevant ACS is just as critical for describing linear acceleration. The resultant linear acceleration is different at all of the locations on the body (*i.e.* resultant magnitude of linear acceleration is different according to the location of the origin that is set by the ACS). This is why it is important for the origin point to reflect the CoM of the head, so linear acceleration of the head can be anatomically described. As for angular acceleration, the orientation of the axes you are using to describe the components of that resultant acceleration will result in different magnitudes of each component (*i.e.* amounts of x, y, z acceleration). Although as previously discussed, isolated linear acceleration is more commonly associated with skull fracture rather than producing DAI (Kleiven 2013). However, a combination of linear and angular acceleration is the most lethal combination for the production of DAI, rather than either one isolated alone (Chen, Go & Mao 2002).

7.4.2 Anatomical significance of the sheep head

In order to describe the distribution of angular acceleration following impact in the ovine model of TBI, this must be done with reference to an ACS which defines an anatomical axis. Either coronal, axial or sagittal rotation will occur about one of these individual axes (*chapter 6.1*). To date, only a single study using the ovine model of TBI has evaluated the biomechanics of impact (Anderson, et al. 2003). Most importantly, as discussed in Chapter 6, the head accelerations were described with reference to an ACS that was not defined with reference to the known CoM of the sheep head or its neutral standing position, which therefore makes it difficult to accurately account for the distribution of angular acceleration that is predominating about any axis following impact. To our knowledge there is no standardised method for

determining an anatomically relevant axis of the head using specified anatomical landmarks in quadrupedal large animals; and more specifically, sheep. This is in part due to the domination of non-impact large animal models of TBI being used in research (Browne et al. 2011; Chen, et al. 1999; Cullen et al. 2016; Smith et al. 1997; Smith et al. 2000). As a result, a novel method for determining an anatomically representative CS for the sheep head was developed for the first time, which involved determining the CoM of the sheep head, which is also unreported in the literature. Whilst the x axis remained relatively unchanged, the new ACS resulted in a reorientation of the z axis becoming more vertical, and the reorientation of the y axis to be angled inferiorly representing the resting stature of the sheep head (*Fig. 6.12)*. This is of paramount importance as axial rotation occurs about the z axis, and coronal rotation occurs about the y axis (Anderson, et al. 2003; Anderson 2000). As these are the angular accelerations to result in the most damaging DAI; the value of being able to describe the distribution of magnitude of acceleration following impact within these axes is unparalleled. The definition of these parameters will allow for better clinical translation between both linear acceleration and, more importantly, angular acceleration determined in ovine models of TBI to those seen in human TBI.

Although this will help the understanding of the biomechanical influence on the production and distribution of DAI. There needs to be a uniform protocol for assessing DAI across all sheep TBI experiments to enhance clinical translation.

7.5 Analyses of DAI and associated pathologies

7.5.1 Axonal pathologies

In order to fully examine the effects of biomechanical forces on AI, it may be necessary to utilise additional methods to determine how axons respond to TBI. There was clearly motion

of the head following impact (*see: Fig. 1.9C in appendix II*), which suggests there should be axonal disruption, yet the axonal responses to stretch injury are still not fully understood at the cellular level in the literature. What is known is that axons are most sensitive and susceptible to stretch injury, and this can result in many different pathological mechanisms (Smith et al. 1999). An increased knowledge and understanding of DAI has emerged in recent years (Atlan, Smith & Margulies 2018; Johnson, Stewart & Smith 2013; Mesfin et al. 2020; Siman et al. 2020; Smith, 2016). As discussed in Chapter 5, a four hour time point may be too acute to see the initial stages of DAI as evidenced by APP+ve induced axonal transport disruption. Although APP+ve swollen axonal profiles are indicative of DAI, the vast majority of axons in white matter tracts appear relatively normal following TBI in all severities of TBI (Johnson, Stewart & Smith 2013; Smith, Meaney & Shull 2003; Smith et al. 2003). TBI induced AI must therefore cause earlier disruptions axons prior to axonal transport interruption and swelling (Smith, 2016). Assessing earlier indicators of AI that would occur prior to the disruption of axonal transport may provide more information into the development of AI following trauma. These earlier stages may provide mechanisms that are more readily treatable. Calcium-mediated axonal damage has been highlighted previously as a potential indicator of early AI (Johnson et al. 2016). Calcium can impair mitochondrial function and is hypothesised to impair fast axonal transport before accumulating at the sites of impaired microtubules via bioenergetic failure (Johnson et al. 2016). This can give rise to a population of axons that have undergone calcium-mediated proteolysis, which can be positively detected with use of SNTF but not APP. Interestingly, elevated serum concentrations of SNTF have been linked clinically to a decline in cognitive performance and abnormal DTI scans following TBI (Siman et al. 2013). Detection of APP via IHC is dependent on substantial impairment of axonal transport before positive axons can be detected and is therefore less sensitive to subtle injury compared to SNTF (Johnson et al. 2016; Siman et al. 2013). Sodium channel proteolysis may be another key early

event following TBI (von Reyn et al. 2009). An *in vitro* model of axonal stretch injury has demonstrated impaired regulation of axonal sodium channels, where the channel inactivation gate is disabled and excessive Na^+ influx is unable to be blocked (Wolf, JA et al. 2001). As a result, the sodium-calcium channel exchangers become reversed and the high-voltage state further maintains the opening of calcium channels, thereby progressively increasing intra-axonal calcium concentrations following injury (Smith, 2016). Finally, the role of neurofilaments in perpetuating DAI as a result TBI has been a topic of recent discussion in the literature (Siedler et al. 2014). Neurofilament compaction (NFC), where interfilament spacing is reduced due to side-arm phosphorylation or proteolysis, is another key determinant of AI pathology (Siedler et al. 2014). Evidence has suggested the possibility of NFC occurring in different subpopulations of axons to those showing impaired axonal transport (DiLeonardi, Huh & Raghupathi 2009; Mohamed, et al. 2020). NFC has been attributed to the blockage of axonal transport following trauma (Siedler et al. 2014). However, recently, it has been suggested that NFC and defective transport, as measured by APP, are separate pathophenotypes of DAI. SMI-32, NF-68 and compacted RMO-14 are all independent markers used to assess neurofilament alterations following trauma (Johnson et al. 2016; Siedler et al. 2014). Interestingly, RMO-14 and NF-68 positive axonal pathology has been shown to exist independently of both SNTF and APP following a pig model of mTBI, further confirming neurofilaments to be a key component in the development of AI (Johnson et al. 2016). Interestingly, the influx of calcium as a result of SNTF changes and sodium channel dysfunction can lead to NFC (Siedler et al. 2014; Staal et al. 2010).

7.5.2 Neuroinflammation

It has been well addressed in the literature that primary DAI sustained at the time of impact signals the recruitment of resident immune cells within the brain (microglia and astrocytes) to

potentiate neuronal recovery through the production of both pro- and anti-inflammatory mediators (Begum et al. 2020; Burda, Bernstein & Sofroniew 2016; Lin & Wen 2013). However, this can also potentiate the production of DAI. Recent research has examined how neuroinflammation modulates AI, with microglial processes converging on APP+ve injured axons within white matter tracts in a large animal porcine TBI model (Lafrenaye et al. 2015). Many large animal experimental models of TBI have found microglial activation, an indicator of neuroinflammation, to be observed as early as 15 minutes and up to six hours post-injury (Browne et al. 2011; Johnson et al. 2016; Lafrenaye et al. 2015; Wofford et al. 2017). Pro-inflammatory cytokines IL-1β, IL-6, and TNF-α, have all been demonstrated to increase following TBI in the brain (Yan et al. 2011). In a rodent model of TBI the expression of these pro-inflammatory cytokines was shown to be enhanced with TBI in conjunction with hypoxia compared to TBI alone (Yan et al. 2011). Interestingly, in results presented in chapter 5.3.9, hypoxia resulted in an increase in peripheral TNF-α and IL-6. TNF-α is a known pro-inflammatory mediator and its action stimulates immunocytes such as natural killer-cells and macrophages/monocytes, and promotes the secretion of several inflammatory factors (Lin & Wen 2013). It can also regulate cell apoptosis (Katschinski et al. 1999). However, more importantly, TNF-α is also able to directly induce primary demyelination and oligodendrocyte apoptosis in neurodegenerative disease (Akassoglou et al. 1998; Previtali, Archelos & Hartung 1997). As such, it can be assumed that TNF-α could contribute to DAI pathologies following TBI; however, the presence of these cytokines would need to be evaluated in brain tissue homogenate. Within this thesis, the neuroinflammatory response to injury was analysed via proliferation of microglia and astrocytes, which has not been completed in any previous work using the ovine model of TBI to date. However, minimal regional differences were noted in both microglial and astrocytic proliferation in results presented in both Chapter 4 and Chapter 5. As such, low APP+ve axons and the paucity of neuroinflammation may suggest that the level

of injury achieved with the use of this model may not be substantial enough to induce significant neuroinflammation.

7.6 Limitations and Future Directions

It was evident from the results of this thesis that skull fracture was unavoidable with the use of this model. It is suggested that further biomechanical modelling be applied to this model to potentially reduce the risk of skull fracture and therefore enhance the translatability of this model for ethical survival of the animal. In previous work by both Lewis *et.al.* and Van den Heuvel *et.al.*, a steel plate was adhered to the bone under the skin to reduce skull fracture. Employing a similar method to future experiments would be desirable (Lewis, et al. 1996; Van den Heuvel et al. 1999; Van den Heuvel et al. 1998). However, it is important to consider in future modelling that such a plate would need to be applied non-invasively/externally to the head in order to allow ethical survival of the animal.

Unfortunately, an unappreciable amount of DAI was produced, however we were able to quantitatively assess DAI via APP+ve staining in the sheep which has not been done before. However, it has been highlighted that only a subpopulation of injured axons are captured by APP staining, especially in more mild forms of TBI. In order to assess the micro-pathological outcomes following TBI more accurately and comprehensively in the sheep, it is suggested that the use of more sensitive markers of DAI are employed in order to capture those subpopulations of injured axons. The use of SNTF along with neurofilament markers (NF-68, RMO-14 and SMI-32) may capture more acute DAI pathologies. Additionally, it is suggested that a four hour time point may be too acute to see significant DAI pathology in this model. Although a four hour time point has been effective in revealing APP+ve staining in the previous model (Anderson, et al. 2003; Lewis, et al. 1996), other large animal models investigating more mild

forms of TBI have successfully found APP+ve staining along with other markers of DAI at the six hour time point (Johnson et al. 2016). In addition to DAI being assessed quantitatively for the first time in the sheep model, neuroinflammatory markers were also effectively used in the evaluation of injury in the sheep which has not been employed in previous TBI models. Whilst both astrocytes and microglia were assessed via IHC (GFAP and IBA-1 respectively), it is strongly encouraged that activation state be further investigated to fully understand the neuroinflammatory response as either pro- or anti-inflammatory. Additionally, ELISA was used to assess the presence of pro-inflammatory cytokines in the peripheral serum. Whilst this provides valuable information into the inflammatory state of the periphery, it is suggested that in future experiments these cytokines be assessed in both fresh brain and CSF samples in order to capture the neuroinflammatory state of the CNS rather than the periphery. A novel period of PTH was implemented in this model which has not been previously reported in a sheep model of TBI before. It appeared this was too acute to elicit a severe enough response to worsen the pathology arising from impact, so a longer period of hypoxia would be desirable to an effect on DAI. Previous work using rodents have successfully exacerbated DAI following injury with the use of a 30 minute PTH period, therefore at least a 30 minute time point is suggested for future experiments.

Unfortunately, this model was unsuccessful in producing an appreciable amount of DAI and associated neuroinflammatory pathologies. However, this model did produce peak resultant magnitudes of both linear and angular acceleration which should have been predictive of considerable DAI. Additional biomechanical evaluation of head acceleration is required in order effectively determine the distribution of angular head acceleration within specific anatomical axes, so to highlight the predominating direction of head rotation (sagittal, coronal or axial). A novel, anatomically representative method of assessing head acceleration in the

sheep was developed in this thesis. However, these anatomical landmarks on the skull of the sheep would require dissection of the head for digitisation during biomechanical calibration and assessment. The skull anatomy of each animal differs slightly, therefore it is suggested that prior to injury each animal undergo CT scanning so to allow the application of a transformation matrix to the head acceleration data in post-processing analyses.

7.7 Conclusion

In conclusion, despite the unsuccessful outcomes, this thesis was able to evaluate different methods for reducing skull fracture in the ovine model of impact acceleration TBI. When these proved unsuccessful in reducing skull fracture, hypoxia was induced in the sheep which is novel and has not been implemented in a large animal model of ovine TBI to date. Biomechanical assessment of both angular and linear head acceleration revealed considerable peak magnitudes which should have been predictive of severe DAI. Finally, the head CoM of the sheep was determined, which to our knowledge is currently unreported in the literature. The CoM was used to create an anatomically representative CS which will help to accurately report both angular and linear head accelerations following impact in the sheep. These results taken together will better inform future troubleshooting of this model, which will overall improve the clinical translation of this model to the human condition.

APPENDIX I: CHAPTER 5 SUPPLEMENTAL DATA: BIOMECHANICAL ANALYSES OF HEAD ACCELERATION

Chapter 5: Characterising the effects of post-traumatic hypoxia on the development of axonal injury in an ovine model of TBI

Appendix I contains supplemental data that is referred to throughout Chapter 5. *Figs. 1.1 – 1.8* depict the linear and angular acceleration of the head throughout the impact event for each of the injured animals. Note the depicted distribution and magnitude of acceleration within each of the x, y and z axes, as well as the resultant acceleration of the head. Additionally, the peak translation of the head following impact is depicted in *Fig. 1.9.*

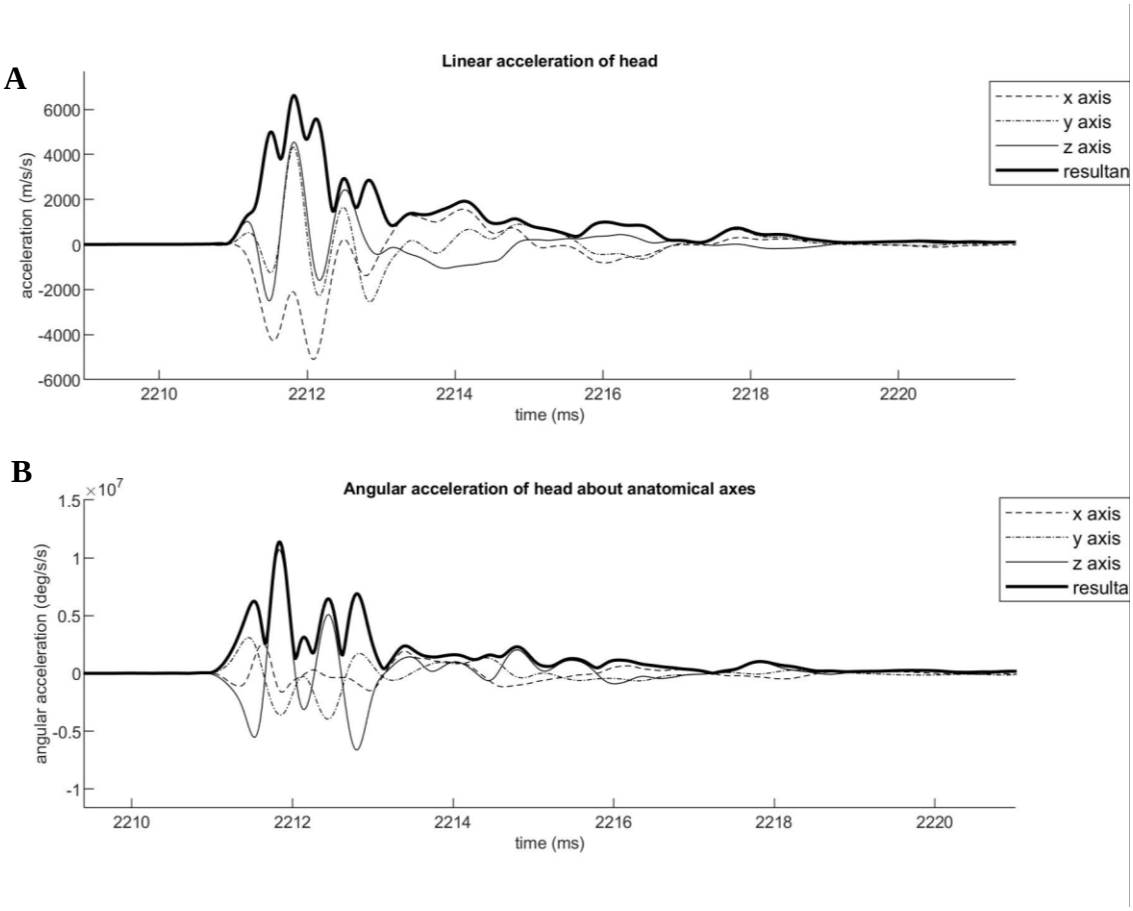

*Figure 1.1: JS007 - Linear (**A**) and angular (**B**) acceleration of the head following impact. Accelerations are depicted in the ACS as defined by (Anderson, 2000).*

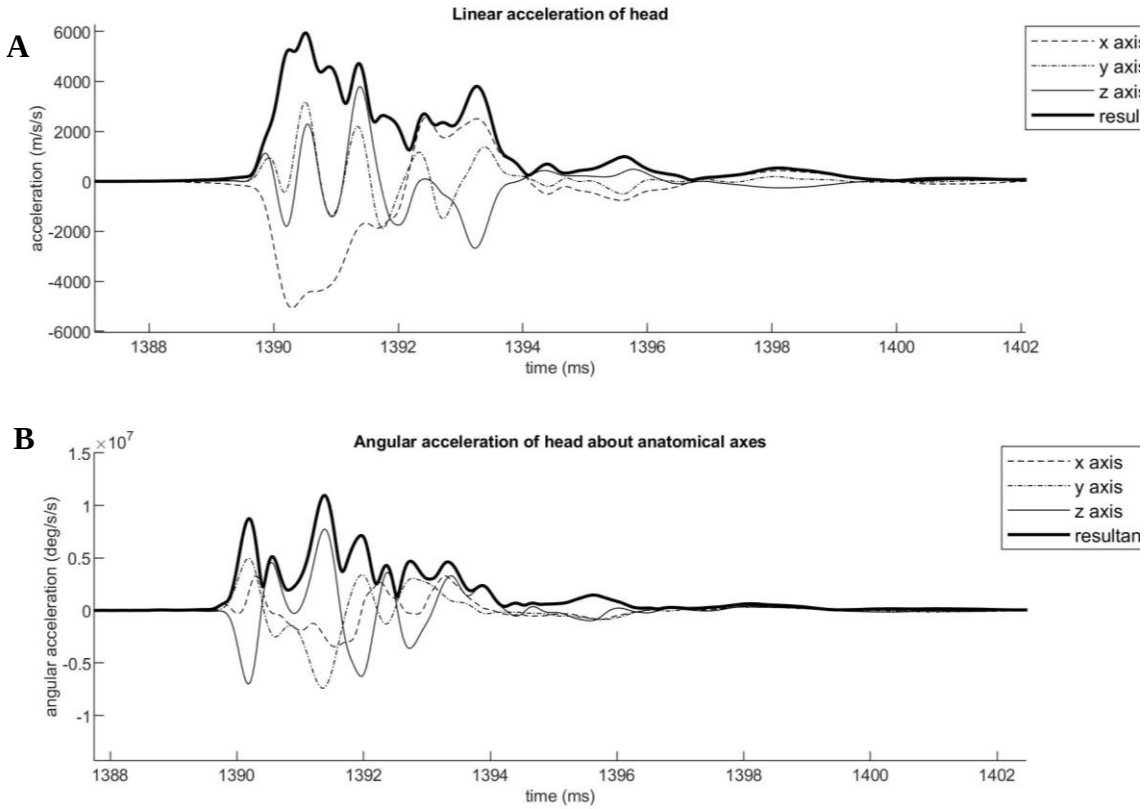

*<u>Figure 1.2:</u> JS009 - Linear (**A**) and angular (**B**) acceleration of the head following impact. Accelerations are depicted in the ACS as defined by (Anderson, 2000).*

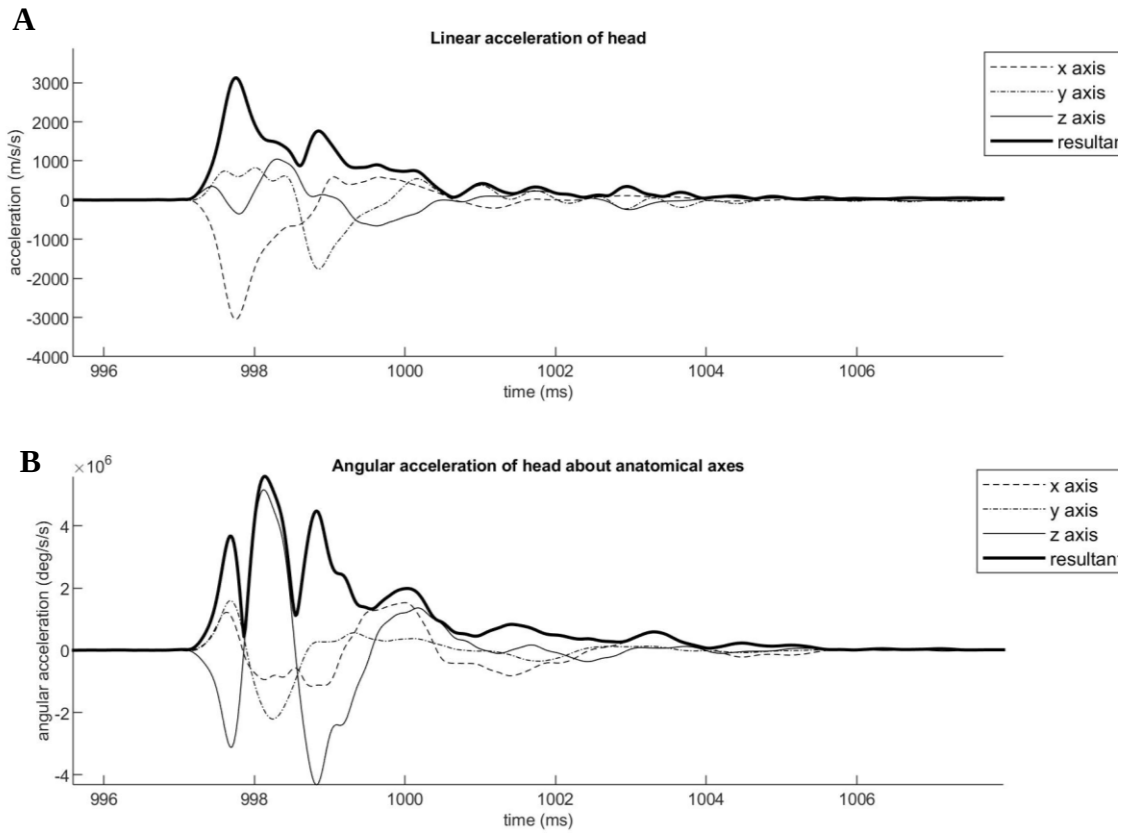

*<u>Figure 1.3:</u> JS010 - Linear (**A**) and angular (**B**) acceleration of the head following impact. Accelerations are depicted in the ACS as defined by (Anderson, 2000).*

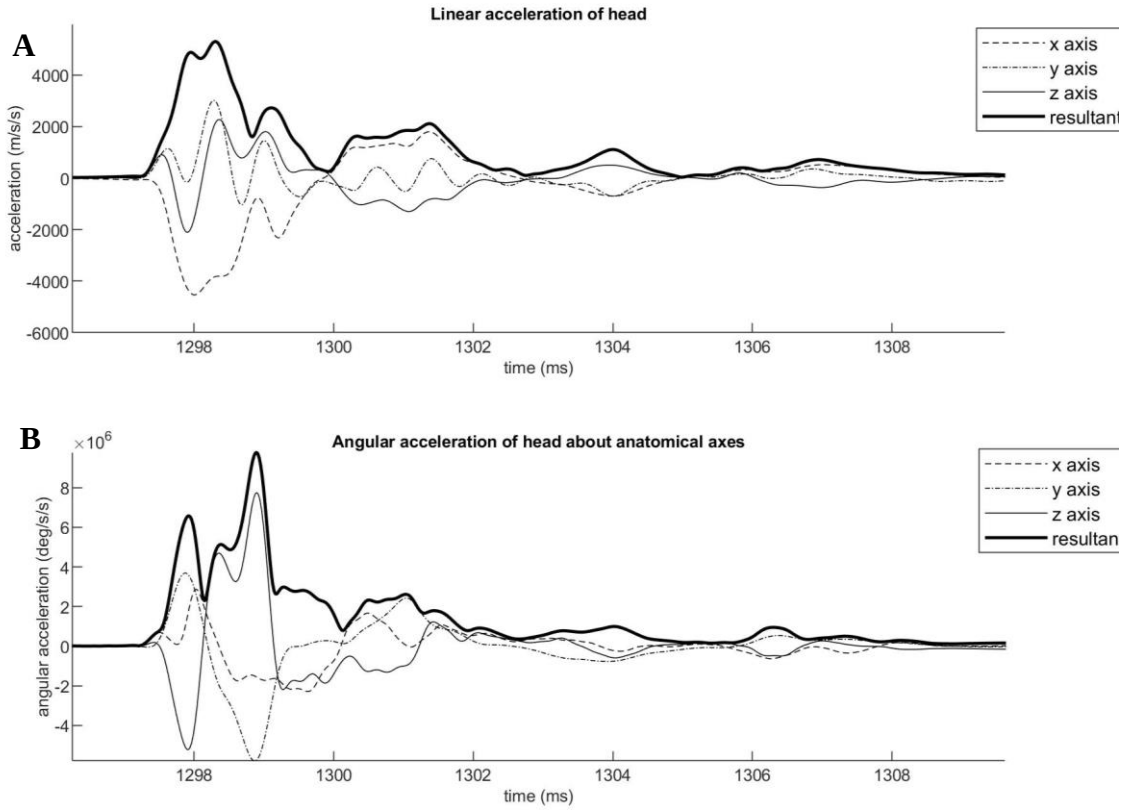

*<u>Figure 1.4:</u> JS011 - Linear (**A**) and angular (**B**) acceleration of the head following impact. Accelerations are depicted in the ACS as defined by (Anderson, 2000).*

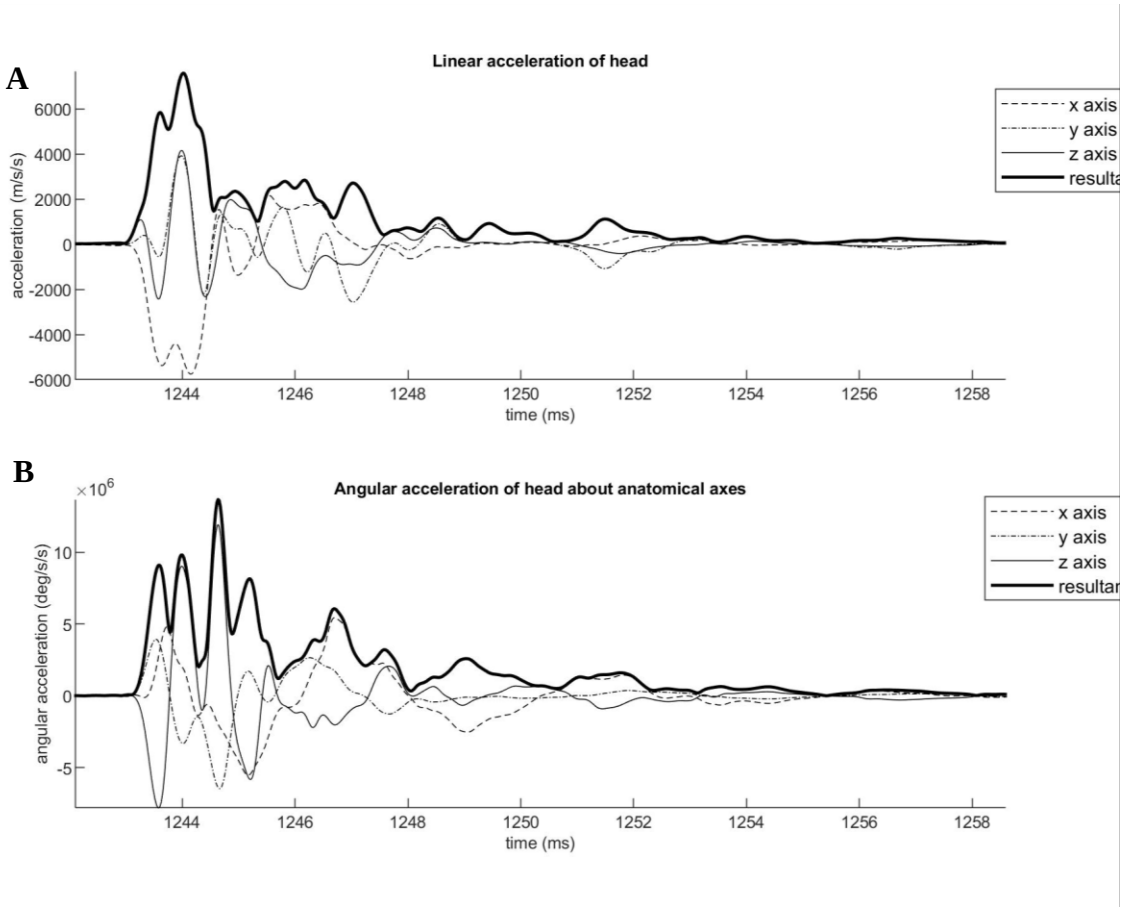

*Figure 1.5: JS012 - Linear (**A**) and angular (**B**) acceleration of the head following impact. Accelerations are depicted in the ACS as defined by (Anderson, 2000).*

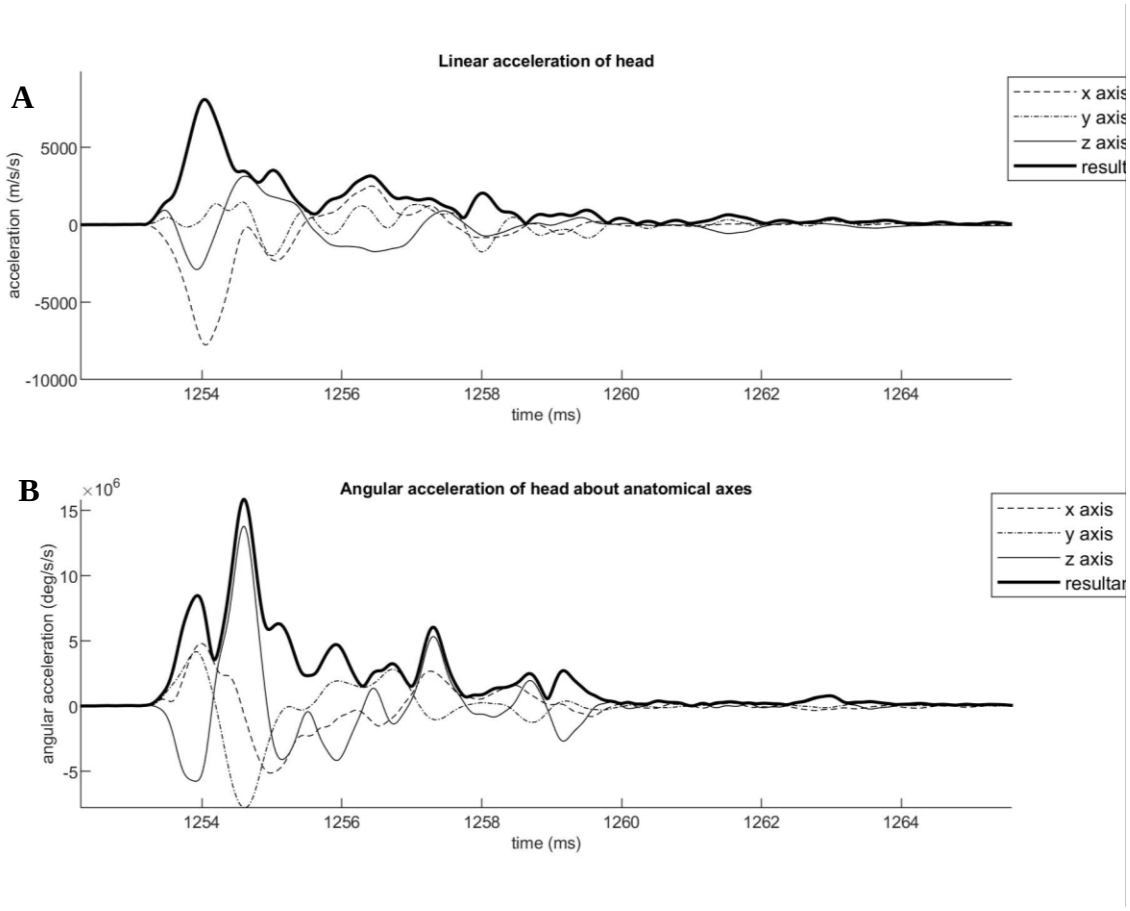

*<u>Figure 1.6:</u> JS013 - Linear (**A**) and angular (**B**) acceleration of the head following impact. Accelerations are depicted in the ACS as defined by (Anderson, 2000).*

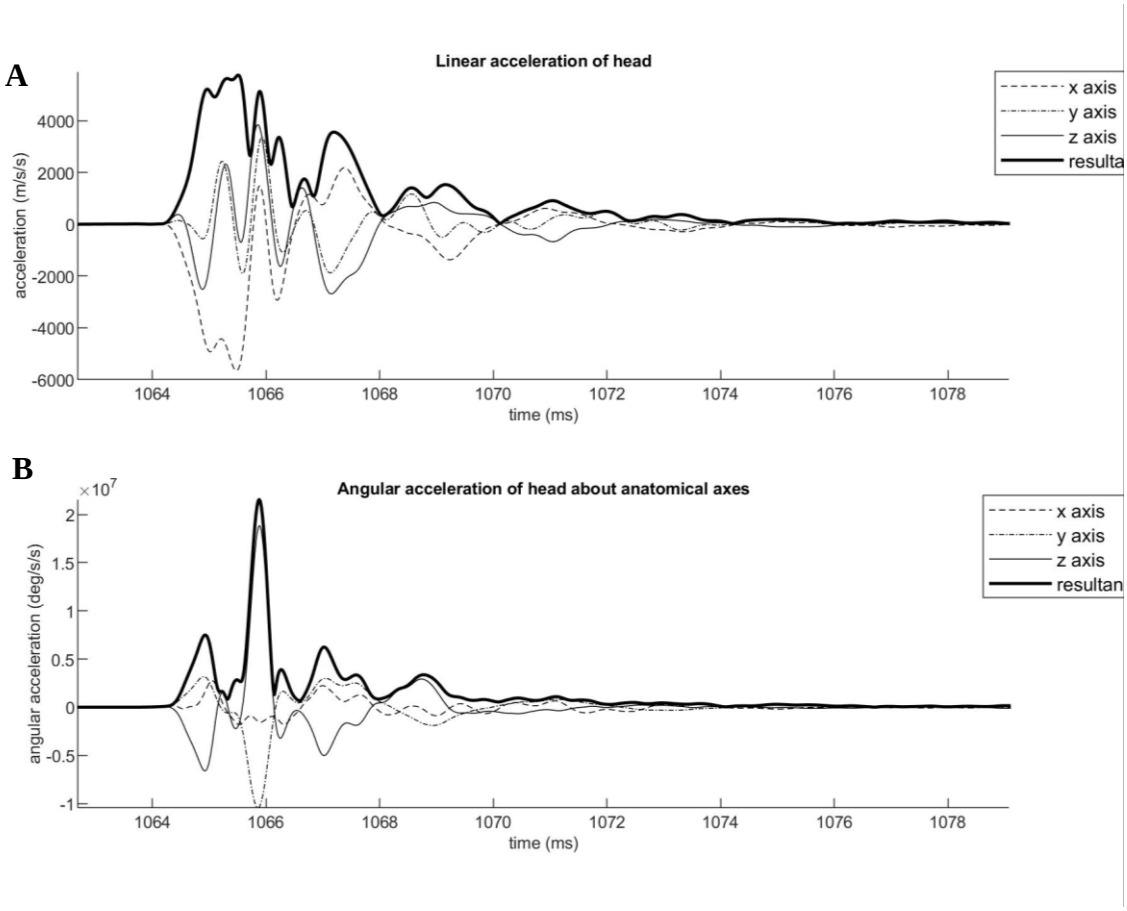

*<u>Figure 1.7:</u> JS016 - Linear (**A**) and angular (**B**) acceleration of the head following impact. Accelerations are depicted in the ACS as defined by (Anderson, 2000).*

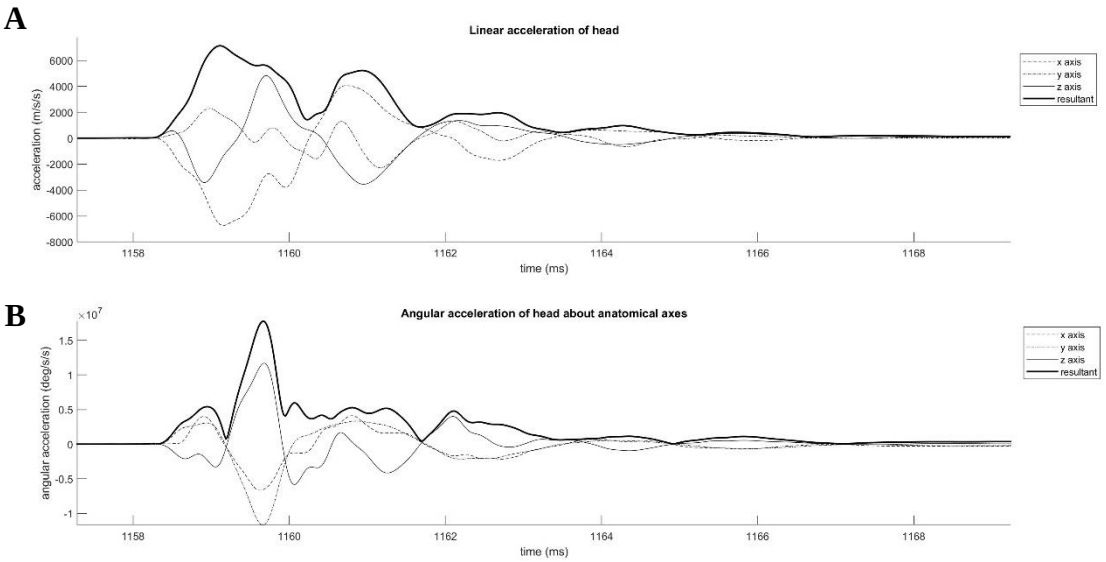

*Figure 1.8: JS017 - Linear (**A**) and angular (**B**) acceleration of the head following impact. Accelerations are depicted in the ACS as defined by (Anderson, 2000).*

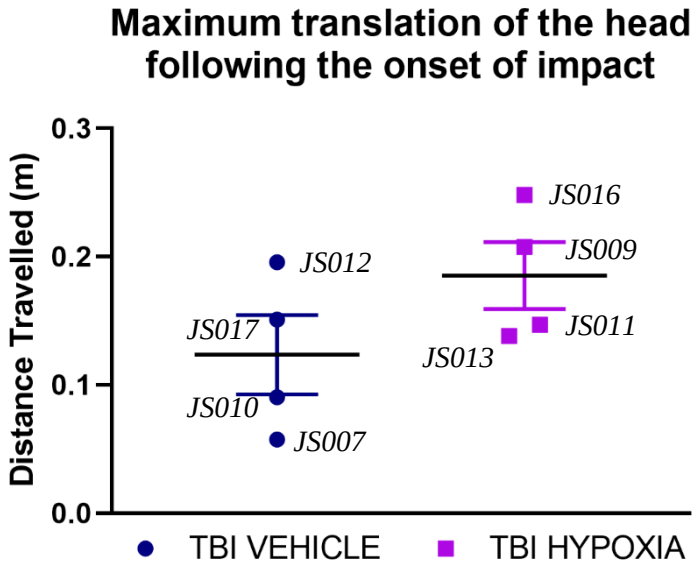

Figure 1.9: JS017 – Maximum translation of the head following impact. Note the lack of distance travelled by JS010

APPENDIX II: CHAPTER 5 SUPPLEMENTAL DATA: ADDITIONAL HISTOLOGICAL DATA

Chapter 5: Characterising the effects of post-traumatic hypoxia on the development of axonal injury in an ovine model of TBI

Appendix II contains the additional heat maps not presented in Chapter 5, which demonstrate the distribution of MBP, IBA-1 and GFAP across the ROI investigated in histological assessment of data in Chapter 5.

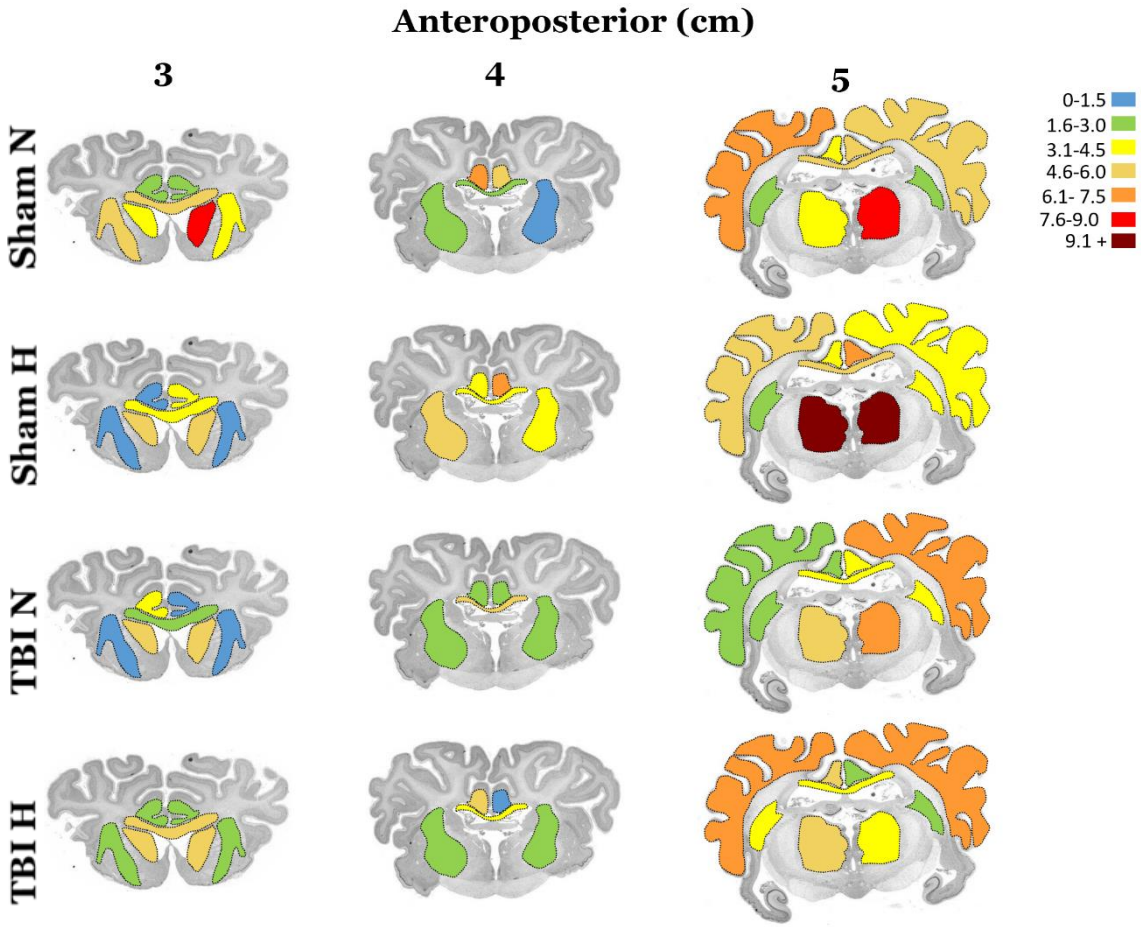

Figure 2.1: Heat map demonstrating the distribution and total length of myelinated fibres in white matter tracts and grey matter regions across three, 1 cm separated anteroposterior brain regions. Scale indicates the length of MBP+ve fibres within the region. N = normoxia, H = hypoxia. Values calculated as the average of n = 3-4 per group.

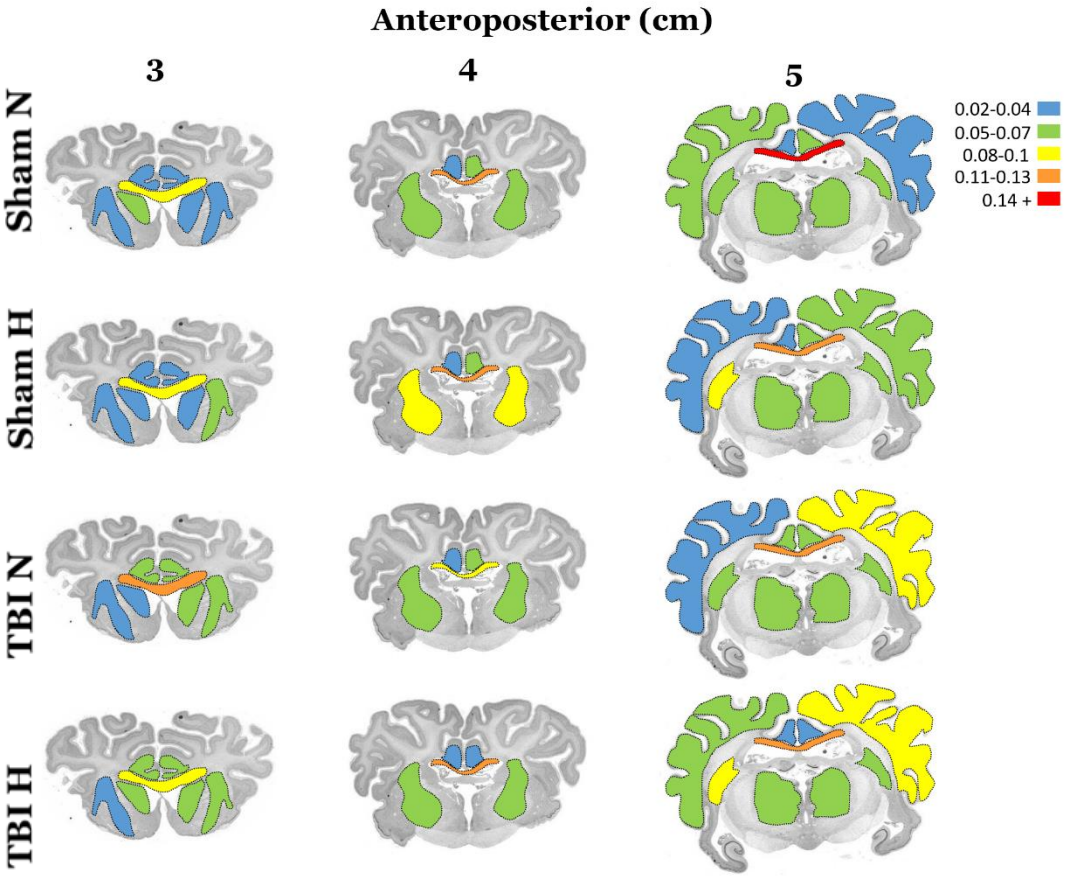

<u>Figure 2.2:</u> Heat map demonstrating the distribution and coherence of myelinated fibres in white matter tracts and grey matter regions across three, 1 cm separated anteroposterior brain regions. Scale indicates the coherence of MBP+ve fibres within the region. N = normoxia, H = hypoxia. Values calculated as the average of n = 3-4 per group.

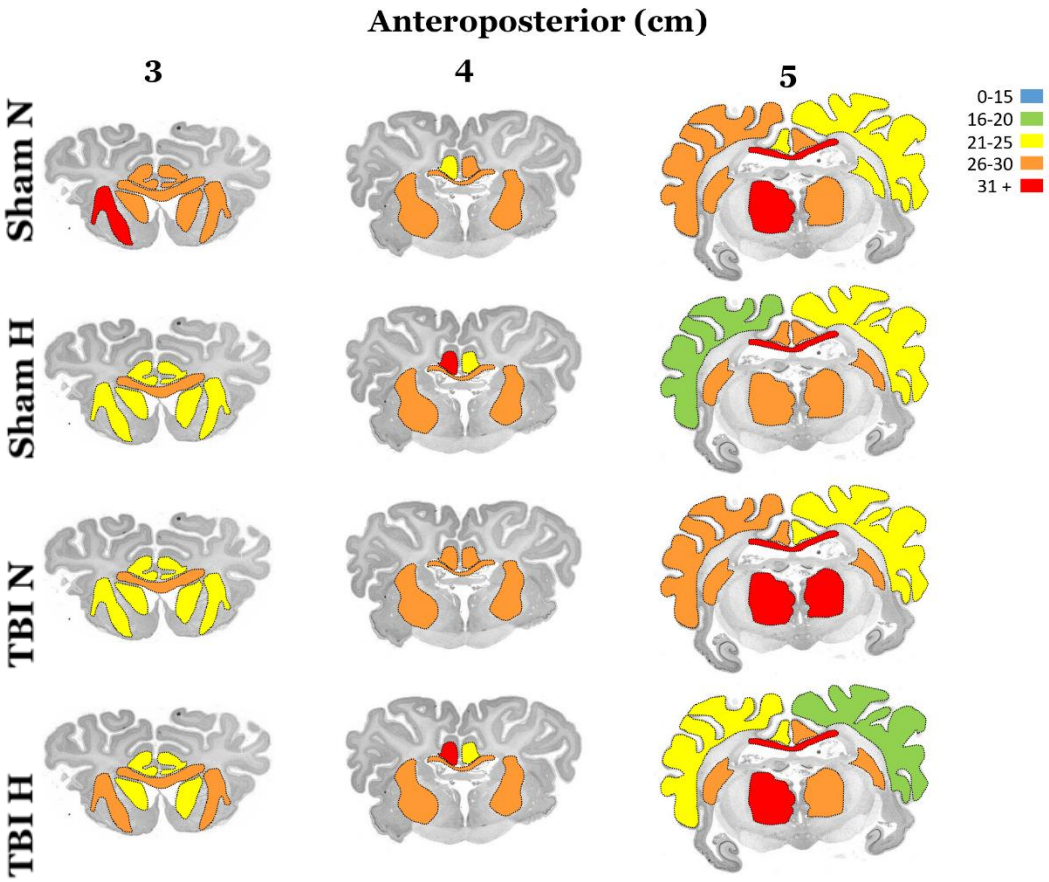

<u>Figure 2.3:</u> Heat map demonstrating the total % of the area of myelinated fibres in white matter tracts and grey matter regions across three, 1 cm separated anteroposterior brain regions. Scale indicates the % / area of MBP+ve fibres within the region. N = normoxia, H = hypoxia. Values calculated as the average of n = 3-4 per group.

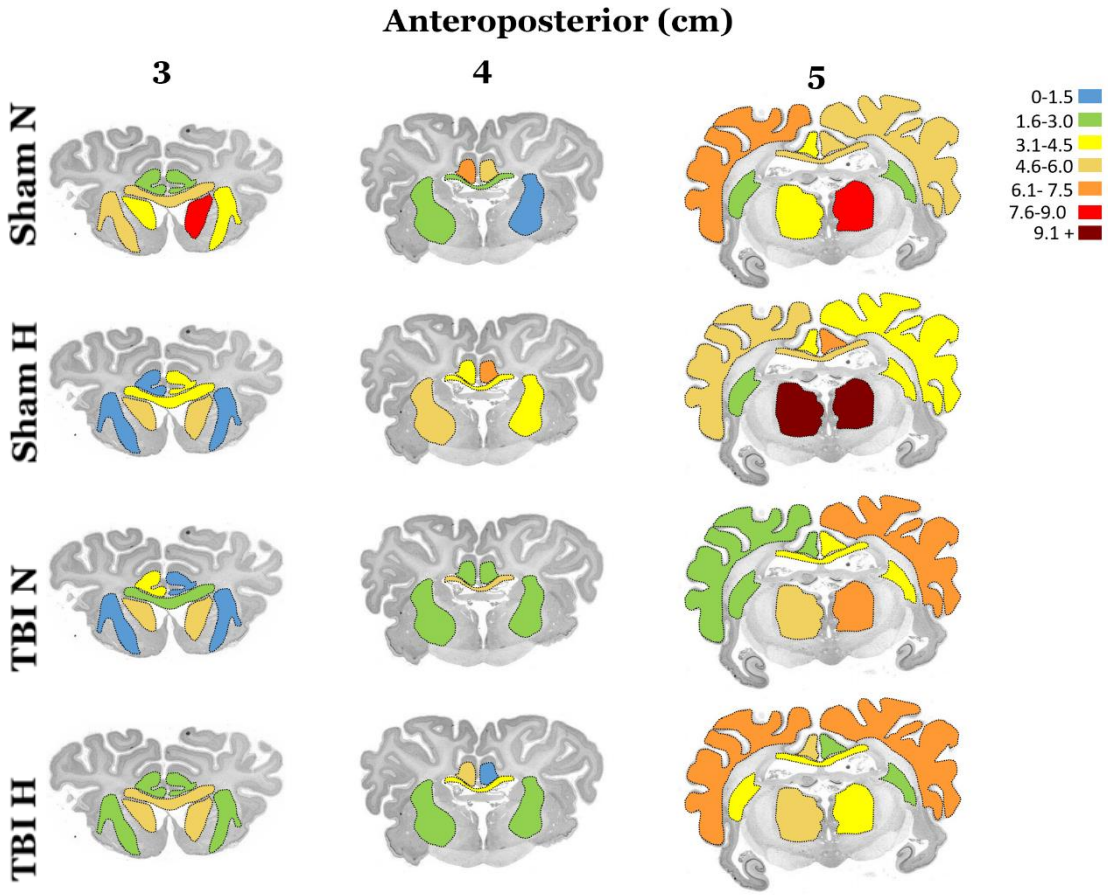

<u>Figure 2.4:</u> Heat map demonstrating the distribution and coherence of myelinated fibres in white matter tracts and grey matter regions across three, 1 cm separated anteroposterior brain regions. Scale indicates the kurtosis of MBP+ve fibres within the region. N = normoxia, H = hypoxia. Values calculated as the average of n = 3-4 per group.

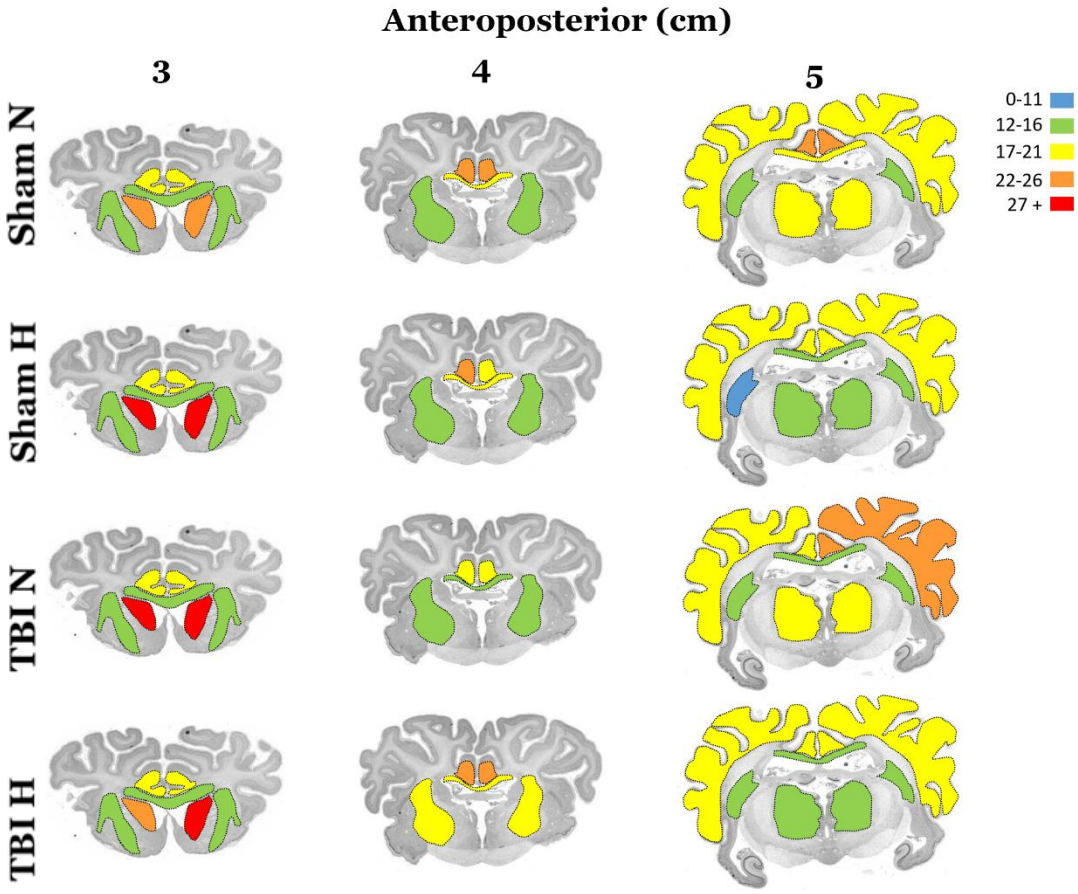

<u>Figure 2.5:</u> Heat map demonstrating the expression and distribution of microglial number in white matter tracts and grey matter regions across three, 1 cm separated anteroposterior brain regions. Scale indicates the % / area of IBA-1+ve fibres within the region. N = normoxia, H = hypoxia. Values calculated as the average of n = 3-4 per group.

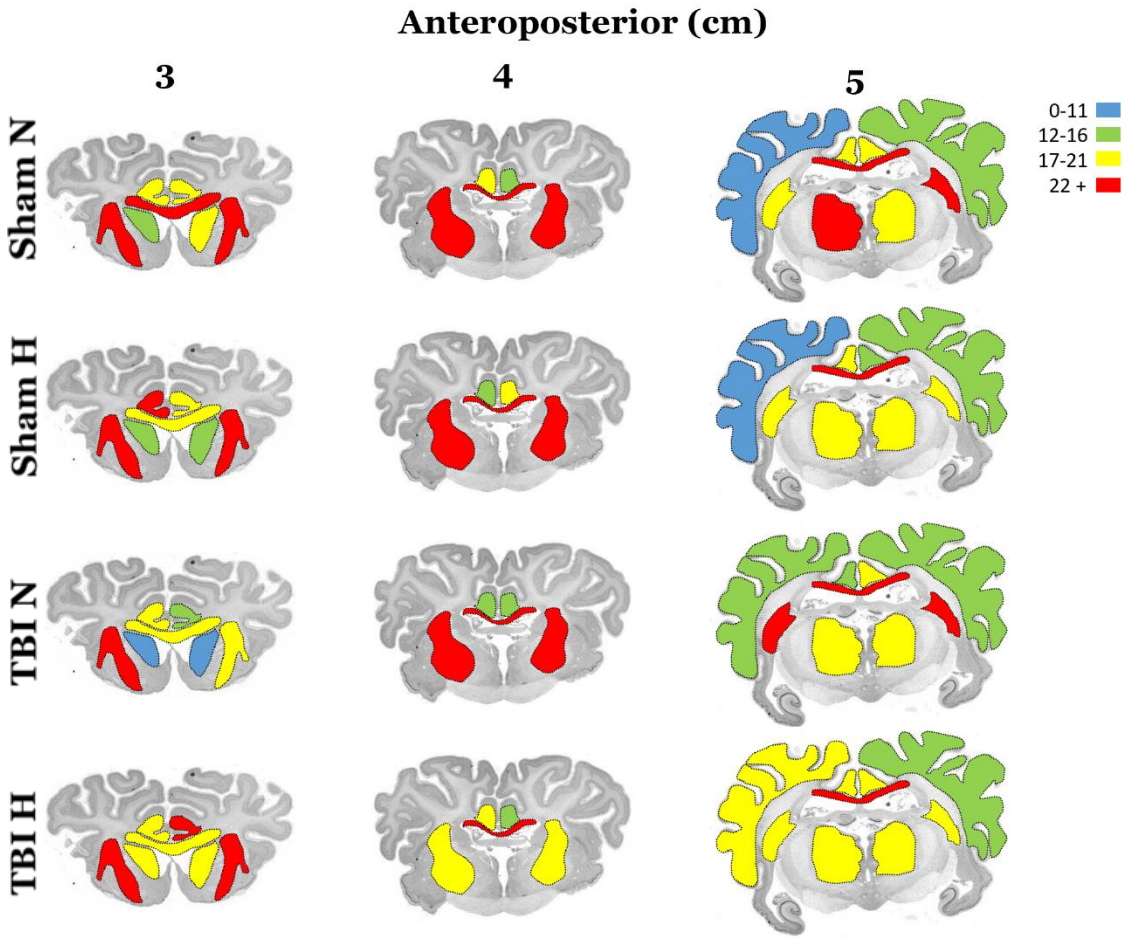

Figure 2.6: Heat map demonstrating the expression and distribution of astroglial number in white matter tracts and grey matter regions across three, 1 cm separated anteroposterior brain regions. Scale indicates the % / area of GFAP+ve fibres within the region. N = normoxia, H = hypoxia. Values calculated as the average of n = 3-4 per group.

APPENDIX III: CHAPTER 6 SUPPLEMENTAL DATA: BIOMECHANICAL ANALYSES OF HEAD ACCELERATION IN AN ACS DEVELOPED WITH REFERENCE TO SHEEP HEAD ANATOMY

Chapter 6: Determining the CoM of the sheep head: Biomechanical optimisation of the ovine model of impact acceleration TBI

Appendix III contains supplemental data that is referred to throughout Chapter 6. *Figs. 3.1 – 3.8* depict the linear and angular acceleration of the head throughout the impact event for each of the injured animals. Note the depicted distribution and magnitude of acceleration within each of the x, y and z axes, as well as the resultant acceleration of the head. These accelerations are those captured from animals injured in Chapter 5 experiments; however, a transformation matrix was applied to each of these data sets which was created from results generated in Chapter 6.

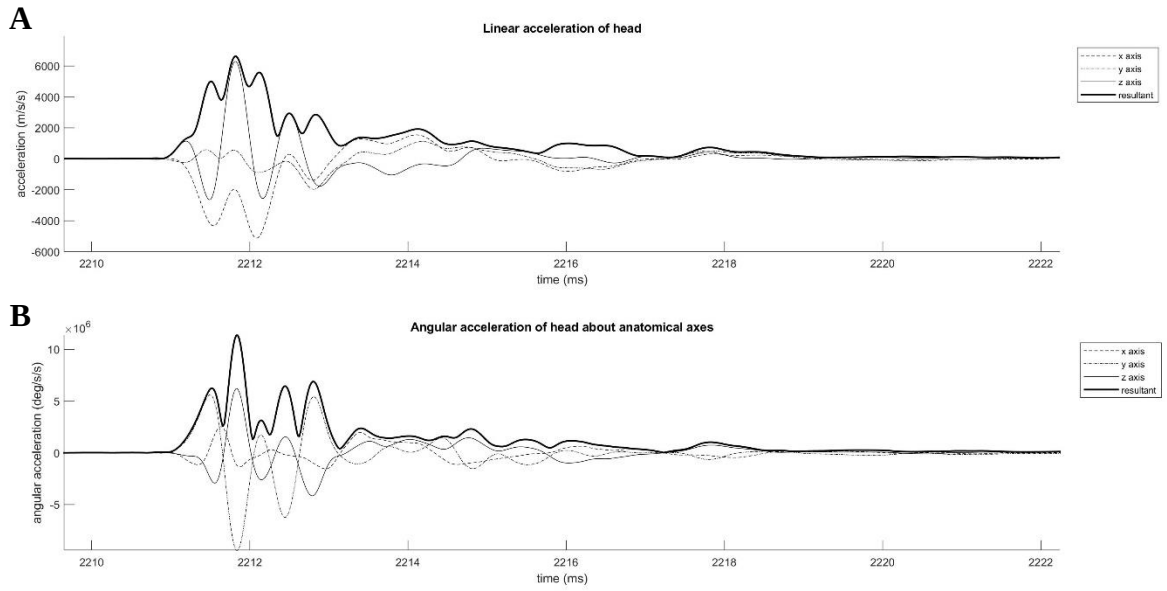

*<u>Figure 3.1:</u> JS007 - Linear (**A**) and angular (**B**) acceleration of the head following impact. Accelerations are depicted in the ACS as defined by results from Chapter 6.*

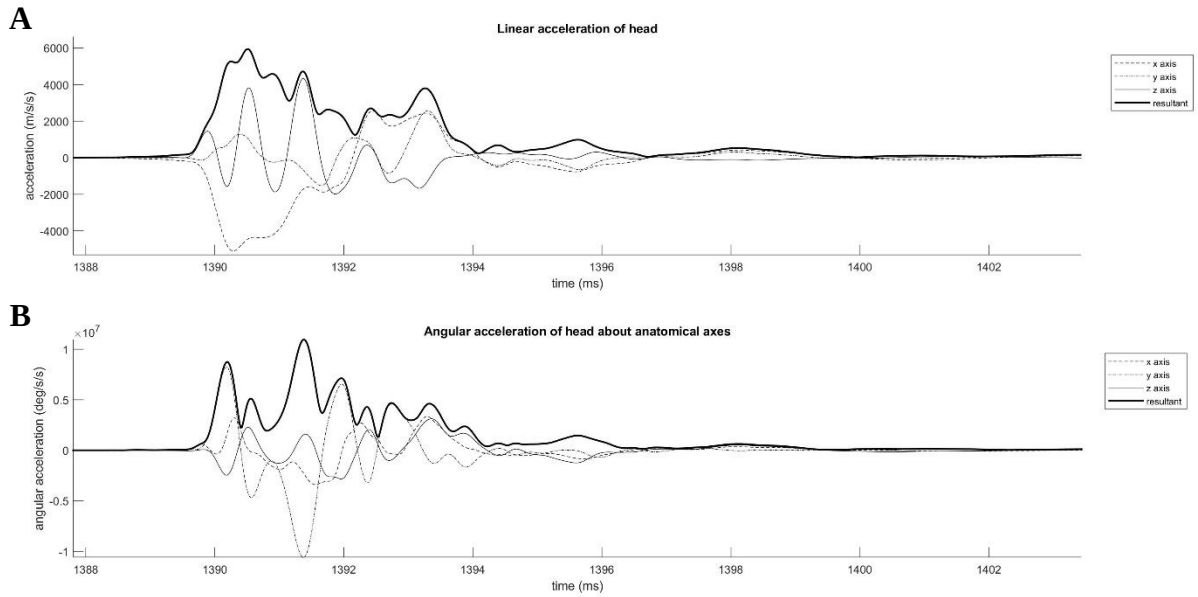

*<u>Figure 3.2:</u> JS009 - Linear (**A**) and angular (**B**) acceleration of the head following impact. Accelerations are depicted in the ACS as defined by results from Chapter 6.*

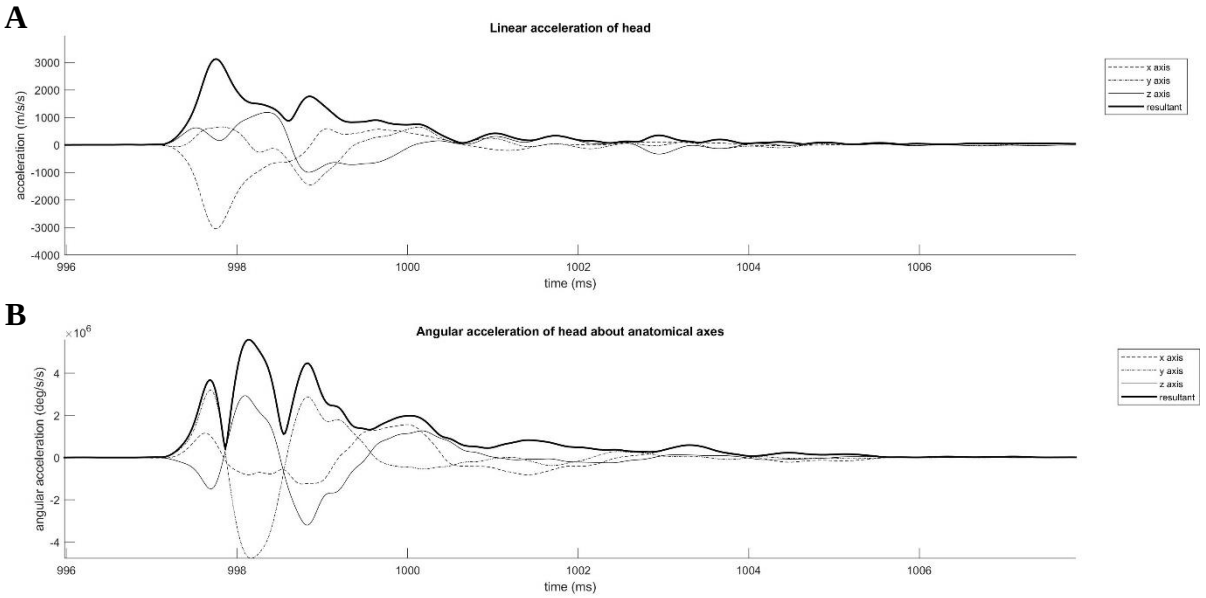

*<u>Figure 3.3:</u> JS010 - Linear (**A**) and angular (**B**) acceleration of the head following impact. Accelerations are depicted in the ACS as defined by results from Chapter 6.*

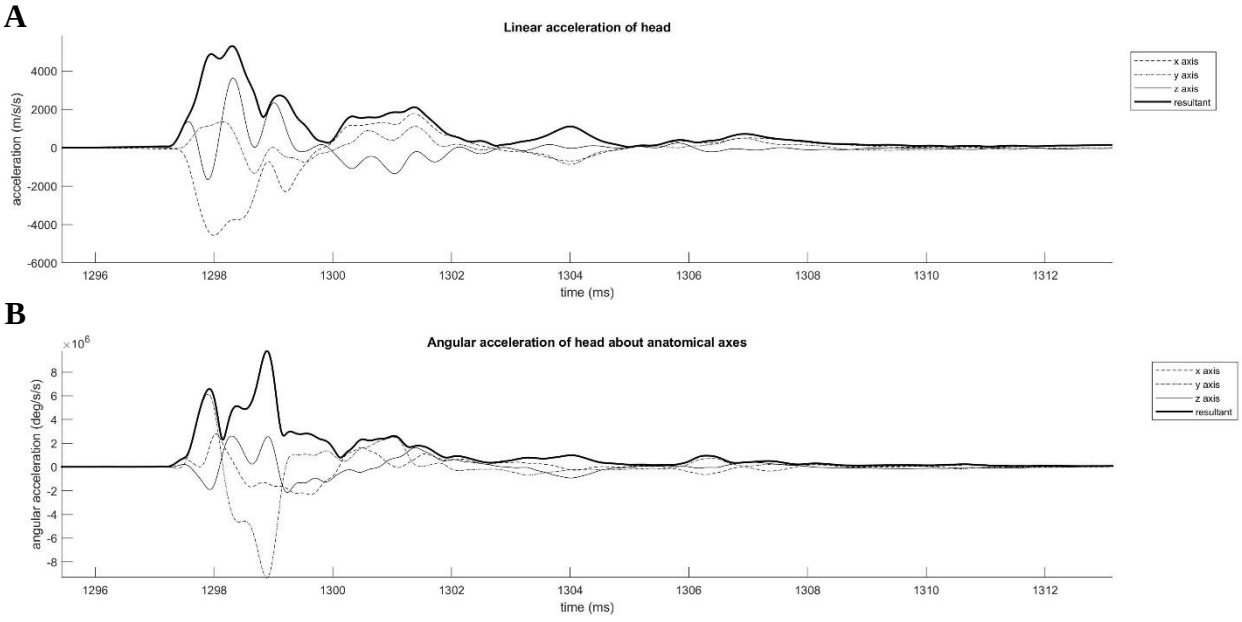

*<u>Figure 3.4:</u> JS011 - Linear (**A**) and angular (**B**) acceleration of the head following impact. Accelerations are depicted in the ACS as defined by results from Chapter 6.*

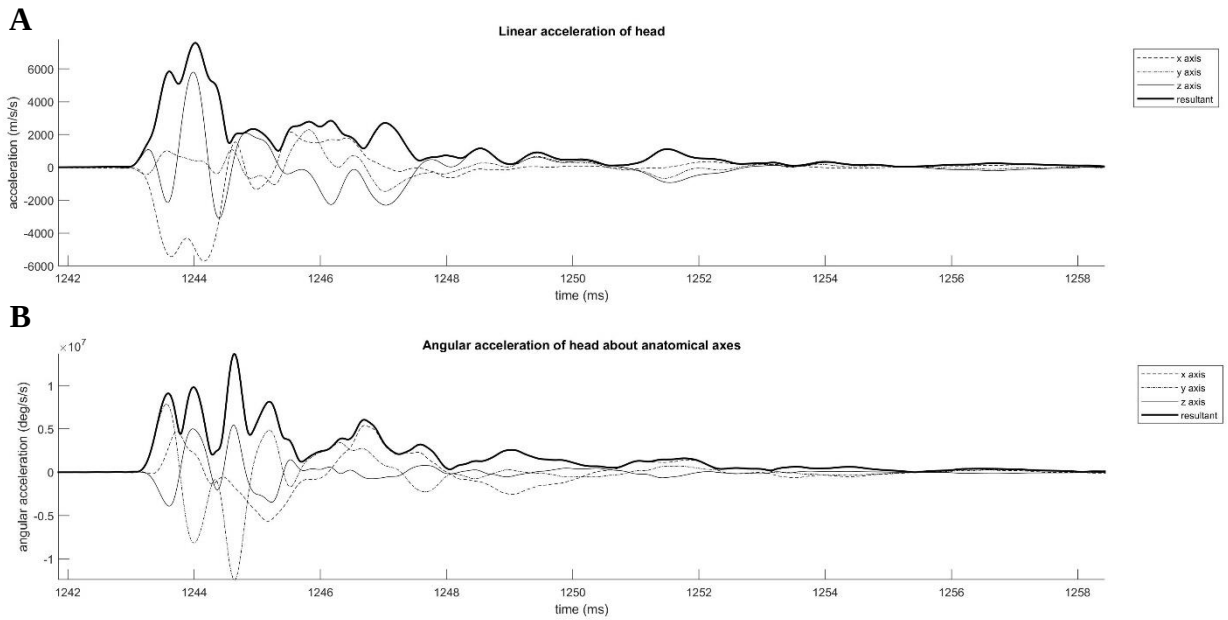

*<u>Figure 3.5:</u> JS012 - Linear (**A**) and angular (**B**) acceleration of the head following impact. Accelerations are depicted in the ACS as defined by results from Chapter 6.*

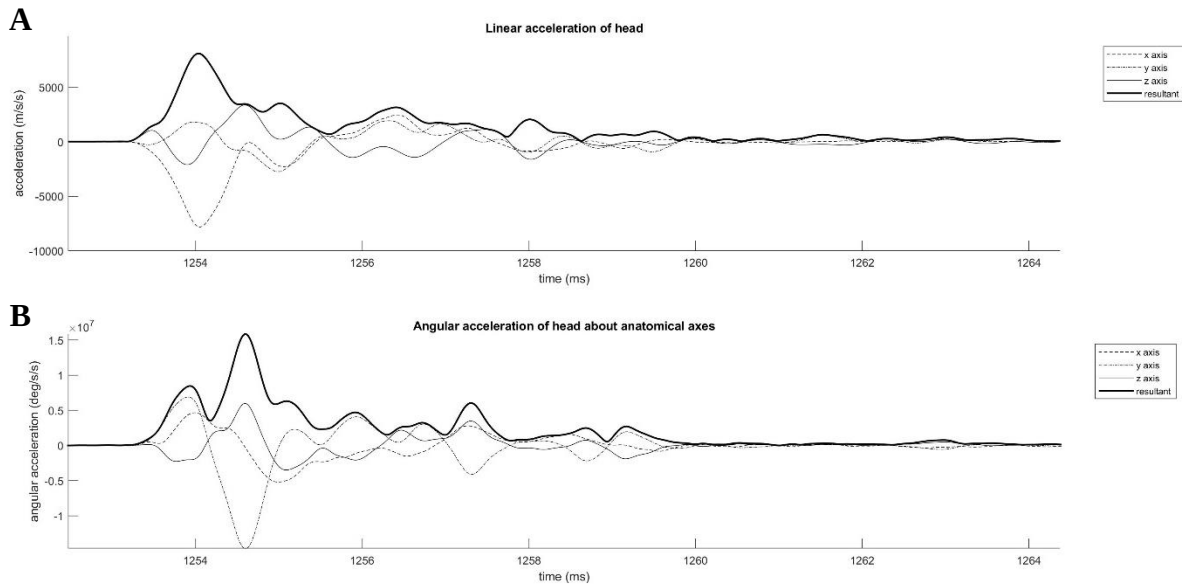

*<u>Figure 3.6:</u> JS013 - Linear (**A**) and angular (**B**) acceleration of the head following impact. Accelerations are depicted in the ACS as defined by results from Chapter 6.*

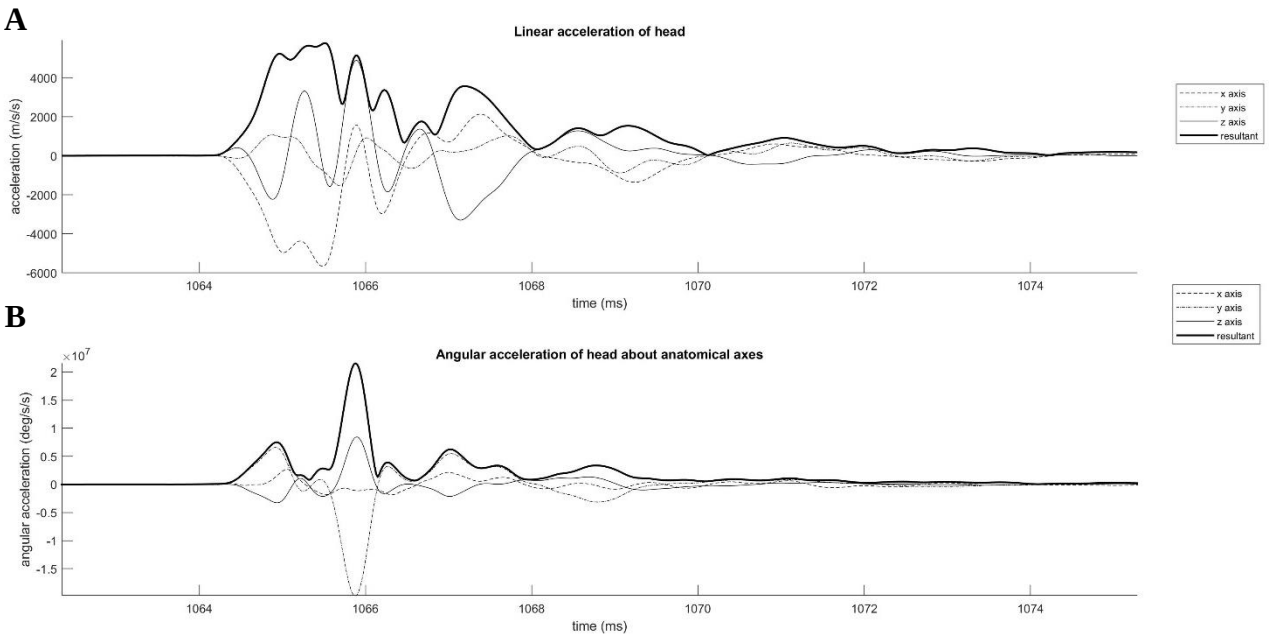

*<u>Figure 3.7:</u> JS016 - Linear (**A**) and angular (**B**) acceleration of the head following impact. Accelerations are depicted in the ACS as defined by results from Chapter 6.*

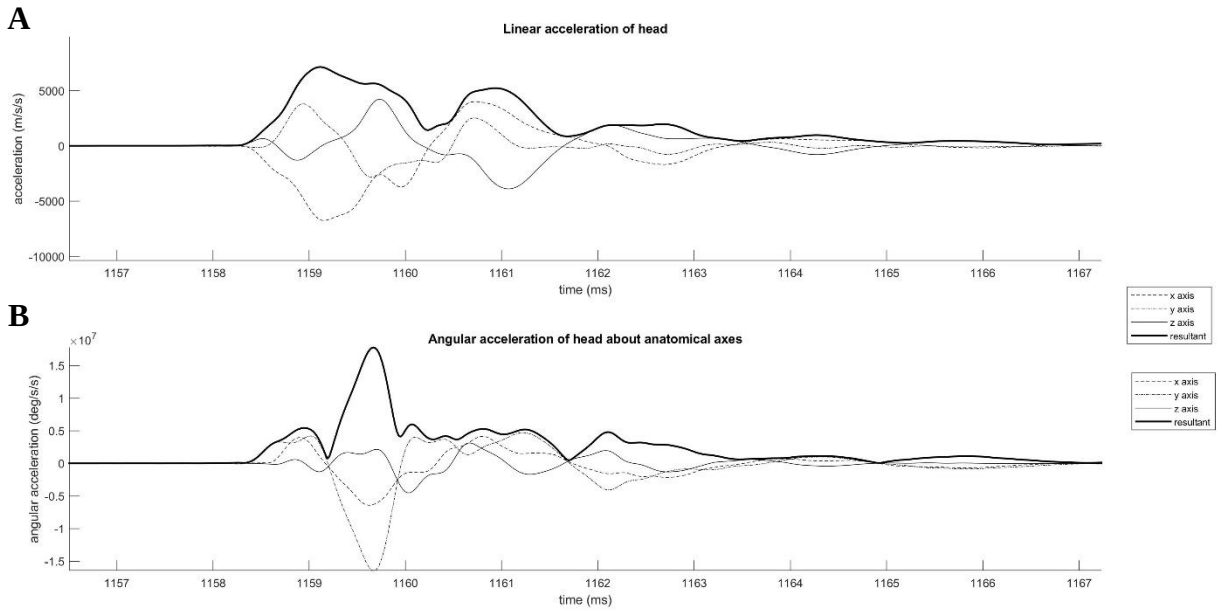

*<u>Figure 3.8:</u> JS017 - Linear (**A**) and angular (**B**) acceleration of the head following impact. Accelerations are depicted in the ACS as defined by results from Chapter 6.*

APPENDIX IV: PUBLISHED MANUSCRIPTS AS PDFS ARISING FROM OUTSIDE THIS THESIS

Published 1st author manuscript: Beyond the Brain: Peripheral Interactions after Traumatic Brain Injury

JOURNAL OF NEUROTRAUMA 37:770–781 (March 1, 2020)

DOI: 10.1089/neu.2019.6885

Beyond the Brain: Peripheral Interactions after Traumatic Brain Injury

Stuart J. McDonald,[1,2,*] Jessica M. Sharkey,[3,*] Mujun Sun,[1] Lola M. Kaukas,[4] Sandy R. Shultz,[1,5] Renee J. Turner,[3] Anna V. Leonard,[3] Rhys D. Brady,[1] and Frances Corrigan[4]

Abstract

Traumatic brain injury (TBI) is a leading cause of death and disability, and there are currently no pharmacological treatments known to improve patient outcomes. Unquestionably, contributing toward a lack of effective treatments is the highly complex and heterogenous nature of TBI. In this review, we highlight the recent surge of research that has demonstrated various central interactions with the periphery as a potential major contributor toward this heterogeneity and, in particular, the breadth of research from Australia. We describe the growing evidence of how extracranial factors, such as polytrauma and infection, can significantly alter TBI neuropathology. In addition, we highlight how dysregulation of the autonomic nervous system and the systemic inflammatory response induced by TBI can have profound pathophysiological effects on peripheral organs, such as the heart, lung, gastrointestinal tract, liver, kidney, spleen, and bone. Collectively, this review firmly establishes TBI as a systemic condition. Further, the central and peripheral interactions that can occur after TBI must be further explored and accounted for in the ongoing search for effective treatments.

Keywords: autonomic dysfunction; infection; inflammation; polytrauma; traumatic brain injury

Introduction

Traumatic brain injury (TBI) is a life-threatening injury, with survivors often experiencing extensive impairments to neurological function. TBI is the leading cause of death and major disability in people under 45 years of age in Western-industrialized countries, especially young adults.[1,2] Deficits post-injury can range from motor, sensory, and physical disability, such as dependency for activities of daily life,[3] to cognitive, emotional, and behavioral/psychosocial impairment, such as spatial reasoning and conceptualization deficits, attention, and concentration deficits, information processing and skills in executive functioning and withdrawal, anxiety, depression, irritability, and impulsivity.[4] Increasing evidence suggests that a TBI is not confined to the central nervous system (CNS) and can have wide-ranging systemic effects, altering the biology and function of the heart, lungs, liver, gut, musculoskeletal, and immune system. There is also evidence that peripheral changes induced by TBI can, in turn, worsen neurological outcome.

These systemic effects are, in part, induced by the deleterious secondary injury cascades initiated by TBI: dysfunction of the autonomic nervous system (ANS) and neuroinflammation. TBI initiates a systemic stress response associated with activation of the hypothalamic-pituitary-adrenal axis and the sympathetic nervous system (SNS), leading to release of glucocorticoids and catecholamines, respectively.[5–8] Indeed, significant activation of the SNS after TBI (i.e., sympathetic storming) is evidenced by a massive release of catecholamines acutely post-injury, with a gradual decrease over time, although levels can remain elevated for up to 14 days.[9] This catecholamine release appears to be proportional to the severity of brain injury, as measured by admission Glasgow Coma Scale (GCS), with admission catecholamine levels also shown to be independently associated with functional outcome, assessed by Glasgow Outcome Scale-Extended (GOSE) at 6 months post-injury.[10] As outlined below, this surge in catecholamine release directly affects the function of a wide range of organs, including the heart, lung, kidney, and lymphoid organs.

The effects of TBI also extend beyond the brain as the result of the release of inflammatory mediators into the systemic circulation.[11] TBI leads to an acute, immediate cascade of inflammatory responses, with release of cytokines and chemokines into the system circulation.[12–14] Of note, the relative increase in systemic

[1]Department Neuroscience, Monash University, Melbourne, Victoria, Australia.
[2]Department of Physiology, Anatomy and Microbiology, La Trobe University, Bundoora, Victoria, Australia.
[3]Discipline of Anatomy and Pathology, Adelaide Medical School, Faculty of Health and Medical Sciences, The University of Adelaide, Adelaide, South Australia, Australia.
[4]School of Health Sciences, University of South Australia, Adelaide, South Australia, Australia.
[5]Department of Medicine, University of Melbourne, Melbourne, Victoria, Australia.
*These authors contributed equally to the work.

levels of cytokines and chemokines corresponds with unfavorable outcome and death post-TBI.[15,16] Intriguingly, this may relate to downstream effects on peripheral organs, with the relationship between systemic cytokines and patient outcomes found to remain significant even after controlling for injury severity.[17]

Extracranial Effects after Traumatic Brain Injury

It has been reported that dysfunction of at least one non-neurologic organ system occurs in around 89% of patients with severe TBI.[18] Further, milder injuries are also known to promote autonomic dysfunction, playing a significant role in early symptomology, including headache, dizziness, nausea, and balance difficulties.[19] However, few studies have directly examined the effects of milder injuries on organ systems, and, as such, this review predominantly focuses on moderate-severe TBI.

Heart

Neurogenic stunned myocardium (NSM) is a phenomenon whereby acute neurological events such as TBI give rise to cardiovascular abnormalities, including echocardiogram (ECG) changes, cardiac arrhythmias, release of cardiac injury biomarkers, and left ventricular dysfunction (LVD).[20] This is partially attributable to the aforementioned surge of catecholamine release that may occur post-TBI leading to systemic vasoconstriction, thereby increasing cardiac afterload, myocardial workload, and myocardial oxygen demand.[20] Given that the coronary arteries may also be similarly vasoconstricted, this increased oxygen demand is not met with increased oxygen delivery, and subendocardial ischemia with impaired ventricular function may result.

Indeed, Prathep and colleagues found evidence of LVD on ECG with reduced left ventricular ejection fraction in 12% of severe TBI patients, with a further 17.5% showing regional wall motion abnormality.[21] Krishnamoorthy and colleagues similarly found that 22% of moderate-severe TBI patients demonstrated evidence of systolic dysfunction within the first 24 h of injury, as reflected by a distinctive hemodynamic profile of acute hypertension and tachycardia followed by a decrease in blood pressure (BP).[22] Levels of cardiac troponin I (cTnI), a cardio-regulatory contractile protein suggestive of myocardial ischemia, were also elevated in 29.8% of blunt TBI patients on admission, with elevated cTnI associated with a lower admission GCS, providing further evidence that NSM may be a consequence of severe TBI.[23]

Even mild TBI (mTBI) may lead to persistent autonomic dysregulation of cardiac function, as indicated by changes in heart rate variability (HRV). HRV refers to normal variations in the time between any two consecutive heart beats (i.e., R-R interval) and thus the relative contributions of the sympathetic and parasympathetic systems. In the first 3 days post-injury, Bishop and colleagues noted significantly decreased HRV (specifically R-R wave mean) after mTBI when standing.[24] Abaji and colleagues also found chronic changes in the low-frequency to high-frequency ratio within the HRV, suggestive of a withdrawal of parasympathetic function upon exercise.[25] Hilz and colleagues observed chronic alterations in autonomic control after mTBI (i.e., at 5–43 months) without exercise challenge, as evidenced by decreased HRV.[26] Upon standing, baroreceptor sensitivity was still reduced compared to supine positioning, and participants did not withdraw parasympathetic or augment sympathetic modulation adequately, indicating impaired autonomic cardiovascular regulation. Another small study revealed that concussed patients had significantly increased systolic BP (SBP), HR, and standing SBP responses after the Valsalva maneuver.[27] These results are thought to represent uncoupling of the ANS from cardiovascular control and could be potentially used as a measure of recovery after mTBI.[28] The long-term effects of these cardiovascular effects on neurological outcome are yet to be determined.

Lung

Lung complications and associated respiratory distress are thought to be one of the most frequent and life-threatening extracranial effects of TBI.[18,29,30] One third of moderate-severe TBI patients will develop acute lung injury (ALI), a condition characterized by bilateral opacities on lung imaging, with respiratory failure occurring within 7 days.[31–33] Moreover, 50% of patients who died within 96 h of an isolated TBI had significantly increased lung weight, potentially attributable to pulmonary edema, congestion, and hemorrhage.[34] Current literature postulates a number of mechanisms that may drive lung injury post-TBI, with the main contributors being development of neurogenic pulmonary edema (NPO) and systemic inflammation.[30,35,36]

Neurogenic pulmonary edema.

NPO is classified as the extravasation of fluid from the blood into the alveolar and interstitial space of the lungs.[30,37] It is thought that NPO can be induced and perpetuated primarily by sympathetic discharge, which forces a shift of circulation from the high-resistance systemic circulation into the low-resistance pulmonary circulation, leading to a dramatic increase in pulmonary vascular pressure.[37,38] This increases hydrostatic pressure within the pulmonary capillaries, causing extravasation of fluid into the interstitial tissue of the lung.[37,39] Experimental studies in brain-injured rats found that by preventing acute hypertensive episodes after injury by pre-treatment of alpha-adrenergic agonists, ALI was reduced and capillary-alveolar integrity was preserved.[40,41]

Systemic inflammatory effects on the lungs.

NPO is also exacerbated by increased levels of circulating proinflammatory mediators, including interleukin (IL)-1β, tumor necrosis factor-α (TNF-α), substance P, and neurokinin-1 after TBI,[37,42,43] which increase vascular permeability. Further, lung epithelial cells have a high expression of receptors which bind high mobility group box 1 (HMGB1), a damage-associated molecular pattern protein released acutely after TBI, leading to a local inflammatory response.[44] Indeed, clinical studies have found elevated concentrations of proinflammatory cytokines within bronchoalveolar lavage fluid from patients who had suffered a fatal TBI,[45] with upregulation of IL-1β and IL-6 similarly observed within the lungs after brain injury in experimental animal models.[46,47] The lung also shows increased expression of intracellular adhesion molecules, which promote significant migration of neutrophils and macrophages into the lungs by 24 h after experimental TBI, further disrupting alveolar structures.[48,49]

Appropriate management of lung injury post-TBI is critical to prevent hypoxemia, which is associated with poor outcome, with decreased cerebral oxygen delivery a known cause of cerebral vasodilatation and an associated increase in intracranial pressure.[50] Further investigations into the contribution of inflammatory mediators from the lung to the neuroinflammatory response post-TBI are warranted.

Gastrointestinal tract

Gastrointestinal (GI) dysfunction is another common complication of TBI. Within the first few weeks after injury, patients who

experience a moderate-severe TBI often present with vomiting and abdominal distension indicative of reduced intestinal contractility, whereas those who survive beyond 1 year post-TBI are more than twice as likely to die of digestive system conditions than the matched general population.[51–53]

The GI tract is comprised of four layers: the mucosa, submucosa, muscle, and serosa or adventitia dependent on location within the tract.[54] The mucosa consists of a lipid bilayer of epithelial cells and tight junctions, that, when functioning normally, works to maintain homeostasis and prevent access of unwanted compounds and pathogens.[55–57]

The gut-brain axis. The gut-brain axis allows monitoring and integration of GI functions, including motility, absorption, and secretion, through bidirectional communication between the CNS and enteric nervous system (ENS), which is found within the wall of the GI tract.[58] Communication occurs by endocrine, immune, and neural methods. Neurologically, the vagus nerve directly links the viscera primarily through the ENS to the brain, containing both afferent and efferent neurons that tonically transmit information from the gut to the brain and *vice versa*.[58,59] Gut microbiota are key regulators of the gut-brain axis, able to communicate directly to the brain by the vagus nerve with bidirectional communication through hormones, such as corticotrophin-releasing hormone, neurotransmitters, including dopamine and serotonin, neuropeptides, and short-chain fatty acids.

Traumatic brain injury effects on the gastrointestinal tract. After moderate-severe TBI, dysautonomia has been shown to promote decreased contractility of the smooth muscle within the GI tract, resulting in reduced motility.[60–62] Experimentally, TBI also causes alterations to the intestinal mucosal morphology, evident as early as 3 h post-injury, with shedding of epithelial cells, fracture of intestinal villi, and mucosal atrophy and reduced expression of intestinal tight junction proteins, including occludin and zonula occluden-1.[63] Acutely post-injury, gut permeability is increased within the jejunum,[53,63,64] whereas chronically at 28 days post-injury, no effect on the jejunum was noted, but large intestine permeability was increased,[65] suggesting regional and time-dependent effects.

TBI patients requiring admission to intensive care similarly show increased intestinal permeability, as measured by translocation of lactulose from the gut to the serum.[66] Increased intestinal permeability results in endotoxemia attributed to translocation of gut bacteria to the systemic circulation,[62,63,67] which may explain why increased intestinal permeability was associated with a greater risk of a systemic inflammatory response (SIR) and multiple organ dysfunction in TBI patients.[66] Given that increased intestinal permeability is often accompanied by increases in cytokine levels, including TNF-α, IL1-β, and IL-6, within the gut,[67] a vicious cycle may be initiated with further gut damage, leakage of gut bacteria, and exacerbation of the SIR. Given that endotoxin-mediated systemic inflammation is known to cause activation of microglia within the CNS,[68] in the context of TBI this may also worsen neurological outcomes.

TBI can also cause alterations in the gut microbiome, with changes evident as early as 2 h after moderate-severe fluid percussion injury (FPI) in rats.[69] Larger brain lesions were associated with decreases in the beneficial bacteria *Firmicutes* and increases in the pathogenic bacteria *Proteobacteria*.[69] Houlden and colleagues similarly reported alterations in *Firmicutes* and *Proteobacteria* within the caecum that correlated with TBI severity.[70] Traegan and colleagues provided further evidence of acute dysbiosis after TBI, finding alterations in *Lactobacillus* and *Ruminococcus* at 24 h after controlled cortical impact (CCI) in mice.[71] Healthy gut microbiota is also integral to the regulation of intestinal barrier permeability[72] and can directly influence CNS function.[73] Indeed, the gut microbiome plays a pivotal role in microglial function and can alter microglial phenotype and behaviour,[74] with further research needed to understand how TBI-induced gut dysbiosis may effect neurological outcome.

Liver

Release of cytokines into the systemic circulation, particularly IL-6 and IL-1β, triggers an acute phase response from the liver, also thought to be augmented by release of norepinephrine as part of the sympathetic response. The acute-phase response is a biological defense to systemic or local tissue injury, with hepatocytes producing acute-phase proteins, including serum amyloid A, C-reactive protein, complement, and fibrinogen, into the systemic circulation. In pre-clinical TBI models, serum amyloid A is noted to be increased by 6 h post-injury, with elevated levels persisting to 7 days[75] and correlated with TBI severity.[76] This is mirrored clinically, suggesting that this is likely a ubiquitous response to trauma.[77] Other acute-phase proteins show a similar pattern, with C-reactive protein and fibrinogen increasing rapidly after TBI, with levels peaking within the first week.

The acute-phase response modulates the peripheral inflammatory response, stimulating the complement system and scavenging free radicals in order to minimize tissue damage and initiate repair. However, the acute-phase response also triggers the production of cytokines and chemokines by the liver, with levels of chemokines C-X-C motif chemokine ligand 1 (CXCL)1 and CXCL10 and cytokines such as IL-1β increased in the liver from 6 h post-CCI in mice, with neutrophil infiltration observed from 3 days post-injury.[78] This may promote local damage to the liver, with increased expression of markers of oxidative stress and mitochondrial dysfunction within hepatocytes,[78] along with an increase in hepatocytes apoptosis at an acute stage after CCI in mice.[75] Nonetheless, the long-term effects of this localized liver damage are not yet known. Studies have, however, shown that liver response to TBI can influence neurological outcome, by promoting neutrophil recruitment within the brain. Importantly, this study also found that by reducing the inflammatory response by injection of a nuclear factor kappa beta repressor into the liver, neutrophil recruitment to the brain was also reduced,[78] suggesting that modifying the peripheral response may play an important role in improving outcome post-TBI.

Kidney

The kidneys are highly vascularized organs that are responsible for maintaining the body's internal environment by the processes of filtration, reabsorption, and secretion.[79] Sympathetic efferent impulses from the CNS regulate renal blood flow, glomerular filtration rate, and sodium handling.[80] The nephron is the functional unit of the kidney consisting of a glomerulus and its associated tubule through which glomerular filtrate passes. Acute kidney injury, as indicated by increases in serum creatinine and reductions in urine output, was reported in 8–36% of severe TBI patients.[81–84] Even TBI patients who do not meet the criteria for acute kidney injury show evidence of acute tubular damage.[85] Importantly, presence of acute kidney injury is associated with a marked increase in mortality compared to patients without acute kidney injury.[86] This may reflect increasing injury severity, given that low admission GCS is

associated with higher levels of acute kidney injury,[83] or, alternatively, it is also possible that increased plasma osmolarity attributable to renal failure may aggravate cerebral edema.[87]

One mechanism driving development of acute kidney injury post-TBI is the aforementioned increase in SNS activity. The increased SNS activation results in reduced renal glomerular perfusion and increased sodium reabsorption.[88] Second, the peripheral inflammatory response induced post-TBI can damage kidney tubule cells, with the application of plasma from TBI patients to *in vitro* cultures of human tubular epithelial cells inducing functional alterations and apoptotic cell death.[85] Importantly, kidney injury not only increases proinflammatory cytokine generation, but also reduces cytokine clearance,[89] increasing the overall inflammatory response and potentially worsening neuroinflammation. Further, neuronal injury may be driven by retention of waste products of nitrogen metabolism leading to increased plasma urea.[90] Given that the blood–brain barrier (BBB) is often disrupted after TBI, increased urea can enter the brain, and although it is initially taken up by astrocytes, this urea can lead to worsening of cerebral edema.[87] To date, relatively few studies have examined the specific mechanisms whereby TBI may lead to kidney injury, and how this may impact upon TBI, with further work needed in this area.

Bone

Several factors involved in secondary injury mechanisms of TBI have the potential to alter bone remodeling, including the aforementioned peripheral inflammatory response and increased sympathetic outflow. In addition, the increased permeability of the BBB post-TBI facilitates the leakage of reactive oxygen species (ROS) into the systemic circulation.[91] Increased SNS activation may result in activation of $\beta 2$ adrenergic receptors on osteoblasts, which can stimulate bone resorption while suppressing bone formation,[92] whereas ROS can elicit the same effects.[93,94] A number of proinflammatory cytokines that are upregulated in circulation post-TBI are also known facilitate osteoclastogenesis and osteoclastic activation, resulting in increased bone resorption.[95,96] In addition to these effects, TBI-induced deficiencies in growth hormone and insulin-like growth factor 1 may also induce bone loss.[97,98]

Human studies indicate that brain-injured patients have an elevated risk of hip fracture and reduced bone mineral density (BMD).[99–102] These changes are often attributed to immobilization after injury given that reduced mechanical loading of bone can activate bone resorption. However, experimentally at 1 and 12 weeks post-FPI in rats, a reduction in femoral cortical and trabecular bone was found without alterations in locomotion.[103] Similarly, CCI in mice led to reduced BMD and bone volume at the distal metaphyseal region of the femur at 8 weeks post-injury.[104] This appears to relate to TBI-induced inflammation within the bone marrow, with increased expression of inflammatory mediators, such as IL-1β, IL-6, and TNF-α, thought to promote osteoclastic differentiation and bone resorption.[104] In rats treated with sodium selenate, a compound previously shown to attenuate brain damage after TBI,[105,106] TBI-induced bone loss was significantly reduced,[107] further emphasizing the association between TBI and loss of bone. Interestingly, although TBI appears to induce bone loss in healthy bone, there is also considerable evidence that TBI induces bone formation in the context of fracture healing.

Bone fracture healing. In the late 1980s, reports of TBI rapidly stimulating bone fracture callus formation began to accumulate in the clinical literature.[108,109] This was subsequently supported by experimental studies, where concomitant CCI and femoral fracture resulted in increased callus volume at 4–8 weeks post-injury.[110–113] Further, the strength of the callus is enhanced, with increased maximum torque at 4 weeks in TBI plus fracture animals compared to fracture alone.[111] Similar findings have been reported in closed-TBI models, with animals undergoing TBI plus tibial fracture demonstrating increased bone volume and superior biomechanical properties at 21 days post-injury compared to fracture alone.[103] With reports to suggest that osteogenesis is enhanced in distant skeletal sites after burr hole defect in rat tibiae,[114] this finding in closed TBI indicates that brain injury is the primary driver of enhanced fracture healing.

To date, the mechanisms that underlie enhanced callus formation after TBI are poorly understood. Preliminary clinical studies speculated that this phenomenon was likely attributed to upregulation of circulating levels of epidermal growth factor, nerve growth factor, and prolactin in patients with both TBI and bone fracture compared to those with fracture only.[115,116] Alternatively, Wei and colleagues suggested that leptin may play a role, with elevated serum leptin in multi-trauma rats and an increased percentage of leptin-positive cells in the callus.[112,113] Intriguingly, mice that received a fracture contralateral to the CCI had increased callus bone volume at 5 days post-injury when compared to fracture-only mice and mice that were given a TBI ipsilateral to the fracture, although this was only noted at 5 days post-injury, with no difference compared to fracture-alone animals at later time points. Nonetheless, these findings led the researchers to suggest that neuronal mechanisms play a significant role in increasing bone formation acutely after TBI by causing contralateral activation of fracture healing.[117]

Future investigations in pre-clinical models are required to concurrently examine post-TBI changes in humoral factors, as well as the activity of peripheral sympathetic nerves at various time points. Characterizing neurotransmitter release from sensory and sympathetic nerves within the callus may provide insight into possible differences in the neuronal regulation of fracture healing between multi-trauma and fracture-only groups. This could then highlight potential therapeutic targets to augment healing in delayed fracture healing and non-union fracture models.

Muscle

Skeletal muscle atrophy is another common systemic complication of TBI.[118] In addition to the effects of prolonged bed stay and immobilization, there is now some evidence that the pathophysiological changes induced by TBI may directly cause loss of skeletal muscle mass. A recent Australian-led study found that rats given a moderate-severity lateral FPI had increased expression of muscle atrophy markers and altered muscle-fiber contractile properties at 12 weeks post-injury.[119] Previous studies in this injury model and laboratory have shown no differences between sham and FPI rats in locomotion in an open field to 12 weeks post-injury,[103] indicating that these muscle alterations may not be the result of reduced activity. Similarly, Shahidi and colleagues found that mice given a moderate-severity CCI had atrophy of the slow twitch soleus muscle and, interestingly, evidence of degeneration and regeneration without atrophy in the fast twitch tibialis anterior.[120] Further study is required to understand the effects of TBI on muscle, and whether these effects are indeed muscle-fiber–type specific.

Traumatic brain injury–induced neurological heterotopic ossification. A common musculoskeletal complication of TBI is the development of neurological heterotopic ossification (NHO).[121]

NHO is characterized by the formation of bone in soft tissue (typically skeletal muscle) and is often initiated after a TBI and simultaneous peripheral injuries (e.g., bone fracture and/or muscle injury).[121] Evidence suggests that NHO affects approximately 5–20% of severe TBI patients with significant peripheral injuries.[122–127] In the context of combat-related trauma, specifically blast-related TBI, the prevalence of NHO may be significantly higher.[128,129] For example, a study that examined the prevalence of blast-related NHO in combat wounded who underwent at least one orthopedic procedure reported that 86% of blast-TBI patients developed NHO.[129]

NHO generally forms within 1–3 months after a TBI (in some cases 12 months) and commonly occurs around the hip, elbow, knee, and shoulder joints.[121,122] As NHO progresses, it can cause severe chronic pain, nerve entrapment, and reduced range of motion, which is associated with difficulty sitting, standing, and walking.[121,122] Currently, the only effective intervention for this affliction is surgical resection after NHOs have matured, which is problematic given that the ossifications often entrap large blood vessels and nerves.[130,131] In addition, surgical intervention can result in recurrence, and often patients are left with functional deficits as a result of musculoskeletal damage.[132]

The lack of treatment options for patients with TBI-induced NHO stems from a limited understanding of the pathobiology of this condition.[121] Localized inflammation, in combination with neurological injury, may drive this abnormal bone formation, by stimulating mineralization of muscle-derived stromal cells.[133,134] To provide a platform to further investigate the pathobiology and treatment of TBI-induced NHO, Brady and colleagues recently developed the first rat model of the condition. The model involves a combination of moderate-severe TBI, muscle crush injury, and a femoral fracture.[135] At 6 weeks post-injury, micro computed tomography images showed evidence of ectopic bone in 70% of rats given all three conditions, 20% of rats given a muscle crush injury and a femoral fracture, and 0% of the sham-injured controls, providing a platform to investigate pathogenesis and hence potential therapeutics.

Lymphoid organs

Resident macrophages in the spleen express adrenergic/cholinergic receptors and therefore demonstrate a heightened sensitivity to changes in autonomic output.[136–138] Indeed, after acute TBI, the massive release of catecholamines stimulates splenic macrophages to release significant amounts of proinflammatory cytokines, such as TNF-α and IL-1β, into the peripheral circulation.[139] These cytokines reach and penetrate the BBB, which is compromised after TBI, and enhance a post-traumatic immunological response.[139] Work from Queensland has shown that after traumatic spinal cord injury (SCI), the majority of infiltrating monocytes to the site of injury subacutely originate from the spleen, and this can be prevented by early splenectomy with improved open-field locomotor activity at 42 days post-SCI.[140] Similar processes appear to occur after TBI, with immediate splenectomy in animal models decreasing mortality rate with decreases in inflammatory cytokine expression within the serum and brain.[141,142]

Importantly, TBI can also induce immunosuppression, which may lead to a decreased capacity to defend against infectious agents.[143,144] Studies in TBI patients suggested that levels of circulating leukocytes, especially lymphocytes, decline during the first week after the injury.[145] Though levels of acute circulating neutrophils are increased after TBI,[91,146] their phagocytic capacity is decreased.[91] Studies in rodents have indicated that numbers of circulating monocytes and lymphocytes decrease within hours after TBI,[147,148] and there is also evidence of depletion-caused thymic atrophy and deficits in T-cell maturation.[148] Given that reductions in circulating T cells have also been reported in some clinical TBI studies, suppression of adaptive immunity may be a significant factor contributing to the increased risk of infection observed in TBI patients.

Infections and Traumatic Brain Injury

Post-traumatic infection is a common complication in patients with moderate-severe TBI, observed in up to 55% of patients,[149–151] resulting in longer hospital stays, unfavorable functional recovery, and increased mortality rates.[144,152–154] Risk of infection is dependent on the severity of the injury, the age of the patient, ventilator use, surgical procedures, and numerous other risk factors.[150,153,154] The most common nosocomial infections experienced by TBI patients include pneumonia/lower respiratory tract infections, urinary tract infections, and surgical site infections.[150,152,153] In addition, a less common, however often life-threatening, complication that may occur in the days or weeks after CNS injury is sepsis, which is classified as organ dysfunction attributed to a substantial SIR.[155] Although sepsis occurs only in 2% of adult trauma patients,[156] it has been reported to occur in up to 75% of severe TBI patients[82] and results in high risk of death attributed to multiple organ failure.[82,157] Indeed, given that sepsis itself is linked to high rates of morbidity,[158] including a higher risk of cognitive impairment present 12 months after admission,[159] as well as neuropsychiatric symptoms, including anxiety[160] and depression,[161] the combination of TBI and sepsis may have an even greater deleterious effect.

It has widely been predicted that concomitant infection may exacerbate TBI. Although several animal studies have demonstrated that pre-conditioning of ''low-dose'' infectious agent is beneficial to a consequent TBI/SCI injury,[162–164] post-injury challenge with infection has generally been found to be detrimental to neurological outcomes. The Toll-like receptor 4 agonist, lipopolysaccharide (LPS), is an activator of immune response and is often used as a model of infection. Systemic administration of LPS after TBI can exacerbate neuroinflammation (e.g., increases levels of brain TNF-α and IL-6), worsen neuronal damage, and exaggerate long-term neurological deficits, including cognitive impairments and depressive-like behavior in rodents.[165,166] Even delayed immune stimuli can alter TBI outcome, with LPS injection at 1 month post-TBI found to exacerbate production of inflammatory cytokines and worsen neurological function in mice,[167,168] and administration of LPS at 8 weeks post-TBI found to enhance neuronal excitability and seizure susceptibility at 24 weeks post-TBI.[169]

Similar findings have been reported with other inflammatory agents, with the peripheral administration of lymphocytic choriomeningitis virus after mTBI disrupting the repair process of the meningeal vasculature.[170] Further, cecal ligation and puncture induced exacerbated neuronal damage and worsened functional impairments, possibly by exacerbating microglia reactivity.[171]

Effects of Peripheral Trauma on Traumatic Brain Injury

High-impact collisions, such as motor vehicle accidents, frequently result in trauma to multiple body regions, a condition known as polytrauma or multi-trauma. There is now substantial evidence that concomitant peripheral trauma can lead to higher mortality rates and poorer GOS scores (see McDonald and colleagues for a detailed review).[172] This is supported by animal

studies where concomitant limb fracture with TBI has been found to exacerbate motor deficits,[173] worsen cognitive outcome,[174] and prolong pain-like behaviors.[175] Exacerbated TBI outcomes in polytrauma may relate to the enhanced systemic inflammatory response with circulating proinflammatory cytokines, such as IL-6 and C-C motif chemokine ligand 2, found to be significantly higher in TBI animals that also had bone fracture or blunt chest trauma.[176–179] This may enhance the neuroinflammatory response, with higher levels of IL-1β found in the injured brain of polytrauma animals with a bone fracture compared to TBI alone,[173] with resultant increases in BBB breakdown and edema formation.

Treatments targeting inflammation have shown some success in mitigating the exacerbated neuropathology after experimental polytrauma, with an IL-1 receptor antagonist[180] and a HMGB1 antibody[181] both found to reduce neuroinflammation and edema in rodents with polytrauma. Interestingly, concomitant skeletal muscle injury was shown to not alter TBI outcomes in the same manner to bone fracture,[72] indicating the likely importance of extracranial injury location and severity. Although further research is required, and other pathophysiological mechanisms are likely involved, the aforementioned findings indicate that neuroinflammation and cerebral edema may be particularly prominent in TBI involving concomitant bone fracture. As such, treatments targeting associated pathways may be particularly promising for treating such TBI cases.

A recent multi-center clinical trial led by Melbourne-based researchers found evidence that concomitant extracranial injuries

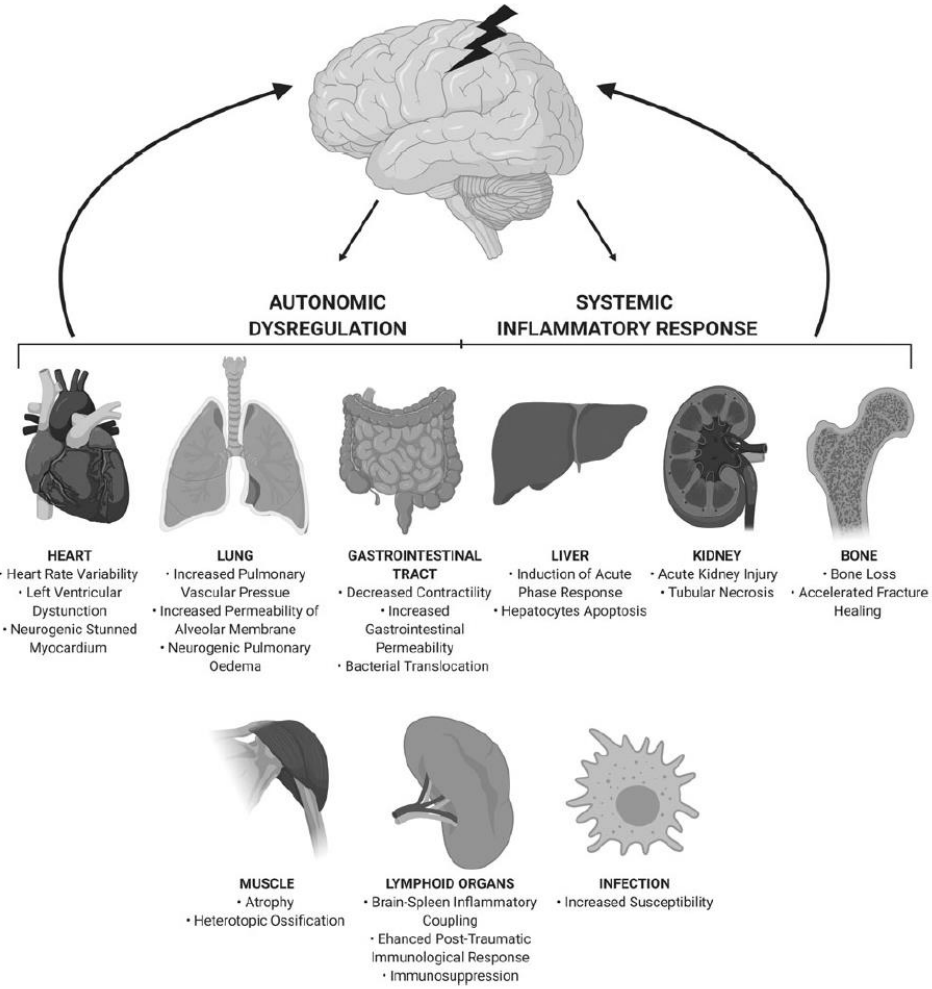

FIG. 1. Downstream effects on peripheral organs of an isolated TBI.

may also have treatment implications for TBI patients.[182] When reanalyzing the efficacy of erythropoietin (EPO) treatment on mortality and GOSE scores for 606 patients with non-penetrating moderate or severe TBI, post-hoc analysis found that mortality was significantly reduced in the ~50% who had concomitant peripheral injuries (i.e., extracranial injury severity score >6). Notably, this protective effect of EPO was not apparent in patients with isolated TBI.[182] Although this finding may be contributed to by EPO actions on peripheral traumas (i.e., indirectly related to secondary brain injury), when considered along with the aforementioned polytrauma findings in rodents, and evidence that EPO dampens neuroinflammation in rodents after TBI,[183,184] it is plausible that the benefit of treatment in polytrauma could be attributed to the prominent neuroinflammatory response in this subset patients. Although preliminary, the accumulating data from both animal and clinical studies indicate that extracranial injuries are likely to have important implications for treatment and should be a factor considered in clinical trials.

In addition to having potential implications for TBI treatment, it also important to note that the presence of concomitant extracranial injuries may directly alter the expression of blood biomarker candidates that have shown promise as biomarkers of TBI. Several proteins that have shown potential as diagnostic or prognostic indicators of TBI have also been shown to lack brain specificity, with proteins such as S100 calcium-binding protein B, ubiquitin carboxy-terminal hydrolase L1, myelin basic protein, and tau all found to be released from extracranial sources (see a review by Agoston).[185] It is therefore likely that extracranial injuries will directly alter the circulating expression of these markers, therefore limiting their clinical utility in the polytrauma setting. Moreover, it is possible that increases in these biomarkers in polytrauma patients may reflect exacerbation of TBI neuropathology by concomitant extracranial injuries. As such, it is paramount that emerging TBI biomarker candidates are assessed along with isolated extracranial trauma control groups.

Conclusions and Future Directions

This review has highlighted the growing appreciation in the pre-clinical and clinical fields that TBI is a systemic condition, with effects on an array of peripheral organs becoming increasingly apparent, as summarized in Figure 1. In addition, there is now substantial evidence that the traumatically injured brain is particularly vulnerable to peripheral factors, such as extracranial injury and infection. These systemic effects are principally driven by autonomic dysfunction post-TBI and induction of an inflammatory response. Further research is needed into autonomic outflow changes to the cardiovascular system, lymphoid organs, and GI tract after TBI, and how these may influence TBI pathology and outcomes. In addition, research should examine how the peripheral inflammatory response influences TBI. For example, the spleen is now recognized to be a major driver of neuroinflammation after ischemic stroke,[192] but the splenic response to TBI is relatively poorly understood. Similarly, several reports have shown that the hepatic acute phase response drives neutrophil and macrophage recruitment to the brain after acute CNS insults, including cerebral inflammation,[193] stroke,[194] and TBI,[79] but how this may exacerbate neuronal injury requires further investigation.

Understanding of the short- and long-term effects that TBI has on peripheral organs requires further attention. For example, TBI has extensive musculoskeletal effects, including increased risk of loss of muscle and bone mass, acceleration of bone fracture healing, as well as significantly increased risk of NHO. There is need for further understanding the pathogenesis of the debilitating NHO which can occur after TBI, with prospective clinical studies required to examine the acute, subacute, and chronic stages of NHO development. TBI also cause significant disruptions to systemic immune function, with increased risk of infection acutely post-TBI that can detrimentally affect recovery. A greater understanding of the mechanisms and temporal patterns of immunosuppression after TBI are likely to help identify specific periods of vulnerability to infection and, potentially, therapies to mitigate this risk. In addition, careful phenotyping of peripheral immune cells and other markers is needed to understand how the altered immune response may predict outcome post-TBI.

Overall, this review has highlighted a plethora of central and peripheral interactions that can occur after TBI. Most important, these findings add to the growing appreciation in the field that the pathophysiology of TBI is highly complex and heterogeneous, with peripheral interactions representing another factor that must be considered in the continued search for optimal treatments for TBI patients.

Funding Information

This work was supported by funding from the Neurosurgical Research Foundation and the National Health and Medical Research Council (APP1145483).

Author Disclosure Statement

No competing financial interests exist.

References

1. Maas, A.I., Stocchetti, N., and Bullock, R. (2008). Moderate and severe traumatic brain injury in adults. Lancet Neurol. 7, 728–741.
2. Finnie, J.W. and Blumbergs, P.C. (2002). Traumatic brain injury. Vet. Pathol. 39, 679–689.
3. Andelic, N., Sigurdardottir, S., Schanke, A.K., Sandvik, L., Sveen, U., and Roe, C. (2010). Disability, physical health and mental health 1 year after traumatic brain injury. Disabil. Rehabil. 32, 1122–1131.
4. Rassovsky, Y., Levi, Y., Agranov, E., Sela-Kaufman, M., Sverdlik, A., and Vakil, E. (2015). Predicting long-term outcome following traumatic brain injury (TBI). J. Clin. Exp. Neuropsychol. 37, 354–366.
5. Rosner, M.J., Newsome, H.H., and Becker, D.P. (1984). Mechanical brain injury: the sympathoadrenal response. J. Neurosurg. 61, 76–86.
6. Koiv, L., Merisalu, E., Zilmer, K., Tomberg, T., and Kaasik, A.E. (1997). Changes of sympatho-adrenal and hypothalamo-pituitary-adrenocortical system in patients with head injury. Acta Neurol. Scand. 96, 52–58.
7. Taylor, A.N., Rahman, S.U., Sanders, N.C., Tio, D.L., Prolo, P., and Sutton, R.L. (2008). Injury severity differentially affects short- and long-term neuroendocrine outcomes of traumatic brain injury. J. Neurotrauma 25, 311–323.
8. Griesbach, G.S., Hovda, D.A., Tio, D.L., and Taylor, A.N. (2011). Heightening of the stress response during the first weeks after a mild traumatic brain injury. Neuroscience 178, 147–158.
9. Rizoli, S.B., Jaja, B.N., Di Battista, A.P., Rhind, S.G., Neto, A.C., da Costa, L., Inaba, K., da Luz, L.T., Nascimento, B., Perez, A., Baker, A.J., and de Oliveira Manoel, A.L. (2017). Catecholamines as outcome markers in isolated traumatic brain injury: the COMA-TBI study. Crit. Care 21, 37.
10. Clifton, G.L., Ziegler, M.G., and Grossman, R.G. (1981). Circulating catecholamines and sympathetic activity after head injury. Neurosurgery 8, 10–14.
11. Ott, L., McClain, C.J., Gillespie, M., and Young, B. (1994). Cytokines and metabolic dysfunction after severe head injury. J. Neurotrauma 11, 447–472.
12. Navarro Solano, J., Damiani, S., Munno, I., Guastamacchia, F., Anglani, S., Baccaro, M.L., Benedetto, G., Megna, M., Ranieri, M., Echevarria Ruiz De Vargas, C., Lancioni, G.E., and Megna, G. (2009). The role of neuroinflammation in severe acquired brain injuries. Preliminary results on subacute and chronic patients. Int. J. Immunopathol. Pharmacol. 22, 13–20.

13. Singhal, G., Jaehne, E.J., Corrigan, F., Toben, C., and Baune, B.T. (2014). Inflammasomes in neuroinflammation and changes in brain function: a focused review. Front. Neurosci. 8, 315.
14. Woodcock, T., and Morganti-Kossmann, M.C. (2013). The role of markers of inflammation in traumatic brain injury. Front. Neurol. 4, 18.
15. Csuka, E., Morganti-Kossmann, M.C., Lenzlinger, P.M., Joller, H., Trentz, O., and Kossmann, T. (1999). IL-10 levels in cerebrospinal fluid and serum of patients with severe traumatic brain injury: relationship to IL-6, TNF-alpha, TGF-beta1 and blood-brain barrier function. J. Neuroimmunol. 101, 211–221.
16. Ayala, A., Wang, P., Ba, Z.F., Perrin, M.M., Ertel, W., and Chaudry, I.H. (1991). Differential alterations in plasma IL-6 and TNF levels after trauma and hemorrhage. Am J Physiol 260, R167–R171.
17. Di Battista, A.P., Rhind, S.G., Hutchison, M.G., Hassan, S., Shiu, M.Y., Inaba, K., Topolovec-Vranic, J., Neto, A.C., Rizoli, S.B., and Baker, A.J. (2016). Inflammatory cytokine and chemokine profiles are associated with patient outcome and the hyperadrenergic state following acute brain injury. J. Neuroinflammation 13, 40.
18. Zygun, D.A., Kortbeek, J.B., Fick, G.H., Laupland, K.B., and Doig, C.J. (2005). Non-neurologic organ dysfunction in severe traumatic brain injury. Crit. Care Med. 33, 654–660.
19. Purkayastha, S., Stokes, M., and Bell, K.R. (2019). Autonomic nervous system dysfunction in mild traumatic brain injury: a review of related pathophysiology and symptoms. Brain Inj. 33, 1129–1136.
20. Gregory, T., and Smith, M. (2011). Cardiovascular complications of brain injury. BJA Education 12, 67–71.
21. Prathep, S., Sharma, D., Hallman, M., Joffe, A., Krishnamoorthy, V., Mackensen, G.B., and Vavilala, M.S. (2014). Preliminary report on cardiac dysfunction after isolated traumatic brain injury. Crit. Care Med. 42, 142–147.
22. Krishnamoorthy, V., Rowhani-Rahbar, A., Chaikittisilpa, N., Gibbons, E.F., Rivara, F.P., Temkin, N.R., Quistberg, A., and Vavilala, M.S. (2017). Association of early hemodynamic profile and the development of systolic dysfunction following traumatic brain injury. Neurocrit. Care 26, 379–387.
23. Salim, A., Hadjizacharia, P., Brown, C., Inaba, K., Teixeira, P.G., Chan, L., Rhee, P., and Demetriades, D. (2008). Significance of troponin elevation after severe traumatic brain injury. J. Trauma 64, 46–52.
24. Bishop, S., Dech, R., Baker, T., Butz, M., Aravinthan, K., and Neary, J.P. (2017). Parasympathetic baroreflexes and heart rate variability during acute stage of sport concussion recovery. Brain Inj. 31, 247–259.
25. Abaji, J.P., Curnier, D., Moore, R.D., and Ellemberg, D. (2016). Persisting effects of concussion on heart rate variability during physical exertion. J. Neurotrauma 33, 811–817.
26. Hilz, M.J., DeFina, P.A., Anders, S., Koehn, J., Lang, C.J., Pauli, E., Flanagan, S.R., Schwab, S., and Marthol, H. (2011). Frequency analysis unveils cardiac autonomic dysfunction after mild traumatic brain injury. J. Neurotrauma 28, 1727–1738.
27. Dobson, J.L., Yarbrough, M.B., Perez, J., Evans, K., and Buckley, T. (2017). Sport-related concussion induces transient cardiovascular autonomic dysfunction. Am. J. Physiol. Regul. Integr. Comp Physiol. 312, R575–R584.
28. La Fountaine, M.F., Heffernan, K.S., Gossett, J.D., Bauman, W.A., and De Meersman, R.E. (2009). Transient suppression of heart rate complexity in concussed athletes. Auton. Neurosci. 148, 101–103.
29. Solenski, N.J., Haley, E.C., Jr., Kassell, N.F., Kongable, G., Germanson, T., Truskowski, L., and Torner, J.C. (1995). Medical complications of aneurysmal subarachnoid hemorrhage: a report of the multicenter, cooperative aneurysm study. Participants of the Multicenter Cooperative Aneurysm Study. Crit. Care Med. 23, 1007–1017.
30. Koutsoukou, A., Katsiari, M., Orfanos, S.E., Kotanidou, A., Daganou, M., Kyriakopoulou, M., Koulouris, N.G., and Rovina, N. (2016). Respiratory mechanics in brain injury: a review. World J. Crit. Care Med. 5, 65–73.
31. Ferguson, N.D., Fan, E., Camporota, L., Antonelli, M., Anzueto, A., Beale, R., Brochard, L., Brower, R., Esteban, A., Gattinoni, L., Rhodes, A., Slutsky, A.S., Vincent, J.L., Rubenfeld, G.D., Thompson, B.T., and Ranieri, V.M. (2012). The Berlin definition of ARDS: an expanded rationale, justification, and supplementary material. Intensive Care Med. 38, 1573–1582.
32. Thompson, B.T., Chambers, R.C., and Liu, K.D. (2017). Acute respiratory distress syndrome. N. Engl. J. Med. 377, 562–572.
33. Holland, M.C., Mackersie, R.C., Morabito, D., Campbell, A.R., Kivett, V.A., Patel, R., Erickson, V.R., and Pittet, J.F. (2003). The development of acute lung injury is associated with worse neurologic outcome in patients with severe traumatic brain injury. J. Trauma 55, 106–111.
34. Rogers, F.B., Shackford, S.R., Trevisani, G.T., Davis, J.W., Mackersie, R.C., and Hoyt, D.B. (1995). Neurogenic pulmonary edema in fatal and nonfatal head injuries. J. Trauma 39, 860–866; discussion, 866–868.
35. Pelosi, P., Colombo, G., and Gamberoni, C. (2002). *Respiratory Failure in Brain Injured Patients*. Springer Milan: Milano, Italy, pps. 381–398.
36. Gonzalvo, R., Marti-Sistac, O., Blanch, L., and Lopez-Aguilar, J. (2007). Bench-to-bedside review: brain-lung interaction in the critically ill—a pending issue revisited. Crit. Care 11, 216.
37. O'Leary, R., and McKinlay, J. (2011). Neurogenic pulmonary oedema. BJA Education 11, 87–92.
38. Theodore, J., and Robin, E. (1975). Pathogenesis of neurogenic pulmonary œdema. Lancet 306, 749–751.
39. Smith, W.S., and Matthay, M.A. (1997). Evidence for a hydrostatic mechanism in human neurogenic pulmonary edema. Chest 111, 1326–1333.
40. Avlonitis, V.S., Wigfield, C.H., Kirby, J.A., and Dark, J.H. (2005). The hemodynamic mechanisms of lung injury and systemic inflammatory response following brain death in the transplant donor. Am. J. Transplant. 5, 4 Pt. 1, 684–693.
41. Schraufnagel, D.E., and Thakkar, M.B. (1993). Pulmonary venous sphincter constriction is attenuated by alpha-adrenergic antagonism. Am. Rev. Respir. Dis. 148, 477–482.
42. Baumann, A., Audibert, G., McDonnell, J., and Mertes, P.M. (2007). Neurogenic pulmonary edema. Acta Anaesthesiol. Scand. 51, 447–455.
43. Campos, M.M., and Calixto, J.B. (2000). Neurokinin mediation of edema and inflammation. Neuropeptides 34, 314–322.
44. Nicolls, M.R., and Laubach, V.E. (2014). Traumatic brain injury: lungs in a RAGE. Sci. Transl. Med. 6, 252fs234.
45. Fisher, A.J., Donnelly, S.C., Hirani, N., Burdick, M.D., Strieter, R.M., Dark, J.H., and Corris, P.A. (1999). Enhanced pulmonary inflammation in organ donors following fatal non-traumatic brain injury. Lancet 353, 1412–1413.
46. Kalsotra, A., Zhao, J., Anakk, S., Dash, P.K., and Strobel, H.W. (2007). Brain trauma leads to enhanced lung inflammation and injury: evidence for role of P4504Fs in resolution. J. Cereb. Blood Flow Metab, 27, 963–974.
47. Skrabal, C.A., Thompson, L.O., Potapov, E.V., Southard, R.E., Joyce, D.L., Youker, K.A., Noon, G.P., and Loebe, M. (2005). Organ-specific regulation of pro-inflammatory molecules in heart, lung, and kidney following brain death. J. Surg. Res. 123, 118–125.
48. Wu, S., Fang, C.X., Kim, J., and Ren, J. (2006). Enhanced pulmonary inflammation following experimental intracerebral hemorrhage. Exp. Neurol. 200, 245–249.
49. Matsumoto, T., Yokoi, K., Mukaida, N., Harada, A., Yamashita, J., Watanabe, Y., and Matsushima, K. (1997). Pivotal role of interleukin-8 in the acute respiratory distress syndrome and cerebral reperfusion injury. J. Leukoc. Biol. 62, 581–587.
50. McHugh, G.S., Engel, D.C., Butcher, I., Steyerberg, E.W., Lu, J., Mushkudiani, N., Hernandez, A.V., Marmarou, A., Maas, A.I., and Murray, G.D. (2007). Prognostic value of secondary insults in traumatic brain injury: results from the IMPACT study. J. Neurotrauma 24, 287–293.
51. Katzenberger, R.J., Ganetzky, B., and Wassarman, D.A. (2015). The gut reaction to traumatic brain injury. Fly 9, 68–74.
52. Harrison, F.E., Hosseini, A.H., and McDonald, M.P. (2009). Endogenous anxiety and stress responses in water maze and Barnes maze spatial memory tasks. Behav. Brain Res. 198, 247–251.
53. Bansal, V., Costantini, T., Kroll, L., Peterson, C., Loomis, W., Eliceiri, B., Baird, A., Wolf, P., and Coimbra, R. (2009). Traumatic brain injury and intestinal dysfunction: uncovering the neuro-enteric axis. J. Neurotrauma 26, 1353–1359.
54. Liao, D.-H., Zhao, J.-B., and Gregersen, H. (2009). Gastrointestinal tract modelling in health and disease. World J. Gastroenterol. 15, 169–176.
55. Podolsky, D.K. (1999). Mucosal immunity and inflammation. V. Innate mechanisms of mucosal defense and repair: the best offense is a good defense. Am. J. Physiol. 277, G495–G499.
56. Balda, M.S., Fallon, M.B., Van Itallie, C.M., and Anderson, J.M. (1992). Structure, regulation, and pathophysiology of tight junctions in the gastrointestinal tract. Yale J. Biol. Med. 65, 725–740.

57. Cheng, L.K., O'Grady, G., Du, P., Egbuji, J.U., Windsor, J.A., and Pullan, A.J. (2010). Gastrointestinal system. Wiley Interdiscip. Rev. Syst. Biol. Med. 2, 65–79.
58. Carabotti, M., Scirocco, A., Maselli, M.A., and Severi, C. (2015). The gut-brain axis: interactions between enteric microbiota, central and enteric nervous systems. Ann. Gastroenterol. 28, 203–209.
59. Pavlov, V.A., and Tracey, K.J. (2015). Neural circuitry and immunity. Immunol. Res. 63, 38–57.
60. Olsen, A.B., Hetz, R.A., Xue, H., Aroom, K.R., Bhattarai, D., Johnson, E., Bedi, S., Cox, C.S., Jr., and Uray, K. (2013). Effects of traumatic brain injury on intestinal contractility. Neurogastroenterol. Motil. 25, 593–e463.
61. Sun, B., Hu, C., Fang, H., Zhu, L., Gao, N., and Zhu, J. (2015). The effects of *Lactobacillus acidophilus* on the intestinal smooth muscle contraction through PKC/MLCK/MLC signaling pathway in TBI mouse model. PLoS One 10, e0128214.
62. Wang, Y.B., Liu, J., and Yang, Z.X. (2011). Effects of intestinal mucosal blood flow and motility on intestinal mucosa. World J. Gastroenterol. 17, 657–661.
63. Hang, C.H., Shi, J.X., Li, J.S., Wu, W., and Yin, H.X. (2003). Alterations of intestinal mucosa structure and barrier function following traumatic brain injury in rats. World J. Gastroenterol. 9, 2776–2781.
64. Feighery, L., Smyth, A., Keely, S., Baird, A.W., O'Connor, W.T., Callanan, J.J., and Brayden, D.J. (2008). Increased intestinal permeability in rats subjected to traumatic frontal lobe percussion brain injury. J. Trauma 64, 131–137; discussion, 137–138.
65. Ma, E.L., Smith, A.D., Desai, N., Cheung, L., Hanscom, M., Stoica, B.A., Loane, D.J., Shea-Donohue, T., and Faden, A.I. (2017). Bi-directional brain-gut interactions and chronic pathological changes after traumatic brain injury in mice. Brain Behav. Immun. 66, 56–69.
66. Faries, P.L., Simon, R.J., Martella, A.T., Lee, M.J., and Machiedo, G.W. (1998). Intestinal permeability correlates with severity of injury in trauma patients. J. Trauma 44, 1031–1035; discussion, 1035–1036.
67. Jin, W., Wang, H., Ji, Y., Hu, Q., Yan, W., Chen, G., and Yin, H. (2008). Increased intestinal inflammatory response and gut barrier dysfunction in Nrf2-deficient mice after traumatic brain injury. Cytokine 44, 135–140.
68. Sandiego, C.M., Gallezot, J.D., Pittman, B., Nabulsi, N., Lim, K., Lin, S.F., Matuskey, D., Lee, J.Y., O'Connor, K.C., Huang, Y., Carson, R.E., Hannestad, J., and Cosgrove, K.P. (2015). Imaging robust microglial activation after lipopolysaccharide administration in humans with PET. Proc. Natl. Acad. Sci. U. S. A. 112, 12468–12473.
69. Nicholson, S.E., Watts, L.T., Burmeister, D.M., Merrill, D., Scroggins, S., Zou, Y., Lai, Z., Grandhi, R., Lewis, A.M., Newton, L.M., Eastridge, B.J., and Schwacha, M.G. (2019). Moderate traumatic brain injury alters the gastrointestinal microbiome in a time-dependent manner. Shock 52, 240–248.
70. Houlden, A., Goldrick, M., Brough, D., Vizi, E.S., Lenart, N., Martinecz, B., Roberts, I.S., and Denes, A. (2016). Brain injury induces specific changes in the caecal microbiota of mice via altered autonomic activity and mucoprotein production. Brain Behav. Immun. 57, 10–20.
71. Treangen, T.J., Wagner, J., Burns, M.P., and Villapol, S. (2018). Traumatic brain injury in mice induces acute bacterial dysbiosis within the fecal microbiome. Front. Immunol. 9, 2757.
72. Li, H., Sun, J., Du, J., Wang, F., Fang, R., Yu, C., Xiong, J., Chen, W., Lu, Z., and Liu, J. (2018). Clostridium butyricum exerts a neuroprotective effect in a mouse model of traumatic brain injury via the gut-brain axis. Neurogastroenterol. Motil. 30, e13260.
73. Ma, Q., Xing, C., Long, W., Wang, H.Y., Liu, Q., and Wang, R.F. (2019). Impact of microbiota on central nervous system and neurological diseases: the gut-brain axis. J. Neuroinflammation 16, 53.
74. Abdel-Haq, R., Schlachetzki, J.C.M., Glass, C.K., and Mazmanian, S.K. (2019). Microbiome-microglia connections via the gut-brain axis. J. Exp. Med. 216, 41–59.
75. Villapol, S., Kryndushkin, D., Balarezo, M.G., Campbell, A.M., Saavedra, J.M., Shewmaker, F.P., and Symes, A.J. (2015). Hepatic expression of serum amyloid A1 is induced by traumatic brain injury and modulated by telmisartan. Am. J. Pathol. 185, 2641–2652.
76. Wicker, E., Benton, L., George, K., Furlow, W., and Villapol, S. (2019). Serum amyloid A protein as a potential biomarker for severity and acute outcome in traumatic brain injury. Biomed. Res. Int. 2019, 5967816.
77. Rael, L.T., Bar-Or, R., Salottolo, K., Mains, C.W., Slone, D.S., Offner, P.J., and Bar-Or, D. (2009). Injury severity and serum amyloid A correlate with plasma oxidation-reduction potential in multitrauma patients: a retrospective analysis. Scand. J. Trauma Resusc. Emerg. Med. 17, 57.
78. Nizamutdinov, D., DeMorrow, S., McMillin, M., Kain, J., Mukherjee, S., Zeitouni, S., Frampton, G., Bricker, P.C., Hurst, J., and Shapiro, L.A. (2017). Hepatic alterations are accompanied by changes to bile acid transporter-expressing neurons in the hypothalamus after traumatic brain injury. Sci. Rep. 7, 40112.
79. Chmielewski, C. (2003). Renal anatomy and overview of nephron function. Nephrol. Nurs. J. 30, 185–190; quiz, 191–182.
80. Freeman, W.D., and Wadei, H.M. (2015). A brain-kidney connection: the delicate interplay of brain and kidney physiology. Neurocrit. Care 22, 173–175.
81. Moore, E.M., Bellomo, R., Nichol, A., Harley, N., Macisaac, C., and Cooper, D.J. (2010). The incidence of acute kidney injury in patients with traumatic brain injury. Ren. Fail. 32, 1060–1065.
82. Corral, L., Javierre, C.F., Ventura, J.L., Marcos, P., Herrero, J.I., and Manez, R. (2012). Impact of non-neurological complications in severe traumatic brain injury outcome. Crit. Care 16, R44.
83. Li, N., Zhao, W.G., and Zhang, W.F. (2011). Acute kidney injury in patients with severe traumatic brain injury: implementation of the acute kidney injury network stage system. Neurocrit. Care 14, 377–381.
84. Ahmed, M., Sriganesh, K., Vinay, B., and Umamaheswara Rao, G.S. (2015). Acute kidney injury in survivors of surgery for severe traumatic brain injury: incidence, risk factors, and outcome from a tertiary neuroscience center in India. Br. J. Neurosurg. 29, 544–548.
85. Civiletti, F., Assenzio, B., Mazzeo, A.T., Medica, D., Giaretta, F., Deambrosis, I., Fanelli, V., Ranieri, V.M., Cantaluppi, V., and Mascia, L. (2019). Acute tubular injury is associated with severe traumatic brain injury: in vitro study on human tubular epithelial cells. Sci. Rep. 9, 6090.
86. Skrifvars, M.B., Moore, E., Martensson, J., Bailey, M., French, C., Presneill, J., Nichol, A., Little, L., Duranteau, J., Huet, O., Haddad, S., Arabi, Y., McArthur, C., Cooper, D.J., and Bellomo, R.; EPO-TBI Investigators and the ANZICS Clinical Trials Group. (2019). Erythropoietin in traumatic brain injury associated acute kidney injury: a randomized controlled trial. Acta Anaesthesiol. Scand. 63, 200–207.
87. Park, C.Y., Choi, H.Y., You, N.K., Roh, T.H., Seo, S.J., and Kim, S.H. (2016). Continuous renal replacement therapy for acute renal failure in patients with traumatic brain injury. Korean J. Neurotrauma 12, 89–93.
88. Nongnuch, A., Panorchan, K., and Davenport, A. (2014). Brain-kidney crosstalk. Crit. Care 18, 225.
89. Andres-Hernando, A., Dursun, B., Altmann, C., Ahuja, N., He, Z., Bhargava, R., Edelstein, C.E., Jani, A., Hoke, T.S., Klein, C., and Faubel, S. (2012). Cytokine production increases and cytokine clearance decreases in mice with bilateral nephrectomy. Nephrol. Dial. Transplant. 27, 4339–4347.
90. Kinsey, G.R., Li, L., and Okusa, M.D. (2008). Inflammation in acute kidney injury. Nephron Exp. Nephrol. 109, e102–e107.
91. Liao, Y., Liu, P., Guo, F., Zhang, Z.Y., and Zhang, Z. (2013). Oxidative burst of circulating neutrophils following traumatic brain injury in human. PLoS One 8, e68963.
92. Nagao, M., Feinstein, T.N., Ezura, Y., Hayata, T., Notomi, T., Saita, Y., Hanyu, R., Hemmi, H., Izu, Y., Takeda, S., Wang, K., Rittling, S., Nakamoto, T., Kaneko, K., Kurosawa, H., Karsenty, G., Denhardt, D.T., Vilardaga, J.P., and Noda, M. (2011). Sympathetic control of bone mass regulated by osteopontin. Proc. Natl. Acad. Sci. U. S. A. 108, 17767–17772.
93. Garrett, I.R., Boyce, B.F., Oreffo, R.O., Bonewald, L., Poser, J., and Mundy, G.R. (1990). Oxygen-derived free radicals stimulate osteoclastic bone resorption in rodent bone in vitro and in vivo. J. Clin. Invest. 85, 632–639.
94. Kondo, H., Takeuchi, S., and Togari, A. (2013). beta-Adrenergic signaling stimulates osteoclastogenesis via reactive oxygen species. Am. J. Physiol. Endocrinol. Metab. 304, E507–E515.
95. Galindo, L.T., Filippo, T.R., Semedo, P., Ariza, C.B., Moreira, C.M., Camara, N.O., and Porcionatto, M.A. (2011). Mesenchymal stem cell therapy modulates the inflammatory response in experimental traumatic brain injury. Neurol Res. Int. 2011, 564089.
96. Hardy, R., and Cooper, M.S. (2009). Bone loss in inflammatory disorders. J. Endocrinol. 201, 309–320.

97. Reed, M.L., Merriam, G.R., and Kargi, A.Y. (2013). Adult growth hormone deficiency—benefits, side effects, and risks of growth hormone replacement. Front. Endocrinol. (Lausanne) 4, 64.
98. Kristensen, E., Hallgrimsson, B., Morck, D.W., and Boyd, S.K. (2012). Microarchitecture, but not bone mechanical properties, is rescued with growth hormone treatment in a mouse model of growth hormone deficiency. Int. J. Endocrinol. 2012, 294965.
99. Beaupre, G.S., and Lew, H.L. (2006). Bone-density changes after stroke. Am. J. Phys. Med. Rehabil. 85, 464–472.
100. Smith, E.M., Comiskey, C.M., and Carroll, A.M. (2009). A study of bone mineral density in adults with disability. Arch. Phys. Med. Rehabil. 90, 1127–1135.
101. Smith, E., Comiskey, C., and Carroll, A. (2016). Prevalence of and risk factors for osteoporosis in adults with acquired brain injury. Ir. J. Med. Sci. 185, 473–481.
102. Oppl, B., Michitsch, G., Misof, B., Kudlacek, S., Donis, J., Klaushofer, K., Zwerina, J., and Zwettler, E. (2014). Low bone mineral density and fragility fractures in permanent vegetative state patients. J. Bone Miner. Res. 29, 1096–1100.
103. Brady, R.D., Grills, B.L., Church, J.E., Walsh, N.C., McDonald, A.C., Agoston, D.V., Sun, M., O'Brien, T.J., Shultz, S.R., and McDonald, S.J. (2016). Closed head experimental traumatic brain injury increases size and bone volume of callus in mice with concomitant tibial fracture. Sci. Rep. 6, 34491.
104. Singleton, Q., Vaibhav, K., Braun, M., Patel, C., Khayrullin, A., Mendhe, B., Lee, B.R., Kolhe, R., Kaiser, H., and Awad, M.E. (2019). Bone marrow derived extracellular vesicles activate osteoclast differentiation in traumatic brain injury induced bone loss. Cells 8, E63.
105. Shultz, S.R., Wright, D.K., Zheng, P., Stuchbery, R., Liu, S.-J., Sashindranath, M., Medcalf, R.L., Johnston, L.A., Hovens, C.M., and Jones, N.C. (2015). Sodium selenate reduces hyperphosphorylated tau and improves outcomes after traumatic brain injury. Brain 138, 1297–1313.
106. Tan, X.L., Wright, D.K., Liu, S., Hovens, C., O'Brien, T.J., and Shultz, S.R. (2016). Sodium selenate, a protein phosphatase 2A activator, mitigates hyperphosphorylated tau and improves repeated mild traumatic brain injury outcomes. Neuropharmacology 108, 382–393.
107. Brady, R., Grills, B., Romano, T., Wark, J., O'Brien, T., Shultz, S., and McDonald, S.J. (2016). Sodium selenate treatment mitigates reduction of bone volume following traumatic brain injury in rats. J. Musculoskelet. Neuronal Interact. 16, 369–376.
108. Hofman, M., Koopmans, G., Kobbe, P., Poeze, M., Andruszkow, H., Brink, P.R., and Pape, H.C. (2015). Improved fracture healing in patients with concomitant traumatic brain injury: proven or not? Mediators Inflamm. 2015, 204842.
109. Morley, J., Marsh, S., Drakoulakis, E., Pape, H.C., and Giannoudis, P.V. (2005). Does traumatic brain injury result in accelerated fracture healing? Injury 36, 363–368.
110. Tsitsilonis, S., Seemann, R., Misch, M., Wichlas, F., Haas, N.P., Schmidt-Bleek, K., Kleber, C., and Schaser, K.D. (2015). The effect of traumatic brain injury on bone healing: an experimental study in a novel in vivo animal model. Injury 46, 661–665.
111. Locher, R.J., Lunnemann, T., Garbe, A., Schaser, K., Schmidt-Bleek, K., Duda, G., and Tsitsilonis, S. (2015). Traumatic brain injury and bone healing: radiographic and biomechanical analyses of bone formation and stability in a combined murine trauma model. J. Musculoskelet. Neuronal Interact. 15, 309–315.
112. Wei, Y., Wang, L., Clark, J.C., Dass, C.R., and Choong, P.F. (2008). Elevated leptin expression in a rat model of fracture and traumatic brain injury. J. Pharm. Pharmacol. 60, 1667–1672.
113. Wang, L., Yuan, J.S., Zhang, H.X., Ding, H., Tang, X.G., and Wei, Y.Z. (2011). Effect of leptin on bone metabolism in rat model of traumatic brain injury and femoral fracture. Chin. J. Traumatol. 14, 7–13.
114. Mueller, M., Schilling, T., Minne, H.W., and Ziegler, R. (1991). A systemic acceleratory phenomenon (South AustraliaP) accompanies the regional acceleratory phenomenon (RAP) during healing of a bone defect in the rat. J. Bone Miner. Res. 6, 401–410.
115. Wildburger, R., Zarkovic, N., Tonkovic, G., Skoric, T., Frech, S., Hartleb, M., Loncaric, I., and Zarkovic, K. (1998). Post-traumatic hormonal disturbances: prolactin as a link between head injury and enhanced osteogenesis. J. Endocrinol. Invest. 21, 78–86.
116. Zhuang, Y.F., and Li, J. (2013). Serum EGF and NGF levels of patients with brain injury and limb fracture. Asian Pac. J. Trop. Med. 6, 383–386.
117. Morioka, K., Marmor, Y., Sacramento, J.A., Lin, A., Shao, T., Miclau, K.R., Clark, D.R., Beattie, M.S., Marcucio, R.S., and Miclau, T. (2019). Differential fracture response to traumatic brain injury suggests dominance of neuroinflammatory response in polytrauma. Sci. Rep. 9, 1–16.
118. Brown, S., Hawker, G., Beaton, D., and Colantonio, A. (2011). Long-term musculoskeletal complaints after traumatic brain injury. Brain Inj. 25, 453–461.
119. Wright, D.K., Liu, S., van der Poel, C., McDonald, S.J., Brady, R.D., Taylor, L., Yang, L., Gardner, A.J., Ordidge, R., O'Brien, T.J., Johnston, L.A., and Shultz, S.R. (2017). Traumatic brain injury results in cellular, structural and functional changes resembling motor neuron disease. Cereb. Cortex 27, 4503–4515.
120. Shahidi, B., Shah, S.B., Esparza, M., Head, B.P., and Ward, S.R. (2018). Skeletal muscle atrophy and degeneration in a mouse model of traumatic brain injury. J. Neurotrauma 35, 398–401.
121. Brady, R.D., Shultz, S.R., McDonald, S.J., and O'Brien, T.J. (2018). Neurological heterotopic ossification: current understanding and future directions. Bone 109, 35–42.
122. Genêt, F., Jourdan, C., Schnitzler, A., Lautridou, C., Guillemot, D., Judet, T., Poiraudeau, S., and Denormandie, P. (2011). Troublesome heterotopic ossification after central nervous system damage: a survey of 570 surgeries. PLoS One 6, e16632.
123. Reznik, J., Biros, E., Marshall, R., Jelbart, M., Milanese, S., Gordon, S., and Galea, M. (2014). Prevalence and risk-factors of neurogenic heterotopic ossification in traumatic spinal cord and traumatic brain injured patients admitted to specialised units in Australia. J. Musculoskelet. Neuronal Interact. 14, 19–28.
124. Simonsen, L.L., Sonne-Holm, S., Krasheninnikoff, M., and Engberg, A.W. (2007). Symptomatic heterotopic ossification after very severe traumatic brain injury in 114 patients: incidence and risk factors. Injury 38, 1146–1150.
125. Hendricks, H.T., Geurts, A., van Ginneken, B.C., Heeren, A.J., and Vos, P.E. (2007). Brain injury severity and autonomic dysregulation accurately predict heterotopic ossification in patients with traumatic brain injury. Clin. Rehabil. 21, 545–553.
126. Potter, B.K., Burns, T.C., Lacap, A.P., Granville, R.R. and Gajewski, D.A. (2007). Heterotopic ossification following traumatic and combat-related amputations: prevalence, risk factors, and preliminary results of excision. J. Bone Joint Surg. Am. 89, 476–486.
127. Almangour, W., Schnitzler, A., Salga, M., Debaud, C., Denormandie, P., and Genet, F. (2016). Recurrence of heterotopic ossification after removal in patients with traumatic brain injury: a systematic review. Ann. Phys. Rehabil. Med. 59, 263–269.
128. Alfieri, K., Forsberg, J., and Potter, B. (2012). Blast injuries and heterotopic ossification. Bone Joint Res. 1, 174–179.
129. Forsberg, J.A., Pepek, J.M., Wagner, S., Wilson, K., Flint, J., Andersen, R.C., Tadaki, D., Gage, F.A., Stojadinovic, A., and Elster, E.A. (2009). Heterotopic ossification in high-energy wartime extremity injuries: prevalence and risk factors. J. Bone Joint Surg. Am. 91, 1084–1091.
130. Cipriano, C.A., Pill, S.G., and Keenan, M.A. (2009). Heterotopic ossification following traumatic brain injury and spinal cord injury. J. Am. Acad. Orthop. Surg. 17, 689–697.
131. Chalidis, B., Stengel, D., and Giannoudis, P.V. (2007). Early excision and late excision of heterotopic ossification after traumatic brain injury are equivalent: a systematic review of the literature. J. Neurotrauma 24, 1675–1686.
132. Garland, D.E. (1991). Surgical approaches for resection of heterotopic ossification in traumatic brain-injured adults. Clin. Orthop. Relat. Res. (263), 59–70.
133. Torossian, F., Guerton, B., Anginot, A., Alexander, K.A., Desterke, C., Soave, S., Tseng, H.-W., Arouche, N., Boutin, L., and Kulina, I. (2017). Macrophage-derived oncostatin M contributes to human and mouse neurogenic heterotopic ossifications. JCI Insight 2, 96034.
134. Genêt, F., Kulina, I., Vaquette, C., Torossian, F., Millard, S., Pettit, A.R., Sims, N.A., Anginot, A., Guerton, B., and Winkler, I.G. (2015). Neurological heterotopic ossification following spinal cord injury is triggered by macrophage-mediated inflammation in muscle. J. Pathol. 236, 229–240.
135. Brady, R.D, Zhao, M.Z., Wong, K.R., Casilla-Espinosa, P.M., Yamakawa, G.R., Wortman, R.C., Sun, M., Grills, B.L., Mychasiuk, R.,

O'Brien, T.J., Agoston, D.V., Lee, P.V.S., McDonald, S.J., Robinson, D.L., and Shultz, S.R. (2020). A novel rat model of heterotopic ossification after polytrauma with traumatic brain injury. Bone 133, 115263.
136. Wang, H., Liao, H., Ochani, M., Justiniani, M., Lin, X., Yang, L., Al-Abed, Y., Wang, H., Metz, C., Miller, E.J., Tracey, K.J., and Ulloa, L. (2004). Cholinergic agonists inhibit HMGB1 release and improve survival in experimental sepsis. Nat. Med. 10, 1216–1221.
137. Rosas-Ballina, M., and Tracey, K.J. (2009). The neurology of the immune system: neural reflexes regulate immunity. Neuron 64, 28–32.
138. Ajmo, C.T., Jr., Collier, L.A., Leonardo, C.C., Hall, A.A., Green, S.M., Womble, T.A., Cuevas, J., Willing, A.E., and Pennypacker, K.R. (2009). Blockade of adrenoreceptors inhibits the splenic response to stroke. Exp. Neurol. 218, 47–55.
139. Tracey, K.J. (2002). The inflammatory reflex. Nature 420, 853–859.
140. Blomster, L.V., Brennan, F.H., Lao, H.W., Harle, D.W., Harvey, A.R., and Ruitenberg, M.J. (2013). Mobilisation of the splenic monocyte reservoir and peripheral CX(3)CR1 deficiency adversely affects recovery from spinal cord injury. Exp. Neurol. 247, 226–240.
141. Chu, W., Li, M., Li, F., Hu, R., Chen, Z., Lin, J., and Feng, H. (2013). Immediate splenectomy down-regulates the MAPK-NF-κB signaling pathway in rat brain after severe traumatic brain injury. J. Trauma Acute Care Surg. 74, 1446–1453.
142. Li, M., Li, F., Luo, C., Shan, Y., Zhang, L., Qian, Z., Zhu, G., Lin, J., and Feng, H. (2011). Immediate splenectomy decreases mortality and improves cognitive function of rats after severe traumatic brain injury. J. Trauma 71, 141–147.
143. Hazeldine, J., Lord, J.M., and Belli, A. (2015). Traumatic brain injury and peripheral immune suppression: primer and prospectus. Front. Neurol. 6, 235.
144. Sun, M., McDonald, S.J., Brady, R.D., O'Brien, T.J., and Shultz, S.R. (2018). The influence of immunological stressors on traumatic brain injury. Brain Behav. Immun. 69, 618–628.
145. Kong, X.-D., Bai, S., Chen, X., Wei, H.-J., Jin, W.-N., Li, M.-S., Yan, Y., and Shi, F.-D. (2014). Alterations of natural killer cells in traumatic brain injury. Neurosci. Bull. 30, 903–912.
146. Junger, W.G., Rhind, S.G., Rizoli, S.B., Cuschieri, J., Baker, A.J., Shek, P.N., Hoyt, D.B., and Bulger, E.M. (2013). Pre-hospital hypertonic saline resuscitation attenuates the activation and promotes apoptosis of neutrophils in patients with severe traumatic brain injury. Shock 40, 366–374.
147. Dong, T., Zhi, L., Bhayana, B., and Wu, M.X. (2016). Cortisol-induced immune suppression by a blockade of lymphocyte egress in traumatic brain injury. J. Neuroinflammation 13, 197.
148. Schwulst, S.J., Trahanas, D.M., Saber, R., and Perlman, H. (2013). Traumatic brain injury-induced alterations in peripheral immunity. J. Trauma Acute Care Surg. 75, 780–788.
149. Valencic, L., Tokmadzic, V.S., Kuharic, J., and Sustic, A. (2015). The incidence of nosocomial infections in patients with isolated severe traumatic brain injury. Sanamed 10, 185–194.
150. Kourbeti, I., Vakis, A., Papadakis, J., Karabetsos, D., Bertsias, G., Filippou, M., Ioannou, A., Neophytou, C., Anastasaki, M., and Samonis, G. (2012). Infections in traumatic brain injury patients. Clin. Microbiol. Infect. 18, 359–364.
151. Mrakovcic-Sutic, I., Tokmadzic, V.S., Laskarin, G., Mahmutefendic, H., Lucin, P., Zupan, Z., and Sustic, A. (2010). Early changes in frequency of peripheral blood lymphocyte subpopulations in severe traumatic brain-injured patients. Scand. J. Immunol. 72, 57–65.
152. Ho, C.-H., Liang, F.-W., Wang, J.-J., Chio, C.-C., and Kuo, J.-R. (2018). Impact of grouping complications on mortality in traumatic brain injury: a nationwide population-based study. PloS One 13, e0190683.
153. Alharfi, I.M., Charyk Stewart, T., Al Helali, I., Daoud, H., and Fraser, D.D. (2014). Infection rates, fevers, and associated factors in pediatric severe traumatic brain injury. J. Neurotrauma 31, 452–458.
154. Sharma, R., Shultz, S.R., Robinson, M.J., Belli, A., Hibbs, M.L., O'Brien, T.J., and Semple, B.D. (2019). Infections after a traumatic brain injury: the complex interplay between the immune and neurological systems. Brain Behav. Immun. 79, 63–74.
155. Sonneville, R., Verdonk, F., Rauturier, C., Klein, I.F., Wolff, M., Annane, D., Chretien, F., and Sharshar, T. (2013). Understanding brain dysfunction in sepsis. Ann. Intensive Care 3, 15.
156. Osborn, T.M., Tracy, J.K., Dunne, J.R., Pasquale, M., and Napolitano, L.M. (2004). Epidemiology of sepsis in patients with traumatic injury. Crit. Care Med. 32, 2234–2240.
157. Selassie, A.W., Fakhry, S.M., and Ford, D.W. (2011). Population-based study of the risk of in-hospital death after traumatic brain injury: the role of sepsis. J. Trauma Acute Care Surg. 71, 1226–1234.
158. Prescott, H.C., Iwashyna, T.J., Blackwood, B., Calandra, T., Chlan, L.L., Choong, K., Connolly, B., Dark, P., Ferrucci, L., Finfer, S., Girard, T.D., Hodgson, C., Hopkins, R.O., Hough, C.L., Jackson, J.C., Machado, F.R., Marshall, J.C., Misak, C., Needham, D.M., Panigrahi, P., Reinhart, K., Yende, S., Zafonte, R., Rowan, K.M., and Angus, D.C. (2019). Understanding and enhancing sepsis survivorship. priorities for research and practice. Am. J. Respir. Crit. Care Med. 200, 972–981.
159. Calsavara, A.J.C., Costa, P.A., Nobre, V., and Teixeira, A.L. (2018). Factors associated with short and long term cognitive changes in patients with sepsis. Sci. Rep. 8, 4509.
160. Dijkstra-Kersten, S.M.A., Kok, L., Kerckhoffs, M.C., Cremer, O.L., de Lange, D.W., van Dijk, D., Needham, D.M., and Slooter, A.J.C. (2020). Neuropsychiatric outcome in subgroups of intensive care unit survivors: implications for after-care. J. Crit. Care 55, 171–176.
161. Davydow, D.S., Hough, C.L., Langa, K.M. and Iwashyna, T.J. (2013). Symptoms of depression in survivors of severe sepsis: a prospective cohort study of older Americans. Am. J. Geriatr. Psychiatry 21, 887–897.
162. Longhi, L., Gesuete, R., Perego, C., Ortolano, F., Sacchi, N., Villa, P., Stocchetti, N., and De Simoni, M.-G. (2011). Long-lasting protection in brain trauma by endotoxin preconditioning. J. Cereb. Blood Flow Metab. 31, 1919–1929.
163. Smithason, S., Moore, S.K., and Provencio, J.J. (2013). Low-dose lipopolysaccharide injection prior to subarachnoid hemorrhage modulates delayed deterioration associated with vasospasm in subarachnoid hemorrhage, in: *Cerebral Vasospasm: Neurovascular Events After Subarachnoid Hemorrhage*. M. Zuccarello, J.F. Clark, G. Pyne-Geithman, N. Andaluz, J. Hartings, and O.M. Adeoye (eds). Springer-Verlag: Vienna, Austria, pps. 253–258.
164. Turner, R.C., Naser, Z.J., Lucke-Wold, B.P., Logsdon, A.F., Vangilder, R.L., Matsumoto, R.R., Huber, J.D., and Rosen, C.L. (2017). Single low-dose lipopolysaccharide preconditioning: neuroprotective against axonal injury and modulates glial cells. Neuroimmunol. Neuroinflammation 4, 6.
165. Hang, C.H., Shi, J.X., Tian, J., Li, J.S., Wu, W., and Yin, H.X. (2004). Effect of systemic LPS injection on cortical NF-kappaB activity and inflammatory response following traumatic brain injury in rats. Brain Res. 1026, 23–32.
166. Corrigan, F., Arulsamy, A., Collins-Praino, L.E., Holmes, J.L., and Vink, R. (2017). Toll like receptor 4 activation can be either detrimental or beneficial following mild repetitive traumatic brain injury depending on timing of activation. Brain Behav. Immun. 64, 124–139.
167. Fenn, A.M., Gensel, J.C., Huang, Y., Popovich, P.G., Lifshitz, J., and Godbout, J.P. (2014). Immune activation promotes depression 1 month after diffuse brain injury: a role for primed microglia. Biol. Psychiatry 76, 575–584.
168. Muccigrosso, M.M., Ford, J., Benner, B., Moussa, D., Burnsides, C., Fenn, A.M., Popovich, P.G., Lifshitz, J., Walker, F.R., and Eiferman, D.S. (2016). Cognitive deficits develop 1month after diffuse brain injury and are exaggerated by microglia-associated reactivity to peripheral immune challenge. Brain Behav. Immun. 54, 95–109.
169. Wang, Y., Miszczuk, D., Andrade, P., and Pitkänen, A. (2017). Peripheral infection after traumatic brain injury augments focal excitability in the perilesional cortex and dentate gyrus. J. Neurol. Sci. 381, 82.
170. Russo, M.V., and McGavern, D.B. (2018). Secondary damage or viral infection following mild traumatic brain injury impedes tissue repair induced by distinct myeloid cell subsets. J. Immnol. 200, 1 Suppl., 108.10.
171. Venturi, L., Miranda, M., Selmi, V., Vitali, L., Tani, A., Margheri, M., De Gaudio, A.R., and Adembri, C. (2009). Systemic sepsis exacerbates mild post-traumatic brain injury in the rat. J. Neurotrauma 26, 1547–1556.
172. McDonald, S.J., Sun, M., Agoston, D.V., and Shultz, S.R. (2016). The effect of concomitant peripheral injury on traumatic brain injury pathobiology and outcome. J. Neuroinflammation 13, 90.

173. Shultz, S.R., Sun, M., Wright, D.K., Brady, R.D., Liu, S., Beynon, S., Schmidt, S.F., Kaye, A.H., Hamilton, J.A., O'Brien, T.J., Grills, B.L., and McDonald, S.J. (2015). Tibial fracture exacerbates traumatic brain injury outcomes and neuroinflammation in a novel mouse model of multitrauma. J. Cereb. Blood Flow Metab. 35, 1339–1347.
174. Suto, Y., Nagata, K., Ahmed, S.M., Jacovides, C.L., Browne, K.D., Cognetti, J., Johnson, V.E., Leone, R., Kaplan, L.J., Smith, D.H. and Pascual, J.L. (2019). Cerebral edema and neurological recovery after traumatic brain injury are worsened if accompanied by a concomitant long bone fracture. J. Neurotrauma 36, 609–618.
175. Sahbaie, P., Tajerian, M., Yang, P., Irvine, K.A., Huang, T.T., Luo, J., Wyss-Coray, T., and Clark, J.D. (2018). Nociceptive and cognitive changes in a murine model of polytrauma. J. Pain 19, 1392–1405.
176. Probst, C., Mirzayan, M.J., Mommsen, P., Zeckey, C., Tegeder, T., Geerken, L., Maegele, M., Samii, A., and van Griensven, M. (2012). Systemic inflammatory effects of traumatic brain injury, femur fracture, and shock: an experimental murine polytrauma model. Mediators Inflamm. 2012, 136020.
177. Weckbach, S., Perl, M., Heiland, T., Braumuller, S., Stahel, P.F., Flierl, M.A., Ignatius, A., Gebhard, F., and Huber-Lang, M. (2012). A new experimental polytrauma model in rats: molecular characterization of the early inflammatory response. Mediators Inflamm. 2012, 890816.
178. Weckbach, S., Hohmann, C., Braumueller, S., Denk, S., Klohs, B., Stahel, P.F., Gebhard, F., Huber-Lang, M.S., and Perl, M. (2013). Inflammatory and apoptotic alterations in serum and injured tissue after experimental polytrauma in mice: distinct early response compared with single trauma or "double-hit" injury. J. Trauma Acute Care Surg. 74, 489–498.
179. Lippert-Gruner, M., Maegele, M., Haverkamp, H., Klug, N., and Wedekind, C. (2007). Health-related quality of life during the first year after severe brain trauma with and without polytrauma. Brain Inj. 21, 451–455.
180. Sun, M., Brady, R.D., Wright, D.K., Kim, H.A., Zhang, S.R., Sobey, C.G., Johnstone, M.R., O'Brien, T.J., Semple, B.D., McDonald, S.J., and Shultz, S.R. (2017). Treatment with an interleukin-1 receptor antagonist mitigates neuroinflammation and brain damage after polytrauma. Brain Behav. Immun. 66, 359–371.
181. Yang, L., Guo, Y., Wen, D., Yang, L., Chen, Y., Zhang, G., and Fan, Z. (2016). Bone Fracture Enhances Trauma Brain Injury. Scand. J. Immunol. 83, 26–32.
182. Skrifvars, M.B., Bailey, M., French, C., Presneill, J., Nichol, A., Little, L., Duranteau, J., Huet, O., Haddad, S., Arabi, Y., McArthur, C., Cooper, D.J., and Bellomo, R.; EPO-TBI investigators and the ANZICS Clinical Trials Group. (2017). Erythropoietin in patients with traumatic brain injury and extracranial injury—a post hoc analysis of the erythropoietin traumatic brain injury trial. J, Trauma Acute Care Surg, 83, 449–456.
183. Yatsiv, I., Grigoriadis, N., Simeonidou, C., Stahel, P.F., Schmidt, O.I., Alexandrovich, A.G., Tsenter, J., and Shohami, E. (2005). Erythropoietin is neuroprotective, improves functional recovery, and reduces neuronal apoptosis and inflammation in a rodent model of experimental closed head injury. FASEB J. 19, 1701–1703.
184. Zhou, Z.W., Li, F., Zheng, Z.T., Li, Y.D., Chen, T.H., Gao, W.W., Chen, J.L., and Zhang, J.N. (2017). Erythropoietin regulates immune/inflammatory reaction and improves neurological function outcomes in traumatic brain injury. Brain Behav. 7, e00827.
185. Agoston, D.V., Shutes-David, A., and Peskind, E.R. (2017). Biofluid biomarkers of traumatic brain injury. Brain Inj. 31, 1195–1203.

Address correspondence to:
Stuart J. McDonald, PhD
Department of Neuroscience
Monash University
The Alfred Centre
99 Commercial Road
Melbourne, Victoria 3004
Australia

E-mail: stuart.mcdonald@monash.edu

REFERENCE LIST

Abel, JM, Gennarelli, TA & Segawa, H 1978, 'Incidence and Severity of Cerebral Concussion in the Rhesus Monkey Following Sagittal Plane Angular Acceleration'.

Abu Hamdeh, S, Marklund, N, Lewén, A, Howells, T, Raininko, R, Wikström, J & Enblad, P 2018, 'Intracranial pressure elevations in diffuse axonal injury: association with nonhemorrhagic MR lesions in central mesencephalic structures', *J Neurosurg*, vol. 131, no. 2, pp. 604-611.

Access Economics 2009, *The Economic Cost of Spinal Cord Injury and Traumatic Brain Injury in Australia*, Victorian Neurotrauma Initiative.

Adams, JH, Doyle, D, Ford, I, Gennarelli, TA, Graham, DI & McLellan, DR 1989, 'Diffuse axonal injury in head injury: definition, diagnosis and grading', *Histopathology*, vol. 15, no. 1, pp. 49-59.

Adams, JH, Graham, DI & Gennarelli, TA 1981, 'Acceleration induced head injury in the monkey. II. Neuropathology', *Acta Neuropathol Suppl*, vol. 7, pp. 26-28.

Adams, JH, Graham, DI, Murray, LS & Scott, G 1982, 'Diffuse axonal injury due to nonmissile head injury in humans: an analysis of 45 cases', *Ann Neurol*, vol. 12, no. 6, pp. 557-563.

Agoston, DV, Shutes-David, A & Peskind, ER 2017, 'Biofluid biomarkers of traumatic brain injury', *Brain Inj*, vol. 31, no. 9, pp. 1195-1203.

Akassoglou, K, Bauer, J, Kassiotis, G, Pasparakis, M, Lassmann, H, Kollias, G & Probert, L 1998, 'Oligodendrocyte apoptosis and primary demyelination induced by local TNF/p55TNF receptor signaling in the central nervous system of transgenic mice: models for multiple sclerosis with primary oligodendrogliopathy', *Am J Pathol*, vol. 153, no. 3, pp. 801-813.

Alahmari, DM, Skiold, B, Barton, SK, Nitsos, I, McDonald, C, Miller, SL, Zahra, V, Galinsky, R, Wu, Q, Farrell, MJ, Moss, TJ, Hooper, SB, Pearson, JT & Polglase, GR 2017, 'Diffusion Tensor Imaging Colour Mapping Threshold for Identification of Ventilation-Induced Brain Injury after Intrauterine Inflammation in Preterm Lambs', *Front Pediatr*, vol. 5, pp. 70.

Allouch, G 2017, 'Functional anatomy of the masticatory mechanism: A comparative study of physical characteristics of jaw-closing and jaw-opening muscles in sheep', *International Journal of Veterinary Sciences and Animal Husbandry*, vol. 38, 11/29, pp. 38-44.

Allsop, DL, Warner, CY, Wille, MG, Schneider, DC & Nahum, AM 1988, 'Facial Impact Response — A Comparison of the Hybrid III Dummy and Human Cadaver', <https://doi.org/10.4271/881719>.

Aly, H, Khashaba, MT, El-Ayouty, M, El-Sayed, O & Hasanein, BM 2006, 'IL-1beta, IL-6 and TNF-alpha and outcomes of neonatal hypoxic ischemic encephalopathy', *Brain Dev*, vol. 28, no. 3, pp. 178-182.

Andelic, N, Sigurdardottir, S, Schanke, AK, Sandvik, L, Sveen, U & Roe, C 2010, 'Disability, physical health and mental health 1 year after traumatic brain injury', *Disabil Rehabil*, vol. 32, no. 13, pp. 1122-1131.

Anderson, RW, Brown, CJ, Blumbergs, PC, McLean, AJ & Jones, NR 2003, 'Impact mechanics and axonal injury in a sheep model', *J Neurotrauma*, vol. 20, no. 10, pp. 961-974.

Anderson, RW, Sandoz, B, Dutschke, JK, Finnie, JW, Turner, RJ, Blumbergs, PC, Manavis, J & Vink, R 2014, 'Biomechanical studies in an ovine model of non-accidental head injury', *J Biomech*, vol. 47, no. 11, pp. 2578-2583.

Anderson, RWG, 2000, ' A study on the biomechanics of axonal injury', Dept. of Mechanical Engineering, Ph.D. thesis, University of Adelaide.

Arulsamy, A, Teng, J, Colton, H, Corrigan, F & Collins-Praino, L 2018, 'Evaluation of early chronic functional outcomes and their relationship to pre-frontal cortex and hippocampal pathology following moderate-severe traumatic brain injury', *Behav Brain Res*, vol. 348, 1, pp. 127-138.

Atlan, LS, Smith, C & Margulies, SS 2018, 'Improved prediction of direction-dependent, acute axonal injury in piglets', *J Neurosci Res*, vol. 96, no. 4, pp. 536-544.

Baguley, IJ, Nicholls, JL, Felmingham, KL, Crooks, J, Gurka, JA & Wade, LD 1999, 'Dysautonomia after traumatic brain injury: a forgotten syndrome?', *J Neurol Neurosurg Psychiatry*, vol. 67, no. 1, pp. 39-43.

Baguley, IJ, Nott, MT, Howle, AA, Simpson, GK, Browne, S, King, AC, Cotter, RE & Hodgkinson, A 2012, 'Late mortality after severe traumatic brain injury in New South Wales: a multicentre study', *Med J Aust*, vol. 196, no. 1 16, pp. 40-45.

Bauman, RA, Ling, G, Tong, L, Januszkiewicz, A, Agoston, D, Delanerolle, N, Kim, Y, Ritzel, D, Bell, R, Ecklund, J, Armonda, R, Bandak, F & Parks, S 2009, 'An introductory characterization of a combat-casualty-care relevant swine model of closed head injury resulting from exposure to explosive blast', *J Neurotrauma*, vol. 26, no. 6, pp. 841-860.

Bazarian, JJ, Cernak, I, Noble-Haeusslein, L, Potolicchio, S & Temkin, N 2009, 'Long-term neurologic outcomes after traumatic brain injury', *J Head Trauma Rehabil*, vol. 24, no. 6, pp. 439-451.

Becelewski, J & Pierzchała, K 2003, 'Cerebrovascular reactivity in patients with mild head injury', *Neurol Neurochir Pol*, vol. 37, no. 2, Mar-Apr, pp. 339-350.

Begum, G, Reddy, R, Yakoub, KM, Belli, A, Davies, DJ & Di Pietro, V 2020, 'Differential Expression of Circulating Inflammatory Proteins Following Sport-Related Traumatic Brain Injury', *Int J Mol Sci*, vol. 21, no. 4.

Bellapart, J, Abi-Fares, C, Cuthbertson, K, Dunster, K, Diab, S, Platts, DG, Raffel, C, Gabrielian, L, Barnett, A, Paratz, J, Boots, R & Fraser, JF 2016, 'Cerebral microcirculation during mild head injury after a contusion and acceleration experimental model in sheep', *Brain Inj*, vol. 30, no. 13-14, pp. 1542-1551.

Bellapart, J, Cuthbertson, K, Dunster, K, Diab, S, Platts, DG, Raffel, OC, Gabrielian, L, Barnett, A, Paratz, J, Boots, R & Fraser, JF 2018, 'Cerebral Microcirculation and Histological Mapping After Severe Head Injury: A Contusion and Acceleration Experimental Model', *Front Neurol*, vol. 9, p. 277.

Berry, C, Ley, EJ, Tillou, A, Cryer, G, Margulies, DR & Salim, A 2009, 'The effect of gender on patients with moderate to severe head injuries', *J Trauma*, vol. 67, no. 5, Nov, pp. 950-953.

Bigler, ED 2001, 'Distinguished Neuropsychologist Award Lecture 1999. The lesion(s) in traumatic brain injury: implications for clinical neuropsychology', *Arch Clin Neuropsychol*, vol. 16, no. 2, pp. 95-131.

Binder, LM, Rohling, ML & Larrabee, GJ 1997, 'A review of mild head trauma. Part I: Meta-analytic review of neuropsychological studies', *J Clin Exp Neuropsychol*, vol. 19, no. 3, pp. 421-431.

Bjork, JM & Grant, SJ 2009, 'Does traumatic brain injury increase risk for substance abuse?', *J Neurotrauma*, vol. 26, no. 7, pp. 1077-1082.

Blennow, K, Brody, DL, Kochanek, PM, Levin, H, McKee, A, Ribbers, GM, Yaffe, K & Zetterberg, H 2016, 'Traumatic brain injuries', *Nat Rev Dis Primers*, vol. 2, p. 16084.

Blennow, K, Hardy, J & Zetterberg, H 2012, 'The neuropathology and neurobiology of traumatic brain injury', *Neuron*, vol. 76, no. 5, pp. 886-899.

Blumbergs, PC, Jones, NR & North, JB 1989, 'Diffuse axonal injury in head trauma', *J Neurol Neurosurg Psychiatry*, vol. 52, no. 7 pp. 838-841.

Bonne, O, Gilboa, A, Louzoun, Y, Kempf-Sherf, O, Katz, M, Fishman, Y, Ben-Nahum, Z, Krausz, Y, Bocher, M, Lester, H, Chisin, R & Lerer, B 2003, 'Cerebral blood flow in chronic symptomatic mild traumatic brain injury', *Psychiatry Res*, vol. 124, no. 3, pp. 141-152.

Brett, FM, Mizisin, AP, Powell, HC & Campbell, IL 1995, 'Evolution of neuropathologic abnormalities associated with blood-brain barrier breakdown in transgenic mice expressing interleukin-6 in astrocytes', *J Neuropathol Exp Neurol*, vol. 54, no. 6, pp. 766-775.

Brown, AW, Leibson, CL, Malec, JF, Perkins, PK, Diehl, NN & Larson, DR 2004, 'Long-term survival after traumatic brain injury: a population-based analysis', *NeuroRehabilitation*, vol. 19, no. 1, pp. 37-43.

Browne, KD, Chen, XH, Meaney, DF & Smith, DH 2011, 'Mild traumatic brain injury and diffuse axonal injury in swine', *J Neurotrauma*, vol. 28, no. 9, pp. 1747-1755.

Buki, A & Povlishock, JT 2006, 'All roads lead to disconnection?--Traumatic axonal injury revisited', *Acta Neurochir (Wien)*, vol. 148, no. 2, pp. 181-193.

Burda, JE, Bernstein, AM & Sofroniew, MV 2016, 'Astrocyte roles in traumatic brain injury', *Exp Neurol*, vol. 275 Pt 3, pp. 305-315.

Bussone, W, Duma, S, Gabler, C, Stitzel, J & Madigan, M 2005, 'Linear and angular head accelerations in daily life'.

Byard, RW, Bhatia, KD, Reilly, PL & Vink, R 2009, 'How rapidly does cerebral swelling follow trauma? Observations using an animal model and possible implications in infancy', *Leg Med (Tokyo)*, vol. 11, no. 1, pp. S128-131.

Byard, RW, Gabrielian, L, Helps, SC, Thornton, E & Vink, R 2012, 'Further investigations into the speed of cerebral swelling following blunt cranial trauma', *J Forensic Sci*, vol. 57, no. 4, pp. 973-975.

Cai, B & Wang, N 2016, 'Large Animal Stroke Models vs. Rodent Stroke Models, Pros and Cons, and Combination?', *Acta Neurochir Suppl*, vol. 121, pp. 77-81.

Campolettano, ET, Gellner, RA & Rowson, S 2018, 'Relationship between Impact Velocity and Resulting Head Accelerations during Head Impacts in Youth Football', *Proc Int IRCOBI Conf Biomech Impacts*, vol. 2018, pp. 326-333.

Carroll, L, Cassidy, JD, Holm, L, Kraus, J & Coronado, V 2004, 'Methodological issues and research recommendations for mild traumatic brain injury: the who collaborating centre task force on mild traumatic brain injury', *Journal of Rehabilitation Medicine*, vol. 36, pp. 113-125.

Castellanos-Pinedo, F, Cid-Gala, M, Duque, P, Ramirez-Moreno, JM & Zurdo-Hernandez, JM 2012, 'Acquired brain injury: a proposal for its definition, diagnostic criteria and classification', *Rev Neurol*, vol. 54, no. 6, pp. 357-366.

Chen, G, Go, L & Mao, B 2002, 'Biomechanical mechanism of diffuse axonal injury', *Sheng Wu Yi Xue Gong Cheng Xue Za Zhi*, vol. 19, no. 3, Sep, pp. 500-504.

Chen, XH, Johnson, VE, Uryu, K, Trojanowski, JQ & Smith, DH 2009, 'A lack of amyloid beta plaques despite persistent accumulation of amyloid beta in axons of long-term survivors of traumatic brain injury', *Brain Pathol*, vol. 19, no. 2, pp. 214-223.

Chen, XH, Meaney, DF, Xu, BN, Nonaka, M, McIntosh, TK, Wolf, JA, Saatman, KE & Smith, DH 1999, 'Evolution of neurofilament subtype accumulation in axons following diffuse brain injury in the pig', *J Neuropathol Exp Neurol*, vol. 58, no. 6, pp. 588-596.

Chesnut, RM 1997, 'The management of severe traumatic brain injury', *Emerg Med Clin North Am*, vol. 15, no. 3, pp. 581-604.

Chio, CC, Chang, CH, Wang, CC, Cheong, CU, Chao, CM, Cheng, BC, Yang, CZ & Chang, CP 2013, 'Etanercept attenuates traumatic brain injury in rats by reducing early microglial expression of tumor necrosis factor-α', *BMC Neurosci*, vol. 14, p. 33.

Christman, CW, Grady, MS, Walker, SA, Holloway, KL & Povlishock, JT 1994, 'Ultrastructural studies of diffuse axonal injury in humans', *J Neurotrauma*, vol. 11, no. 2, pp. 173-186.

Clifton, GL, Robertson, CS, Kyper, K, Taylor, AA, Dhekne, RD & Grossman, RG 1983, 'Cardiovascular response to severe head injury', *J Neurosurg*, vol. 59, no. 3, pp. 447-454.

Cloots, RJ, Gervaise, HM, van Dommelen, JA & Geers, MG 2008, 'Biomechanics of traumatic brain injury: influences of the morphologic heterogeneities of the cerebral cortex', *Ann Biomed Eng*, vol. 36, no. 7, pp. 1203-1215.

Collins-Praino, LE, Arulsamy, A, Katharesan, V & Corrigan, F 2018, 'The effect of an acute systemic inflammatory insult on the chronic effects of a single mild traumatic brain injury', *Behav Brain Res*, vol. 336, pp. 22-31.

Collins-Praino, LE & Corrigan, F 2016, 'Does neuroinflammation drive the relationship between tau hyperphosphorylation and dementia development following traumatic brain injury?', *Brain Behav Immun*.

Cullen, DK, Harris, JP, Browne, KD, Wolf, JA, Duda, JE, Meaney, DF, Margulies, SS & Smith, DH 2016, 'A Porcine Model of Traumatic Brain Injury via Head Rotational Acceleration', *Methods Mol Biol*, vol. 1462, pp. 289-324.

Dancewicz, OL, Sylvander, SR, Markwell, TS, Crowe, SB & Trapp, JV 2017, 'Radiological properties of 3D printed materials in kilovoltage and megavoltage photon beams', *Phys Med*, vol. 38, pp. 111-118.

Daneshvar, DH, Nowinski, CJ, McKee, AC & Cantu, RC 2011, 'The epidemiology of sport-related concussion', *Clin Sports Med*, vol. 30, no. 1, pp. 1-17, vii.

Dashnaw, ML, Petraglia, AL & Bailes, JE 2012, 'An overview of the basic science of concussion and subconcussion: where we are and where we are going', *Neurosurg Focus*, vol. 33, no. 6, pp. E5: 1-9.

Davceva, N, Basheska, N & Balazic, J 2015, 'Diffuse Axonal Injury-A Distinct Clinicopathological Entity in Closed Head Injuries', *Am J Forensic Med Pathol*, vol. 36, no. 3, pp. 127-133.

Davceva, N, Sivevski, A & Basheska, N 2017, 'Traumatic axonal injury, a clinical-pathological correlation', *J Forensic Leg Med*, vol. 48, pp. 35-40.

Davidsson, J & Risling, M 2011, 'A new model to produce sagittal plane rotational induced diffuse axonal injuries', *Front Neurol*, vol. 2, p. 41.

Deb, S, Lyons, I & Koutzoukis, C 1999, 'Neurobehavioural symptoms one year after a head injury', *Br J Psychiatry*, vol. 174, pp. 360-365.

Demetriades, D, Kuncir, E, Murray, J, Velmahos, GC, Rhee, P & Chan, L 2004, 'Mortality prediction of head Abbreviated Injury Score and Glasgow Coma Scale: analysis of 7,764 head injuries', *J Am Coll Surg*, vol. 199, no. 2, pp. 216-222.

Dewar, D, Yam, P & McCulloch, J 1999, 'Drug development for stroke: importance of protecting cerebral white matter', *Eur J Pharmacol*, vol. 375, no. 1-3, pp. 41-50.

DiLeonardi, AM, Huh, JW & Raghupathi, R 2009, 'Impaired axonal transport and neurofilament compaction occur in separate populations of injured axons following diffuse brain injury in the immature rat', *Brain Res*, vol. 1263, pp. 174-182.

Dixon, B & MacLeod, DB 2020, 'Assessment of a Non Invasive Brain Oximeter in Volunteers Undergoing Acute Hypoxia', *Med Devices (Auckl)*, vol. 13, pp. 183-194.

Dixon, B, Turner, R & Christou, C 2019, 'Assessment of a Non-Invasive Brain Oximeter in a Sheep Model of Acute Brain Injury', *Med Devices (Auckl)*, vol. 12, pp. 479-487.

Dollé, JP, Jaye, A, Anderson, SA, Ahmadzadeh, H, Shenoy, VB & Smith, DH 2018, 'Newfound sex differences in axonal structure underlie differential outcomes from in vitro traumatic axonal injury', *Exp Neurol*, vol. 300, pp. 121-134.

Dowdell, J, Kim, J, Overley, S & Hecht, A 2018, 'Biomechanics and common mechanisms of injury of the cervical spine', *Handb Clin Neurol*, vol. 158, pp. 337-344.

Drake, A, Haut Donahue, TL, Stansloski, M, Fox, K, Wheatley, BB & Donahue, SW 2016, 'Horn and horn core trabecular bone of bighorn sheep rams absorbs impact energy and reduces brain cavity accelerations during high impact ramming of the skull', *Acta Biomater*, vol. 44, pp. 41-50.

Dutschke, Jea 2016, 'A Biomechanical Model of Traumatic Contusional Injury Produced by Controlled Cerebrocortical Indentation in Sheep', paper presented at International Research Council on Biomechanics of Injury Conference, Malaga, Spain.

Esterov, D & Greenwald, BD 2017, 'Autonomic Dysfunction after Mild Traumatic Brain Injury', *Brain Sci*, vol. 7, no. 8.

Evans, RW 1992, 'The postconcussion syndrome and the sequelae of mild head injury', *Neurol Clin*, vol. 10, no. 4, pp. 815-847.

Fearnside, MR, Cook, RJ, McDougall, P & McNeil, RJ 1993, 'The Westmead Head Injury Project outcome in severe head injury. A comparative analysis of pre-hospital, clinical and CT variables', *Br J Neurosurg*, vol. 7, no. 3, pp. 267-279.

Fehily, B & Fitzgerald, M 2017, 'Repeated Mild Traumatic Brain Injury: Potential Mechanisms of Damage', *Cell Transplant*, vol. 26, no. 7, pp. 1131-1155.

Feng, J, Zhao, X, Gurkoff, GG, Van, KC, Shahlaie, K, Lyeth, BG 2012, 'Post-traumatic hypoxia exacerbates neruonal cell death in the hippocampus', *J Neurotrauma*, vol. 29, no. 6, pp. 1167-1179

Finnie, J 2001, 'Animal models of traumatic brain injury: a review', *Aust Vet J*, vol. 79, no. 9, pp. 628-633.

Finnie, J, Lewis, S, Manavis, J, Blumbergs, P, Van den Heuvel, C & Jones, N 1999, 'Traumatic axonal injury in lambs: a model for paediatric axonal damage', *J Clin Neurosci*, vol. 6, no. 1, pp. 38-42.

Finnie, JW & Blumbergs, PC 2002, 'Traumatic brain injury', *Vet Pathol*, vol. 39, no. 6, pp. 679-689.

Finnie, JW, Blumbergs, PC, Manavis, J, Summersides, GE & Davies, RA 2000, 'Evaluation of brain damage resulting from penetrating and non-penetrating captive bolt stunning using lambs', *Aust Vet J*, vol. 78, no. 11, pp. 775-778.

Finnie, JW, Manavis, J, Blumbergs, PC & Summersides, GE 2002, 'Brain damage in sheep from penetrating captive bolt stunning', *Aust Vet J*, vol. 80, no. 1-2, pp. 67-69.

Finnie, JW, Van den Heuvel, C, Gebski, V, Manavis, J, Summersides, GE & Blumbergs, PC 2001, 'Effect of impact on different regions of the head of lambs', *J Comp Pathol*, vol. 124, no. 2-3, Feb-Apr, pp. 159-164.

Fisher, MW, Bray, AR & Johnstone, PD 2010, 'Implications of removing or altering the testicles of ram lambs on the financial returns from carcasses', *New Zealand Journal of Agricultural Research*, vol. 53, no. 2, pp. 135-143.

Fleminger, S & Ponsford, J 2005, 'Long term outcome after traumatic brain injury', *Bmj*, vol. 331, no. 7530, pp. 1419-1420.

Frank, D, Melamed, I, Gruenbaum, BF, Grinshpun, J, Kuts, R, Shvartsur, R, Azab, AN, Assadi, MH, Vinokur, M & Boyko, M 2020, 'Induction of Diffuse Axonal Brain Injury in Rats Based on Rotational Acceleration', *J Vis Exp*, no. 159.

Gaetz, M 2004, 'The neurophysiology of brain injury', *Clin Neurophysiol*, vol. 115, no. 1, pp. 4-18.

Gardner, RC & Yaffe, K 2015, 'Epidemiology of mild traumatic brain injury and neurodegenerative disease', *Mol Cell Neurosci*, vol. 66, no. Pt B, pp. 75-80.

Gennarelli, TA, Adams, JH & Graham, DI 1981, 'Acceleration induced head injury in the monkey I The model, its mechanical and physiological correlates', *Acta Neuropathol Suppl*, vol. 7, pp. 23-25.

Gennarelli, TA, Thibault, LE, Adams, JH, Graham, DI, Thompson, CJ & Marcincin, RP 1982, 'Diffuse axonal injury and traumatic coma in the primate', *Ann Neurol*, vol. 12, no. 6, pp. 564-574.

Gennarelli, TA, Thibault, LE & Ommaya, AK 1972, 'Pathophysiologic Responses to Rotational and Translational Accelerations of the Head', <https://doi.org/10.4271/720970>.

Gennarelli, TA, Thibault, LE, Tomei, G, Wiser, R, Graham, D & Adams, J 1987, 'Directional Dependence of Axonal Brain Injury due to Centroidal and Non-Centroidal Acceleration', <https://doi.org/10.4271/872197>.

Gentleman, SM, Leclercq, PD, Moyes, L, Graham, DI, Smith, C, Griffin, WS & Nicoll, JA 2004, 'Long-term intracerebral inflammatory response after traumatic brain injury', *Forensic Sci Int*, vol. 146, no. 2-3, pp. 97-104.

Ghawami, H, Sadeghi, S, Raghibi, M & Rahimi-Movaghar, V 2017, 'Executive functioning of complicated-mild to moderate traumatic brain injury patients with frontal contusions', *Appl Neuropsychol Adult*, vol. 24, no. 4, pp. 299-307.

Giza, CC & Hovda, DA 2001, 'The Neurometabolic Cascade of Concussion', *J Athl Train*, vol. 36, no. 3, pp. 228-235.

Giza, CC & Hovda, DA 2014, 'The new neurometabolic cascade of concussion', *Neurosurgery*, vol. 75, no. 4, pp. S24-33.

Golding, EM, Steenberg, ML, Contant, CF, Jr., Krishnappa, I, Robertson, CS & Bryan, RM 1999, 'Cerebrovascular reactivity to CO(2) and hypotension after mild cortical impact injury', *Am J Physiol*, vol. 277, no. 4, pp. H1457-1466.

Goodman, MD, Makley, AT, Huber, NL, Clarke, CN, Friend, LA, Schuster, RM, Bailey, SR, Barnes, SL, Dorlac, WC, Johannigman, JA, Lentsch, AB & Pritts, TA 2011, 'Hypobaric hypoxia exacerbates the neuroinflammatory response to traumatic brain injury', *J Surg Res*, vol. 165, no. 1, pp. 30-37.

Goodrich, JA, Kim, JH, Situ, R, Taylor, W, Westmoreland, T, Du, F, Parks, S, Ling, G, Hwang, JY, Rapuano, A, Bandak, FA & de Lanerolle, NC 2016, 'Neuronal and glial changes in the brain resulting from explosive blast in an experimental model', *Acta Neuropathol Commun*, vol. 4, no. 1, pp. 124.

Greve, MW & Zink, BJ 2009, 'Pathophysiology of traumatic brain injury', *Mt Sinai J Med*, vol. 76, no. 2, pp. 97-104.

Grimmelt, AC, Eitzen, S, Balakhadze, I, Fischer, B, Wölfer, J, Schiffbauer, H, Gorji, A & Greiner, C 2011, 'Closed traumatic brain injury model in sheep mimicking high-velocity, closed head trauma in humans', *Cent Eur Neurosurg*, vol. 72, no. 3, pp. 120-126.

Gultekin, SH & Smith, TW 1994, 'Diffuse axonal injury in craniocerebral trauma. A comparative histologic and immunohistochemical study', *Arch Pathol Lab Med*, vol. 118, no. 2, pp. 168-171.

Guskiewicz, KM, Weaver, NL, Padua, DA & Garrett, WE, Jr. 2000, 'Epidemiology of concussion in collegiate and high school football players', *Am J Sports Med*, vol. 28, no. 5, pp. 643-650.

Hajiaghamemar, M, Wu, T, Panzer, MB & Margulies, SS 2020, 'Embedded axonal fiber tracts improve finite element model predictions of traumatic brain injury', *Biomech Model Mechanobiol*, vol. 19, no. 3, pp. 1109-1130.

Hall, RC, Hall, RC & Chapman, MJ 2005, 'Definition, diagnosis, and forensic implications of postconcussional syndrome', *Psychosomatics*, vol. 46, no. 3, pp. 195-202.

Haque, A, Polcyn, R, Matzelle, D & Banik, NL 2018, 'New Insights into the Role of Neuron-Specific Enolase in Neuro-Inflammation, Neurodegeneration, and Neuroprotection', *Brain Sci*, vol. 8, no. 2.

Hardy, WN, Foster, CD, Mason, MJ, Yang, KH, King, AI & Tashman, S 2001, 'Investigation of Head Injury Mechanisms Using Neutral Density Technology and High-Speed Biplanar X-ray', *Stapp Car Crash J*, vol. 45, pp. 337-368.

Hawryluk, GW & Manley, GT 2015, 'Classification of traumatic brain injury: past, present, and future', *Handb Clin Neurol*, vol. 127, pp. 15-21.

Australian Instituite of Health & Welfare 2010, *Health system expenditure on disease and injury in Australia, 2004-05*, AIHW, Canberra, <https://www.aihw.gov.au/reports/health-welfare-expenditure/expenditure-disease-injury-2004-05>.

Hellewell, SC, Yan, EB, Agyapomaa, DA, Bye, N & Morganti-Kossmann, MC 2010, 'Post-traumatic hypoxia exacerbates brain tissue damage: analysis of axonal injury and glial responses', *J Neurotrauma*, vol. 27, no. 11, pp. 1997-2010.

Hergenroeder, GW, Moore, AN, McCoy, JP, Jr., Samsel, L, Ward, NH, 3rd, Clifton, GL & Dash, PK 2010, 'Serum IL-6: a candidate biomarker for intracranial pressure elevation following isolated traumatic brain injury', *J Neuroinflammation*, vol. 7, p. 19.

Hernández, JA, Lepe, M, Macedo, R, Arredondo, V, Cortez, CE, García, LJ & Prado, O 2017, 'Morphological study of Socorro Island Merino sheep and its crosses with hair breeds', *Trop Anim Health Prod*, vol. 49, no. 1, pp. 173-178.

Hillier, SL, Hiller, JE & Metzer, J 1997, 'Epidemiology of traumatic brain injury in South Australia', *Brain Inj*, vol. 11, no. 9, pp. 649-659.

Ho, J & Kleiven, S 2009, 'Can sulci protect the brain from traumatic injury?', *J Biomech*, vol. 42, no. 13, pp. 2074-2080.

Hofmann, E, Fimmers, R, Schmid, M, Hirschfelder, U, Detterbeck, A & Hertrich, K 2016, 'Landmarks of the Frankfort horizontal plane : Reliability in a three-dimensional Cartesian coordinate system', *J Orofac Orthop*, vol. 77, no. 5, pp. 373-383.

Holbourn, A 1943, 'Mechanics of Head Injury Lancet'.

Huang, L, Coats, JS, Mohd-Yusof, A, Yin, Y, Assaad, S, Muellner, MJ, Kamper, JE, Hartman, RE, Dulcich, M, Donovan, VM, Oyoyo, U & Obenaus, A 2013, 'Tissue vulnerability is increased following repetitive mild traumatic brain injury in the rat', *Brain Res*, vol. 1499, pp. 109-120.

Iaccarino, C, Carretta, A, Nicolosi, F & Morselli, C 2018, 'Epidemiology of severe traumatic brain injury', *J Neurosurg Sci*, vol. 62, no. 5, pp. 535-541.

Iwata, A, Stys, PK, Wolf, JA, Chen, XH, Taylor, AG, Meaney, DF & Smith, DH 2004, 'Traumatic axonal injury induces proteolytic cleavage of the voltage-gated sodium channels modulated by tetrodotoxin and protease inhibitors', *J Neurosci*, vol. 24, no. 19, pp. 4605-4613.

Jagnoor, J & Cameron, ID 2014, 'Traumatic brain injury--support for injured people and their carers', *Aust Fam Physician*, vol. 43, no. 11, pp. 758-763.

Johnson, VE, Stewart, JE, Begbie, FD, Trojanowski, JQ, Smith, DH & Stewart, W 2013, 'Inflammation and white matter degeneration persist for years after a single traumatic brain injury', *Brain*, vol. 136, no. 1, pp. 28-42.

Johnson, VE, Stewart, W & Smith, DH 2013, 'Axonal pathology in traumatic brain injury', *Exp Neurol*, vol. 246, pp. 35-43.

Johnson, VE, Stewart, W, Weber, MT, Cullen, DK, Siman, R & Smith, DH 2016, 'SNTF immunostaining reveals previously undetected axonal pathology in traumatic brain injury', *Acta Neuropathol*, vol. 131, no. 1, pp. 115-135.

Johnson, VE, Weber, MT, Xiao, R, Cullen, DK, Meaney, DF, Stewart, W & Smith, DH 2018, 'Mechanical disruption of the blood-brain barrier following experimental concussion', *Acta Neuropathol*, vol. 135, no. 5, pp. 711-726.

Jünger, EC, Newell, DW, Grant, GA, Avellino, AM, Ghatan, S, Douville, CM, Lam, AM, Aaslid, R & Winn, HR 1997, 'Cerebral autoregulation following minor head injury', *J Neurosurg*, vol. 86, no. 3, pp. 425-432.

Karnabatidis, D, Katsanos, K, Diamantopoulos, A, Kagadis, GC & Siablis, D 2006, 'Transauricular arterial or venous access for cardiovascular experimental protocols in animals', *J Vasc Interv Radiol*, vol. 17, no. 11 Pt 1, pp. 1803-1811.

Karve, IP, Taylor, JM & Crack, PJ 2016, 'The contribution of astrocytes and microglia to traumatic brain injury', *Br J Pharmacol*, vol. 173, no. 4, pp. 692-702.

Katschinski, DM, Robins, HI, Schad, M, Frede, S & Fandrey, J 1999, 'Role of tumor necrosis factor alpha in hyperthermia-induced apoptosis of human leukemia cells', *Cancer Res*, vol. 59, no. 14, pp. 3404-3410.

Kettenmann, H, Hanisch, UK, Noda, M & Verkhratsky, A 2011, 'Physiology of microglia', *Physiol Rev*, vol. 91, no. 2, pp. 461-553.

Kim, JB, Lim, CM, Yu, YM & Lee, JK 2008, 'Induction and subcellular localization of high-mobility group box-1 (HMGB1) in the postischemic rat brain', *J Neurosci Res*, vol. 86, no. 5, pp. 1125-1131.

Kinoshita, K 2016, 'Traumatic brain injury: pathophysiology for neurocritical care', *J Intensive Care*, vol. 4, p. 29.

Kleiven, S 2013, 'Why Most Traumatic Brain Injuries are Not Caused by Linear Acceleration but Skull Fractures are', *Front Bioeng Biotechnol*, vol. 1, p. 15.

Kraus, MF, Susmaras, T, Caughlin, BP, Walker, CJ, Sweeney, JA & Little, DM 2007, 'White matter integrity and cognition in chronic traumatic brain injury: a diffusion tensor imaging study', *Brain*, vol. 130, no. 10, pp. 2508-2519.

Krishnamoorthy, V, Chaikittisilpa, N, Kiatchai, T & Vavilala, M 2017, 'Hypertension After Severe Traumatic Brain Injury: Friend or Foe?', *J Neurosurg Anesthesiol*, vol. 29, no. 4, pp. 382-387.

Krishnamoorthy, V, Mackensen, GB, Gibbons, EF & Vavilala, MS 2016, 'Cardiac Dysfunction After Neurologic Injury: What Do We Know and Where Are We Going?', *Chest*, vol. 149, no. 5, pp. 1325-1331.

Kuo, C, Fanton, M, Wu, L & Camarillo, D 2018, 'Spinal constraint modulates head instantaneous center of rotation and dictates head angular motion', *J Biomech*, vol. 76, pp. 220-228.

Lafrenaye, AD, Mondello, S, Wang, KK, Yang, Z, Povlishock, JT, Gorse, K, Walker, S, Hayes, RL & Kochanek, PM 2020, 'Circulating GFAP and Iba-1 levels are associated with pathophysiological sequelae in the thalamus in a pig model of mild TBI', *Sci Rep*, vol. 10, no. 1, pp. 13369.

Lafrenaye, AD, Todani, M, Walker, SA & Povlishock, JT 2015, 'Microglia processes associate with diffusely injured axons following mild traumatic brain injury in the micro pig', *J Neuroinflammation*, vol. 12, pp. 186.

Langlois, JA, Rutland-Brown, W & Wald, MM 2006, 'The epidemiology and impact of traumatic brain injury: a brief overview', *J Head Trauma Rehabil*, vol. 21, no. 5, pp. 375-378.

LaPlaca, MC, Simon, CM, Prado, GR & Cullen, DK 2007, 'CNS injury biomechanics and experimental models', *Prog Brain Res*, vol. 161, pp. 13-26.

Laskowski, RA, Creed, JA & Raghupathi, R 2015, 'Frontiers in Neuroengineering Pathophysiology of Mild TBI: Implications for Altered Signaling Pathways', in FH Kobeissy (ed.), *Brain Neurotrauma: Molecular, Neuropsychological, and Rehabilitation Aspects*, CRC Press/Taylor & Francis (c) 2015 by Taylor & Francis Group, LLC., Boca Raton (FL).

Lazaridis, C, Rusin, CG & Robertson, CS 2019, 'Secondary brain injury: Predicting and preventing insults', *Neuropharmacology*, vol. 145, Pt B, pp. 145-152.

Lee, W, Lee, SD, Park, MY, Foley, L, Purcell-Estabrook, E, Kim, H & Yoo, SS 2015, 'Functional and diffusion tensor magnetic resonance imaging of the sheep brain', *BMC Vet Res*, vol. 11, p. 262.

Len, TK, Neary, JP, Asmundson, GJ, Candow, DG, Goodman, DG, Bjornson, B & Bhambhani, YN 2013, 'Serial monitoring of CO2 reactivity following sport concussion using hypocapnia and hypercapnia', *Brain Inj*, vol. 27, no. 3, pp. 346-353.

Lewis, A & Elks, PM 2019, 'Hypoxia Induces Macrophage tnfa Expression via Cyclooxygenase and Prostaglandin E2 in vivo', *Front Immunol*, vol. 10, p. 2321.

Lewis, SB, Finnie, JW, Blumbergs, PC, Scott, G, Manavis, J, Brown, C, Reilly, PL, Jones, NR & McLean, AJ 1996, 'A head impact model of early axonal injury in the sheep', *J Neurotrauma*, vol. 13, no. 9, pp. 505-514.

Lin, Y & Wen, L 2013, 'Inflammatory response following diffuse axonal injury', *Int J Med Sci*, vol. 10, no. 5, pp. 515-521.

Lippert-Gruner, M, Kuchta, J, Hellmich, M & Klug, N 2006, 'Neurobehavioural deficits after severe traumatic brain injury (TBI)', *Brain Inj*, vol. 20, no. 6, pp. 569-574.

Loane, DJ & Byrnes, KR 2010, 'Role of microglia in neurotrauma', *Neurotherapeutics*, vol. 7, no. 4, pp. 366-377.

Lyne, A & Hollis, D 1973, 'Development of horns in Merino sheep', *Australian Journal of Zoology*, vol. 21, no. 2, pp. 153-169.

Maas, AI, Stocchetti, N & Bullock, R 2008, 'Moderate and severe traumatic brain injury in adults', *Lancet Neurol*, vol. 7, no. 8, pp. 728-741.

Maloney-Wilensky, E, Gracias, V, Itkin, A, Hoffman, K, Bloom, S, Yang, W, Christian, S & LeRoux, PD 2009, 'Brain tissue oxygen and outcome after severe traumatic brain injury: a systematic review', *Crit Care Med*, vol. 37, no. 6, pp. 2057-2063.

Margulies, SS & Thibault, LE 1992, 'A proposed tolerance criterion for diffuse axonal injury in man', *J Biomech*, vol. 25, no. 8, pp. 917-923.

Margulies, SS, Thibault, LE & Gennarelli, TA 1990, 'Physical model simulations of brain injury in the primate', *J Biomech*, vol. 23, no. 8, pp. 823-836.

Mariotti, GV 2019, 'Head Injury Criterion: Mini Review', *Am J Biomed Sci & Res*, vol. 5, no. 5, pp. 406-407.

Marmarou, A, Foda, MA, van den Brink, W, Campbell, J, Kita, H & Demetriadou, K 1994, 'A new model of diffuse brain injury in rats. Part I: Pathophysiology and biomechanics', *J Neurosurg*, vol. 80, no. 2, pp. 291-300.

Martin, P, Hall, G, Crandall, J & Pilkey, W 1998, 'Measuring the Acceleration of a Rigid Body', *Shock and Vibration*, vol. 5, pp. 211-224.

Marzban Abbasabadi, B, Hajian, O & Rahmati, S 2020, 'Investigating the Morphometric Characteristics of Male and Female Zell Sheep Skulls for Sexual Dimorphism', *Anatomical Sciences Journal*, vol. 17, no. 1, pp. 13-20.

Mateika, JH & Duffin, J 1995, 'A review of the control of breathing during exercise', *Eur J Appl Physiol Occup Physiol*, vol. 71, no. 1, pp. 1-27.

McCrory, P, Meeuwisse, WH, Aubry, M, Cantu, B, Dvorak, J, Echemendia, RJ, Engebretsen, L, Johnston, K, Kutcher, JS, Raftery, M, Sills, A, Benson, BW, Davis, GA, Ellenbogen, RG, Guskiewicz, K, Herring, SA, Iverson, GL, Jordan, BD, Kissick, J, McCrea, M, McIntosh, AS, Maddocks, D, Makdissi, M, Purcell, L, Putukian, M, Schneider, K, Tator, CH & Turner, M 2013, 'Consensus statement on concussion in sport: the 4th International Conference on Concussion in Sport held in Zurich, November 2012', *Br J Sports Med*, vol. 47, no. 5, pp. 250-258.

McDonald, SJ, Sharkey, JM, Sun, M, Kaukas, LM, Shultz, SR, Turner, RJ, Leonard, AV, Brady, RD & Corrigan, F 2020, 'Beyond the Brain: Peripheral Interactions after Traumatic Brain Injury', *J Neurotrauma*, vol. 37, no. 5, pp. 770-781.

McGinn, MJ & Povlishock, JT 2015, 'Cellular and molecular mechanisms of injury and spontaneous recovery', *Handb Clin Neurol*, vol. 127, pp. 67-87.

McIntosh, TK, Vink, R, Noble, L, Yamakami, I, Fernyak, S, Soares, H & Faden, AL 1989, 'Traumatic brain injury in the rat: characterization of a lateral fluid-percussion model', *Neuroscience*, vol. 28, no. 1, pp. 233-244.

McKee, AC, Stein, TD, Kiernan, PT & Alvarez, VE 2015, 'The neuropathology of chronic traumatic encephalopathy', *Brain Pathol*, vol. 25, no. 3, pp. 350-364.

McQuire, JC, Sutcliffe, JC & Coats, TJ 1998, 'Early changes in middle cerebral artery blood flow velocity after head injury', *J Neurosurg*, vol. 89, no. 4, pp. 526-532.

Meaney, DF, Morrison, B & Bass, DC 2014, 'The mechanics of traumatic brain injury: a review of what we know and what we need to know for reducing its societal burden', *J Biomech Eng*, vol. 136, no. 2, pp. 021008.

Meaney, DF & Smith, DH 2011, 'Biomechanics of concussion', *Clin Sports Med*, vol. 30, no. 1, pp. 19-31, vii.

Meaney, DF, Smith, DH, Shreiber, DI, Bain, AC, Miller, RT, Ross, DT & Gennarelli, TA 1995, 'Biomechanical analysis of experimental diffuse axonal injury', *J Neurotrauma*, vol. 12, no. 4, pp. 689-694.

Mertz, H, Prasad, P & Irwin, A 1997, Injury Risk Curves for Children and Adults in Frontal and Rear Collisions.

Mesfin, FB, Gupta, N, Hays Shapshak, A & Taylor, RS 2020, 'Diffuse Axonal Injury (DAI)', in *StatPearls*, StatPearls Publishing., Copyright © 2020, StatPearls Publishing LLC., Treasure Island (FL).

Meythaler, JM, Peduzzi, JD, Eleftheriou, E & Novack, TA 2001, 'Current concepts: diffuse axonal injury-associated traumatic brain injury', *Arch Phys Med Rehabil*, vol. 82, no. 10, pp. 1461-1471.

Millen, JE, Glauser, FL & Fairman, RP 1985, 'A comparison of physiological responses to percussive brain trauma in dogs and sheep', *J Neurosurg*, vol. 62, no. 4, pp. 587-591.

Mittenberg, W, Canyock, EM, Condit, D & Patton, C 2001, 'Treatment of post-concussion syndrome following mild head injury', *J Clin Exp Neuropsychol*, vol. 23, no. 6, pp. 829-836.

Mohamed, AZ, Corrigan, F, Collins-Praino, LE, Plummer, SL, Soni, N & Nasrallah, FA 2020, 'Evaluating spatiotemporal microstructural alterations following diffuse traumatic brain injury', *NeuroImage: Clinical*, vol. 25, pp. 102136.

Mohamed, R, Driscoll, M & Mootoo, N 2016, 'Clinical Anatomy of the skull of the Barbados Black Belly Sheep in Trinidad'.

Moorin, R, Miller, TR & Hendrie, D 2014, 'Population-based incidence and 5-year survival for hospital-admitted traumatic brain and spinal cord injury, Western Australia, 2003-2008', *J Neurol*, vol. 261, no. 9, pp. 1726-1734.

Mustafa, AG, Singh, IN, Wang, J, Carrico, KM & Hall, ED 2010, 'Mitochondrial protection after traumatic brain injury by scavenging lipid peroxyl radicals', *J Neurochem*, vol. 114, no. 1, pp. 271-280.

Mustafa, AG, Wang, JA, Carrico, KM & Hall, ED 2011, 'Pharmacological inhibition of lipid peroxidation attenuates calpain-mediated cytoskeletal degradation after traumatic brain injury', *J Neurochem*, vol. 117, no. 3, pp. 579-588.

Myburgh, JA, Cooper, DJ, Finfer, SR, Venkatesh, B, Jones, D, Higgins, A, Bishop, N & Higlett, T 2008, 'Epidemiology and 12-month outcomes from traumatic brain injury in australia and new zealand', *J Trauma*, vol. 64, no. 4, pp. 854-862.

Nahum, AM, Gatts, JD, Gadd, CW & Danforth, J 1968, 'Impact Tolerance of the Skull and Face', <https://doi.org/10.4271/680785>.

Namjoshi, DR, Cheng, WH, McInnes, KA, Martens, KM, Carr, M, Wilkinson, A, Fan, J, Robert, J, Hayat, A, Cripton, PA & Wellington, CL 2014, 'Merging pathology with biomechanics using CHIMERA (Closed-Head Impact Model of Engineered Rotational Acceleration): a novel, surgery-free model of traumatic brain injury', *Mol Neurodegener*, vol. 9, p. 55.

Newcombe, VF, Williams, GB, Scoffings, D, Cross, J, Carpenter, TA, Pickard, JD & Menon, DK 2010, 'Aetiological differences in neuroanatomy of the vegetative state: insights from diffusion tensor imaging and functional implications', *J Neurol Neurosurg Psychiatry*, vol. 81, no. 5, pp. 552-561.

Nguyen, H & Zaroff, JG 2009, 'Neurogenic stunned myocardium', *Curr Neurol Neurosci Rep*, vol. 9, no. 6, pp. 486-491.

O'Donnell, JC, Browne, KD, Kilbaugh, TJ, Chen, HI, Whyte, J & Cullen, DK 2019, 'Challenges and demand for modeling disorders of consciousness following traumatic brain injury', *Neurosci Biobehav Rev*, vol. 98, pp. 336-346.

O'Leary R, A & Nichol, AD 2018, 'Pathophysiology of severe traumatic brain injury', *J Neurosurg Sci*, vol. 62, no. 5, pp. 542-548.

Oddo, M, Levine, JM, Mackenzie, L, Frangos, S, Feihl, F, Kasner, SE, Katsnelson, M, Pukenas, B, Macmurtrie, E, Maloney-Wilensky, E, Kofke, WA & LeRoux, PD 2011, 'Brain hypoxia is associated with short-term outcome after severe traumatic brain injury independently of intracranial hypertension and low cerebral perfusion pressure', *Neurosurgery*, vol. 69, no. 5, pp. 1037-1045.

Okonkwo, DO & Povlishock, JT 1999, 'An intrathecal bolus of cyclosporin A before injury preserves mitochondrial integrity and attenuates axonal disruption in traumatic brain injury', *J Cereb Blood Flow Metab*, vol. 19, no. 4, pp. 443-451.

Ommaya, AK & Gennarelli, TA 1974, 'Cerebral concussion and traumatic unconsciousness. Correlation of experimental and clinical observations of blunt head injuries', *Brain*, vol. 97, no. 4, pp. 633-654.

Ommaya, AK, Goldsmith, W & Thibault, L 2002, 'Biomechanics and neuropathology of adult and paediatric head injury', *Br J Neurosurg*, vol. 16, no. 3, pp. 220-242.

Ommaya, AK, Grubb, RL, Jr. & Naumann, RA 1971, 'Coup and contre-coup injury: observations on the mechanics of visible brain injuries in the rhesus monkey', *J Neurosurg*, vol. 35, no. 5, pp. 503-516.

Ommaya, AK & Hirsch, AE 1971, 'Tolerances for cerebral concussion from head impact and whiplash in primates', *J Biomech*, vol. 4, no. 1, pp. 13-21.

Ommaya, AK, Yarnell, P, Hirsch, AE & Harris, EH 1967, 'Scaling of Experimental Data on Cerebral Concussion in Sub-Human Primates to Concussion Threshold for Man', <https://doi.org/10.4271/670906>.

Ono, K, Kikuchi, A, Nakamura, M, Kobayashi, H & Nakamura, N 1980, 'Human Head Tolerance to Sagittal Impact Reliable Estimation Deduced from Experimental Head Injury Using Subhuman Primates and Human Cadaver Skulls', <https://doi.org/10.4271/801303>.

Otsuka, N, Tomonaga, M & Ikeda, K 1991, 'Rapid appearance of beta-amyloid precursor protein immunoreactivity in damaged axons and reactive glial cells in rat brain following needle stab injury', *Brain Res*, vol. 568, no. 1-2, pp. 335-338.

Parés Casanova, P-M 2015, 'Discrete sexual size dimorphism in domestic sheep', *Annals of Biological Research, 2015*, vol. 6, no. 10, p. 43-48.

Park, J & Lakes, RS 1992, *Biomaterials: An Introduction*, 2 edn, vol. 72, Plenum Press, New York.

Patel, S, Miao, JH, Yetiskul, E, Anokhin, A & Majmundar, SH 2020, 'Physiology, Carbon Dioxide Retention', in *StatPearls*, StatPearls Publishing., Copyright © 2020, StatPearls Publishing LLC., Treasure Island (FL).

Penkowa, M, Giralt, M, Lago, N, Camats, J, Carrasco, J, Hernández, J, Molinero, A, Campbell, IL & Hidalgo, J 2003, 'Astrocyte-targeted expression of IL-6 protects the CNS against a focal brain injury', *Exp Neurol*, vol. 181, no. 2, pp. 130-148.

Pertab, JL, Merkley, TL, Cramond, AJ, Cramond, K, Paxton, H & Wu, T 2018, 'Concussion and the autonomic nervous system: An introduction to the field and the results of a systematic review', *NeuroRehabilitation*, vol. 42, no. 4, pp. 397-427.

Pettus, EH, Christman, CW, Giebel, ML & Povlishock, JT 1994, 'Traumatically induced altered membrane permeability: its relationship to traumatically induced reactive axonal change', *J Neurotrauma*, vol. 11, no. 5, pp. 507-522.

Pettus, EH & Povlishock, JT 1996, 'Characterization of a distinct set of intra-axonal ultrastructural changes associated with traumatically induced alteration in axolemmal permeability', *Brain Res*, vol. 722, no. 1-2, pp. 1-11.

Pfenninger, EG, Reith, A, Breitig, D, Grünert, A & Ahnefeld, FW 1989, 'Early changes of intracranial pressure, perfusion pressure, and blood flow after acute head injury. Part 1: An experimental study of the underlying pathophysiology', *J Neurosurg*, vol. 70, no. 5, pp. 774-779.

Pierce, JE, Smith, DH, Trojanowski, JQ & McIntosh, TK 1998, 'Enduring cognitive, neurobehavioral and histopathological changes persist for up to one year following severe experimental brain injury in rats', *Neuroscience*, vol. 87, no. 2, pp. 359-369.

Pieri, V, Trovatelli, M, Cadioli, M, Zani, DD, Brizzola, S, Ravasio, G, Acocella, F, Di Giancamillo, M, Malfassi, L, Dolera, M, Riva, M, Bello, L, Falini, A & Castellano, A 2019,

'In vivo Diffusion Tensor Magnetic Resonance Tractography of the Sheep Brain: An Atlas of the Ovine White Matter Fiber Bundles', *Front Vet Sci*, vol. 6, p. 345.

Plummer, SL, Van den Heuvel, C, Thornton, E, Corrigan, F & Cappai, R 2016, 'The Neuroprotective Properties of the Amyloid Precursor Protein Following Traumatic Brain Injury', *Aging Dis*, vol. 7, no. 2, Mar, pp. 163-179.

Plummer, SL, Corrigan, F, Thornton, E, Woenig, JA, Vink, R, Cappai, R & Van den Heuvel, C 2018, 'The amyloid precursor protein derivative, APP96-110, is efficacious following intravenous administration after traumatic brain injury', *PLoS One*, vol. 13, no. 1, p. e0190449.

Ponsford, J, Olver, J, Ponsford, M & Nelms, R 2003, 'Long-term adjustment of families following traumatic brain injury where comprehensive rehabilitation has been provided', *Brain Inj*, vol. 17, no. 6, pp. 453-468.

Povlishock, JT 2013, 'The window of risk in repeated head injury', *J Neurotrauma*, vol. 30, no. 1, pp. 1.

Povlishock, JT & Katz, DI 2005, 'Update of neuropathology and neurological recovery after traumatic brain injury', *J Head Trauma Rehabil*, vol. 20, no. 1, pp. 76-94.

Pozzato, I, Tate, RL, Rosenkoetter, U & Cameron, ID 2019, 'Epidemiology of hospitalised traumatic brain injury in the state of New South Wales, Australia: a population-based study', *Aust N Z J Public Health*, vol. 43, no. 4, pp. 382-388.

Previtali, SC, Archelos, JJ & Hartung, HP 1997, 'Modulation of the expression of integrins on glial cells during experimental autoimmune encephalomyelitis. A central role for TNF-alpha', *Am J Pathol*, vol. 151, no. 5, pp. 1425-1435.

Pushkarna, A, Bhatoe, HS & Sudambrekar, SM 2010, 'Head Injuries', *Med J Armed Forces India*, vol. 66, no. 4, pp. 321-324.

Quintana, A, Molinero, A, Borup, R, Nielsen, FC, Campbell, IL, Penkowa, M & Hidalgo, J 2008, 'Effect of astrocyte-targeted production of IL-6 on traumatic brain injury and its impact on the cortical transcriptome', *Dev Neurobiol*, vol. 68, no. 2, pp. 195-208.

Rassovsky, Y, Levi, Y, Agranov, E, Sela-Kaufman, M, Sverdlik, A & Vakil, E 2015, 'Predicting long-term outcome following traumatic brain injury (TBI)', *J Clin Exp Neuropsychol*, vol. 37, no. 4, pp. 354-366.

Reeves, TM, Phillips, LL, Lee, NN & Povlishock, JT 2007, 'Preferential neuroprotective effect of tacrolimus (FK506) on unmyelinated axons following traumatic brain injury', *Brain Res*, vol. 1154, pp. 225-236.

Reeves, TM, Phillips, LL & Povlishock, JT 2005, 'Myelinated and unmyelinated axons of the corpus callosum differ in vulnerability and functional recovery following traumatic brain injury', *Exp Neurol*, vol. 196, no. 1, pp. 126-137.

Ren, L, Wang, D, Liu, X, Yu, H, Jiang, C & Hu, Y 2020, 'Influence of Skull Fracture on Traumatic Brain Injury Risk Induced by Blunt Impact', *Int J Environ Res Public Health*, vol. 17, no. 7.

Rensch, B 1950, 'Die Abhängigkeit der relativen Sexualdifferenz von der Körpergrösse', *Bonner Zoologische Beiträge*, vol. 1, pp. 58-69.

Rivara, FP & Graham, R 2014, 'Sports-related concussions in youth: report from the Institute of Medicine and National Research Council', *Jama*, vol. 311, no. 3, pp. 239-240.

Ross, DT, Meaney, DF, Sabol, MK, Smith, DH & Gennarelli, TA 1994, 'Distribution of forebrain diffuse axonal injury following inertial closed head injury in miniature swine', *Exp Neurol*, vol. 126, no. 2, pp. 291-299.

Roth, G & Dicke, U 2012, 'Evolution of the brain and intelligence in primates', *Prog Brain Res*, vol. 195, pp. 413-430.

Roush, GC 2010, 'Finding Cadaveric Human Head Masses and Center of Gravity: A Comparison of Direct Measurement to 3D ing', Wright State University. Thesis.

Santiago, LA, Oh, BC, Dash, PK, Holcomb, JB & Wade, CE 2012, 'A clinical comparison of penetrating and blunt traumatic brain injuries', *Brain Inj*, vol. 26, no. 2, pp. 107-125.

Schiffner, R, Bischoff, SJ, Lehmann, T, Rakers, F, Rupprecht, S, Matziolis, G, Schubert, H, Schwab, M, Huber, O, Lemke, C & Schmidt, M 2018, 'Underlying mechanism of subcortical brain protection during hypoxia and reoxygenation in a sheep model - Influence of α1-adrenergic signalling', *PLoS One*, vol. 13, no. 5, p. e0196363.

Schonberger, M, Ponsford, J, Gould, KR & Johnston, L 2011, 'The temporal relationship between depression, anxiety, and functional status after traumatic brain injury: a cross-lagged analysis', *J Int Neuropsychol Soc*, vol. 17, no. 5, pp. 781-787.

Schwaninger, M, Sallmann, S, Petersen, N, Schneider, A, Prinz, S, Libermann, TA & Spranger, M 1999, 'Bradykinin induces interleukin-6 expression in astrocytes through activation of nuclear factor-kappaB', *J Neurochem*, vol. 73, no. 4, pp. 1461-1466.

Selassie, AW, Zaloshnja, E, Langlois, JA, Miller, T, Jones, P & Steiner, C 2008, 'Incidence of long-term disability following traumatic brain injury hospitalization, United States, 2003', *J Head Trauma Rehabil*, vol. 23, no. 2, pp. 123-131.

Semple, BD, Zamani, A, Rayner, G, Shultz, SR & Jones, NC, 'Affective, neurocognitive and psychosocial disorders associated with traumatic brain injury and post-traumatic epilepsy', *Neurobiol Dis*, vol. 123, pp. 27-41.

Sharp, DJ & Jenkins, PO 2015, 'Concussion is confusing us all', *Pract Neurol*, vol. 15, no. 3, pp. 172-186.

Shiozaki, T 2005, 'Hypertension and head injury', *Curr Hypertens Rep*, vol. 7, no. 6, pp. 450-453.

Shohami, E, Novikov, M, Bass, R, Yamin, A & Gallily, R 1994, 'Closed head injury triggers early production of TNF alpha and IL-6 by brain tissue', *J Cereb Blood Flow Metab*, vol. 14, no. 4, pp. 615-619.

Siedlecki, P, Sanzo, P, Zerpa, C & Newhouse, I 2018, 'End-tidal carbon dioxide levels in patients with post-concussion syndrome during neurocognitive and physical tasks compared to a normative control group', *Brain Inj*, vol. 32, no. 13-14, pp. 1824-1833.

Siedler, DG, Chuah, MI, Kirkcaldie, MT, Vickers, JC & King, AE 2014, 'Diffuse axonal injury in brain trauma: insights from alterations in neurofilaments', *Front Cell Neurosci*, vol. 8, p. 429.

Siegler, S, Caravaggi, P, Tangorra, J, Milone, M, Namani, R & Marchetto, PA 2015, 'The envelope of motion of the cervical spine and its influence on the maximum torque generating capability of the neck muscles', *J Biomech*, vol. 48, no. 13, pp. 3650-3655.

Siman, R, Cui, H, Wewerka, SS, Hamel, L, Smith, DH & Zwank, MD 2020, 'Serum SNTF, a Surrogate Marker of Axonal Injury, Is Prognostic for Lasting Brain Dysfunction in Mild TBI Treated in the Emergency Department', *Front Neurol*, vol. 11, p. 249.

Siman, R, Giovannone, N, Hanten, G, Wilde, EA, McCauley, SR, Hunter, JV, Li, X, Levin, HS & Smith, DH 2013, 'Evidence That the Blood Biomarker SNTF Predicts Brain Imaging Changes and Persistent Cognitive Dysfunction in Mild TBI Patients', *Front Neurol*, vol. 4, p. 190.

Simard, JM & Bellefleur, M 1989, 'Systemic arterial hypertension in head trauma', *Am J Cardiol*, vol. 63, no. 6, pp. 32c-35c.

Singhal, G, Jaehne, EJ, Corrigan, F, Toben, C & Baune, BT 2014, 'Inflammasomes in neuroinflammation and changes in brain function: a focused review', *Front Neurosci*, vol. 8, pp. 315.

Slykhouse, L, Zaseck, LW, Miller, C, Humm, JR, Alai, A, Kang, YS, Dooley, C, Sherman, D, Bigler, B, Demetropoulos, CK, Reed, MP & Rupp, JD 2019, 'Anatomically-based skeletal coordinate systems for use with impact biomechanics data intended for anthropomorphic test device development', *J Biomech*, vol. 92, pp. 162-168.

Smith, DH 2016, 'Neuromechanics and Pathophysiology of Diffuse Axonal Injury in Concussion', *Bridge (Washington, D.C)*, vol. 46, no. 1, Spring, pp. 79-84.

Smith, DH, Chen, XH, Xu, BN, McIntosh, TK, Gennarelli, TA & Meaney, DF 1997, 'Characterization of diffuse axonal pathology and selective hippocampal damage following inertial brain trauma in the pig', *J Neuropathol Exp Neurol*, vol. 56, no. 7, pp. 822-834.

Smith, DH, Hicks, R & Povlishock, JT 2013, 'Therapy development for diffuse axonal injury', *J Neurotrauma*, vol. 30, no. 5, pp. 307-323.

Smith, DH, Meaney, DF & Shull, WH 2003, 'Diffuse axonal injury in head trauma', *J Head Trauma Rehabil*, vol. 18, no. 4, pp. 307-316.

Smith, DH, Nonaka, M, Miller, R, Leoni, M, Chen, XH, Alsop, D & Meaney, DF 2000, 'Immediate coma following inertial brain injury dependent on axonal damage in the brainstem', *J Neurosurg*, vol. 93, no. 2, pp. 315-322.

Smith, DH, Uryu, K, Saatman, KE, Trojanowski, JQ & McIntosh, TK 2003, 'Protein accumulation in traumatic brain injury', *Neuromolecular Med*, vol. 4, no. 1-2, pp. 59-72.

Smith, DH, Wolf, JA, Lusardi, TA, Lee, VM & Meaney, DF 1999, 'High tolerance and delayed elastic response of cultured axons to dynamic stretch injury', *J Neurosci*, vol. 19, no. 11, pp. 4263-4269.

Sorby-Adams, AJ, Vink, R & Turner, RJ 2018, 'Large animal models of stroke and traumatic brain injury as translational tools', *Am J Physiol Regul Integr Comp Physiol*, Mar 14.

'Sports concussion assessment tool - 5th Edition ', 2017, *Br J Sports Med* vol. 51, pp. 851-858.

Staal, JA, Dickson, TC, Gasperini, R, Liu, Y, Foa, L & Vickers, JC 2010, 'Initial calcium release from intracellular stores followed by calcium dysregulation is linked to secondary axotomy following transient axonal stretch injury', *J Neurochem*, vol. 112, no. 5, pp. 1147-1155.

Staal, JA & Vickers, JC 2011, 'Selective vulnerability of non-myelinated axons to stretch injury in an in vitro co-culture system', *J Neurotrauma*, vol. 28, no. 5, pp. 841-847.

Stocchetti, N & Zanier, ER 2016, 'Chronic impact of traumatic brain injury on outcome and quality of life: a narrative review', *Crit Care*, vol. 20, no. 1, pp. 148.

Strebel, S, Lam, AM, Matta, BF & Newell, DW 1997, 'Impaired cerebral autoregulation after mild brain injury', *Surg Neurol*, vol. 47, no. 2, pp. 128-131.

Su, E & Bell, M 2016, 'Frontiers in Neuroscience Diffuse Axonal Injury', in D Laskowitz & G Grant (eds), *Translational Research in Traumatic Brain Injury*, CRC Press/Taylor and Francis Group(c) 2016 by Taylor & Francis Group, LLC., Boca Raton (FL).

Sugiyama, K, Kondo, T, Higano, S, Endo, M, Watanabe, H, Shindo, K & Izumi, S 2007, 'Diffusion tensor imaging fiber tractography for evaluating diffuse axonal injury', *Brain Inj*, vol. 21, no. 4, pp. 413-419.

Teasdale, G & Jennett, B 1974, 'Assessment of coma and impaired consciousness. A practical scale', *Lancet*, vol. 2, no. 7872, pp. 81-84.

Teng, SX, Katz, PS, Maxi, JK, Mayeux, JP, Gilpin, NW & Molina, PE 2015, 'Alcohol exposure after mild focal traumatic brain injury impairs neurological recovery and exacerbates localized neuroinflammation', *Brain Behav Immun*, vol. 45, pp. 145-156.

Thelin, EP, Frostell, A, Mulder, J, Mitsios, N, Damberg, P, Aski, SN, Risling, M, Svensson, M, Morganti-Kossmann, MC, Bellander, B 2016, ' Lesion Size Is Exacerbated in Hypoxic Rats Whereas Hypoxia-Inducible Factor-1 Alpha and Vascular Endothelial Growth Factor Increase in Injured Normoxic Rats: A Prospective Cohort Study of Secondary Hypoxia in Focal Traumatic Brain Injury', *Front Neurol*, vol. 7, no. 23.

Thomas, M & Dufour, L 2009, 'Challenges of diffuse axonal injury diagnosis', *Rehabil Nurs*, vol. 34, no. 5, pp. 179-180.

Trivedi, M & Coles, JP 2009, 'Blood pressure management in acute head injury', *J Intensive Care Med*, vol. 24, no. 2, pp. 96-107.

Tu, TW, Williams, RA, Lescher, JD, Jikaria, N, Turtzo, LC & Frank, JA 2016, 'Radiological-pathological correlation of diffusion tensor and magnetization transfer imaging in a closed head traumatic brain injury model', *Ann Neurol*, vol. 79, no. 6, pp. 907-920.

Ueno, K & Melvin, JW 1995, 'Finite element model study of head impact based on Hybrid III head acceleration: the effects of rotational and translational acceleration', *J Biomech Eng*, vol. 117, no. 3, pp. 319-328.

Van den Heuvel, C, Blumbergs, P, Finnie, J, Manavis, J, Lewis, S, Jones, N, Reilly, P & Pereira, R 2000, 'Upregulation of amyloid precursor protein and its mRNA in an experimental model of paediatric head injury', *J Clin Neurosci*, vol. 7, no. 2, pp. 140-145.

Van den Heuvel, C, Blumbergs, PC, Finnie, JW, Manavis, J, Jones, NR, Reilly, PL & Pereira, RA 1999, 'Upregulation of amyloid precursor protein messenger RNA in response to traumatic brain injury: an ovine head impact model', *Exp Neurol*, vol. 159, no. 2, pp. 441-450.

Van den Heuvel, C, Finnie, JW, Blumbergs, PC, Manavis, J, Jones, NR, Reilly, PL & Pereira, RA 2000, 'Upregulation of neuronal amyloid precursor protein (APP) and APP mRNA following magnesium sulphate (MgSO4) therapy in traumatic brain injury', *J Neurotrauma*, vol. 17, no. 11, pp. 1041-1053.

Van den Heuvel, C, Lewis, S, Wong, M, Manavis, J, Finnie, J, Blumbergs, P, Jones, N & Reilly, P 1998, 'Diffuse neuronal perikaryon amyloid precursor protein immunoreactivity in a focal head impact model', *Acta Neurochir Suppl*, vol. 71, pp. 209-211.

van der Naalt, J, van Zomeren, AH, Sluiter, WJ & Minderhoud, JM 1999, 'One year outcome in mild to moderate head injury: the predictive value of acute injury characteristics related to complaints and return to work', *J Neurol Neurosurg Psychiatry*, vol. 66, no. 2, pp. 207-213.

Vink, R 2018, 'Large animal models of traumatic brain injury', *J Neurosci Res*, vol. 96, no. 4, pp. 527-535.

Vink, R, Bahtia, KD & Reilly, PL 2008, 'The relationship between intracranial pressure and brain oxygenation following traumatic brain injury in sheep', *Acta Neurochir Suppl*, vol. 102, pp. 189-192.

Vink, R, Gabrielian, L & Thornton, E 2017, 'The Role of Substance P in Secondary Pathophysiology after Traumatic Brain Injury', *Front Neurol*, vol. 8, p. 304.

von Reyn, CR, Spaethling, JM, Mesfin, MN, Ma, M, Neumar, RW, Smith, DH, Siman, R & Meaney, DF 2009, 'Calpain mediates proteolysis of the voltage-gated sodium channel alpha-subunit', *J Neurosci*, vol. 29, no. 33, pp. 10350-10356.

Wang, G, Zhang, J, Hu, X, Zhang, L, Mao, L, Jiang, X, Liou, AK, Leak, RK, Gao, Y & Chen, J 2013, 'Microglia/macrophage polarization dynamics in white matter after traumatic brain injury', *J Cereb Blood Flow Metab*, vol. 33, no. 12, pp. 1864-1874.

Wang, YT, Kent, RD, Duffy, JR, Thomas, JE & Weismer, G 2004, 'Alternating motion rate as an index of speech motor disorder in traumatic brain injury', *Clin Linguist Phon*, vol. 18, no. 1, pp. 57-84.

Weil, ZM, Gaier, KR & Karelina, K 2014, 'Injury timing alters metabolic, inflammatory and functional outcomes following repeated mild traumatic brain injury', *Neurobiology of Disease*, vol. 70, pp. 108-116.

Wells, AJ 2014, 'A surgical model of middle cerebral artery occlusive stroke in the sheep.', School of Medical Science, PhD Thesis, The University of Adelaide.

Wells, AJ, Vink, R, Blumbergs, PC, Brophy, BP, Helps, SC, Knox, SJ & Turner, RJ 2012, 'A surgical model of permanent and transient middle cerebral artery stroke in the sheep', *PLoS One*, vol. 7, no. 7, p. e42157.

Wijdicks, EF & Cranford, RE 2005, 'Clinical diagnosis of prolonged states of impaired consciousness in adults', *Mayo Clin Proc*, vol. 80, no. 8, pp. 1037-1046.

Willer, B & Leddy, JJ 2006, 'Management of concussion and post-concussion syndrome', *Curr Treat Options Neurol*, vol. 8, no. 5, pp. 415-426.

Williams, AM, Bhatti, UF, Brown, JF, Biesterveld, BE, Kathawate, RG, Graham, NJ, Chtraklin, K, Siddiqui, AZ, Dekker, SE, Andjelkovic, A, Higgins, GA, Buller, B & Alam, HB 2020, 'Early single-dose treatment with exosomes provides neuroprotection and improves blood-brain barrier integrity in swine model of traumatic brain injury and hemorrhagic shock', *J Trauma Acute Care Surg*, vol. 88, no. 2 pp. 207-218.

Wofford, KL, Harris, JP, Browne, KD, Brown, DP, Grovola, MR, Mietus, CJ, Wolf, JA, Duda, JE, Putt, ME, Spiller, KL & Cullen, DK 2017, 'Rapid neuroinflammatory response localized to injured neurons after diffuse traumatic brain injury in swine', *Exp Neurol*, vol. 290, pp. 85-94.

Wofford, KL, Loane, DJ & Cullen, DK 2019, 'Acute drivers of neuroinflammation in traumatic brain injury', *Neural Regen Res*, vol. 14, no. 9, pp. 1481-1489.

Wolf, JA, Stys, PK, Lusardi, T, Meaney, D & Smith, DH 2001, 'Traumatic axonal injury induces calcium influx modulated by tetrodotoxin-sensitive sodium channels', *J Neurosci*, vol. 21, no. 6, pp. 1923-1930.

Wolf, SA, Boddeke, HW & Kettenmann, H 2017, 'Microglia in Physiology and Disease', *Annu Rev Physiol*, vol. 79, pp. 619-643.

Wood, T, Moralejo, D, Corry, K, Snyder, JM, Traudt, C, Curtis, C, Nance, E, Parikh, P & Juul, SE 2018, 'A Ferret Model of Encephalopathy of Prematurity', *Dev Neurosci*, vol. 40, no. 5-6, pp. 475-489.

Woodroofe, MN, Sarna, GS, Wadhwa, M, Hayes, GM, Loughlin, AJ, Tinker, A & Cuzner, ML 1991, 'Detection of interleukin-1 and interleukin-6 in adult rat brain, following mechanical injury, by in vivo microdialysis: evidence of a role for microglia in cytokine production', *J Neuroimmunol*, vol. 33, no. 3, pp. 227-236.

World Health Organization 2014, *Injuries and violence: the facts 2014*, World Health Organization, Geneva.

World Health Organisation 2006, 'Neurological Disorders Report'.

Xiong, Y, Mahmood, A & Chopp, M 2013, 'Animal models of traumatic brain injury', *Nat Rev Neurosci*, vol. 14, no. 2, pp. 128-142.

Yamamoto, M, Marmarou, CR, Stiefel, MF, Beaumont, A & Marmarou, A 1999, 'Neuroprotective effect of hypothermia on neuronal injury in diffuse traumatic brain injury coupled with hypoxia and hypotension', *J Neurotrauma*, vol. 16, no. 6, pp. 487-500.

Yan, EB, Hellewell, SC, Bellander, BM, Agyapomaa, DA & Morganti-Kossmann, MC 2011, 'Post-traumatic hypoxia exacerbates neurological deficit, neuroinflammation and cerebral metabolism in rats with diffuse traumatic brain injury', *J Neuroinflammation*, vol. 8, pp. 147.

Yang, SH, Gustafson, J, Gangidine, M, Stepien, D, Schuster, R, Pritts, TA, Goodman, MD, Remick, DG & Lentsch, AB 2013, 'A murine model of mild traumatic brain injury exhibiting cognitive and motor deficits', *J Surg Res*, vol. 184, no. 2, pp. 981-988.

Yavuz, MS, Asirdizer, M, Cetin, G, Günay Balci, Y & Altinkok, M 2003, 'The correlation between skull fractures and intracranial lesions due to traffic accidents', *Am J Forensic Med Pathol*, vol. 24, no. 4, pp. 339-345.

Yoganandan, N, Pintar, FA, Zhang, J & Baisden, JL 2009, 'Physical properties of the human head: mass, center of gravity and moment of inertia', *J Biomech*, vol. 42, no. 9, pp. 1177-1192.

Yuen, TJ, Browne, KD, Iwata, A & Smith, DH 2009, 'Sodium channelopathy induced by mild axonal trauma worsens outcome after a repeat injury', *J Neurosci Res*, vol. 87, no. 16, pp. 3620-3625.

Zhang, YP, Cai, J, Shields, LB, Liu, N, Xu, XM & Shields, CB 2014, 'Traumatic brain injury using mouse models', *Transl Stroke Res*, vol. 5, no. 4, pp. 454-471.